Studies in Systems, Decision and Control 388

Olexandr Kyrylenko · Andrii Zharkin · Oleksandr Butkevych · Ihor Blinov · Ievgen Zaitsev · Artur Zaporozhets *Editors*

Power Systems Research and Operation

Selected Problems

Springer

Studies in Systems, Decision and Control

Volume 388

The series “Studies in Systems, Decision and Control” (SSDC) covers both new developments and advances, as well as the state of the art, in the various areas of broadly perceived systems, decision making and control–quickly, up to date and with a high quality. The intent is to cover the theory, applications, and perspectives on the state of the art and future developments relevant to systems, decision making, control, complex processes and related areas, as embedded in the fields of engineering, computer science, physics, economics, social and life sciences, as well as the paradigms and methodologies behind them. The series contains monographs, textbooks, lecture notes and edited volumes in systems, decision making and control spanning the areas of Cyber-Physical Systems, Autonomous Systems, Sensor Networks, Control Systems, Energy Systems, Automotive Systems, Biological Systems, Vehicular Networking and Connected Vehicles, Aerospace Systems, Automation, Manufacturing, Smart Grids, Nonlinear Systems, Power Systems, Robotics, Social Systems, Economic Systems and other. Of particular value to both the contributors and the readership are the short publication timeframe and the world-wide distribution and exposure which enable both a wide and rapid dissemination of research output.

Indexed by SCOPUS, DBLP, WTI Frankfurt eG, zbMATH, SCImago.

All books published in the series are submitted for consideration in Web of Science.

More information about this series at http://www.springer.com/series/13304

Olexandr Kyrylenko · Andrii Zharkin ·
Oleksandr Butkevych · Ihor Blinov ·
Ievgen Zaitsev · Artur Zaporozhets
Editors

Power Systems Research and Operation

Selected Problems

Springer

Editors
Olexandr Kyrylenko
Institute of Electrodynamics
National Academy of Sciences of Ukraine
Kyiv, Ukraine

Andrii Zharkin
Institute of Electrodynamics
National Academy of Sciences of Ukraine
Kyiv, Ukraine

Oleksandr Butkevych
Institute of Electrodynamics
National Academy of Sciences of Ukraine
Kyiv, Ukraine

Ihor Blinov
Institute of Electrodynamics
National Academy of Sciences of Ukraine
Kyiv, Ukraine

Ievgen Zaitsev
Institute of Electrodynamics
National Academy of Sciences of Ukraine
Kyiv, Ukraine

Artur Zaporozhets
Institute of Engineering Thermophysics
National Academy of Sciences of Ukraine
Kyiv, Ukraine

ISSN 2198-4182 ISSN 2198-4190 (electronic)
Studies in Systems, Decision and Control
ISBN 978-3-030-82925-4 ISBN 978-3-030-82926-1 (eBook)
https://doi.org/10.1007/978-3-030-82926-1

This Springer imprint is published by the registered company Springer Nature Switzerland AG
The registered company address is: Gewerbestrasse 11, 6330 Cham, Switzerland

Preface

Ensuring operational reliability and safety of objects integrated power system of Ukraine's complex task. Solution of which is related to the optimization of operating modes of electric power facilities and their control systems, information and measuring systems and metrological support in the electric power industry, ensuring the functioning of the electric power system in the conditions of a competitive market of the electric power.

Monograph presents the research results aimed at covering solutions to current scientific and practical problems, occuring during the operation of integrated power system of Ukraine in modern market condition in the next areas:

- implementation of new approaches to the calculation of the capacity of intersections between power systems or their parts;
- study of power system stability by frequency with considering account the influence of renewable generation sources and the operation of frequency emergency automation devices of power plants;
- research methods for identification of dominant modes of low-frequency electromechanical oscillations are suitable for use in real time in monitoring systems;
- development of new methods of flow distribution analysis in electric networks of arbitrary structure, which allows to take into account the limitations of power flows when modelling the decentralized combination of electricity markets in the market segment "day ahead";
- studies of short-term forecasting electricity generated by renewable energy sources and development new neural deep learning networks architecture;
- development structural and parametric operating modes optimization methods for main electric networks with considering design features of ultra-high-voltage power transmission lines and coronation effects in their wires;
- development methods and devices for improving metrological and technical characteristics of measuring systems for monitoring and diagnosing generating equipment of power plants.

Develop these areas, the monograph covers new technologies and methods related to the management of large interconnected power systems, solving a stable and reliable problem of electricity generation, ensuring optimal operation of transmission lines taking into account the probabilistic nature of corona losses, sources of electricity from renewable sources and energy sources. Devices with remote control, which is reasonable in the case of cyclical and long-term changes in load, as well as assessing the impact of transmission network constraints on electricity exchange in the context of integration of electricity markets into the European electricity market. So, the monograph can be divided into several main sections.

The main part of the monograph is devoted to the management of power systems. Total transmission power is an important indicator of any system interfaces used to maintain system stability in a market environment. Information about the total transmission power for power systems management used. In addition, total transmission power daily or even hourly to estimate the reliability margins for all power transmissions through the interfaces of each network. According to the proposed approach, users spend their time setting up and preparing big data for calculations. This approach significantly reduces the number of errors of operational staff when performing calculations. To optimize the modes of operation of the transmission line, proposed to solve problems of voltage and reactive power optimization. Power lines operating mode monitoring consists of correct choice of the composition of the charging power compensation devices in order to regulate the voltage levels and power coefficients at the bus terminals. By using modern devices for controlled compensation of power line charging, it is possible to achieve deeper regulation of reactive power and voltage, and, accordingly, to minimize the loss of active power. Interconnected mathematical models set to determine the economic effect of optimizing the mode of operation of the electrical network with ultra-high power lines in terms of voltage and reactive power, taking into account the probabilistic nature of corona losses. Methods, algorithms and methods of operative optimization of operating modes of separate power lines taking into account corona losses are developed.

Methods for solving the problem of choosing the optimal places of disconnection in electricity distribution networks and implementing its results are considered. This shown that a universal solution is the use of power electronic devices, which makes it possible to form the so-called “soft points” of the distribution circuits in the active control and reactive power flows to ensure minimum power loss due to rapid response to changes in electrical load and/or modes of production and energy storage in the presence of scattered sources of production means and electricity storage. New technological solutions are proposed that allow to effectively reduce electricity losses in distribution networks with local sources of energy production and storage due to the possibility of dynamic management of the network configuration.

Devoted to the analysis model checking technique applicability in energetics scenarios. Proven and widely adopted TLC (TLA checker) model checker has been considered as an instrument for design solutions verification. To this end, the Temporal Logic of Actions (TLA) and corresponding formalisms—TLA+ and PlusCal—have been applied to formally specify the functional properties provided

as block-diagrams. Power systems management scenarios taking place in electricity markets have been approached as promising problem domain.

Unsatisfactory accuracy of RES electricity generation forecasts leads to additional production and/or consumption disparities and additional costs for settling these imbalances. In such circumstances, it is possible to improve the quality of decision-making when planning regimes, using accurate forecasts for the markets for the day ahead and intraday. For this purpose, a new architecture developed for short-term energy forecasting of aggregate RES production.

The other part of the monograph on the monitoring and control system designed to identify the danger of disruption of the stability of self-energy and its equipment. To assess the condition of generators as mechanical systems, a structural system of systems and a new type of mechanical parameters meter proposed. The use of the system and sensors allows for depth monitoring of the condition of individual generator units in real time, in order to implement the automatic ability to decide on the possibility of operating the generator based on the use of identification systems and artificial intelligence.

In power systems, especially in interconnected ones, Low-Frequency oscillations (LF) periodically occur, leading to accidents with severe consequences. The study of frequency stability in power systems based on the consideration of local frequency control to mitigate the impact of renewable generation on high-load linear flows and the impact of frequency stability considered frequency alarm systems and AGC modelling. The results of researches of various methods of signal analysis for their use in real time for detection of modes of electromechanical oscillations in power systems presented. Using real-time methods under certain conditions, different results of LFO mode identification obtained. This approach allows you to get a more reliable estimate of the parameters of the LFO modes more reliably.

The presented research results in monograph allow increasing the reliability and efficiency of operation of energy facilities and ensuring the stability of power systems, the introduction of effective methods and tools for forecasting electricity supply, optimize power systems, suggest road map to integrate electricity markets taking into account network constraints in modern conditions of electricity markets.

The authors of the monograph are mainly from Institute of Electrodynamics of the National Academy of Sciences of Ukraine.

Kyiv, Ukraine
April 2021

Olexandr Kyrylenko
Andrii Zharkin
Oleksandr Butkevych
Ihor Blinov
Ievgen Zaitsev
Artur Zaporozhets

Contents

Decentralized Market Coupling with Taking Account Power Systems Transmission Network Constraints

Ihor Blinov, Olexandr Kyrylenko, Euvgen Parus, and Oksana Rybina

Abstract The chapter is devoted to the development of theoretical and methodological bases for assessing the impact of transmission network constraints on electricity exchange in the context of integration of electricity markets into the European electricity market. The chapter presents theoretical substantiations of models for assessing the impact of network constraints on the exchange of electricity through the electric section on the pricing processes in the electricity day-ahead market segment on the base of the decentralized market coupling concept. A general description of the existing methods of congestion management for market coupling is given. One of the most important and actual tasks of operability assurance of the day-ahead market is to determine the cross-border congestion management methods. The latter approach is more promising and actively developing now. The most known implementations of market coupling are the flow-based market coupling (FBC) and decentralized market coupling (DMC), including trilateral market coupling (TMC). The main FBC disadvantage is the necessity of linearization of electricity demand function. It prevents from adequately taking into account the demand and offer structure, which is generated from linear and discrete type bids. As a result, the wrong choices of increment of iterative process and the missing of the global extremum are possible. DMC uses mathematical apparatus of net export curves (NECs), which correctly reflect the potential of the export and import of electricity for a local market area in the common electricity market. However, the use of NEC is complicated in case of a coupling of more than two electricity markets. Also, there is the problem of the formal presentation of relations structure between the coupling markets. Approaches to the analysis of restrictions on the exchange of electricity by electric cross-section as a task of multi-purpose optimization of the welfare function of electricity market participants are formalized. Methods and models of analysis of processes of decentralized market coupling of a group of price zones of free configuration are given.

I. Blinov (✉) · O. Kyrylenko · E. Parus · E. Parus · O. Rybina · O. Rybina
Institute of Electrodynamics of NAS of Ukraine, Kyiv, Ukraine

O. Kyrylenko
e-mail: kyrylenko@ied.org.ua

O. Rybina
e-mail: rybina@ied.org.ua

O. Kyrylenko et al. (eds.), *Power Systems Research and Operation*, Studies in Systems, Decision and Control 388, https://doi.org/10.1007/978-3-030-82926-1_1

The principles of solving practical problems of determining the optimal configuration of price zones in the day-ahead electricity market are considered. An example of assessing the feasibility of integrating a separate price zone of the Integrated Power System (IPS) of Ukraine into the European electricity market is shown.

Keywords Day-ahead electricity market · Decentralized market coupling · Cross-border capacity · Congestion management · Net export curves

1 Introduction

Today, in Ukraine the requirements for reliability and efficiency of electricity transmission between energy systems [1–9] and electricity markets are growing [10, 11]. In pursuance of the Law "On the Electricity Market" [12] a new electricity market has been operating in Ukraine from July 1, 2019. The market model defined by the Law corresponds to the generally accepted European model [13] and meets the requirements of the third energy package. At present, the world has accumulated considerable experience in modeling electricity markets, research on the organization and functioning of new models of electricity markets, for example, [14, 15] is being carried out. It should be noted that the scientific and practical principles of introduction of different components of the electricity market [16, 17] created in Ukraine, developed methods and models for solving problems of optimizing operation of power systems, providing ancillary services [19] in the market conditions, forecasting of prices, and forecasting of electricity supply by RES producers [20, 21] do not completely solve the problems of complex modeling of market coupling [11, 22].

The analysis [23–33] has shown that in the electricity markets of European countries the issue of taking into account network constraints on the day-ahead market (DAM) segment is solved based on the characteristics of both the structure of production and consumption of electricity and the structure of electricity networks. Both factors caused the implementation of different approaches to the organization and carrying out of bids in the electricity markets of European countries. Even in the context of merging national electricity markets into transnational market associations, differences in approaches to the organization and carrying out of bids have not been completely eliminated. Therefore, the issue of creating a single method or set of methods of pricing the aim at combining existing markets, taking into account technological constraints on the electricity exchange between them, the basic implementation principles of which are defined in the European Commission Regulations [34, 35]. Thus, the tasks of studying the feasibility of taking into account in this segment of technological constraints on the electricity exchange in main electricity networks and developing appropriate methods and means of such consideration based on the experience of European electricity markets in addressing such tasks become especially actual.

It should be noted that in European energy systems cross-border electricity exchange is carried out based on different principles: from explicit auctions of trade of individual crossings capacity to the formation of transnational exchanges with implicit taking into account the capacity of cross-border crossings based on the methods of coupling or dividing price zones. Therefore and at present, the task of comparing the features of the demand/supply of IPS of Ukraine and related energy systems is still relevant for the development of measures for the effective development of the cross-border electricity trading market, starting with the liberalization of processes of trading cross-border crossings and ending with full integration of the Ukrainian electricity market into respective European market associations.

An analysis of the features of European market associations [36–41] and the provisions of the EU Commission regulations on taking into account cross-border capacity, including Commission Regulation (EU) 2015/1222 [35], as well as the requirements of ENTSO-E, has shown that at present in the electricity markets of European countries the following approaches to solving system constraints have been developed [22]:

- addressing systemic constraints using exclusively balancing market (BM) mechanisms, which is typical of many national electricity markets in Europe, where system constraints do not have a significant impact on the performance of the electricity market as a whole;
- allocation of permanent price zones and exchange of electricity between them with the involvement of explicit auctions of trading the capacity of main electric lines, which is primarily typical of the processes of cross-border trade in electricity between organizationally independent national markets;
- allocation of price zones into which the market is divided, if the bid results lead to such values of electricity flows in the main lines, which violate the relevant system constraints (Market Splitting mechanism);
- preliminary allocation of price zones and coupling to form the uniform price of those zones for which, according to the bid results in the DAM, system constraints between them are not violated (the Market Coupling mechanism).

2 Network Congestion Management Constraints in the Context of European Electricity Market Coupling

2.1 Flow-Based Market Coupling Mechanism

The Flow-Based Market Coupling (FB MC) method is considered as introduced in Europe's cross-border market associations. The method is based on the analysis of electricity flow distribution in the alternative circuit of electrical networks with the objective function of maximizing well-being:

$$\begin{cases} \Sigma_{i\in Area}\left[\int_0^{q_i^d} p_i(q)\cdot dq - \int_0^{q_i^S} c_i(q)\cdot dq\right] \to \max \\ q_i^d \geq 0 \\ q_i^S \geq 0 \\ \begin{bmatrix} R_{Line1}^{AreaA} & \dots & R_{Line1}^{AreaZ} \\ \vdots & & \vdots \\ R_{Linep}^{AreaA} & \dots & R_{Linep}^{AreaZ} \end{bmatrix} \cdot \begin{bmatrix} q_{AreaA}^S - q_{AreaA}^d \\ \vdots \\ q_{AreaZ}^S - q_{AreaZ}^d \end{bmatrix} \leq \begin{bmatrix} \Phi_{Line1}^{\max} \\ \vdots \\ \Phi_{Linep}^{\max} \end{bmatrix}, \end{cases}$$

where q_i^d is the demand for electricity satisfied as a result of bids in area i; $p_i(q)$ is the price function dependent on the volumes of the satisfied demand in area i; q_i^s is the electricity supply as a result of bids in area i; $c_i(q)$ is the price function dependent on the volumes of the accepted offer in area i; R_{Linep}^{AreaX} is Power Transfer Distribution Factor (PTDF) for line p in area X; $\Phi_{Linep}^{\max}$ is physical capacity limitation of line p.

In FB MC, the structure of electrical networks is represented by a topological graph, and price zones is represented by the areas where in the absence of constraints on the electricity exchange a single marginal price is set. Therefore, in the case of performing optimization calculations, FB MC operates not with the ratio of flows in the lines and loads of nodes, but rather with the ratio of flows between areas to the lines of the electrical network model. Thus, the structure of electrical networks in FB MC is represented by a PTDF matrix. The input of power plants in the total coverage of the load schedule is determined by constant coefficients called Generation Shift Keys (GSKs) that link the balance change in the node of the substitution scheme (price zone) with the change in load coverage structure in each node. Relationship between critical cross-sections and cross-border electricity import/export operations for the electricity network consisting of Z of price areas, p of lines and q of nodes:

$$\begin{bmatrix} ptdf_{Line1}^{AreaA} & \dots & ptdf_{Line1}^{AreaZ} \\ \vdots & & \vdots \\ ptdf_{Linep}^{AreaA} & \dots & ptdf_{Linep}^{AreaZ} \end{bmatrix} = \begin{bmatrix} ptdf_{Line1}^{Node1} & \dots & ptdf_{Line1}^{Nodeq} \\ \vdots & & \vdots \\ ptdf_{Linep}^{Node1} & \dots & ptdf_{Linep}^{Nodeq} \end{bmatrix} \cdot \begin{bmatrix} GSK_{Node1}^{AreaA} & \dots & GSK_{Nodeq}^{AreaZ} \\ \vdots & & \vdots \\ GSK_{Node1}^{AreaA} & \dots & GSK_{Nodeq}^{AreaZ} \end{bmatrix}.$$

The FB MC method is invariant both to the structure of the scheme of electrical couplings between price zones and to the structure of electrical networks in price zones. In this case, the most problematic part of the method is the calculation of GSK, which corresponds to the value of the angle of deviation of the linearized supply function from the axis of electricity volumes. The need for linearizing the

supply function results in an error in calculations and increasing the probability of skipping the global extremum. As a result, the risks of obtaining a suboptimal solution increase.

2.2 Decentralized Market Coupling Concept

An alternative mechanism for taking into account constraints on the electricity exchange between price zones is based on the method of Decentralized Market Coupling (DMC). The DMC method analyzes coupling of two electricity markets or two price areas of one market and is based on the use of apparatus of Net Export Curves (NEC) that reflect the algebraic difference between supply and demand (Fig. 1) at the same electricity price.

It should be noted that NECs are used in many macroeconomic models to assess the potential for interaction between individual market areas and determine the balance of imports/exports between them. Similarly, for the electricity markets, NEC enables comparing the export potential and import capacity of individual market areas to assess the opportunities for trade between them (Fig. 2). Thus, at the point of inter-

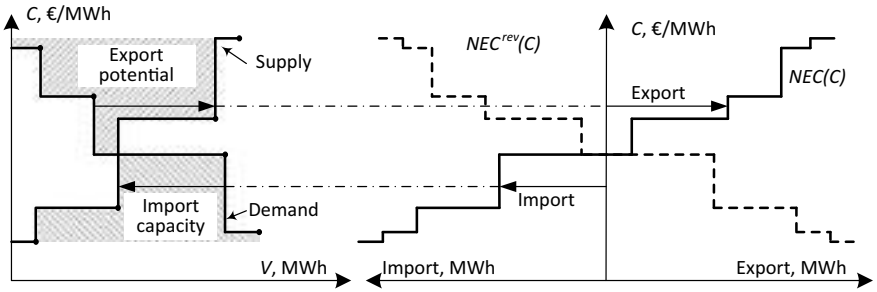

Fig. 1 Plotting the net export function

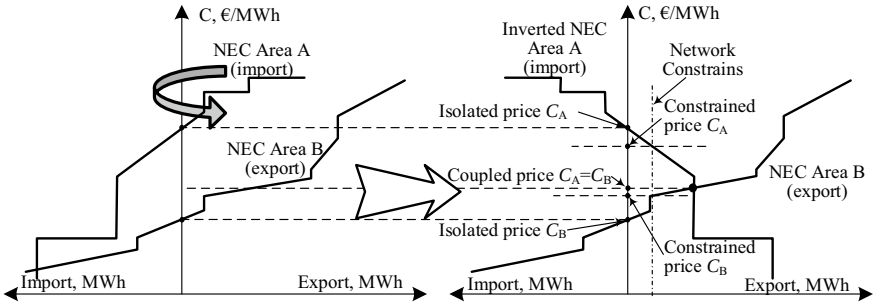

Fig. 2 Taking into account constraints on electricity exchange between price zones using the net export functions

section of the graphs of the NEC of the exporter area and the inverse NEC of the importer area, the optimal volumes of electricity exchange are determined, in case of which the coupled zones completely "merge", i.e. the results of bids in these areas become identical to the result of bids at the joint auction. At the same time, the marginal prices in the coupled areas are equalized and the maximum total welfare of the electricity market for these areas is achieved. If the technological constrains of the intersystem electric connection capacity do not allow to achieve the optimal volumes of electricity exchange, the difference in marginal prices remains non-zero in the coupled areas. In this case, the implementation of electricity exchange at the level of the maximum technologically possible volume results in obtaining the maximum possible value of total welfare under these constraints, which is a priori greater than the total welfare of isolated bids in these areas.

The use of NEC in DMC allows to take into account the features of the structure of supply and demand in the coupled areas. However, this method involves the analysis of only one electrical section between two price zones. The Trilateral Market Coupling (TMC) DMC extension does not use a formal description of the structure of electrical couplings. As a result, TMC is limited to an analysis of situations specific only to coupling of the electricity markets of France, Belgium and the Netherlands. Thus, the main disadvantages of DMC and TMC are their non-invariance toward the structure of electrical networks.

Based on the results of the analysis of existing methods and algorithms for calculating the results of bids in the DAM, a conclusion was made about the problematical character of solving the problem of taking into account constraints on electricity exchange between the coupled areas of the single market. In addition, in view of the

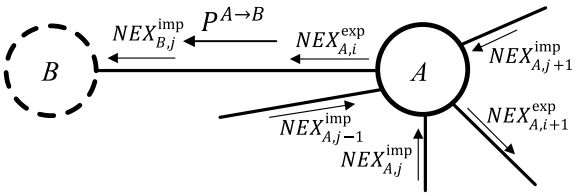

Fig. 3 The task of finding the optimal values of flows between price zones, in which the difference in marginal prices in these zones is minimized

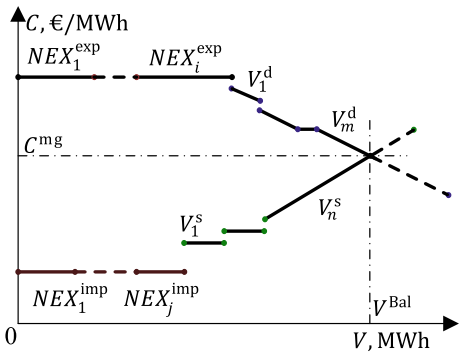

Fig. 4 The task of maximizing welfare in the price zone

processes of integration of the electricity market of Ukraine with EU countries, it is necessary to take into account the warning of the (EU) Commission Regulation 2015/1222 on the likelihood of situations where the price coupling process does not result in a single price in the coupled markets, and, consequently, such coupling does not occur. For cases of this type, it is recommended to develop alternative addressing of the tasks set at the national and regional levels, which, in turn, allows to begin the process of integration of the electricity market of Ukraine into the European associations without introducing a single European platform.

Based on the analysis, it is proposed to develop a new method for addressing the task set using the NEC apparatus to display the structure of supply and demand of the coupled areas and formally describing the structure of relations between them, the description of which is provided in the next section of this work.

For Ukraine, the cross-border electricity exchange is currently carried out using explicit auctions for capacity trading in conditions of imperfect competition, which does not contribute to the efficiency of functioning and development of this segment of the electricity market. The lack of market mechanisms for using the available capacity of cross-border crossings in the IPS of Ukraine for the needs of electricity markets of neighboring countries defines the relevance of developing and implementing methods of using cross-border electrical couplings for electricity exchange between different countries through the IPS of Ukraine; primarily Hungary, the Slovak Republic, the Czech Republic, and Romania (4 M MC) are involved.

3 New Approach to Decentralized Market Coupling Taking into Account Power Systems Network Constraints

In accordance with the research results, there is provided a new method for taking into account network constraints on the DAM by minimizing the difference in marginal prices in the coupled areas of the electricity market. The method is developed to improve the DMC for an arbitrary number of coupled electricity markets with an arbitrary structure of electrical couplings between these markets and is based on the use of the net export curves (NECs) apparatus. If supply and demand for the DAM are provided as the corresponding functional connections of volumes to price, $P_i^d(C_i)$ and $P_i^s(C_i)$, NEC is denoted as the algebraic difference between these functional connections:

$$NEC(C) = P_i^{\mathrm{s}}(C) - P_i^{\mathrm{d}}(C).$$

While the above formula clearly demonstrates the principles of NEC construction, for developing the new method of taking into account network constraints on the DAM it has been necessary to clarify it in order to study the NEC properties as a reflection of export potential and import capacity at different ratios of electricity supply and demand. According to the research results, eight options of the ratios

between the supply and demand functions have been identified, for which the NEC value is calculated using a separate formula. Each of these eight cases is uniquely identified by the ratios of the set price to the values of the maximum and minimum prices of the supply and demand functions. In addition, a special case of the ratios between supply and demand is identified, for which it is impossible to generate a balance. It is shown that in this case it is impossible to generate a balance between supply and demand and by means of the import/export of electricity, and therefore it should be assumed that the bids did not take place. This case does not directly affect the NEC mathematical model, but should be taken into account when developing an algorithm for calculating the bid results.

3.1 Universal Mathematical Model of Net Export Curves

A universal mathematical model of NEC has been developed, which takes into account all ratios between supply and demand of the local electricity market. If the demand at the hourly auction is submitted as a set of divisible price bids, arranged in the direction of decreasing the marginal price of electricity purchase, the demand graph will be displayed as a set of price pairs, $M^d \ni \left\{\left(C_1^d, P_1^d\right), \left(C_2^d, P_2^d\right), ..., \left(C_i^d, P_i^d\right), \ldots, \left(C_n^d, P_n^d\right)\right\}$, where C_i^d, P_i^d are the price and volume of electricity, respectively, at break points in the demand graph. Then the demand function is represented by an interpolation polynomial which establishes the dependence of the electricity purchase volumes on the marginal price at the auction:

$$P_i^{\mathrm{d}}(C_i) = P_k^{\mathrm{d}} + \frac{P_{k+1}^{\mathrm{d}} - P_k^{\mathrm{d}}}{C_{k+1}^{\mathrm{d}} - C_k^{\mathrm{d}}}\left(C_i - C_k^{\mathrm{d}}\right), C_{k+1}^{\mathrm{d}} \le C_i \le C_k^{\mathrm{d}}.$$

Similarly, the supply function at the hourly auction of electricity is presented as follows:

$$P_i^{\mathrm{s}}(C_i) = P_k^{\mathrm{s}} + \frac{P_{k+1}^{\mathrm{s}} - P_k^{\mathrm{s}}}{C_{k+1}^{\mathrm{s}} - C_k^{\mathrm{s}}}\left(C_i - C_k^{\mathrm{s}}\right), C_k^{\mathrm{s}} \le C_i \le C_{k+1}^{\mathrm{s}}.$$

The minimum and maximum values of prices for the demand graph are determined as C_{min}^d and C_{max}^d, respectively, and the minimum and maximum values of prices for the supply graph as C_{min}^s and C_{max}^s, respectively. Then NEC will be calculated by the following formula:

$$NEC(C) = \begin{cases} -P^{\mathrm{d}}\left(C^{\mathrm{d}}_{min}\right), C < C^{\mathrm{s}}_{min}; C \le C^{\mathrm{d}}_{max} \\ P^{\mathrm{s}}(C) - P^{\mathrm{d}}\left(C^{\mathrm{d}}_{min}\right), C^{\mathrm{s}}_{min} \le C \le C^{\mathrm{s}}_{max}; C < C^{\mathrm{d}}_{min} \\ P^{\mathrm{s}}\left(C^{\mathrm{s}}_{max}\right) - P^{\mathrm{d}}\left(C^{\mathrm{d}}_{min}\right), C > C^{\mathrm{s}}_{max}; C < C^{\mathrm{d}}_{min} \\ P^{\mathrm{s}}\left(C^{\mathrm{s}}_{max}\right) - P^{\mathrm{d}}(C), C > C^{\mathrm{s}}_{max}; C^{\mathrm{d}}_{min} \le C \le C^{\mathrm{d}}_{max} \\ P^{\mathrm{s}}\left(C^{\mathrm{s}}_{max}\right), C^{\mathrm{s}}_{min} \le C; C > C^{\mathrm{d}}_{max} \\ P^{\mathrm{s}}(C) - P^{\mathrm{d}}(C), C^{\mathrm{s}}_{min} \le C \le C^{\mathrm{s}}_{max}; C^{\mathrm{d}}_{min} \le C \le C^{\mathrm{d}}_{max} \end{cases}.$$

In the general case, NEC is displayed as a broken line dashed along the price axis. This makes it impossible to implement the analysis methods using derivatives. In addition, if there are "all or nothing" price bids at the auction, discrete or combined linear-discrete methods should be used for the analysis of NEC.

In order to develop a typical method for taking into account the constraints on the electricity exchange between the coupled areas of the DAM with an arbitrary number of price areas for any structure of electrical networks, an in-depth analysis of the NEC properties that affect the results of solving the problem is performed. The areas of definition and values of supply $P^d(C)$ and demand $P^s(C)$ functions are as follows:

$$\begin{cases} P^d(C) \in [0,\ V^d_{\max}] \mid V^d_{\max} = P^d(C^d_{\min}),\ C^d_{\min} \le C \le C^d_{\max} \\ P^S(C) \in [0,\ V^S_{\max}] \mid V^S_{\max} = P^{\Pi p 0 \Pi}(C^S_{\max}),\ C^S_{\min} \le C \le C^S_{\max} \end{cases}.$$

The NEC value is calculated as $NEC(C) = P^s_i(C) - P^d_i(C)$. It is easy to demonstrate that NEC will be determined in the marginal price interval $\left[min\left(C^d_{min}, C^s_{min}\right), max\left(C^d_{max}, C^s_{max}\right)\right]$ and will acquire the following values in this interval, $-V^d_{max} \le NEC(C) \le V^s_{max}$. Thus, NECs have areas of positive and negative values of electricity volumes. The interval in which $NEC(C) > 0$ shows the export potential of the price area, and the interval with $NEC(C) < 0$ shows the capacity for electricity imports in the price area.

Studies of different ratios between NECs have shown that the sequence of analysis provided in the DMC algorithm description gives adequate results only if NEC graphs of the two price areas have an intersection point. Otherwise, there are a number of contradictions, for elimination of which additional calculations need to be made. In order to develop unified methods of NEC analysis for different ratios between supply and demand in the DAM, the properties of NEC were studied, which influence the results of solving the problem of taking into account constraints on electricity exchange along main lines during bidding in the DAM. Two reasons have been identified that result in incomplete coupling of the electricity market. The first reason is the impossibility of electricity exchange implementation due to the limited capacity of intersystem relations. Taking into account these constraints leads to a decrease in the welfare of the electricity market, while the change in the electricity cost is caused solely by the ratios between supply and demand. The second reason for incomplete market coupling is insufficient export potential and the capacity of electricity import in the coupled price zones to equalize marginal prices. This case cannot be traced when modeling using the method of division into price zones without performing

additional calculations at the level of individual zones, and when modeling using the method of coupling price zones there are contradictions in the logic of pricing. The feature of this case is the complete displacement of the own demand of the exporter zone or the complete displacement of the own supply of the importer zone. In this case, the marginal price in one of the coupled price zones is actually formed based on the ratios of supply and demand of another price zone.

3.2 Concept of Development of Decentralized Market Coupling and Method of the Optimal Volume Electricity Exchange Determination to Minimize Prices in Coupled Markets

Based on the research results, the concept of taking into account the constraints on the electricity exchange between price zones in the DAM segment has been formed.

(1) Addressing the task set should be carried out by the method of coupling, i. e. the electricity market is pre-divided into price zones, which are intercoupled by potentially problematic electrical connections. Then the task of finding the optimal electricity distribution between zones has to be addressed, in which the difference in marginal prices in these zones is minimized, and the method of addressing this task should allow the possibility of optimization according to discrete variables.
(2) At the step of calculating the volumes of electricity exchange between price zones, marginal prices in individual zones are to be determined based on the results of balancing supply and demand, taking into account the current balance of electricity import/export.
(3) In order to generate a single marginal price (if this is not made at the previous step of calculations), the results of the joint auction should be calculated, in which only those price bids will be accepted which have been accepted based on the results of the calculation of the volumes of electricity exchange between price areas.

The use of the objective function of minimizing the difference in marginal prices in the coupled zones enabled coupling the formalisms of topological graph analysis and bilateral auction analysis. Thus, the structure of the electrical network is presented by a topological graph, in which price zones are represented by a set of nodes Z, and electrical connections between them are represented by a set of branches L. Main characteristics of nodes $z \in Z$ of the topological graph are as follows: marginal price in the price zone C_z as a characteristic that allows to assess the possibility of carrying out electricity import/export; NEC of the price zone NEC_z as a characteristic that allows to calculate the volumes of electricity import/export; net position of the price zone NP_z as a characteristic that reflects the numerical value of the total balance of electricity import/export for this zone.

The main characteristics of the branches $l \in L$ of the topological graph are as follows: constraints on electricity flows $P_{l(max)}^{(beg)\to(end)}$ and $P_{l(max)}^{(end)\to(beg)}$ separately for each direction relative to the formally defined beg and end of line l; the value of electricity flow $P_l^{(beg)\to(end)}$ in branch l as a result of simulation.

At the level of analysis of the topological graph, optimization is carried out using the objective function of minimizing marginal prices in adjacent price zones:

$$\left|C_{l,h}^{Z(beg)} - C_{l,h}^{Z(end)}\right| \to \min \ \forall(l \in L,\ z(beg) \cup z(end) \in Z,\ h \in \{1, 2, \ldots, 24\}),$$

where $C_{l,h}^{z(beg)}$, $C_{l,h}^{z(end)}$ are marginal prices in the beg $z(beg)$ and the end $z(end)$ nodes of the branch l per hour h.

Volumes of electricity exchange $V_{Coup}^{A\to B}$, the implementation of which will minimize the difference in marginal prices in adjacent price zones A and B, taking into account the constraints on the electricity exchange from zone A to zone B $V_{max}^{A\to B}$ and in the reverse direction $V_{max}^{B\to A}$ are calculated by the formula:

$$V_{Coup}^{A\to B} = \begin{cases} -\min\left(\max\left(NEC^B\left(C^B\right)\right), \min\left(NEC^A\left(C^A\right)\right), V_{max}^{B\to A}\right), C^A \geq C^B, C_{Isol}^A > C_{Isol}^B \\ \min\left(\min\left(NEC^B\left(C^B\right)\right), \max\left(NEC^A\left(C^A\right)\right), V_{max}^{A\to B}\right), C^A \leq C^B, C_{Isol}^A < C_{Isol}^B \\ 0, C_{Isol}^A = C_{Isol}^B \end{cases},$$

where C_{Isol}^A, C_{Isol}^B are marginal prices based on the results of isolated bids in price zones A and B, respectively.

If there is more than one branch of the topological graph (more than two nodes), the calculations are performed using iterative sequential analysis of each branch to achieve a stable optimal solution.

Relationship between electricity flow in branch l and net positions of electricity exchange in adjacent nodes $z(beg)$ and $z(end)$ is described by the system of equality constraints:

$$P_{l,h}^{z(beg\to z(end)} = NEX_{i,h}^{z(beg)} = -NEX_{j,h}^{z(end)} \forall l \in L \equiv I \cup J, h \in \{1, 2, \ldots, 24\}.$$

At the level of the price zone (topological graph node) the problem of optimizing the balance between supply and demand is solved taking into account the balance of electricity import/export according to the criterion of maximizing welfare.

Suppose that at the joint auction, in which all price zones $z \epsilon Z$ participate, the market participants are registered that apply for bidding, for each hour of the day $h \epsilon \{1, 2, \ldots, 24\}$, price bids $b \epsilon B$ on the electricity purchase $\left(V_{b,h}^{B,z}, C_{b,h}^{B,z}\right)$ and price

bids for the electricity sale $\left(V_{b,h}^{D,z}, C_{b,h}^{D,z}\right)$, in which the electricity volumes ($V_{b,h}^{B,z}$ and $V_{b,h}^{D,z}$, respectively) and price ($C_{b,h}^{B,z}$ and $C_{b,h}^{D,z}$, respectively). Then the objective function of the problem of optimizing the balance between supply and demand in the price zone z for the hour of day h is as follows:

$$\sum_{b\in B}(V_{b,h}^{B,z}\cdot C_{b,h}^{B,z}) - \sum_{b\in B}\left(V_{b,h}^{D,z}\cdot C_{b,h}^{D,z}\right) \to max \forall z \in Z, h\epsilon\{1,2,\ldots,24\}.$$

The balance of supply and demand is formed taking into account the components of electricity import/export:

$$\sum_{b\in B}(V_{b,h}^{B,z} - V_{b,h}^{D,z}) + NP_{z,h} = 0 \forall z \in Z, h\epsilon\{1,2,\ldots,24\},$$

where $NP_{z,h}$ is the net position of zone z for an hour of the day, h.

Value $NP_{z,h}$ shows the total balance of electricity import/export in the price zone:

$$NP_{z,h} = \sum_{i\in I} NEX_{i,h}^{z} + \sum_{j\in J} NEX_{j,h}^{z} \forall z \in Z, h\epsilon\{1,2,\ldots,24\},$$

where $NEX_{i,h}^{z}$ is the value of the net exchange position for the ith connection, through which from the zone z for an hour of the day, h, the electricity export is carried out; $NEX_{j,h}^{z}$ is the value of the net position of electricity exchange for the ith connection, through which from zone z for an hour of the day, h, electricity import is carried out.

The value of the net position $NP_{z,h}$ in the price zone z is used to adjust the current location of the graph NEC_z relative to the axis of zero balance of import/export. The adjusted NEC of zone z is used in the next cycle of iterative calculations of optimal volumes of electricity exchange at the level of topological graph analysis.

The proposed method for taking into account network constraints when bidding in the DAM is devoid of the shortcomings inherent in the known basic methods of solving the problem set. It does not require the linearization of the supply function and does not impose any constraints on the types of price bids that can be used by the DAM participants. The developed method is a development of DMC for an arbitrary number of coupled price zones and, in contrast with DMC and TMC, uses a unified representation of the structure of electrical connections between coupled markets and allows for analysis for an arbitrary structure of electrical networks taking into account different types of price bids. The practical implementation of the developed method for modeling bids in the DAM allowed to more flexibly take into account the needs of the participants in this electricity market segment and search for aspects of integration of the electricity market of Ukraine into the markets of European countries. The results of such a research were practically used to develop the Ukraine DAM implementation concept, which defines the possibilities of explicit

and implicit consideration of network constraints. In addition, the developed method was used to assess the effectiveness of solutions at different steps of integration of the electricity market of Ukraine into the electricity markets of European countries.

4 Example of Assessing the Feasibility of Integrating a Separate Price Zone of the Ukrainian Power System into the European Electricity Market

The developed model of coupling price areas in the DAM segment is used in researches of various options of integration of the IPS of Ukraine and the national electricity market into the European market associations. Based on the research results, a number of problems have been identified, which should addressed before the beginning of such integration. While Ukraine, in particular the Burshtyn TPP Energy Island, generally has a significant export potential (up to 928 MWh per day), there are time intervals (mostly at night time) when market mechanisms for purchasing/selling electricity will result in importing electricity from European energy systems to the IPS of Ukraine. Therefore, the obligatory precondition for the integration of the Ukrainian electricity market into European market associations should be the coordination of cross-border electricity trade and the research for the steps of such integration, taking into account both technological factors and national interests of Ukraine.

In particular, the results of simulation modeling of the processes of coupling the IPS of Ukraine with the energy systems of Hungary and Romania at the level of the DAM revealed the incompatibility of the structure of supply and demand in the electricity markets. Thus, even if all technological constraints on cross-border electricity exchange are eliminated, price equalization in the DAM segments on the Burshtyn TPP Energy Island (BEI) in the energy systems of neighboring countries is not always carried out. At the same time, significant changes in the volumes of electricity exchange at cross-border electricity crossings (up to 1569 MWh for Hungary and up to 1603 MWh for Romania) in adjacent hours of the day will result in increased risks for maintaining the operational security of the respective energy systems. Therefore, the analysis of projects on modernization of the cross-border electrical crossings of the IPS of Ukraine with Romania, Hungary and other European countries should be carried out not only based on economic criteria, but also taking into account systemic constraints due to the requirements for operational regimes safety maintenance of national energy systems.

For the Ukrainian electricity market, one of the significant negative consequences of the merger with European countries in the DAM segment in the context of the existing infrastructure of the IPS networks of Ukraine is the increase of the BEI regime regulation problems.

Figure 5 shows, by way of example, a comparison of the hourly actual graph of the Energy Island load coverage by the energy units of the Burshtyn TPP for the day of 08/16/2020 with the model of the graph of hourly loading (Burshtyn TPP) in

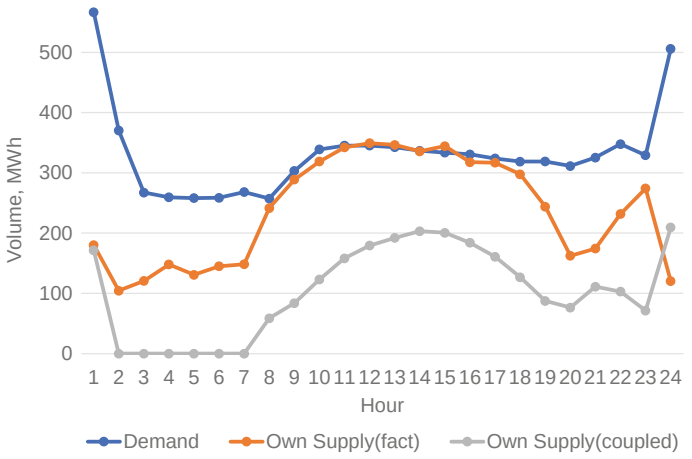

Fig. 5 Demand coverage by the Burshtyn TPP (actual and subject to coupling with ENTSO-E) on 08/16/2020

the conditions of coupling in the DAM segment with the markets of Romania and Hungary. As seen in Fig. 5, in night hours of this day, the production capacities of the Burshtyn TPP are completely replaced by electricity imported from European energy systems.

Similar results were obtained when modeling the processes of coupling the BEI with ENTSO-E on retrospective data on June 23, 2016. Comparative graphs of hourly load of the Burshtyn TPP are shown in Fig. 6.

As can be seen, introducing a liberalized model of the electricity market in Ukraine has not fundamentally changed the ratio between supply and demand at the BEI. This

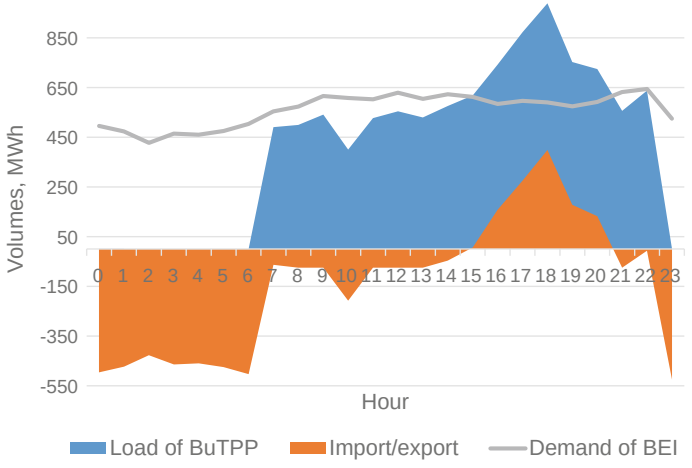

Fig. 6 Load of the Burshtyn TPP (actual and subject to coupling with ENTSO-E) on 06/23/2016

is due to the fact that during night and morning hours the Burshtyn TPP, actually the only electricity producer in the BEI, is not able to compete with a large share of cheaper supply from Romanian and Hungarian electricity producers. It was found that this problem becomes especially relevant in the spring and summer periods. Seasonal decrease in electricity consumption stimulates lower prices in the DAM segments of the European countries. Under these conditions, the Burshtyn TPP generally loses competitiveness compared to power plants that remain under load in the energy systems of neighboring countries. On the contrary, in the day and evening hours of the day, it is economically feasible for the Burshtyn TPP to maximally load production capacities for electricity exporting, especially in the autumn and winter periods. However, in case of implementing such a scenario in most hours of the day for the BEI there will be no reserves of production capacities to regulate the regime.

The Burshtyn TPP is actually a monopoly electricity producer in trade, which leads to a significantly higher market value of electricity during the seasonal decrease in electricity consumption, as shown in Fig. 7.

The researches have shown that the urgency of this problem is not solved by mechanical connection of additional production capacities to the BEI. Thus, the plans of the "'Ukraine EU' Energy Bridge" project provided for the synchronization of the KhNPP power unit No.2 with the BEI. However, according to calculations significant volumes of unregulated generation of the KhNPP No.2 nuclear power unit will almost completely displace a priori the more expensive supply by the Burshtyn TPP. Therefore, the integration of the IPS of Ukraine and its individual components into European electricity markets should be preceded by the introduction of a competitive market of ancillary services, as well as a comprehensive analysis of potential consequences of implementing management decisions on the organization and operation

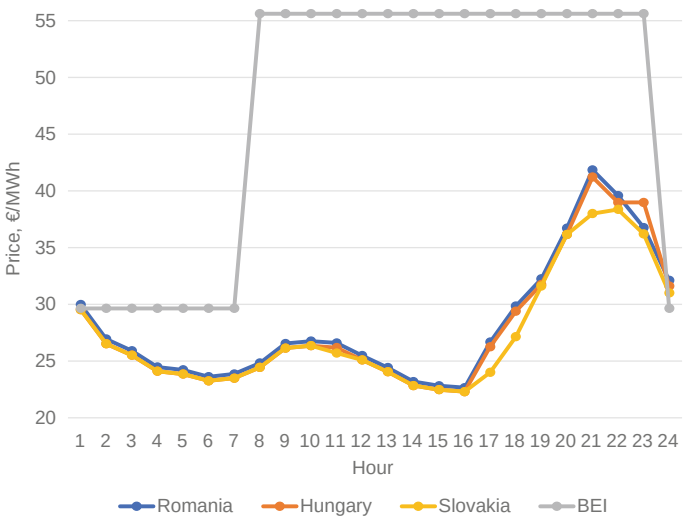

Fig. 7 Hourly marginal prices of the DAM on 08/16/2020

of the DAM segment of Ukraine based on modeling the results of market integration and mutual influence of integrated electricity markets of Ukraine and European countries. Currently, the market of ancillary services in the BEI regulation area is not competitive, as the Burshtyn TPP is the only provider of ancillary services.

An assessment of the export potential of the IPS of Ukraine under the existing technical conditions and taking into account the features of operation of the DAM of Ukraine based on the examples of different options for market coupling of the BEI with the energy systems of Hungary and Romania. In general, sufficient capacity of cross-border electric crossings in case of coupling of the BEI as a separate price zone with the DAM of Hungary and insufficient capacity of such crossings to realize potential of electricity import/export in case of coupling to the DAM of Romania are noted. It is shown that in the future coupling of the BEI to ENTSO-E in the DAM segment will result in importing electricity to the BEI in night hours of the day and in exporting electricity from the BEI in the day hours of the day.

In general, for the calculation period of 1 year, for the BEI a positive balance of electricity import/export is received, as well as expansion of capacities of cross-border electricity crossings, and expansion of the BEI due to connection of the Khmelnytskyi NPP power unit No.2, which will result in increasing annual volumes of electricity export to 7.6 million kWh per year. This confirms the presence of export potential, a sufficient level of competitiveness of the Burshtyn TPP (in general for the year) compared to electricity producers in European countries in the DAM segment, as well as broad prospects for increasing the export potential of the BEI.

An in-depth analysis of the impact of cross-border electricity trade in the DAM of Ukraine (primarily, the BEI) has been performed. To this end, various aspects of the implementation of the pilot project of the "Ukraine—European Union" energy bridge in the DAM segment (Fig. 8) have been analyzed, namely: (1) coupling of the DAM of the Burshtyn Energy Island, Hungary and Romania taking into account the current constraints on electricity flows between these energy systems; (2) coupling of the DAM of the Burshtyn Energy Island, Hungary and Romania without taking into account constraints on electricity flows between these energy systems; (3) coupling of the DAM of the Burshtyn Energy Island, Khmelnytskyi NPP power unit No.2, Hungary and Romania, taking into account the current constraints on electricity flows between these energy systems; (4) coupling of the DAM of the Burshtyn Energy Island, Khmelnytskyi NPP power unit No.2, Hungary and Romania without taking into account constraints on electricity flows between these energy systems.

It is revealed that the modernization of cross-border electric crossings of the BEI for full implementation of electricity import/export does not lead to a significant increase in the cost of electricity for the consumer. The maximum increase in the cost of electricity for the BEI to 3.78% was recorded when modeling bids in the warm season, during which electricity import volumes increase. Expansion of the BEI's production potential by the Khmelnytskyi NPP power unit No.2 will lead to a significant reduction in the cost of electricity for consumers.

With the full implementation of the BEI's export potential, the annual cost of electricity will decrease by 15.1%. Thus, in general, the implementation of the "'Ukraine-EU' energy bridge" project will lead to positive consequences for the BEI consumers.

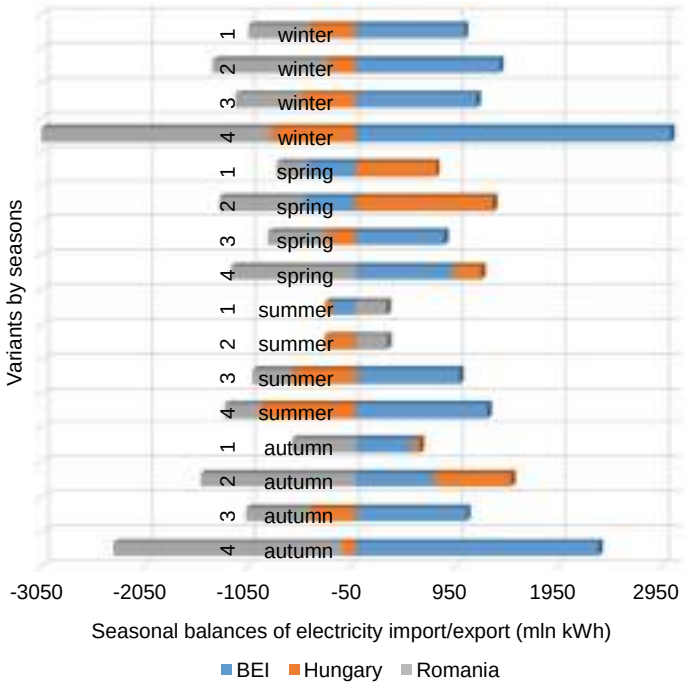

Fig. 8 Comparative diagrams of import/export of electricity under different conditions

On the other hand, the problem of lack of production capacities to regulate the BEI regime is noted. Indeed, for a significant period of the day (Fig. 5), the BuTPP power units will be outside the zone of readiness for providing the system operator with services for frequency regulation and active power. Similarly, with different options for integration of the BEI with EU markets in different seasons of the year, an insufficient level of loading of the BuTPP power units for the state of readiness for providing ancillary services (Fig. 9). Based on the technical requirements of ENTSO-E for the minimum level of reserves with Secondary Frequency Control (SFC) in the energy system, for the Burshtyn Energy Island for different calculation periods of time it is necessary to provide for reserves of production capacities with SFC in volumes of 19 to 39 MW. Therefore, the required minimum level of guaranteed load of the Burshtyn TPP for different calculation periods of the year should be 144 to 281 MW.

Based on the results of these and other researches, it was concluded that the introduction of a competitive market of ancillary services should be a mandatory component of the processes of integration of Ukrainian energy systems with ENTSO-E.

Figure 9 shows that for the BuTPP as a participant in the electricity market the most cost-effective option is to increase the capacity of cross-border electrical crossings without changes in the supply/demand structure. The expansion of the Burshtyn Energy Island by the Khmelnytskyi NPP power unit No.2 will result in significant

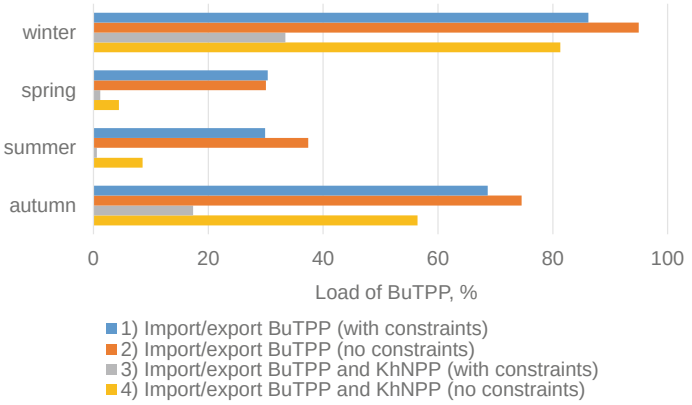

Fig. 9 Levels of loading of the BuTPP power units according to different options of coupling the BEI with EU countries in the DAM

displacing the production capacities of the BuTPP from the local electricity market, even if the capacity of cross-border electric crossings is increased. The analysis of the options for coupling the BEI with the energy systems of Hungary and Romania showed the potential benefits for these countries from expanding the economic possibilities to use the additional route of electricity export from Romania to Hungary through the BEI in the DAM segment and the possibility of Hungarian and Romanian electricity markets to export electricity to the BEI in night hours of the day.

5 Conclusions

The chapter provides an alternative method of addressing tasks of taking into account technological limitations in the organization of cross-border electricity trade. The provided method, in contrast to that used in European electricity markets, allows to accurately take into account the structure of production capacities. In contrast to existing methods, this method requires no linearization of the supply function, imposes no constraints on the types of price bids submitted that can be used and is based on a unified representation of the structure of electrical connections between coupled markets, which allows for analysis of electrical networks of an arbitrary structure.

The application of the provided method based on retrospective data allowed to identify technological hindrances to the integration of the IPS of Ukraine into European electricity markets in terms of ensuring the operational security of modes of the IPS of Ukraine. The actual implementation of plans to integrate the Ukrainian electricity market into European cross-border market associations should be preceded by increased competition in the market of ancillary services, primarily in terms of increasing the number of providers of such services for the secured provision

of resources of the regime regulation in the regimes of both minimum and peak electricity consumption.

References

1. Butkevich, O.F., Yuneeva, N.T., Gureeva, T.M.: On the issue of placement of energy storage in the Ukrainian UES. Techn. Electrodyn. **6**, 59–64. (2019). (Ukr). https://doi.org/10.15407/techned2019.06.059
2. Kyrylenko, O., Pavlovsky, V., Steliuk, A., Vyshnevskyi, M.: Simulation of the normal and emergency operation of interconnected power system of Ukraine for frequency stability study. Techn. Electrodyn. **2**, 57–60. (2017). (Ukr). https://doi.org/10.15407/techned2017.02.057
3. Pavlovsky, V., Steliuk, A., Lenga, O., Zaychenko, V., Vyshnevskyi, M.: Frequency stability simulation considering under-frequency load shedding relays, special protection automatics and AGC software models. In: Proceedings of IEEE Power Tech Conference, Manchester **2017**,(2017). https://doi.org/10.1109/PTC.2017.7981043
4. Popov, O., Iatsyshyn, A., Kovach, V., Artemchuk, V., Taraduda, D., Sobyna, V., Sokolov, D., Dement, M., Yatsyshyn, T., Matvieieva, I.: Analysis of possible causes of NPP emergencies to minimize risk of their occurrence. Nucl. Radiation Safety **1**(81), 75–80 (2019) https://doi.org/10.32918/nrs.2019.1(81).13
5. Blinov, I.V., Zaitsev, I.O., Kuchanskyy V.V.: Problems, Methods and Means of Monitoring Power Losses in Overhead Transmission lines. Part of the Studies in Systems, Decision and Control Book Series (SSDC, volume 298), pp. 123–136. Springer (2020). https://doi.org/1007/978-3-030-48583-2_8
6. Kuchanskyy, V., Malakhatka, D., Blinov, I: Application of reactive power compensation devices for increasing efficiency of bulk electrical power systems. In: 2020 IEEE 7th International Conference on Energy Smart Systems (ESS), pp. 83–86. Kyiv, Ukraine (2020). https://doi.org/10.1109/ESS50319.2020.9160072.
7. Kuchanskyy, V., Zaitsev, I.O.: Corona discharge power losses measurement systems in extra high voltage transmissions lines. In: 2020 IEEE 7th International Conference on Energy Smart Systems (ESS), Kyiv, Ukraine, pp. 48–53 (2020). https://doi.org/10.1109/ESS50319.2020.9160088.
8. Kulyk, M., Zgurovets, O.: Modeling of power systems with wind, solar power plants and energy storage. Part of the Studies in Systems, Decision and Control book series (SSDC, volume 298), pp. 231–245. Springer, Cham (2020). https://doi.org/10.1007/978-3-030-48583-2_15
9. Pavlovskyi, V.V., Steliuk, A.O., Lukianenko, L.M., Lenga, O.V.: Analysis of the frequency change in IPS of Ukraine in case of the generating unit disconnection of the nuclear power plant. Tech Electrodynam. **4**, 89–94 (2018) https://doi.org/10.15407/techned2018.04.089
10. Blinov, I., Tankevych, S.: The harmonized role model of electricity market in Ukraine. In: 2016 2nd International Conference on Intelligent Energy and Power Systems, IEPS 2016 Conference Proceedings (2016). https://doi.org/10.1109/IEPS.2016.7521861
11. Blinov, I.V., Parus, Y.V., Ivanov, H.A.: Imitationmodeling of the balancing electricity market functioning taking into accountsystem constraints on the parametersof the IPS of Ukraine mode. Tech. Electrodynam. **6**, 72–79 (Ukr). (2017). https://doi.org/10.15407/techned2017.06.072
12. On Electricyty Market: The Law of Ukraine (2017) 13.04.2017 No 2019-VIII.
13. Ivanov, H., Blinov, I., Parus, Ye.: Simulation model of new electricity market in Ukraine. In: 2019 IEEE 6th International Conference on Energy Smart Systems (ESS), pp. 339–342 (2019) https://doi.org/10.1109/ESS.2019.8764184
14. Lin, J., Magnago, F.: Electricity markets: theories and applications. IEEE Press Ser. Power. 352 (2017)
15. Momoh, J., Mili, L.: Economic market design and planning for electric power systems. Int Electr Electron Eng. 277 (2009). https://doi.org/10.1002/9780470529164

16. Kyrylenko, O.V., Blinov, I.V., Parus, E.V., Ivanov, G.A.: Simulation model of the day-ahead electricity market with implicit consideration of power systems network constraints. Tekhnichna Elektrodynamika. **5**, 60–67. (Ukr) (2019). https://doi.org/10.15407/techned2019.05.060
17. Blinov, I.V., Parus, E.V.: Congestion management and minimization of price difference between coupled electricity markets. Techn. Electrodyn. **4**, 81–88. (2015). (Ukr)
18. Saukh, S., Borysenko, A.: Representation of transmission and distribution networks in the mathematical model of the electricity market equilibrium. In: 2019 IEEE 20th International Conference on Computational Problems of Electrical Engineering (CPEE) (2019). https://doi.org/10.1109/CPEE47179.2019.8949116
19. Blinov, I., Parus, E.: Approach of reactive power pricing for ancillary service of voltage control in Ukraine. Intelligent Energy and Power Systems (IEPS). In: 2014 IEEE International Conference on, pp. 145–148 (2014). https://doi.org/10.1109/IEPS.2014.6874167
20. Ivanov, H.A., Blinov, I.V., Parus, E.V., Miroshnyk, V.O.: Components of model for analysis of influence of renewables on the electricity market price in Ukraine. Techn. Electrodyn. **4**, 72–75. (2020). https://doi.org/10.15407/techned2020.04.072
21. Lezhniuk, P., Kravchuk, S., Netrebskiy, V., Komar, V., Lesko, V.: Forecasting hourly photovoltaic generation on day ahead, In: 2019 IEEE 6th International Conference on Energy Smart Systems (ESS). (2019). https://doi.org/10.1109/ESS.2019.8764245
22. Blinov, I.V.: New approach to congestion management for decentralized market coupling using net export curves. CIGRE Session **46** (2016)
23. Kumar, A., Srivastava, S.C., Singh, S.N.: Congestion management in competitive power market: a bibliographical survey. Elect. Power Syst. Res. **76**(1–3), 153–164 (2005)
24. Moulin, H.: Fair division and Collective Welfare. Cambridge, Massachusetts: MIT Press **2004**, 295 (2004). https://doi.org/10.7551/mitpress/2954.001.0001
25. Klemperer, P.: Auctions: Theory and Practice. Princeton University Press, p 246 (2004)
26. Tierney, S., Schatzki, T., Mukerji, R.: Uniform-pricing versus Pay-as-bid in Wholesale Electricity Markets. Analysis Group and ISO New York, p 24 (2008)
27. EuroPEX Position Paper on Cross-Border Congestion Management and Market Coupling. 6th of October (2006)
28. Basagoiti, P., Gonzalez, J.J., Alvarez, M.: An algorithm for the decentralized market coupling problem. Electricity Market. 2008. EEM 2008. In: 5th International Conference on European. Lisboa, Portugal. 28–30 May (2008). https://doi.org/10.1109/EEM.2008.4579046
29. Basagoiti, P., Gonzalez, J.J., Alvarez, M.: An algorithm for the decentralized market coupling problem. Electricity Market. EEM 2008. In: 5th International Conference on European (2008)
30. Sleisz, A., Sörés, P., Raisz, D.: Algorithmic properties of the all-european day-ahead electricity market. In: 11h International Conference on the European Energy Market (EEM14). Krakow. Poland. May 2014 (2014). https://doi.org/10.1109/EEM.2014.6861275
31. László, V.: Regional market integration. Why and how. Magyar Energia Hivatal, p. 22 (2006)
32. Bjorndal, M., Jornsten, K.: Zonal pricing in a deregulated electricity market. Energ. J. **2001**, 51–73 (2001)
33. Bjorndal, M., Jornsten, K., Pignon, V.: Congestion management in the Nordic power market—counter purchases and zonal pricing. J. Netw. Ind. **2003**(3), 271–292 (2003)
34. Commission Regulation (EU) 2016/1719 of 26 September 2016 establishing a guideline on forward capacity allocation. Offic. J. Eur. Union **259**, 42–68 (2016)
35. Commission Regulation (EU) 2015/1222 of 24 July 2015 establishing a guideline on capacity allocation and congestion management. Offic. J. Eur. Union, **58**, 24–72 (2015)
36. ENTSO-E Capacity Allocation and Nomination System (ECAN): Implementation Guide. ENTSO-E. 2011. Version 6.0, p. 235 (2011)
37. EUPHEMIA Public Description Single Price Coupling Algorithm. NEMO Committee, p. 55 (2019)
38. Trilateral market coupling algorithm: Powernext, APX. March 2006, p. 25 (2006)
39. Elspot Market Regulations: Nord Pool Spot Physical Market. Nord Pool Spot AS, Version, p. 1. 7 (2001)

40. Using Implicit Auctions to Manage Cross-Border Congestion: Decentralised Market Coupling: Paper by EuroPEX, Tenth Meeting of the European Electricity Regulatory Forum, 8 July 2003.CWE Enhanced Flow-Based MC feasibility report. (2011) CWE Steering Committee, p. 99 (2003)
41. CWE Enhanced Flow-Based MC intuitiveness report: CWE Steering Committee, p. 62 (2012)
42. Rezinkina, M.M., Sokol, Y.I., Zaporozhets, A.O., Gryb, O.G., Karpaliuk, I.T., Shvets, S.V.: Monitoring of energy objects parameters with using UAVs. In: Sokol, Y.I., Zaporozhets, A.O. (eds) Control of Overhead Power Lines with Unmanned Aerial Vehicles (UAVs). Studies in Systems, Decision and Control, vol. 359. Springer, Cham. (2021). https://doi.org/10.1007/978-3-030-69752-5_1

Improving the Reliability and Power Quality in Distribution Networks with Sources of Dispersed Generation

Andrii Zharkin, Volodymyr Novskyi, Volodymyr Popov, and Serhii Palachov

Abstract Methods for solving the problem of selecting optimal switch-off locations in electrical distribution networks and implementing its results are considered. It is shown that in modern electrical distribution systems, in the context of the widespread use of dispersed sources of energy generation and its storage, the traditional approach to solving this problem loses its effectiveness. As an alternative can be the use of remote-controlled switching devices, what is reasonable in the case of cyclic and rather prolonged changes in the load as well as output power of dispersed energy sources, when energy storage devices are turned on or off. New technological solutions are proposed that make it possible to effectively reduce electric energy losses in distribution networks with local sources of energy generation and storage due to the possibility of dynamic management of the network configuration. The expediency of implementing a strategy for rational use of remote-controlled switching devices are substantiated, taking into account their switching resource, and an algorithm for their operation is developed. It is shown that now the universal solution is the use of power electronics devices, which makes it possible to form the so-called "soft points" of opening the distribution network circuits when controlling active and reactive power flows to ensure a minimum of electrical energy losses due to rapid response to changes in electrical load and/or modes of energy generation and storage in the presence of dispersed sources of electricity generation and storage facilities. For the introduction of new technical means on the way to implementing even individual components of the concept of "Smart Grid", an appropriate methodology for

A. Zharkin (✉) · V. Novskyi · S. Palachov
Institute of Electrodynamics of NAS of Ukraine, Kyiv, Ukraine
e-mail: zhark@ied.org.ua

V. Novskyi
e-mail: novsky@ied.org.ua

S. Palachov
e-mail: palp@ukr.net

V. Popov
National Technical University of Ukraine "Igor Sikorsky Kyiv Polytechnic Institute", Kyiv, Ukraine
e-mail: tig@ukr.net

O. Kyrylenko et al. (eds.), *Power Systems Research and Operation*, Studies in Systems, Decision and Control 388, https://doi.org/10.1007/978-3-030-82926-1_2

economic justification of such decisions has been developed, which allows one to objectively take into account the positive consequences of their implementation, at least from the point of view of improving the reliability and efficiency of power supply, reducing voltage deviations, etc.

Keywords Dispersed generation · Electrical energy losses · Remote-controlled switching devices · Soft open points · Power electronics

1 Introduction

Reconfiguration of distribution electrical networks is the most common method of multifunctional control of their modes. If earlier this problem was solved mainly in order to minimize power losses, then in the future, understanding the influence of the network topology on system reliability and voltage quality, various indicators that characterize the reliability of power supply and the level of voltage deviations also began to be considered as an objective functions. In the future, a fairly independent area of research has become comprehensive solution of this optimization problem, additionally taking into account the indicators of the operating modes of electrical networks of adjacent voltage levels.

It should be noted that in recent years there has been a constant tightening of requirements for the reliability of power supply and the quality of electric energy supplied to consumers. At the same time, it is necessary to take into account the fact that the owners (operators) of dispersed generation sources and electric networks are different commercial structures, whose interests often do not coincide. Power companies are interested in connecting dispersed generation sources to electric networks at a higher rated voltage in order to reduce their impact on power quality characteristics, primarily on the voltage deviations.

In such conditions, the problem of choosing the optimal distribution network configuration becomes significantly more complicated and it cannot be effectively solved within the old formulation, without focusing on new technical means and outside the context of other issues related to the development and management of modes, in particular, by the choice of conditions for the voltage regulation and reactive power compensation equipment, coordination of relay protection devices, implementation of measures to ensure the reliability of power supply without a comprehensive assessment of the final effect.

In the implementation of projects using dispersed generation, the problem of ensuring the optimal level of reliability of power supply, in the opinion of the authors, are the most complex and debatable. The difficulties that arise here are caused by a number of factors, and the possible ways to solve this problem largely depend on the legislative and regulatory framework as well as technical factors.

First of all, it is necessary to take into account the possible “legalized” conditions for the operation of electric networks with dispersed generators, in particular, the

admissibility or inadmissibility of "islanding" operation; the nomenclature of parameters for the reliability assessment, determined by the relevant regulatory documents; the availability and methods of monitoring the level of power supply reliability; the technical level of facilities in electrical networks (primarily automatic switching devices, and protection and automation equipment) and other.

2 The Main Ways to Improve the Reliability of Power Supply in Distribution Networks with Dispersed Generators

In the world practice, there is no generally accepted common approach to modeling reliability indicators and justifying the choice of optimal measures to improve it, even in traditional electric networks, not to mention distribution systems with dispersed power sources. The expediency of taking into account the reliability factor when choosing the optimal option for using the dispersed generators (DG) or for assessing the consequences of such decisions is obvious.

If the "island" operation of the network is unacceptable and it is not possible to operate the DG in post fault modes on a localized load, then this generation source practically does not affect the reliability of the power supply. This is due to the fact that in the event of any damage to the network, the main source of centralized power supply and the DG source will be turned off almost simultaneously by the appropriate means of relay protection and automation and can be connected to the network only after the complete elimination of the fault.

Of much greater practical interest is the option when power grid provides for the possibility of operating the DG sources on a localized load. Two situations need to be considered here. So, let's consider the first case when there is no regulation of power supply reliability. Then the implementation of the DG will be associated only with the need to place the appropriate switching and protective devices in the network (practically always automatic), which will allow in the case of a network failure to separate a localized load – a group of sections and load nodes of the network, that will continue to receive stable power from the DG source in the post-fault mode.

It is obvious that for various scenarios of the DG implementation, significantly different investments may be required, for example, related to the need to purchase new switching equipment, its installation, modernization of relay protection and automation equipment, as well as the implementation of other necessary technical and organizational measures. It is logical to assume that the effects in changes in certain reliability indicators may also differ. Then, to evaluate and compare different options for the implementation of the DG, it is proposed to use an indicator that reflects the degree of improvement in the reliability characteristics per unit of investments associated with the acquisition and installation of DG sources (with different technical characteristics of the equipment), as well as with the technical support for their integration into electrical networks.

Currently, in most industrialized countries the authorized regulatory authorities set limits for certain indicators of the electricity supply reliability and fairly strict control over their compliance is carried out. In this case, regardless of the places and conditions of integration of distributed generation facilities in electric networks, the same level of reliability must be provided.

However, to achieve this result, different investments may be required. Therefore, in this case, the effectiveness of the various options for the use of the DG in terms of the reliability of the power supply can be estimated based on the amount of investment required for the implementation of a particular project.

At the same time, it should be taken into account that in order to achieve the maximum effect in solving the above issues, careful coordination of the projects for the placement and selection of the parameters of the DG sources is required, taking into account the development of electrical networks and their equipment with modern switching and protective devices (sectioning devices). The fulfillment of these conditions allows in many cases to significantly reduce the costs associated with the implementation of technical conditions for connecting generating sources to electric distribution networks (DN) that imposed by energy supply companies, and with ensuring the reliability of electricity supply in the conditions of rationing of its characteristic.

Thus, before proceeding to the solution of the problem of assessing the reliability of various options for integrating DG into centralized distribution systems, it is necessary to consider such issues as the definition of the nomenclature of integral reliability indicators, possible approaches to their modeling, methods for optimizing reliability in the conditions of the use of DG, and the quantitative assessment of the required investments.

In this book, it is proposed to use integral indicators for assessing reliability, which are based on the IEEE standards [1]: SAIFI (System Average Interruption Frequency Index) – a system index of number of interruptions in power supply per year, SAIDI (System Average Interruption Duration Index) – a system index of average duration of interruption in the power supply indicated in hours per year, EENS (Expected Energy Not Served) - a index indicated in kW•hour per year, ASIDI (Average System Interruption Duration Index) – a index indicated in hours per year, ASIFI (Average System Interruption Frequency Index) – a index indicated in of number of interruptions in power supply per year.

In the technical literature, several approaches to modeling (quantifying) integral reliability indexes, in particular the expected amount of energy unserved, are proposed. At the same time, it should be taken into account that according to statistical data in the electric power industry of any country, in terms of reliability, the most vulnerable part are the distribution systems [2]. The main number of failures in these systems falls on the DN, primarily on overhead lines with a voltage of 6–20 kV. Therefore, in the practice of analyzing the reliability of DS, these elements that are the main object of research.

From the methodological point of view and from the point of view of clarity, it is convenient to use structural-logical matrixes to evaluate integral reliability indexes [3]. However, from the standpoint of the effectiveness of formalization and practical

implementation of this procedure, it is more appropriate to focus on the following approach. As an example of its application, let us consider the definition of such an integral index of reliability as the expected amount of the energy not served. In general, this index is calculated by the formula.

$$EENS = \sum_{m=1}^{M} z_{0m} K_m r_b P, \tag{1}$$

where z_{0m}—specific fault rate of the m-th element of the system; K_m—the number of elements of the m-th type in the system; r_b—the average time of restoration of power supply; P—the average value of the load that is disconnected due to fault; M—the total nomenclature of elements in the system.

The main difficulty in analyzing reliability is due to the need to calculate the index (1) for a certain structure (substation, distribution line, load node, etc.), taking into account the topology of the electrical network, its parameters, the type and location of switching and protective devices. For this purpose, the average recovery time for power supply is usually differentiated as follows [3]:

- r_l—the time from the moment of receiving information about the damage in the network to its localization;
- r_i—the time from the moment of receiving a signal about the damage to the moment of re-commutations in the network associated with the partial restoration of power supply;
- r_p—the time from the moment of receiving information about the damage to the complete restoration of power supply, including the time required to repair or replace the damaged element.

For example, in the distribution medium-voltage overhead line (Fig. 1) are

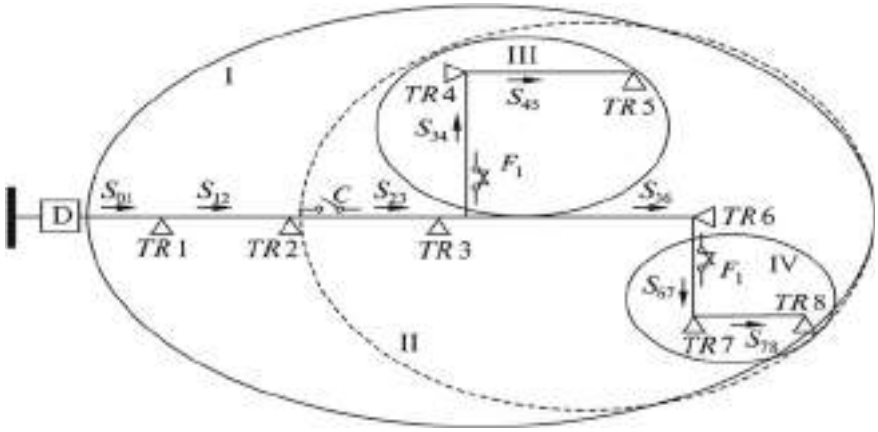

Fig. 1 Overhead distribution line with switching devices

Table 1 Operation areas of protective and switching devices

Sector	Facilities	Area	Load P, kW	Coverage area	Active area
0—1	D	I—IV	P_{01}	$\ell_{01} + \ell_{12}+\ell_{23} + \ell_{34}+$ $+\ell_{45} + \ell_{36}+\ell_{67} + \ell_{78}$	$\ell_{01} + \ell_{12}$
1—2		I—IV	P_{12}		
2—3	C	II—IV	P_{23}	$\ell_{23} + \ell_{34}+\ell_{45} + \ell_{36}+$ $+\ell_{67} + \ell_{78}$	$\ell_{23} + \ell_{36}$
3—4	F	III	P_{34}	$\ell_{34} + \ell_{45}$	$\ell_{34} + \ell_{45}$
4—5		III	P_{45}		
3—6		V	P_{36}		
6—7	F	IV	P_{67}	$\ell_{67} + \ell_{78}$	$\ell_{67} + \ell_{78}$
7—8		IV	P_{78}		

installed: power transformers TR for power supply of consumers, circuit breaker D, fuse switch disconnector F, disconnector C. The essence of the proposed algorithm is to allocate the protection zones (solid line) and the zones of switching devices (dotted line) for all protective and switching devices installed in the line (Table 1).

In this example, the expected amount of underutilized electricity is determined by three components. The first component depends on the active zone of the circuit breaker installed at the substation, and, accordingly, the relay protection devices placed there:

$$\mathrm{EENS}_1 = z_0 P_{01} \ell_{Da} r_\mathrm{p},$$

where z_0 is the specific frequency of damage to the line as a whole; P_{01} is the total load of the line; ℓ_{Da}—the active area of the circuit breaker (relay protection); r_p – the total time of restoration of power supply.

The second component is determined by the active zones of fuse switch disconnector:

$$\mathrm{EENS}_2 = \sum_{i=1}^{m} z_0 P_{Fi} \ell_{Fai} r_\mathrm{p},$$

where m—the number of devices of this type installed in the line; P_{Fi}—the load power of the section where the i-th switching device of this type is installed; ℓ_{Fai}—the active zone of the i-th fuse switch disconnector; r_p—the total time for restoring power supply.

The third component of the total value of the not-supplied electricity is determined by the active zones of the disconnectors:

$$EENS_3 = \sum_{j=1}^{q} z_0 \ell_{Caj}\left[P_{Cj}\left(r_p - r_i\right) + P_{01} r_p\right],$$

where q—number of disconnectors installed in the line; P_{Cj}—load power of the section where the j-th disconnector is installed; ℓ_{Caj}—active area of the j-th disconnector; P_{01}—total line load power; r_i—the time to restore the power supply, determined by the actions associated with the detection and localization of fault, as well as operation of the disconnector switching.

Thus, the total expected amount of not delivered electricity for the distribution line shown in Fig. 1 can be calculated using the formula:

$$\begin{aligned} EENS = z_0\big[&P_\Sigma(\ell_{01} + \ell_{12}) r_p + P_{34}(\ell_{34} + \ell_{45}) r_p + P_{67}(\ell_{67} + \ell_{78}) r_p + \\ &+ P_{23}(\ell_{23} + \ell_{36})\left(r_p - r_i\right) P_\Sigma(\ell_{23} + \ell_{36}) r_i\big]. \end{aligned} \tag{2}$$

This method of evaluating the integral reliability indicator can also be used to analyze the reliability of a DN with integrated DG by allocating the corresponding active zone, determined by the amount of load that can be powered by these sources during the isolated operation of the selected network fragment (Fig. 1).

In particular, for such a scheme of the electric network, assuming that, if necessary, the power of the DG source is sufficient to provide electricity to all consumers of nodes TR6, TR7 and TR8, the expected amount of not delivered electricity can be calculated by the formula

$$\begin{aligned} EENS = z_0\big[&(P_\Sigma - P_{36})(\ell_{01} + \ell_{12}) r_p + P_{34}(\ell_{34} + \ell_{45}) r_p + P_{67}(\ell_{67} + \ell_{78}) r_p + \\ &+ P_{23}\ell_{23}\left(r_p - r_i\right) + P_\Sigma \ell_{23} r_i + (P_{23} - P_{36})\ell_{23} r_p + P_{23}\ell_{23} r_i + P_{36}\ell_{36} r_p\big]. \end{aligned} \tag{3}$$

Comparing expressions (2) and (3), it is possible to estimate, due to what and in which extent the level of reliability of power supply changes when the corresponding local power sources appear in the network.

It is obvious that, regardless of the availability of DG, the composition and placement of switching devices in overhead lines significantly affect the reliability of power supply. Therefore, the problem of optimal sectioning of electrical networks, associated with the reasonable choice and placement of switching devices of a certain type, is the key to solving the problem of providing a normalized level of reliability. For this purpose, the algorithm based on the method of normalized functions, which was proposed for the analysis of a wide class of discrete problems, was successfully used. A number of studies have shown that this iterative algorithm provides a quasi-optimal solution obtained with a very limited number of steps. Consequently, it is devoid of the disadvantages that inherent in exact methods of discrete optimization [4].

The main essence of the algorithm, which is iterative in nature, is that the following operations are performed at each iteration.

1. Switching devices in turn are placed on each of the network sections from a pre-defined discrete sequence, formed starting from the simplest, and therefore the cheapest device. If a switching device was already installed on some of the sections in the previous iteration, then it is replaced with a more efficient one.
2. For each of the obtained options of equipping the electric line with sectioning devices, considering the objective function and corresponding restrictions, the appropriate integral reliability indexes are calculated. In particular, we have:

$$\begin{aligned} SAIDI^L\left(x_n^k\right) &= \frac{\sum Rdt_j^L\left(x_n^k\right)NP_j}{\sum NP_j}, SAIFI^L\left(x_n^k\right) = \frac{\sum Tf_j^L\left(x_n^k\right)NP_j}{\sum NP_j}, \\ ASIDI^L\left(x_n^k\right) &= \frac{\sum Rdt_j^L\left(x_n^k\right)P_j}{\sum P_j}, ASIFI^L\left(x_n^k\right) = \frac{\sum Tf_j^L\left(x_n^k\right)P_j}{\sum P_j}, \end{aligned} \tag{4}$$

where $Rdt_i^L\left(x_n^k\right)$—the average duration, $Tf_i^L\left(x_n^k\right)$—the average frequency of disconnections when installing an n-type sectioning device at the k-th location of the line (x_n^k); NPj—the number of electricity consumption metering points linked to the load node j; Pj—the average load of the node j (kW).

3. Under the conditions of setting the reliability indicators, for each controlled integral reliability criterion, its so-called relative significance index is calculated as follows:

$$S_i^L = \frac{R_i^{L-1}(x) - R_i^T}{R_i^T}, \tag{5}$$

when R_i^T—the target value of the i-th index; $R_i^{L-1}(\mathbf{x})$ — the value of this index obtained in the previous $(L-1)$-th iteration. In this case, if $S_i^L < 0$ or $0 < S_i^L \le \varepsilon$, where ε — the user-defined degree of approximation to R_i^T, then we accept $S_i^L = 0$. If $\sum\limits_j S_j^L = 0$ it is assumed that the problem is solved and further calculations are stopped. Otherwise, the weight coefficient of the i-th criterion on the L-th iteration is defined as

$$w_i^L = \frac{S_i^L}{\sum\limits_j S_j^L}. \tag{6}$$

With this approach, the index whose value (in normalized form) is further from its target value at the current iteration gains more weight. If there are no norms for reliability indexes, then the corresponding weight coefficients are assumed to be equal to each other or must be determined experimentally, provided that their sum is equal to one.

4. Calculate a normalized generalized index of improving reliability, for example

$$\Delta NRI^{L}\left(x_n^k\right) = w_{\text{SAIDI}}\frac{\text{SAIDI}^{L-1} - \text{SAIDI}^{L}\left(x_n^k\right)}{\text{SAIDI}^{L-1}} + \\ + w_{\text{SAIFI}}\frac{\text{SAIFI}^{L-1} - \text{SAIFI}^{L}\left(x_n^k\right)}{\text{SAIFI}^{L-1}} + w_{\text{EENS}}\frac{\text{EENS}^{L-1} - \text{EENS}^{L}\left(x_n^k\right)}{\text{EENS}^{L-1}}, \tag{7}$$

or

$$\Delta NRI^{L}\left(x_n^k\right) = w_{ASIDI}\frac{\text{ASIDI}^{L-1} - \text{ASIDI}^{L}\left(x_n^k\right)}{\text{ASIDI}^{L-1}} + \\ + w_{\text{SAIFI}}\frac{\text{ASIFI}^{L-1} - \text{ASIFI}^{L}\left(x_n^k\right)}{\text{ASIFI}^{L-1}} + w_{\text{EENS}}\frac{\text{EENS}^{L-1} - \text{EENS}^{L}\left(x_n^k\right)}{\text{EENS}^{L-1}}, \tag{8}$$

depending for which reliability indexes the limit values are set. At the same time, at the first iteration, the values of the integral indexes SAIDI^{L-1}, SAIFI^{L-1}, ASIDI^{L-1} are determined for the case when there are no switching devices in the line under consideration.

5. Calculate the characteristic $\frac{\Delta NRI^{L}\left(x_n^k\right)}{\Delta C\left(x_n^k\right)}$, where $\Delta C^{L}(x_n^k)$ —is the relative increment of the cost of improving reliability after installing x_n^k sectioning device in the line. It is found like this:
6. if a new sectioning device is to be installed, then

$$\Delta C^{L}(x_n^k) = C(x_n)/C_{MIN};$$

7. if they are considering replacing the (n – 1)-type sectioning device with the nearest more efficient and expensive n-type device from a initially given sequence, then

$$\Delta C^{L}(x_n^k) = (C(x_n) - C(x_{n-1}))/C_{MIN}.$$

In the above expressions C(xn–1), C(xn), CMIN – respectively, the cost of sectioning devices of the n–1, n-th type and the cheapest of all the sectioning devices included in the discrete sequence that are planned for use.

8. The optimal option for placing sectioning devices in the line at this iteration is determined in accordance with the condition

$$\frac{\Delta NRI^{L}\left(x_n^k\right)}{\Delta C\left(x_n^k\right)} \rightarrow \max.$$

In addition, it is obvious that when using the DG and the possibility of organizing the power supply of the localized load by this source in post-fault modes, the corresponding switching devices must be placed in strictly defined places, depending both on the power of the generating source and the loads in the network nodes [5].

At the same time, it is necessary to solve the problem of the necessary degree of interconnection when making decisions about the composition and placement of

switching devices on the basis of optimal sectioning of the electrical network and providing the power supply of a localized load in the presence of DG and setting norms for reliability indexes.

The results of the relevant studies are presented in [6]. Here was considered 10 kV overhead line with the branches, for which the normalized level of reliability was defined as a requirement to reduce the value of the expected amount of not delivered electricity by at least 35% compared to the initial value for the same line in the absence of sectioning devices.

To solve the problem, the above algorithm for optimal sectioning was used. The necessary result was obtained by placing in the line two reclosers—automatic sectioning devices.

Then the DG was connected to the different points of this line. Along with this, it was determinated a localized load that could be powered from this source in the post-fault modes by using existing or additional automatic switching devices. We also tried to minimize the costs associated with the formation of a dedicated load while observing the normalized limits of power supply reliability indexes.

When solving this problem, a number of assumptions were made. Thus, when evaluating reliability indexes, only stable damages were taken into account, assuming that unstable ones would be eliminated by an automatic re-activation device of reclosers or of line switch; at the same time only automatic devices were considered as sectioning devices (reclosers and sectionalizers—automatic disconnector); it was considered that the specified switching equipment is configured for coordinated operation. Fs a result, in the case of line fault, power supply of the localized load will be provided automatically.

In the process of economic evaluation of various options, the costs of recloser installing, its transfer to another location, as well as purchasing and installing the sectionalizer were determined as a percentage of the cost of the recloser itself.

Based on the results of the research, the following conclusions can be drawn.

In most cases, to achieve the goal, it was enough to transfer one or two reclosers (already available in the line) without the use of additional sectioning devices. In addition, two groups of solutions were identified:

1. After the formation of the localized load, the expected amount of not delivered electricity exceeded the permissible level. Therefore, to meet the required condition, it is necessary to install additional sectioning devices in the network—one or two sectionalizers, and in some cases-an additional recloser (if the use of a sectionalizer is impossible).
2. When using the DG, the expected amount of not delivered electricity has become significantly lower (more than 1.5 times) than the required level. Here, the presence of a single recloser in the network was sufficient to form a localized load. Then we can assume that the removal of the second recloser will not lead to an increase in the expected amount of not delivered electricity above the permissible level. This fact was confirmed by experimental calculations.

Thus, the results of the research have shown that, depending on the point of the DG connection, even with a relatively small variation in its power, the costs for implementing the considered project can differ more than twice.

It follows from the above that in case of reliability indexes normalization, the availability of DG requires a strictly coordinated solution for sectioning the DN and forming a localized load in order to reduce cost. In this regard, the algorithm described above for optimal sectioning of the distribution networks under the conditions of the presence of the DG requires modification, which consists in the following.

Initially, switching devices are placed in the network, allowing to allocate a load that can be stably powered from the DG source in the post-fault modes. When performing the first point of the optimal sectioning algorithm, these switching devices are considered as fixed and in the future, in the process of optimal sectioning of the network, they are not considered. In addition, when performing calculations in accordance with (6) or (7) at the first iteration, the values of the corresponding integral reliability indexes are determined taking into account the installed switching devices to form a localized load of the DG.

It should be emphasized that in addition to the independent application (optimal sectioning of the distribution network), the proposed algorithm can also be used when comparing alternative options for using DG in terms of their impact on the reliability of power supply or to take into account the reliability factor, for example, when comparing these alternatives in a multi-criteria manner.

Let us consider the problem of determining the optimal amount of investment in the implementation of DG in the case of setting reliability indexes.

In this case, regardless of the places and conditions of integration of the DG in the electrical networks, the required uniform level of reliability must ultimately be achieved. It is necessary to minimize the total costs when choosing protective and switching equipment that ensures the fulfillment of the technical conditions for the possibility of operating the DG on a localized load, by optimal transfer existing sectioning devices and equipping (if necessary) networks with additional switching devices to meet the regulatory requirements for the reliability of power supply.

If we are talking about comparing several alternative variants of the DG applications, then, given that each of them should provide identical reliability indexes, but significantly different costs may be required to achieve this goal, it is the amount of investment required for the implementation of a particular project that can serve as a comparative assessment.

The procedure for solving the problem includes three interrelated submodules:

Submodule A.

Step 1. Set the target values of the integrated reliability indicators SAIDIT, SAIFIT, ASIDIT and ASIFIT, which should be achieved during the optimization process. Based on these indexes, system constraints for optimization problem is formed. In particular, for the conditions of Ukraine (taking into account the national regulations), the restrictions can be given in the form of

$$\begin{cases} SAIDI(x) \le SAIDI^T; \\ ASIDI(x) \le ASIDI^T, \end{cases} \tag{9}$$

where x—the vector that characterizes the composition and location of the sectioning devices and the DG.

Step 2. For each option (V) under consideration, calculate the amount of investment CV(DG) required to meet the technical requirements for integrating the DG source into the DN, taking into account the possibility of power supply for localized load in the post-fault modes. They are defined as the sum of the costs for the purchase and installation of the DG; the purchase and installation of switching and protective devices that are necessary to connect the DG source to the network; the purchase and installation of sectioning devices providing the formation of a localized load; upgrading the relay protection and automation; transferring (if necessary) sectioning devices already installed in the network, etc. In addition, it is necessary to determine the values of the corresponding reliability indexes (for example, SAIDI V(DG) and ASIDI V(DG) after integrating the DG into the DN.

Step 3. Check the system of restrictions (9). If they are met and at the same time in the network there were no sectioning devices before placing the DG, then we can assume that the solution has been obtained. If sectioning devices have already been installed in the network, then proceed to step 4 (Submodule B) regardless of whether the restrictions are met or not. If the restrictions are not met and sectioning devices have not been previously installed in the network, then proceed to step 6 (Submodule C).

Submodule B.

When implementing this block, the goal is to consider the reasonability of transferring to other sections as well as excluding some of the already existing (not related to the source of the DG) switching devices due to appearance of sectioning devices in the network that provide the formation of a localized load of the DG.

Step 4. The modified algorithm for optimal sectioning is implemented in relation to switching devices that already exist in distribution lines, from which the corresponding discrete sequence is formed.

Step 5. Perform a check of the constraint system (9). If the conditions are met, the optimization process is completed. Otherwise, proceed to the next (L + 1) th iteration. If at the end of all iterations the constraints (9) are not met, then proceed to step 6.

Submodule C.

Step 6. In accordance with the above requirements, a discrete sequence of additional sectioning devices is formed, which are supposed to be placed in the network.

Step 7. Implement the optimal sectioning algorithm in relation to the switching devices accepted for consideration.

Step 8. Check the system of constraints (9). If the conditions are met, the optimization process is completed and the transition to step 9 is performed. Otherwise, the transition to the next (L + 1)-th iteration is performed.

If the ultimate goal of using this method is to compare several options for integrating DG sources, then it is necessary to additionally implement two more stages of calculations.

Step 9. To obtain the optimal solution for each variant of network sectioning to provide the set reliability indexes, an assessment of additional CV(OPT) investments for the purchase and installation of sectioning devices is performed.

Step 10. For each variant (V) under consideration, calculate:

- total investment $C_{\sum}^{V} = C^{V}(DG) + C^{V}(OPT)$;
- relative investment $C_{NP}^{V} = C_{\sum}^{V} \Big/ \sum NP_j^V$ (USD/points) and $C_P^V = C_{\sum}^{V} \Big/ \sum P_j^V$ (USD/кW), where $\sum NP_j^V$ and $\sum P_j^V$ — the total number of points of sale of electrical energy and the total average load of the line under consideration, accordingly.

Step 11. Based on a quantitative comparison of the defined above characteristics, it can be concluded which variant of the DG integration with providing the set level of reliability indicators is preferable to use. In this case, the decision-maker can use the first or second criteria to make the final choice, or turn to the procedure of multi-criteria comparison of alternatives, considering both criteria simultaneously.

In circumstance where the regulator does not set limits for the reliability indexes, in order to compare alternative options for the use of local power sources (which generally differ in the type, parameters and places of connection to the network) in terms of their impact on the reliability of power supply, an indicator should be used that reflects the degree of improvement in the reliability characteristics per unit of investments associated with the acquisition and installation of generating sources, as well as technical support for their integration into electric networks.

These results can be used to determine the optimal (from the point of view of power supply reliability) conditions for the integration of generating sources, as well as to solve the problem in a more general form, focused on a multi-criteria comparison of alternative of their application [7].

When integrating DG, in addition to increasing the reliability of power supply, an important factor is the optimal control of the modes of the electrical network, which ensures a minimum of electrical energy losses, in particular, by the dynamic control of the network configuration.

3 Improving the Efficiency of Distribution Network Operation When Using Dispersed Sources of Generation

Distribution networks are traditionally operated with open topology, which allows the use of simple and not very expensive relay protection systems that provide quick isolation of damaged elements and restore power supply. At the same time, in the absolute majority of cases, switching devices with manual operation were used here. In this regard, choosing the optimal disconnection points was considered as a problem

of medium-term planning. The so-called normal schemes of distribution network are formed twice a year and maintained unchanged within the conditionally winter and summer seasons.

In recent years, significant changes have taken place in the global electric power industry, primarily due to the appearance of DG and energy storage devices in the structure of electric power distribution systems. At the same time, in most cases, in distribution networks, various renewable energy sources have an important feature—the fluctuation of the generated power. This leads to unexpected significant changes in the load flow of different durations, which no longer corresponds to the conditions under which the optimal places of opening the circuits of distribution lines were determined. These circumstances dramatically reduce the effectiveness of the implementation of such a task as the choice of optimal opening points, when this problem is considered within the traditional statement.

To solve this problem, it is necessary to determine the conditions for the feasibility of implementation and the strategy of rational use of remote-controlled switching devices, taking into account their limited switching resource, and the means of power electronics for the formation in the distribution network so called "Soft Open Points" (SOP) for effective reduction of electric energy losses due to rapid response to changes in the electrical load and/or outputs of dispersed sources of energy generation and storage.

One of the possible ways to achieve this goal can be a gradual replacement commutation apparatus (CA) with manual control to automatic or remotely controlled ones, which will make it possible to quickly change the topology of the network and to balance the generation and consumption in case of islanding operation [8]. However, it is necessary to take into account the high cost of the switching equipment itself, the cost of creation the information infrastructure for its operation (including channels for remote control) as well as the limited service life of switches [9].

Taking into account these factors, currently we can only talk about the installation of these CA in separate distribution lines, where they can provide the maximum efficiency. In this regard, the general problem of optimal placement of remote-controlled CA is not considered here, but the emphasis is placed on determining the strategy for the most rational use of them by conducting the following stages of its implementation:

1. A number of circuits in distribution networks are determined in which it would be advisable to install remotely controlled CA. Here the main criterion is the daily heterogeneity of power flows in individual sections of the circuit. This may be determined either on the basis of the direct analysis of load flow; or based on coefficients which reflect the ratio of the power of the certain node load (i) or DG output in the time τ, which corresponds to the period of the maximum total load of the line, to the maximum load or DG output in this node $K_{\Sigma i} = P_{i\tau}/P_{i\,\max}$; or by expert estimates, for example, taking into account the fact of renewable DG availability in the circuit, for example, such as photovoltaic, whose generation schedules are not only stable, but also in most cases do not coincide with the typical load curves of distribution network nodes.

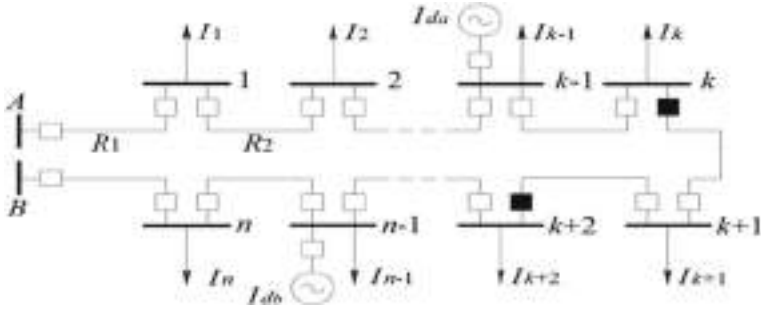

Fig. 2 Loop distribution network with remotely controlled switching devices

2. For the selected circuits of the distribution network for various periods of time, using the typical daily curves of node loads and DG outputs, the problem of choosing the optimal places for their disconnection is solved, with the objective to minimize power losses. For circuits in which, for various instances the optimal places of their disconnection do not coincide, it is necessary to determine the reasonable locations of remotely controlled CA installation.

In the process of DN operation, the decision regarding the reasonability of changing the state of remotely controlled CA is made on the basis of an index similar to the one proposed in [7]. This index is improved here to be able to take into account DG and facility of energy storage installed in the circuit (Fig. 2).

Even without taking into account the change in the node loads, the reasonability to change the state of remotely controlled CA can be caused by a change in output power of DG sources. So, for example, the reasonability of transfer the point of circuit disconnection from the section k, k + 1 to the section k + 1, k + 2 (Fig. 2) can be acquitted in case of an increase in the output power of the generation source (current injection Ida to the network) connected to one of the nodes of the upper part of the circuit and a decrease at the same time in the loads of the nodes of the same part of the circuit, or in case of a decrease in the output power from the second generation source (Idb) connected to the lower part of the circuit and a increase in the load of this part of the circuit.

Provided that switching on/off the sources of dispersed generation does not lead to a change in the direction of load flow in distribution line, the corresponding relationship can be presented in the following form:

- it is reasonable to move the point of disconnection to the left if

$$M_A - M_B + M_{d_B} - M_{d_A} > \frac{I_{tr} R_{\sum}}{2}; \tag{10}$$

- it is reasonable to move the point of disconnection to the right if

$$M_B - M_A - M_{d_B} + M_{d_A} > \frac{I_{tr} R_{\sum}}{2}, \tag{11}$$

where for any arbitrary s-th node with source of DG IEq50$M_{ds} = I_{ds} \sum_{j \in \Pi s} R_j$, M_{d_A}, M_{d_B}represent the sum of similar indexes, that are determined taking into account all DG sources connected to the left and right parts of the distribution circuit

$$M_A = \sum_{i=1}^{k} M_i,\ M_B = \sum_{i=h+1}^{n} M_i,\ R_\Sigma \sum_{j=1}^{m} R_j, M_i = I_i \sum\nolimits_{j \in \Pi_i} R_j. \qquad (12)$$

where n, m—respectively the number of nodes and sections in the circuit; ΣR—the total resistance of the circuit; Itr—the value of the load transferred from one "half–loop" of the circuit to another one in the process of changing the states of CA (in this case $I_{tr} = I_k$); $j \in \prod_i$—the index of the network sections that lies on the power supply path of the i–th load node.

Similarly, the presence of energy storage devices (considering charge/discharge modes) in the circuit of the DN can also be taken into account. Conditions (10) and (11) make it possible to determine variation in the load flow (by continuously monitoring of the distribution line mode), when it is advisable to change the state of the corresponding remotely controlled switching devices. However, the adoption of this decision requires additional analysis.

3. The problem of determining the rational frequency of commutation of remotely controlled CA has to be solved. In the simplest case, knowing the switching resource of CA and the design period of the project T, it is possible to determine the maximum number of commutation within a day. This makes it possible to take into account not only the fact that conditions (10) and (11) are met, but also the duration of the corresponding mode change, in order to avoid exceeding the daily switching limit, when making decisions regarding the feasibility of the distribution line reconfiguring.

It should be noted that the realization of this stage requires knowledge of the predicted loads and DGs outputs. Based on this data, the predicted values of the parameters MA, MB, M_{d_A}, M_{d_B}, Itr are calculated with a given discreteness interval. If the condition (10) or (11) is not met for the predicted values of the above parameters, then no actions are performed with the CA. If one of these conditions is met, the process of predicting the loads and the power of DGs continues with increasing intervals. Thus, essentially, a "scan" of a pre-defined time interval Θ is performed. If the corresponding changes in the mode parameters are stable (Fig. 3), then a command is sent to change the state of CA.

The forecasting procedure plays an important role in making decisions about change of point of disconnection in the distribution line. In this regard, it is proposed to apply the so-called "adaptive" method of predicting the necessary parameters, which must be carried out continuously and based on the simultaneous use of a number of different forecasting methods [10].

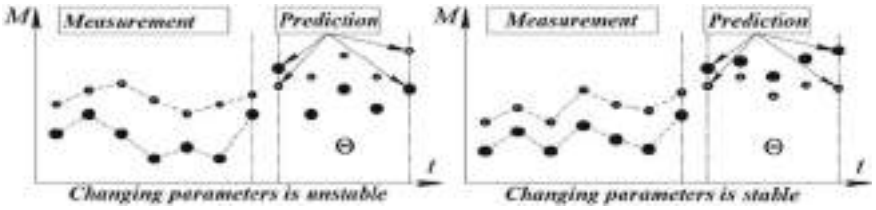

Fig. 3 Load forecasting

4. At this stage the structure of the forecasting procedure can be presented as follows:

$$Y_f(t+l) = \varphi_f[t,\ l,\ Y(t-ql)],\ f = 1,\ldots,F, q = 1,\ldots,Q.$$

After obtaining the actual value of the predicted parameter, the forecast error ε_f is estimated for each method to be used. In the next step, when evaluating the feasibility of changing the state of CA, must be used such prediction model φ*, that in the previous step provided the minimum forecast error $\left(\varepsilon^* = \min\left|\varepsilon_f\right|\right), f = 1, \ldots, F$

$$Y^*(t+nl) = \varphi^*[t,\ l,\ Y(t-ql)],\ n = 1,\ldots,N, q = 1,\ldots,Q.$$

In the above expressions, φ_f is a function that defines a specific forecasting method; F is the number of predictive models used; l is the prediction interval; N is the number of prediction intervals ($Nl = \Theta$); Q is the number of retrospective measurements.

Thus, the above sequence of calculations for stages 1–4 of the proposed strategy for optimal use of remote-controlled switches in DN, taking into account their switching resource and features of the modes of consumption and generation of electric energy, allows to minimize energy losses in these networks and, indirectly, to improve the voltage profile. At the same time, taking into account a rather large, but still limited switching resource, the use of remotely controlled CA will be advisable only in the case of sufficiently prolonged changes in loads.

This also applies to the availability of cyclic changes in the output power of DGs in accordance with natural daily alterations in the level of solar insolation, wind speed, etc. If there are sudden and frequent changes in the load and / or output power from alternative energy sources connected to the DN, then the use of remote-controlled CA will be economically unreasonable. In these conditions, other technical solutions are required, in particular, related to the use of power electronics [11–15].

4 Formation of "Soft" Points of Disconnection of the Distribution Network Circuits to Ensure Reliable and Efficient Operation of Power Distribution Systems with Dispersed Generation Sources

There are various proposals to ensure the reliable and efficient operation of distribution networks with DGs and energy accumulating facilities, among which the possibility of operating these networks in a closed mode is considered. This will automatically make it possible to optimally reallocate the power flows, minimize the loss of electrical energy, but at the same time this solution leads to an increase in short-circuit currents, which may require the replacement of switching equipment, increases the risk of large-scale outages. Therefore quite complex and expensive relay protection devices must be installed in the network in order to avoid this.

In this regard, in recent years, the question of the reasonability and effectiveness of the use of power electronics in DNs for forming the so called "soft points" of circuits disconnection has been discussed (concept «*Soft Open Points*» or «*SOP*») [16]. Installation of the corresponding power electronic device in the network node (Fig. 3) will allow combining the advantages arising from the operation of DNs in open and closed modes, and at the same time to eliminate the disadvantages of each of them.

Instead of simply switching on/off by CA, realization of technology "SOP" in distribution networks makes it possible to provide smoothly control of the flow of active power between parts of the DNs, consume or generate reactive power, regulate the voltage in normal mode, as well as isolate faults and restore power supply in post-emergency modes [17]. In addition, in distribution networks, in the presence of both consumers with drastically variable power consumption and dispersed energy sources with frequent fluctuations of output power, the use of appropriate power electronics is certainly advisable, primarily due to the lack of control inertia and switching restrictions.

A variety of power electronics tools can be used to organize the SOP. As studies show (for example, [7, 18]), the most acceptable solution is the use of "Voltage Source Converter" (VSC) of "Back-to-back" type with a DC link (Fig. 4).

Connected in series through a capacitor on the DC side, both VSC converters allow to generate a voltage with the desired amplitude and phase angle. This allows to control the active power flows through the DC link, the generation of reactive power on both its buses, and also reduce the voltage ripple due to the appropriate connection of IGBT modules in the VSC. The presence of filter reactors with an inductance of L provide the mitigation of higher harmonics, the limitation of short-circuit currents, and facilitates the control of power flows.

Although the principles of operation of such converters are known from the experience of their use in power systems [19], however, the strategy of their applying in distribution networks will be fundamentally different. Technical limitations for the VSC type converters used in SOP are the permissible power (currents) and voltage on their buses, as well as the requirement to maintain the balance of active power

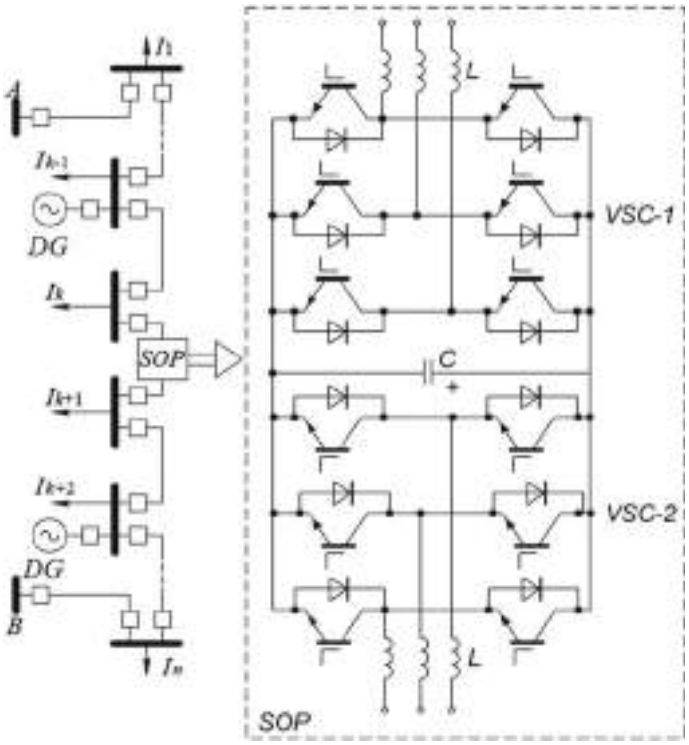

Fig. 4 SOP in distribution network

$$\sqrt{P_{VSC}^2 + Q_{VSC}^2} \leq S_{VSC_H} U_{VSC} \leq U_{VSC_H}, P_{inj}^A + P_{inj}^B + \Delta P_{SOP} = 0, \quad (13)$$

where P_{inj}^A, P_{inj}^B—active power, that entering to the right and left parts of the circuit (Fig. 4); ΔP_{SOP}—losses of active power in *VSC*.

In general, losses in SOP include: losses in semiconductors and passive elements (capacitor bank and filter reactors) of VSC1 and VSC2, in transformers and the cooling system of converters depend non-linearly (quadratically) on the values of the current that flows through them, in particular, on the exchange of active and reactive power in the AC network. The issues of their determination are discussed in [20].

The justification of the optimal conditions for the SOP operation has significant importance. In particular, in [18], two statements of this problem were considered, respectively related to minimizing active power losses

$$\Delta P = \sum R_k \frac{P_k^2 + Q_k^2}{U_k^2} + \Delta P_{SOP} \rightarrow \min, \quad (14)$$

as well as minimizing the unbalance of line loads

$$LBI = \sum_k \left(\frac{I_k}{I_{knom}} \right)^2 \rightarrow \min,$$

where k is the number of the line section, I_k i I_{knom}—the actual and nominal currents of the k-th section of the line, respectively.

Then the optimal parameters of the SOP operation are determined in the process of minimizing the objective function $Z\left[P^I_{s\_inj},\ Q^I_{s\_inj},\ Q^J_{s\_inj}\right]^T$, that includes restrictions on the voltage in nodes and currents in sections in the form of corresponding penalty functions.

At the same time, the resulting solution cannot be considered really optimal, since in this case the greatest interest is to minimize the loss of electrical energy, and not to improve individual characteristics of SOP mode.

Therefore, in distinction to the existing studies, a new SOP control strategy is proposed here. According to it, at each moment of time, the power flow in the circuit has to be distributed in such a way as to be as close as possible to load flow that would take place in the case of loop mode operation.

In this case, the load of one of the network sections that is adjacent to the SOP is monitored. The unbalance between the actual load on this section and its desired value (the one that should have been when working in closed mode) is compensated by additional power generation (positive or negative) from the SOP. In addition, the mode of operation of the DN obtained by this way will automatically provide the most favorable voltage profile in it.

For example (Fig. 5), the output of active power to the left side of the circuit at each moment of time t must be $P^l_{ot} - P^l_{ct}$ (where P^l_{ot}—the value of the active power on the Sects. 2 and 3 when network is operating in open mode, P^l_{3t}—is the same when the network is operating in closed mode). At the same time, from the right side of the circuit, there should be absorbed a active power equal to $P^l_{ot} - P^l_{ct} + \Delta P_{SOP}$ (where ΔP_{SOP}—losses of active power in SOP).

At the same time, in terms of reactive power, the left side of the circuit in relation to the SOP has to be considered as a consumer with a load $Q^l_{ct} - Q^l_{ot}$. In this case, the generation of reactive power from the SOP to the right side of the circuit will be $Q^l_{ct} - Q^l_{ot} + \Delta Q_{SOP}$.

It is important to note that in the presence in the network distributed generation sources, they in many cases provide only active power to the network. Then there are possible modes of operation when the optimal flows of active and reactive power do not coincide. SOP technology allows taking into account this situation due to the independence of active and reactive power generation operation [21].

However, it is impossible to provide optimal power flows simultaneously in both sections adjacent to the SOP buses due to (13). If the solution obtained in this case, when the optimal load is provided only on one of the network sections adjacent to the SOP, does not satisfy the decision maker, then the problem under consideration

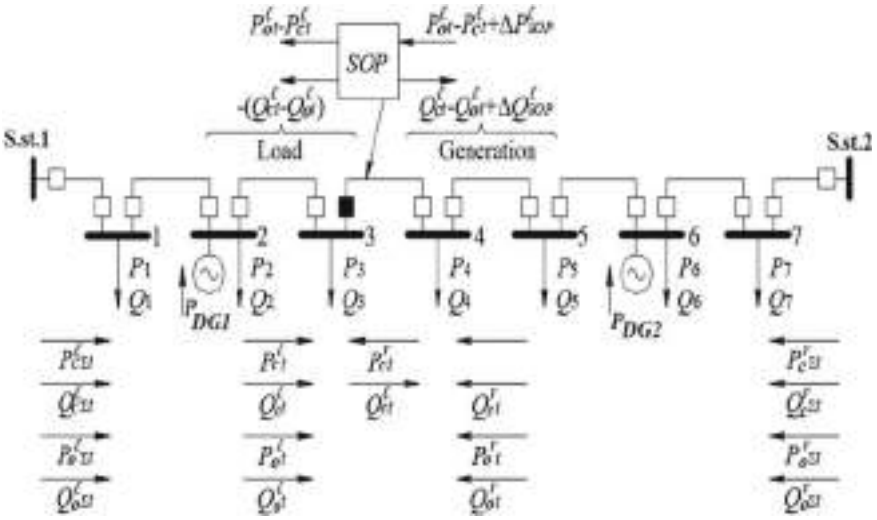

Fig. 5 Principle of SOP operation

is formed according to (14). This will allow one to determine the load flows on both sections of the network adjacent to the SP, and the operating modes of the specified VSC in the process of solving the corresponding optimization problem. The implementation of this strategy avoids a number of technical problems with the broad integration of alternative energy sources with variable and difficult-to-predict output power into distribution networks, while ensuring the most efficient mode of their operation [22].

It is clear that the implementation of sufficiently expensive new technical solutions to improve the efficiency of operation of DNs cannot be justified only from the point of view of reducing electric energy losses. For this, in addition to technical indicators, it is necessary to take into account such factors as an increase of electrical networks capability, a delay in the need for their reconstruction, the widespread (often uncontrolled) integration of alternative energy sources that need the use of energy storage systems with bidirectional converters to ensure the balance of energy in the system between the energy generated by renewable energy sources and the load, improvement of the environmental components and a number of other factors.

5 Conclusion

It is shown that the widespread use of DG and energy storage facilities in DN, complicate the problem of choosing the optimal configuration of distribution networks, which is considered as the most effective means of minimizing electric energy losses.

In many cases, this factor does not make it possible to ensure the desired effectiveness of solutions. This is especially relevant for DNs that integrate renewable energy sources with varying power output.

It is noted that a possible solution in this situation is automation of distribution networks with a focus on the use of fundamentally new switching devices. The use of remotely controlled switches, due to their limited operation resource, can be reasonable in case of infrequent and rather prolonged changes of the load and DG output power, due, for example, to cyclic daily changes of solar insolation or wind speed as well as when switching on/off energy storage batteries.

The algorithm for operating remotely controlled CA is developed. The proposed approach allows one to determine the strategy of rational use of remote-controlled switching devices, taking into account their switching resource, and, in such a way, to implement dynamic reconfiguration of distribution network circuits in order to minimize energy losses in the case of cyclic changes of the load or output power of dispersed generation sources of energy and means of its accumulation.

The main conditions for the expediency of using power electronics are substantiated, and a new approach to managing their operation in the form of the so-called "soft" opening points in distribution lines (the concept of "SOP") is developed, which makes it possible, while maintaining an open network topology, provide independent rational control of active and reactive power flows in real time, responding to changes in power consumption and modes of local generation to minimize total energy losses.

References

1. IEEE Std 1366–2012.: IEEE guide for electric power distribution reliability indices, 43 p. IEEE Inc., USA (2012). https://doi.org/10.1109/IEEESTD.2012.6209381
2. Korchagin, M.I.: Technological violations at the objects of electric networks of power transmission organizations in 2010: analytical reference. Derzhavna inspektsiia z enerhetychnoho nahliadu za rezhymamy spozhyvannia elektrychnoi ta teplovoi enerhii (2011). 250 p
3. Zorin, V.V., Tislenko, V.V., Kleppel', F., Adler, G.: Reliability of power supply systems. Kyiv. Vyshha shkola 192 (1984)
4. Zharkin, A.F., Popov, V.A., Tkachenko, V.V.: Optimal sectionalizing of overhead distribution networks under the condition of distributed generation implementation. Tekhnichna Elektrodynamika (2), 61–69 (2017) (Rus). https://doi.org/10.15407/techned2017.
5. Popov, V., Tkachenko, V., Fedosenko, M., Yarmoliuk, O., Frolov, I.: Optimal distribution networks sectionalizing to comply Smart Grid concept, in *IEEE 7-th International Conference on Energy Smart Systems (ESS 2020)*, Kyiv, 12–14 May 2020. https://doi.org/10.1109/ESS
6. Sahragard, S.B., Popov, V.A., Tkachenko, V.V., et al. Estimation of the costs of the power supply company for maintaining the normalized level of reliability of power supply to consumers in the conditions of distributed generation. Vostochno-Evropejskij zhurnal peredovyh tehnologij. Jenergosberegajushhie tehnologii i oborudovanie **1/8** (79), 58–63 (2016). https://doi.org/10.15587/1729-4061.2016.59616
7. Zarkin, A.F., Denysiuk, S.P., Popov, V.A.: Power supply systems with distributed generation sources, 232 p. Naukova dumka, Kyiv (2017) (Rus)
8. Xu, Y., Liu, C.C., Schneider, K.P., Ton, D.T.: Placement of remote-controlled switches to enhance distribution systems restoration capability. Proc. IEEE Trans. Power Syst. **31**, 1139–1150 (2016). https://doi.org/10.1109/TPWRS.2015.2419616

9. Spitsa, V., Ran, X., Salcedo, R., Martinez, J.F., Uosef, R.E., de Leon, F., Czarkowski, D., Zabar, Z.: On the transient behaviour of large-scale distribution networks during automatic feeder reconfiguration. Proc. IEEE Trans. Smart Grid. **3**(2), 887–896 (2012). https://doi.org/10.1109/TSG.2012.2186319
10. Garcia, E.D., Pereira, P.R., Canha, L.N., Popov, V.: Grid functional blocks methodology to dynamic operation and decision making in Smart Grid. Proc. Electr Power Energy Syst. **103**, 267–276 (2018). https://doi.org/10.1016/j.ijepes.2018.06.002
11. Shydlovskyi, A.K., Novskyi, V.O., Zharkin, A.F.: Stabilization of electrical parameters in three-phase systems by semiconductor corrective devices. K.: Instytut elektrodynamiky NAN Ukrainy, Typ. «Nash format» (2013), 378 p
12. Bayoumi, E.H.E.: Power electronics in smart grid power transmission systems: a review. Int. J. Indus. Electron. Drives **2**(2), 98–115 (2015). https://doi.org/10.1504/IJIED
13. Patil, G., Shashikant Mathpati, S., Aspalli, M.S.: Impact of power electronics on global warming. Int. J. Res. Eng. Technol. **03**(03), 233-236 (2014)
14. Prasad, I.: Smart grid technology: Application and control. Int. J. Adv. Res. Electr. Electr. Instrument. Eng. (An ISO3297: 2007 Certified Organization) **3**(5), 9533–9542 (2014)
15. Srivastava, S.: Role of power electronics in nonrenewable and renewable energy systems. Int. J. Techn. Res. Appl. **1**(3), 91–94 (2013)
16. Ohada, N., Takasaki, M., Sakai, H., Ketoh, S.: Development of a 6, 6 kV – 1 MVA transformer less loop balance controller, in *Proceedings of the IEEE Power Electronics Specialists Conference*, pp. 1087–1091 (2007). https://doi.org/10.1109/PESC.2007.4342144
17. Simanjorang, R., Miura, Y., Ise, T., Sugimoto, S., Fujita, H.: Application of series type BTB converter for minimizing circulating current and balancing power transformers in loop distribution lines, in *Proceedings of the IEEE Conference on Power Conversion*, pp. 997–1004. Nagoya, 2007. https://doi.org/10.1109/PCCON.2007.373088
18. Cao, W., Wu, J., Jenkins, N., Wang, Ch., Green, T.: Benefits analysis of soft open points for electrical distribution network operation. Appl. Energy **165**, 36–47 (2016). https://doi.org/10.1016/j.apenergy.2015.12.022
19. Flourentzou N., Adelidis V.G., Demetriades C.D. VSC – based HVDC power transmission systems: an overview. Proc. IEEE Trans. Power Electron. **24**, 592–602 (2009). https://doi.org/10.1109/TPEL.2008.2008441
20. Daelemans, G., Srivastava, K., Reza, M., Cole, S., Belmans, R. Minimization of steady state losses in meshed networks using VSC HVDC. Proc. IEEE Power Energy Soc (General Meet) 1–5 (2009). https://doi.org/10.1109/PES.2009.5275450
21. Govorov, P.P., Novskiy, V.O., Govorov, V.P., Kindinova, A.K.: Management of modes of distributive electric networks of cities under conditions of weak correlation of graphics of active and reactive power. Tekhnichna Elektrodynamika (4) 60–66 (2020). https://doi.org/10.15407/techned2020.04.060
22. Zharkin, A.F., Novsky, V.O., Palachov, S.O.: Technical regulation of voltage quality in electrical grids with sources of distributed generation. Tekhnichna Elektrodynamika (3), 55–57 (2016). https://doi.org/10.15407/techned2016.03.055

Some Features of Electromechanical Oscillations Modes Identification in Power Systems

Oleksandr Butkevych and Volodymyr Chyzhevskyi

Abstract Power systems are the high-order time-varying nonlinear systems. In power systems, especially in interconnected ones, low-frequency oscillations (LFO) occur from time to time leading to accidents with severe consequences. Modern LFO monitoring systems based on Phasor Measurement Units (PMU) are designed to timely identify the danger of the power system stability violation. This monograph chapter presents some results of studies various signal analysis methods to their use in real-time to identify the modes of electromechanical oscillations in power systems. Comparison application results of different signal analysis methods oriented to real-time use is presented. It is shown that when these methods are using in real-time under certain conditions the differing identification results of LFO modes may be obtained. To provide required reliability of the LFO modes identification few the most suitable for real-time application in LFO monitoring systems methods were selected. Taking into account the possibility of obtaining by such methods differing identification results the special procedure was proposed to process and to generalize corresponding identification results. Such approach makes it possible to obtain adequate estimates of LFO modes parameters more reliably. Two examples of the LFO analysis using PMU data are given. During such analyzing the ensemble of selected methods and the data obtained from PMU were used. These LFO arose in the Interconnected Power System of Ukraine on February 16, 2016 and on February 18, 2017.

Keywords Low-frequency oscillations mode · Identification · Signal analysis methods · Monitoring · Power system stability

O. Butkevych (✉)
Institute of Electrodynamics of NAS of Ukraine, Kyiv, Ukraine

O. Butkevych · V. Chyzhevskyi
National Technical University of Ukraine "Igor Sikorsky Kyiv Polytechnic Institute", Kyiv, Ukraine

O. Kyrylenko et al. (eds.), *Power Systems Research and Operation*, Studies in Systems, Decision and Control 388, https://doi.org/10.1007/978-3-030-82926-1_3

1 Introduction

The causes of the LFO occurrence in the power systems are well known. Such oscillations are electromechanical oscillations. Electromechanical oscillations can be classified by the nature of their initiation, by the frequency and by the influence on the power systems' stability. Generalization of different classifications [1–7] leads to the following conclusions:

- control modes—wide frequency range;
- torsional modes—10…46 Hz;
- intra-plant modes—2.0…3.0 Hz;
- local plant modes—1.0…3.0 Hz;
- intra-area modes—0.3…1.0 Hz;
- inter-area modes—less than 0.3 Hz.

A lot of power systems' outages in recent years were directly or indirectly caused by LFO initiated by different reasons. The major of these outages are pointed in [8–16].

An analysis of extensive data related to the power systems accidents caused by LFO leads to the conclusion that intra-area and inter-area LFO are most dangerous for the power systems by negative consequences.

According to the degree of damping LFO can be classified as follows [6]:

- normal (positively damped)—the amplitude of LFO decreases in time without corrective action;
- sustained (undamped)—the amplitude of LFO is constant so the oscillations do not fade away in time without corrective action;
- negatively damped—the amplitude of the LFO is increasing in time until it reaches a value that results to the overloading of the power systems' elements losing of the subsystems' synchronism etc.

To provide the effective damping of LFO in power systems FACTS technologies and power system stabilizers are used [17–23]. The study results analysis shows that the effectivity of LFO damping systems highly depends on their settings, which must be adjusted according to actual LFO frequencies. Thus, the task of the LFO modes identification is a priority one to provide the effective damping of LFO in power systems.

2 Methods' Testing and Selection to Identify LFO Modes in Real-Time. Identification Results Generalization

In power system small-signal stability analysis linearized mathematical model is used. Such model makes possible to calculate the eigenvalues ($\lambda_i = \sigma_i \pm j\omega_i$, $i = 1, \ldots, n$) of corresponding characteristic matrix A of a certain power system

operational condition. Mathematical model and power system operational condition determine the quantitative and qualitative eigenvalues' composition and the eigenvectors U_i and V_i $(i = 1, \ldots, n)$ of the matrixes A and A^T correspondently. Thus, the state variables vector Δx can be given as follow

$$\Delta x(t) = \sum_{i=1}^{i=n} e^{\lambda i t} U_i V_i^T \Delta x(0) = U e^{\Lambda t} U^{-1} \Delta x(0), \quad (1)$$

where $\Delta x(0)$ is $\Delta x(t = 0)$, U – modal matrix formed from the matrix A eigenvectors, e^{Λ} – diagonal matrix with modes as non-zero elements.

Every i mode is characterized by the amplitude, damping constant σ_i, frequency ω_i [rad/s] or $f_i = \omega_i / 2\pi\,[Hz]$; damping ratio ξ_i where $\xi_i = -\sigma_i (\sigma_i^2 + \omega_i^2)^{-0.5}$.

To analyze the power systems stability in real-time the LFO monitoring system including signal analysis means can be used. Voltage, frequency and active power signals in the digital form can be obtained for analysis from PMU forming the Wide-Area Measurement System's object level.

Main requirements to the means of LFO modes identification in real-time are based on LFO modes analysis results and can be formulated as follow:

- LFO modes with frequencies less than 1 Hz should be reliably identified;
- resolution by the frequency values should be no less than 0.1 Hz due to the possibility of the multimodal oscillations with the close dominant frequencies values [24];
- low sensitivity of the dominant modes' identification results to the noises in analyzed signals.

The possibility and feasibility of signal analysis methods using depend on the signals themselves, analysis conditions and the requirements to the analysis results obtained. All processes in the power systems are non-linear and non-stationary, but most of signal analysis methods can only be used for the analysis of stationary signals (only Hilbert-Huan transform is considered as the method suitable to analyze non-linear and non-stationary processes [25]). Thus, selection of appropriate signal analysis methods which can provide in real-time minimal errors of analysis results is one of the major tasks of the LFO monitoring system development. The selection mentioned above has covered such signal analysis methods:

- discrete Fourier transform (DFT) and fast Fourier transform (FFT) [26];
- non-parametric: periodogram, spectrogram, Welch, Thomson (Multitaper method) [27, 28];
- parametric autoregressive model: Yule-Walker, Burg, covariation, modified covariation [26, 27];
- parametric exponential model: multiple signal classification (MUSIC), eigenvector (EV), Hankel total least squares (HTLS), matrix pencil (MP), Prony, Prony modified (with using of the singular values decomposition method based on the least-squares method) [26, 29–31];

- wavelet transform (WT)—Haar wavelet, Morlet wavelet, "mexican hat" wavelet [32];
- Stockwell transform (ST) and ST modified (with enhanced frequency resolution) [33, 34];
- Hilbert-Huang transform (HHT) and two HHT modifications (MHHT-1—with using the mirror image of extreme near the edges of the analyzed signal's sample to reduce edge-effects of the empirical modes decomposition (EMD), and MHHT-2—with single interpolation using for every sifting during the iterative identification of the intrinsic mode function (IMF) to reduce calculations) [25, 35, 36].

To solve the problem of the parametric model order determination the minimum description length (MDL) principle was used [37]. Comparison of this approach with another ones (exponentially embedded family (EEF) method and model structure determination (MSD) criterion) has showed a little bit excessive model order is determined according to the MDL principle that can increase the reliability of the dominant modes' identification when the signal is noised [27, 38].

Preselection of the signals' analysis methods has been made with using of the 3-component synthesized test signal (denote this signal by TS-1):

$$y(t) = 100 + 2\sin(2\pi \cdot 0.1t) + \sin(2\pi \cdot 0.2t). \tag{2}$$

TS-1 contains 0.1 and 0.2 Hz components which are corresponding to the inter-area oscillations frequency spectrum. Some results of the TS-1 (10 s sample) spectral analysis by different methods using are presented in Figs. 1 and 2, and in Table 1.

Preselection results analysis has shown that HTLS, MP, Prony, Prony modified, Morlet WT and HHT modifications (MHHT-1 and MHHT-2) with different effectiveness are able to identify dominant modes' frequencies. There is high dependence of the obtained results from the signal's sample window width (Table 2).

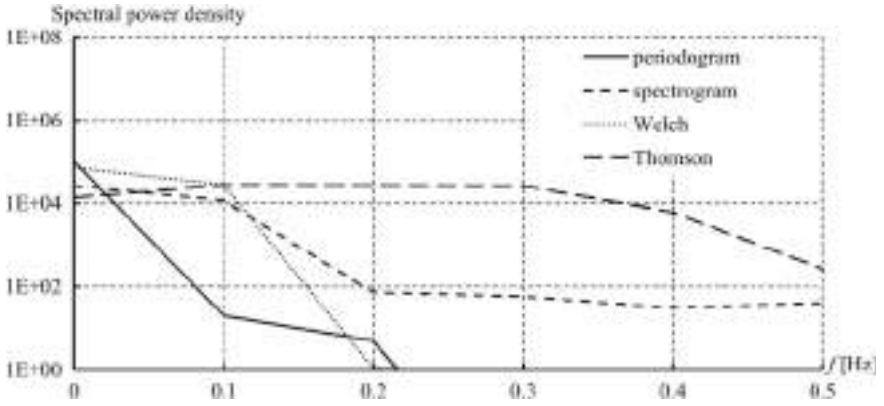

Fig. 1 Spectral analysis results of TS-1 (10 s sample)

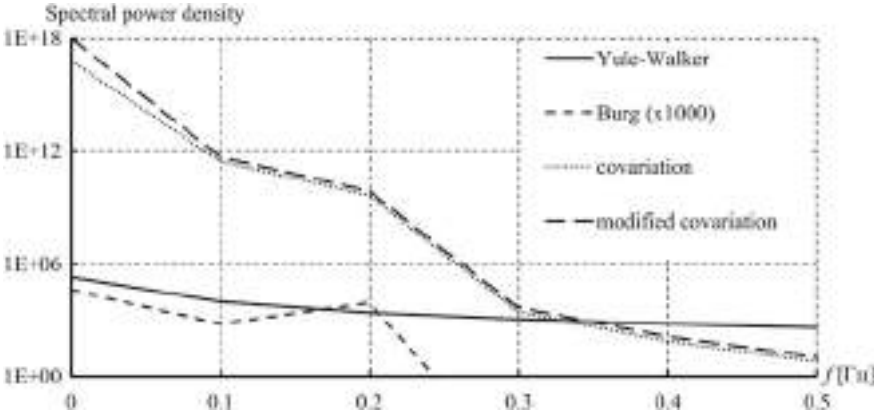

Fig. 2 TS-1 (10 s sample) spectral analysis results

Table 1 TS-1 (10 s sample) spectral analysis results

Analysis method	Estimated components' parameters of TS-1		
	Frequency, Hz	Amplitude	Damping ratio
MUSIC	0.12	2.3	–
	0.21	1.2	–
EV	0.13	2.6	–
	0.22	1.1	–
HTLS	0.10	2.0	0.0
	0.20	1.0	0.0
MP	0.10	2.0	0.0
	0.20	1.0	0.0
Prony	0.10	2.0	0.0
	0.20	1.0	0.0
Prony modified	0.10	2.0	0.0
	0.20	1.0	0.0
HHT	0.04	106.9	–
	0.31	2.5	–
MHHT-1	0.29	0.8	–
MHHT-1 (with 5% both sides IMF vectors trimming)	0.23	0.8	–
MHHT-2	0.10	2.1	–
MHHT-2 (with 1% both sides IMF vectors trimming)	0.10	2.1	–

Table 2 TS-1 spectral analysis results (different sample window width in time)

Analysis method	Time range [s]														
	0…1			0…2			0…3			0…5			0…10		
	f [Hz]	A	ξ	f [Hz]	A	ξ	f [Hz]	A	ξ	f [Hz]	A	ξ	f [Hz]	A	ξ
HTLS	0.10	2.0	0.0	0.10	2.0	0.0	0.10	2.0	0.0	0.10	2.0	0.0	0.10	2.0	0.0
	0.20	1.0	0.0	0.20	1.0	0.0	0.20	1.0	0.0	0.20	1.0	0.0	0.20	1.0	0.0
MP	0.19	1.8	0.0	0.10	2.0	0.0	0.10	2.0	0.0	0.10	2.0	0.0	0.10	2.0	0.0
				0.20	1.0	0.0	0.20	1.0	0.0	0.20	1.0	0.0	0.20	1.0	0.0
Prony	0.10	1.9	0.0	0.10	2.0	0.0	0.10	2.0	0.0	0.10	2.0	0.0	0.10	2.0	0.0
	0.20	1.0	0.0	0.20	1.0	0.0	0.20	1.0	0.0	0.20	1.0	0.0	0.20	1.0	0.0
Prony modified	0.18	1.9	−0.1	0.19	1.7	−0.1	0.19	1.9	−0.1	0.19	1.9	−0.1	0.10	2.0	0.0
													0.20	1.0	0.0
Morlet WT	0.34	7.8	–	0.36	5.5	–	0.33	4.5	–	0.35	3.5	–	0.30	2.4	–
	1.49	2.7	–	1.14	1.9	–	1.47	1.5	–	1.50	1.2	–	1.50	0.9	–
MHTT-1	–	–	–	–	–	–	–	–	–	–	–	–	0.23	0.8	–
MHTT-2	0.96	0.8	–	0.47	1.0	–	0.34	0.9	–	0.2	1.3	–	1.0	2.1	–

Table 2 data show inappropriate accuracy of the dominant modes' frequencies and amplitudes identification by WT and MHHT-2 methods, so these methods were withdrawn from the further selection.

Increasing in time of LFO dominant modes' amplitudes is the main menace sign of the power system's stability loss, so the timely identification of such menace is the main goal of the LFO monitoring system. To test the sensitivity of signal analysis methods to dominant modes' amplitudes changes a five-component test signal was synthesized (denote this signal by TS-2):

$$\begin{aligned} y(t) =& 100 + (1+t)\cdot\sin(2\pi\cdot 0.1t) + (1+1.1t)\cdot\sin(2\pi\cdot 0.15t) + (1+1.3t)\cdot\sin(2\pi\cdot 1.5t) \\ &+ (1+1.1t)\cdot\sin(2\pi\cdot 1.9t). \end{aligned} \tag{3}$$

TS-2 identification results with the 2 s signal's sample window width are presented in Figs. 3 and 4.

The Figs. 3 and 4 show that with the 2 s signal's sample window width considered analysis methods are unable to separate components of 0.1 and 0.15 Hz. To overcome this problem signal's sample window width must be increased to 3 s at least.

To test the sensitivity of signal analysis methods to dominant modes' frequencies changes a three-component test signal was synthesized (denote this signal by TS-3):

$$y(t) = 100 + A_1(t)\cdot\sin(2\pi t\cdot(0.30+0.01t)) + A_2(t)\cdot\sin(2\pi\cdot 0.80t). \tag{4}$$

TS-3 contains a component with the variable frequency increasing from 0.3 to 0.5 Hz in 10 s time. The amplitudes A_1 and A_2 of the TS-3 are changing as follow:

$$\begin{aligned} A_1(t) &= \exp(0.25t) - 1, \text{ if } t = [0;\ 10]\text{s}; \\ A_2(t) &= \begin{cases} \exp(0.60t) - 1, & \text{if } t = [0;\ 5]\text{s}; \\ \exp(0.60\cdot 5) - 1, & \text{if } t = (5;\ 6)\text{s}; \\ \exp(0.60\cdot 5) - \exp(0.70t), & \text{if } t = [6;\ 10]\text{s}. \end{cases} \end{aligned} \tag{5}$$

TS-3 modes identification results with the 2 s signal's sample window width are presented in Figs. 5 and 6.

From the analysis of the above figures (Figs. 4, 5, and 6) it follows that relative errors of frequency estimations by analysis methods are significantly less than errors of amplitude estimations, and accuracy of the dominant modes' parameters estimation highly depends on the signal form and the sample window width. Further studies were carried out with the signals obtained as a result of the electromechanical transients modelling in the 4-machines test system (denote this system by S-I) and 6-machines test system (denote this system by S-II) by Matlab. All data related to S-I and S-II are presented in [3] and [39] correspondently.

In S-I with synchronous generators equipped with automatic voltage regulators DC1A type with the settings according to [40] and without power system stabilizers LFO were initiated by increasing of the active power transfer by the 230 kV transmission lines from 390 to 490 MW (see Fig. 7, denote this signal by TS-4).

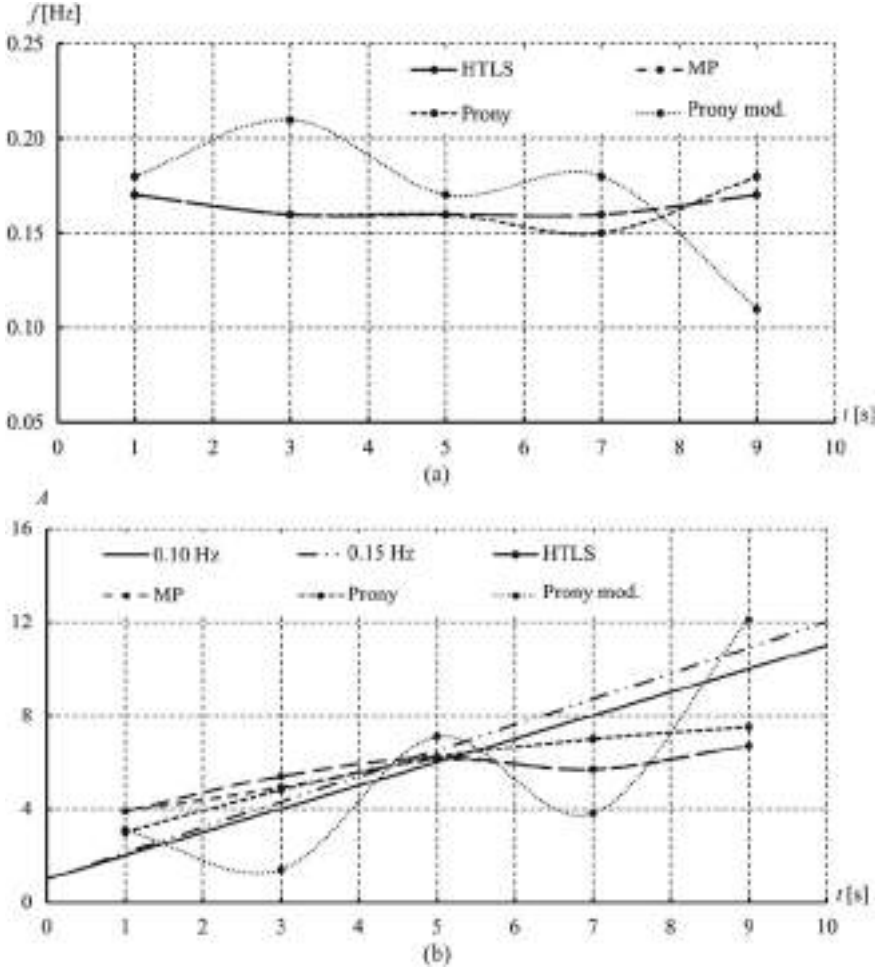

Fig. 3 TS-2 modes frequencies (**a**) and amplitudes (**b**) identification results (2 s sample window width)

The main feature of this signal is the low-speed increasing of the oscillation amplitude. Modal analysis of the TS-4 gives three modes having respectively: $f_1 =$ 0.55 Hz ($\xi_1 = -0.001$), $f_2 = 1.06Hz$ ($\xi_2 = 0.081$), $f_3 = 1.10Hz$ ($\xi_3 = 0.070$). It is obvious that oscillations amplitude increasing is caused by 0.55 Hz mode. Identification results of TS-4 modes parameters with the 2 s signal's sample window width are presented in Figs. 8, 9, and 10.

Identification results of TS-4 modes parameters show that: considered analysis methods are not able to separate modes with the frequencies of 1.06 and 1.10 Hz; only Prony method was able to identify the increasing of the 0.55 Hz dominant mode's amplitude in time; MHHT-1 and MHHT-2 methods are not able to identify any modes

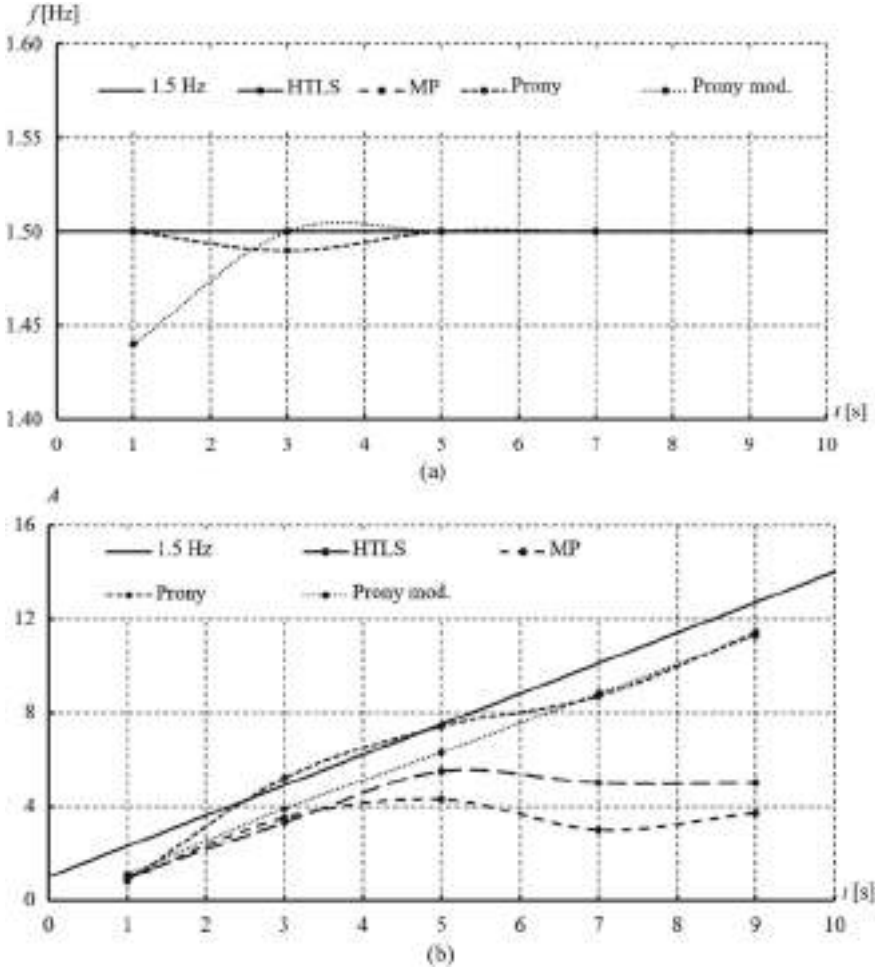

Fig. 4 TS-2 modes frequencies (**a**) and amplitudes (**b**) identification results (2 s sample window width)

of TS-4. It is known [39] that for S-II operational conditions two oscillations' modes with the frequencies 0.79 and 1.34 Hz exist. To assess the ability of selected signal analysis methods to adequately identify indicated oscillations' modes the various disturbing influences were simulated to cause power system operational condition parameters' oscillations. One of the examples of such oscillations occurrence is shown in Fig. 11 (denote the corresponding signal by TS-5; this is active power flow by transmission line 4–100 of S-II).

TS-5 analysis results with the 2 s sample window width are presented in Figs. 12 and 13.

Identification results of the TS-5 modes parameters show that:

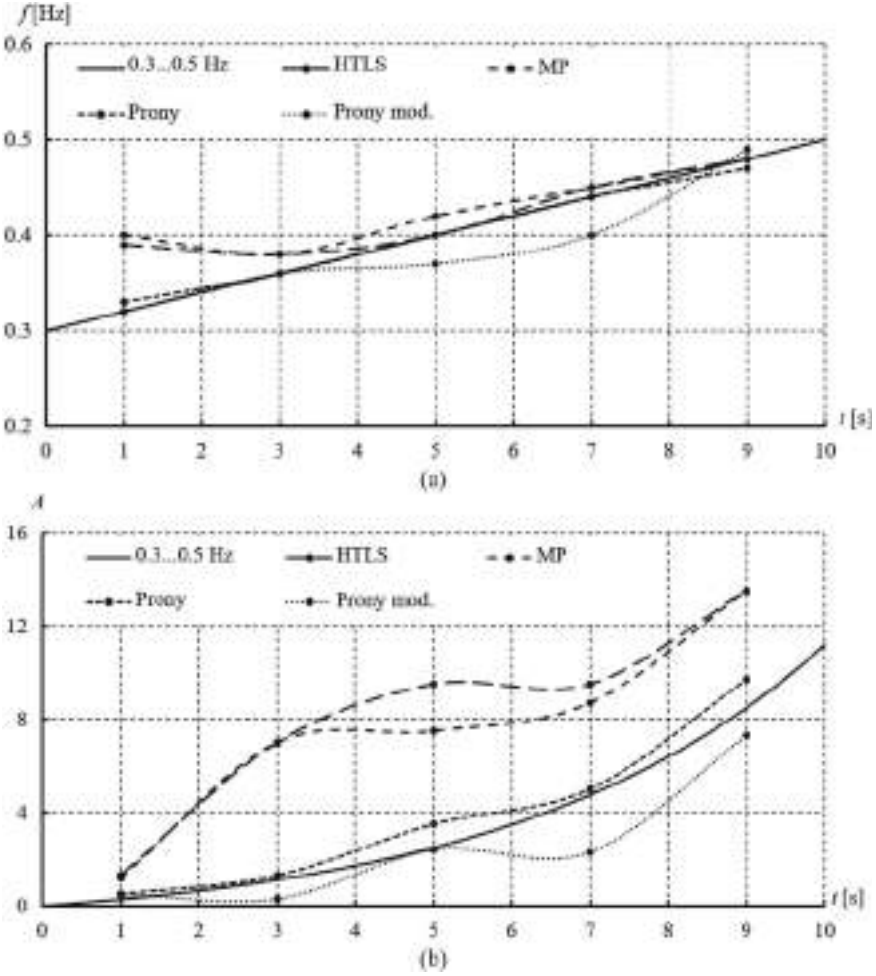

Fig. 5 TS-3 modes frequencies (**a**) and amplitudes (**b**) identification results (2 s sample window width)

- Prony method is not able to separate modes with the frequencies of 0.79 and 1.34 Hz;
- MHHT-1 and MHHT-2 methods provide adequate frequencies analysis results.

The possibilities of considered methods to provide the adequate LFO modes estimation' results also depend on the noise level in the analyzed signals. In steady-states power system operational condition the signals measured by PMU can be characterized by the signal-to-noise-ratio (SNR) of 80…120 dB [41, 42], but SNR may drop to 2…10 dB in the first moments after disturbance [43]. Spectral analysis results of

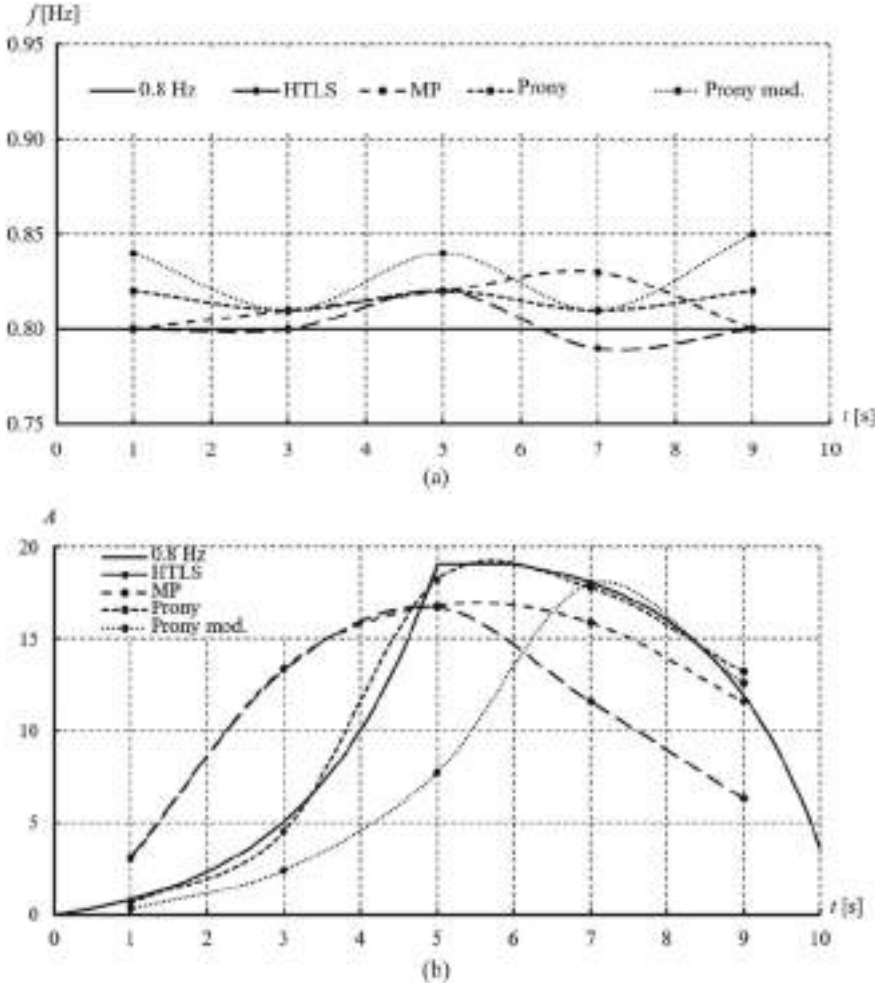

Fig. 6 TS-3 modes' frequencies (**a**) and amplitudes (**b**) identification's results (2 s sample window width)

the TS-4 with different SNR ("white" noise) and with the 2 s signal's sample window width are presented in Table 3.

In the case of the signal's SNR below the values pointed in Table 3 preliminary digital filtering is needed.

TS-1–TS-5 analysis results lead to the conclusion that it is impossible to select only one the best analysis method for real-time using. Therefore, to use the ensemble of the selected methods with the generalization of the results obtained with them is expedient. Taking into account all study results two groups of signal analysis methods for the ensemble can be proposed:

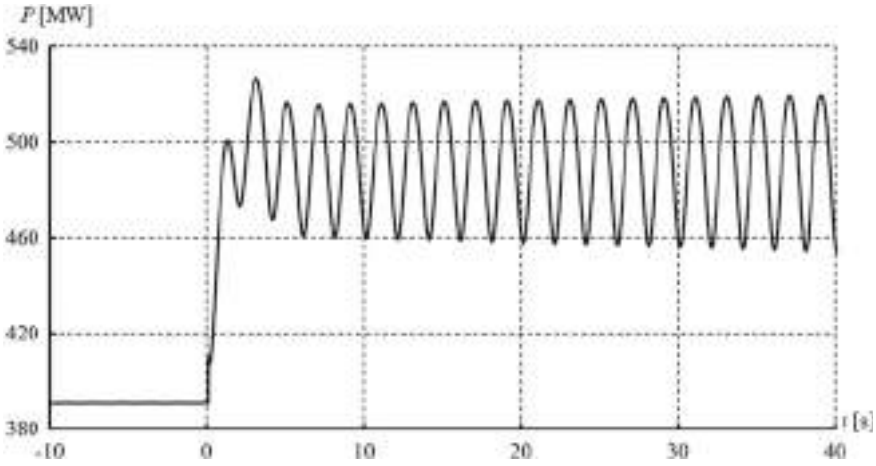

Fig. 7 The active power transfer by 230 kV transmission lines

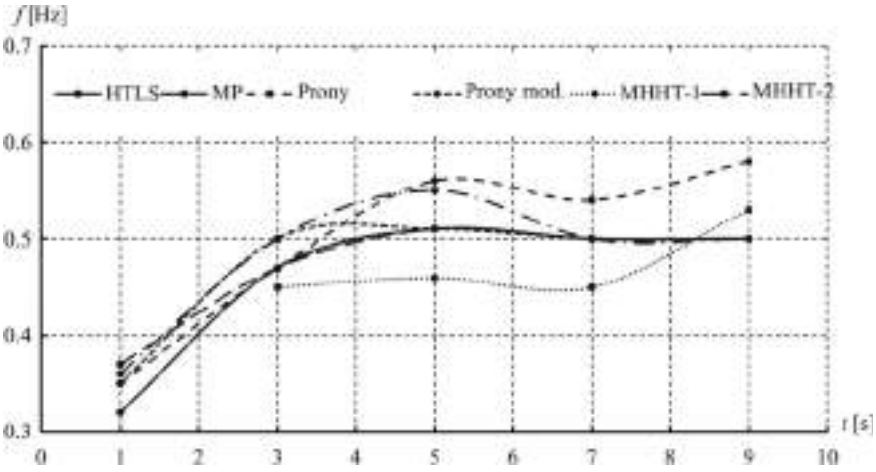

Fig. 8 Identification results of the TS-4 first mode frequency (2 s sample window width)

- main: HTLS, MP, Prony, and modified Prony methods;
- additional: MHHT-2 method (the results are taking into account only if there is no alignment between the main group methods).

LFO dominant modes' parameters' identification results generalization may be provided under next conditions:

1. During one method results generalization it is considered that:
   a. the modes with frequency differences less than Δf_1 are counted as one mode:

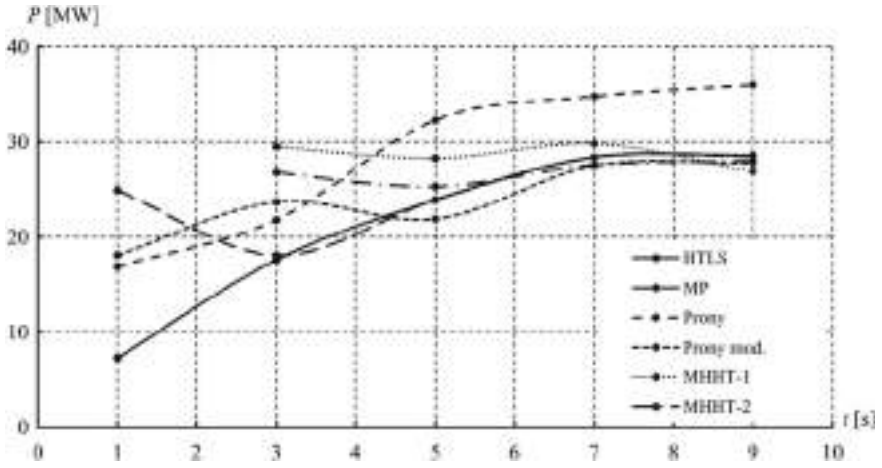

Fig. 9 Identification results of the TS-4 first mode amplitude (2 s sample window width)

(1) frequency and amplitude of such generalized mode equal the ones of the mode with the bigger amplitude;
(2) damping character of the generalized mode can be estimated by means of amplitude' changes in time analysis using three series observation windows, because:
   i. taking into account the possibility of the presence variable-frequency mode in analyzed signal's samples in the (k–2) and (k–1) observation windows the modes with the frequency deviation of $\pm\ \Delta$ from the considering mode frequency in k observation windows have to be taking into consideration;
   ii. damping of the generalized mode is considered as stable negative in the case of increasing of its amplitude in three consecutive observation windows;
   iii. damping of the generalized mode is considered as possibly negative in the case of the increasing of its amplitude for first and second or for first and third observation windows;
   iv. damping of the generalized mode is considered as stable positive in the case of decreasing of its amplitude for three consecutive observation windows;
(3) amplitude of the generalized mode less than threshold value A′ is not taking into account in the further processing;
(4) amplitude of the generalized mode greater than threshold value A″ is considered as error and is not taking into account. A″ value for the k observation window can be estimated as follow

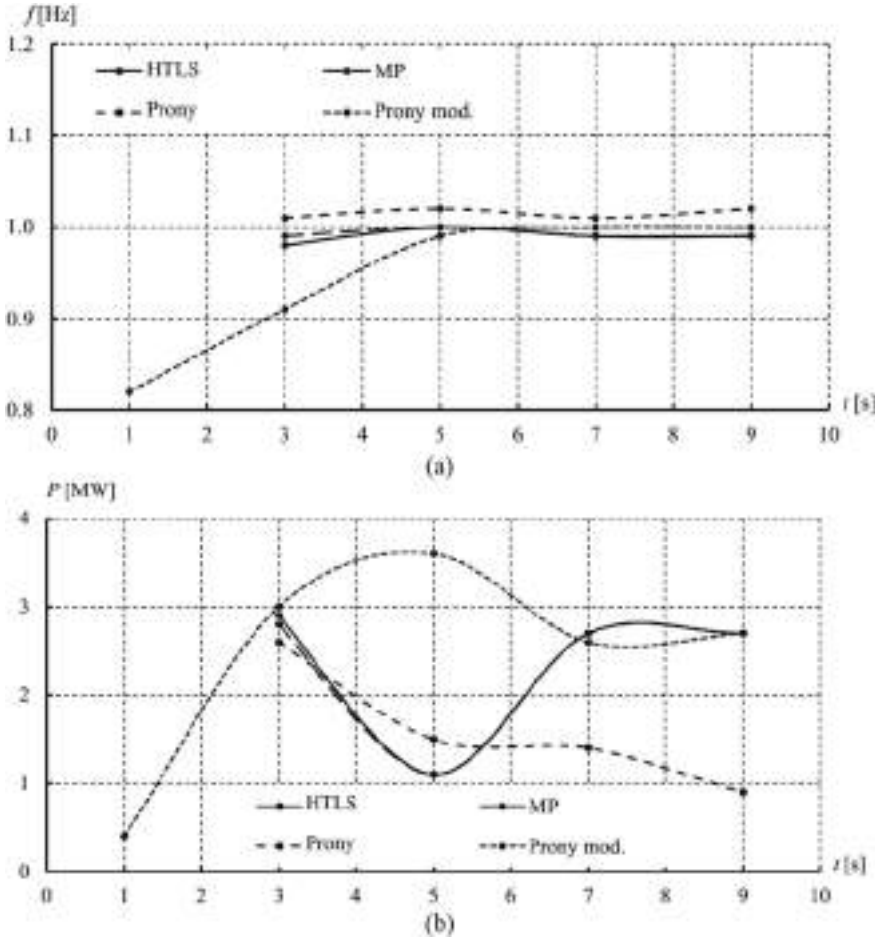

Fig. 10 Identification results of the TS-4 s mode frequency (**a**) and amplitude (**b**)

$$A'' = \begin{cases} S_{\max}, & \text{if } 0 < S_{\min} < S_{\max}; \\ |S_{\min}|, & \text{if } 0 > S_{\max} > S_{\min}; \\ S_{\max} - S_{\min}, & \text{if } (S_{\max} > 0) \wedge (S_{\min} < 0), \end{cases} \tag{6}$$

where $S_{\max}$ and $S_{\min}$ are the maximum and minimum signal value in the k observation window.

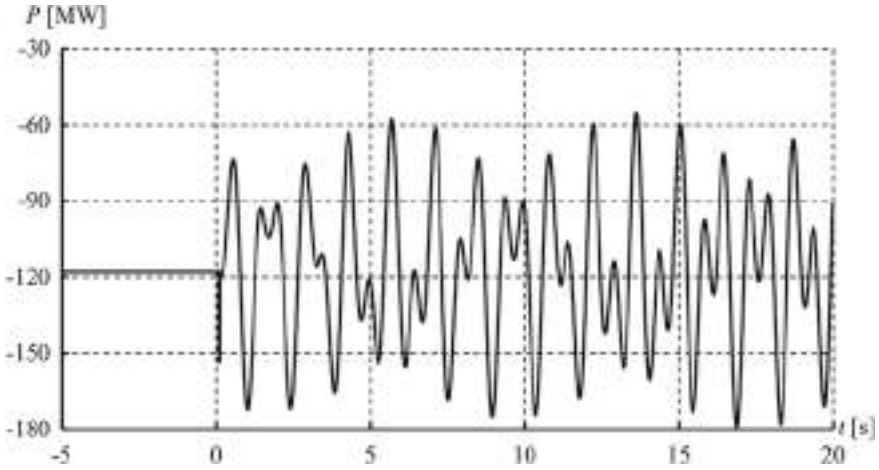

Fig. 11 The active power flow change in time

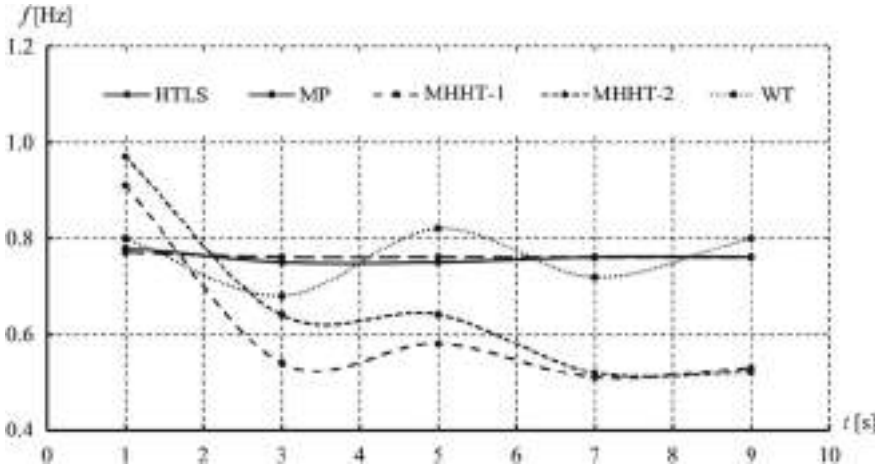

Fig. 12 The 1st mode frequency estimation results (real frequency equals 0.79 Hz)

2. During the ensemble methods results generalization it is considered that
   a. results obtained with different ensemble's main group methods are equally reliable;
   b. the modes with the frequency differences less than Δf_2 are the same modes:
      (1) frequency and amplitude of the generalized mode is defined as the mean of corresponding parameters, calculated with using of main group signal analysis methods (with taking into account modes filtering by A' and A'' threshold values during the single method results generalization);

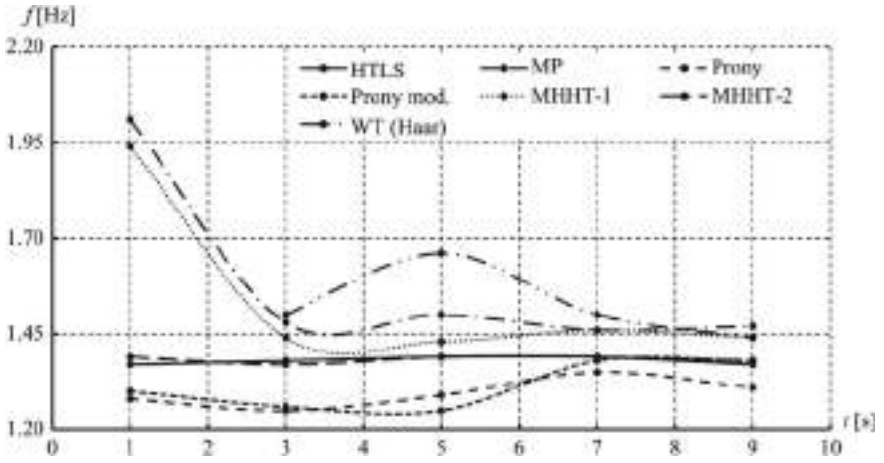

Fig. 13 The 2nd mode frequency estimation results (real frequency equals 1.34 Hz)

Table 3 Spectral analysis results of the TS-4 with "white" noise and 2 s sample window width

Analysis method	Conditions of adequate assessment	
	Adequate assessment of modes' frequencies	Adequate assessment of modes' amplitudes
HTLS	SNR > (10…20 dB)	partially provided, SNR > (60…80 dB)
MP	SNR > (10…20 dB)	partially provided, SNR > (60…80 dB)
Prony	SNR > (80…100 dB)	SNR > (80…100 dB)
Prony modified	SNR > (40…60 dB)	partially provided, SNR > (40…60 dB)
Morlet WT	not provided	not provided
MHHT-1	not provided	not provided
MHHT-2	not provided	not provided

(2) damping of the generalized mode is considered as stable negative in the case of at least one of the main group analysis method has identified damping of this mode as stable negative;
(3) damping of the generalized mode is considered as stable positive if all the main group analysis methods have identified damping of this mode as stable positive;

c. generalized mode is considered as existing if it was identified by at least two methods of the main group or by one method of the main group and by the method of the additional group;
d. generalized mode is considered as dangerous if it's amplitude is greater than predetermined threshold value A_{lim}.

3 Two Examples of Electromechanical Oscillations' Modes Identification Using PMU Data

Proposed generalization algorithm was used to identify dominant modes' parameters in the signals measured by PMU in the Interconnected Power System of Ukraine. The measured signal (see Fig. 14, denote this signal by MS-1) is the change in time the active power flow of the phase A of the 750 kV overhead transmission line connecting the Khmelnytska Nuclear Power Plant and Chornobylska Nuclear Power Plant on February 16, 2016.

Some partial results of the MS-1 dominant modes' parameters identification using proposed algorithm are presented in Table 4. Data processing was carried out with such settings: $\Delta f_1 = 0.02\text{Hz}$, $\Delta f_2 = 0.05\text{Hz}$, $\Delta = 0.10\text{Hz}$, $A^{'} = 1\text{MW}$.

Table 4 data analysis shows the presence in the signal of the main dominant mode with variable frequency 0.29…0.35 Hz and strongly negative damping. Second mode with variable frequency 0.59…0.70 Hz also has negative damping, but much lower amplitude. Analyzed signal characterized by the low SNR that is why Prony method was not able to identify modes parameters.

The second signal is the phase A voltage measured on the 750 kV bus of the Kyivska substation on February 18, 2017 (see Fig. 15, denote this signal by MS-2).

Partial results of the MS-1 dominant modes' parameters identification using proposed algorithm are presented in Table 5. Data processing was carried out with such settings: $\Delta f_1 = 0.02\text{Hz}$, $\Delta f_2 = 0.05\text{Hz}$, $\Delta = 0.10\text{Hz}$, $A^{'} = 0.1\text{kV}$.

Table 5 data analysis shows that dominant modes with the frequencies approximately equal 0.60 and 0.80 Hz and with the strong negative damping are present in the signal.

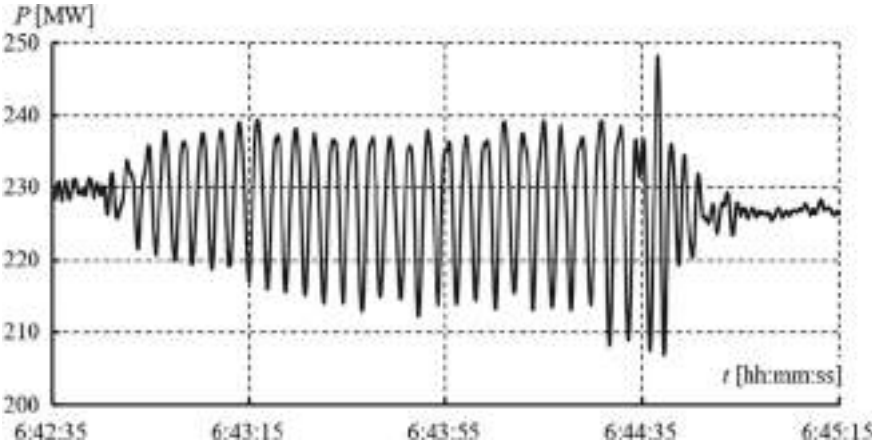

Fig. 14 750 kV transmission line phase A active power change in time

Table 4 MS-1 modes' parameters identification results

Time period [s]	Analysis methods												Summarization		
	HTLS			MP			Prony			Prony modified					
	f, Hz	A, MW	ξ	f, Hz	A, MW	ξ	f, Hz	A, MW	ξ	f, Hz	A, MW	ξ	f, Hz	A, MW	damp
5 s sample window width															
1–6	0.53	1.1	−0.01	0.53	1.1	−0.01	–	–	–	0.58	1.7	−0.04	0.53	1.1	–
2–7	0.29	3.7	−0.75	0.31	3.0	−0.70	–	–	–	0.54	1.9	−0.09	0.30	3.4	–
3–8	0.63	1.3	−0.09	0.63	1.3	−0.09	–	–	–	0.51	2.0	−0.16	0.63	1.3	–
4–9	0.31	1.2	−0.03	0.31	1.2	−0.05	–	–	–	–	–	–	0.31	1.2	–
…	…	…	…	…	…	…	…	…	…	…	…	…	…	…	…
7–12	0.46 0.66	1.4 1.1	−0.11 −0.06	0.46 0.66	1.4 1.1	−0.11 −0.06	–	–	–	–	–	–	0.46 0.66	1.4 1.1	– –
8–13	0.70	1.9	−0.02	0.70	1.9	−0.05	–	–	–	–	–	–	0.70	1.9	–
9–14	0.43 0.68	2.8 1.6	−0.13 −0.02	0.43 0.68	2.7 1.6	−0.13 −0.01	–	–	–	0.58	1.5	0.018	0.43 0.68	2.8 1.6	
…	…	…	…	…	…	…	…	…	…	…	…	…	…	…	…
17–22	0.27	10.2	−0.12	0.27	10.1	−0.12	–	–	–	0.28	4.6	0.07	0.27	8.3	–
18–23	0.29	7.9	−0.04	0.29	7.9	−0.04	–	–	–	0.29	5.7	0.04	0.29	7.2	–
…	…	…	…	…	…	…	…	…	…	…	…	…	…	…	…
120–125	0.33 0.67 1.06	21.4 3.4 3.2	−0.05 −0.04 −0.06	0.33 0.67 1.06	21.4 3.5 3.1	−0.05 −0.04 −0.06	–	–	–	0.33	12.4	0.066	0.33 0.67 1.03	18.4 3.4 3.2	– – –
121–126	0.33 0.64	21.2 4.6	−0.02 −0.08	0.33 0.64	21.4 4.4	−0.02 −0.08	–	–	–	0.35	17.4	0.012	0.34 0.64	20.0 4.5	– –

(continued)

Table 4 (continued)

Time period [s]	Analysis methods												Summarization		
	HTLS			MP			Prony			Prony modified					
	f, Hz	A, MW	ξ	f, Hz	A, MW	ξ	f, Hz	A, MW	ξ	f, Hz	A, MW	ξ	f, Hz	A, MW	damp
122–127	0.34 0.59 0.84	9.3 3.0 1.0	0.083 0.046 0.014	0.34 0.59	9.3 2.9	0.084 0.050	–	–	–	0.38	21.2	−0.060	0.35 0.59	13.3 3.0	– +

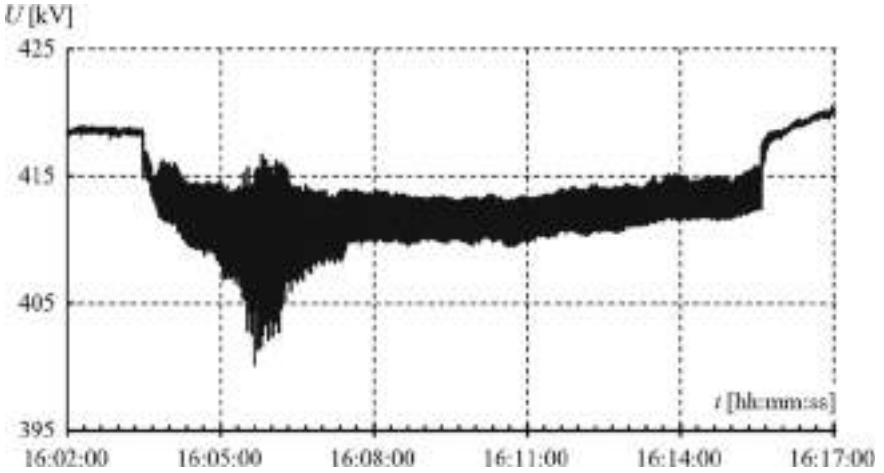

Fig. 15 750 kV substation bus phase voltage change in time

4 Conclusions

Researches results show that not all signal analysis methods are suitable for real-time application in monitoring systems to reliably identify LFO modes.

Customization and use of an ensemble of preselected the most suitable signal analysis methods to identify LFO modes in real time leads to some differences in the results obtained, but together with the proposed procedure for processing these results such approach makes it possible to more reliably obtain adequate estimates of the LFO modes parameters.

Obvious expediency of using this approach to identifying LFO modes is confirmed by the results of its application to synthesized test and real signals.

Table 5 MS-2 modes' parameters identification results

Time period [s]	Analysis methods												Summarization		
	HTLS			MP			Prony			Prony modified					
	f, Hz	A, kV	ξ	f, Hz	A, kV	ξ	f, Hz	A, kV	ξ	f, Hz	A, kV	ξ	f, Hz	A, kV	damp
5 s sample window width															
102–107	0.90	1.4	−0.05	0.90	1.4	−0.05	–	–	–	0.90	0.4	0.05	0.9	1.1	–
103–108	0.89	1.6	−0.03	0.89	1.6	−0.03	0.71	2.6	0.769	0.89	0.7	0.03	0.89	1.3	–
	1.80	0.2	−0.04	1.80	0.2	−0.04							1.80	0.2	–
104–109	0.90	1.7	−0.02	0.90	1.7	−0.02	0.92	0.7	0.567	0.90	1.1	0.02	0.9	1.3	–
	1.81	0.3	−0.03	1.81	0.3	−0.03				1.64	1.5	−0.62	1.81	0.3	–
105–110	0.19	0.9	−0.40	0.19	0.9	−0.40	1.06	0.9	0.19	0.89	1.4	0.01	0.19	0.9	–
	0.89	2.0	−0.02	0.89	2.0	−0.02							0.89	1.8	–
	1.79	0.2	−0.01	1.79	0.2	−0.01				1.83	0.4	−0.13	1.80	0.3	–
…	…	…	…	…	…	…	…	…	…	…	…	…	…	…	…
201–206	0.62	1.9	−0.02	0.62	1.9	−0.02	0.81	3.1	0.14	0.52	3.6	−0.64	0.62	1.9	–
	0.80	3.6	−0.03	0.80	3.6	−0.03							0.80	3.5	–
	1.33	1.2	−0.08	1.33	1.2	−0.08				0.81	4.6	−0.05	1.33	1.2	–
	1.58	0.7	−0.03	1.58	0.7	−0.03				2.59	0.4	−0.58	1.58	0.7	–
202–207	0.54	2.6	−0.11	0.54	2.6	−0.11	0.80	2.3	0.13	0.56	4.1	−0.45	0.54	3.1	–
	0.83	2.3	0.01	0.83	2.3	0.01				0.79	2.8	−0.01	0.82	2.5	–
203–208	0.54	4.6	−0.12	0.54	4.6	−0.12	0.78	3.1	0.09	0.62	9.6	−0.29	0.54	4.6	–
	0.68	5.7	−0.42	0.68	5.7	−0.42							0.69	5.2	–
	0.83	2.6	0.01	0.83	2.6	0.01							0.82	2.8	+
	1.82	0.3	0.00	1.82	0.3	0.00				0.73	3.8	−0.00	1.82	0.3	+

References

1. Report on Power System oscillations experienced in Indian Grid on 9th. 10th. 11th and 12th August 2014. POSOCO. (2014)
2. Grigsby, L.L.: The power system stability and control. Taylor & Francis Group. London. (2001). https://doi.org/10.4324/b12113
3. Kundur, P.: Power system stability and control. McGraw-Hill, New York (1994)
4. Debasish, M., Chakrabarti, A., Sengupta, A.: Power system small signal stability analysis and control. Waltham Mass: Academic Press. London. (2014). doi: https://doi.org/10.1016/C2013-0-18470-X
5. Bikash, P., Balarko, Ch.: Robust control in power systems. Springer Inc. New York. (2005). doi: https://doi.org/10.1007/b136490
6. Zhang, G.: EPRI power systems dynamics tutorial. Final Report. Electric power research institute. Palo Alto. (2009)
7. Wang, X.-F., Song, Y., Irving, M.: Modern power systems. Springer Science & Business Media. New York. (2010). doi: https://doi.org/10.1007/978-0-387-72853-7
8. Prasertwong, K., Mirthulananthan, N., Thakur, D.: Understanding low frequency oscillation in power systems. Int. J. Electr. Eng. Educ. **47**(3), 248–262 (2010). https://doi.org/10.7227/IJEEE.47.3.2
9. Yang, J.-Z., Liu, C.-W.-G.: A hybrid method for the estimation of power system low-frequency oscillation parameters. IEEE Trans. Power Systems **22**(4), 2115–2123 (2007). https://doi.org/10.1109/PES.2008.4595986
10. Shi, J.H., Li, P., Wu, X.C. et al.: Implementation of an adaptive continuous real-time control system based on WAMS. Paper presented at the CIGRÉ 2-nd International Conference "Monitoring of Power System Dynamics Performance". Saint Petersburg. Russian Federation. 28–30 April 2008. (2008)
11. UCTE Final Report—System Disturbance on 4 November 2006 (2007). https://www.entsoe.eu/fileadmin/user_upload/_library/publications/ce/otherreports/Final-Report-20070130.pdf. Accessed 06 Mar 2021
12. Duan, G., Sun, X., Wu, J.T. et al.: Low frequency oscillation monitoring and assessment in CSS200 WAMS. Paper presented at the CIGRÉ 2-nd International Conference "Monitoring of Power System Dynamics Performance". Saint Petersburg. Russian Federation. 28–30 April 2008. (2008)
13. Arango, O.J., Sanchez, H.M., Wilson, D.H.: Low frequency oscillations in the Colombian power system—identification and remedial actions. Paper presented at the CIGRE Session. Paris. France. August 22–27. (2010)
14. Despa, D., Mitani, Y., Li, Ch. et al.: Inter-area power oscillation mode for Singapore–Malaysia interconnected power system based on phasor measurements with auto spectrum analysis. In Proceedings of the 17th Power Systems Computation Conference (PSCC) 2011. Stockholm. Sweden. 22–26 August 2011. vol 2: 847–852. (2011)
15. Analysis of CE Inter-Area Oscillations of 19 and 24 February 2011. ENTSO-E SG SPD Report. (2011). https://www.entsoe.eu/fileadmin/user_upload/_library/publications/entsoe/RG_SOC_CE/Top7_110913_CE_inter-area-oscil_feb_19th_24th_final.pdf. Accessed 06 Mar 2021
16. Report on the Grid Disturbances on 30th July and 31st July 2012. (2012). http://www.cercind.gov.in/2012/orders/Final_Report_Grid_Disturbance.pdf. Accessed 06 Mar 2021
17. Khanna, R., Manrai, P.: Damping of low frequency oscillations using GA based unified power flow controller. Intern. J. Eng. Adv. Technol. **2**(1), 307–311 (2010)
18. Zhang, L., Harnefors, L., Rey, P.: Power system reliability and transfer capability improvement by VSCHVDC (HVDC Light©). Paper presented at the CIGRÉ Regional Meeting "Security and Reliability of Electric Power Systems". Tallinn. Estonia. 18–20 June 2007. (2007)
19. Abraham, R.J., Patra, D.A.: Damping oscillations in Tie-power and Area frequencies in a Thermal power system with SMES-TCPS combination. J. Elect. Syst. **7**(1), 71–80 (2011)

20. Neely, J.C., Byrne, R.H., Elliott, R.T. et al.: Damping of inter-area oscillations using energy storage. In Proceedings of the 2013 IEEE Power & Energy Society General Meeting. Vancouver. British Columbia. Canada. 21–25 July 2013. Curran Associates. Inc.. pp. 2808–2812. (2013). doi: https://doi.org/10.1109/PESMG.2013.6672775
21. Sui, X., Tang, Y., He, H.: Energy-storage-based low-frequency oscillation damping control using particle swarm optimization and heuristic dynamic programming. IEEE Trans. Power Syst. **29**(5), 2539–2548 (2014). https://doi.org/10.1109/TPWRS.2014.2305977
22. Febres, C.A.T., Araujo, P.B., Furini, M.A.: Damping of low-frequency oscillations by supplementary control of power system stabilizers. Trends Appl. Comput. Mathemat. **9**(2), 223–232 (2008). https://doi.org/10.5540/tema.2008.09.02.0223
23. Kamwa, I., Samantaray, S.R., Joos, G.: Optimal integration of disparate C37.118 PMUs in wide-area PSS with electromagnetic transients. IEEE Trans. Power Syst. **28**(4), 4760–4770. (2013). doi: https://doi.org/10.1109/TPWRS.2013.2266694
24. Messina, A.R., Vittal, V.: Nonlinear. Non-stationary analysis of interarea oscillations via Hilbert spectral analysis. IEEE Trans. Power Syst. **21**(3), 1234–1241. (2006). doi: https://doi.org/10.1109/TPWRS.2006.876656
25. Huang, N.E., Shen, Zh., Long, S.R. et al.: The empirical mode decomposition and the Hilbert spectrum for nonlinear and non-stationary time series analysis. Proc. Royal Soc. A **454**(1971), 903–995. (1998). doi: https://doi.org/10.1098/rspa.1998.0193
26. Sergienko, A.B.: Tsifrovaya obrabotka signalov (Signal digital processing). BHV-Peterburg. Sankt-Peterburg. (Rus). (2011)
27. Marple, S.L., Jr.: Digital spectral analysis. Dover Publications. Inc., New York (2019)
28. Thomson, D.J.: Spectrum estimation and harmonic analysis. Proc. IEEE **70**(9), 1055–1096 (1982). https://doi.org/10.1109/PROC.1982.12433
29. Liu, G., Quintero, J., Venkatasubramanian, V.: Oscillation monitoring system based on wide area synchrophasors in power systems. In Proceedings of the 2007 iREP Symposium-Bulk Power System Dynamics and Control – VII Revitalizing Operational Reliability. Charleston. South Carolina. USA. 19–24 August 2007. Curran Associates. Inc. pp 340–350. (2007). doi: https://doi.org/10.1109/IREP.2007.4410548
30. Hua, Y., Sarkar, T.K.: Matrix pencil method for estimating parameters of exponentially damped/undamped sinusoids in noise. IEEE Transactions on Acoustics. Speech. Signal Proc. **38**(5), 814–824. (1990). doi: https://doi.org/10.1109/29.56027
31. Gong, Y., Guzmán, A.: Synchrophasor-based online modal analysis to mitigate power system interarea oscillation. J. Reliable Power **2**(2), 42–47 (2011)
32. Dyakonov, V.P.: Veyvlety. Ot teorii - k praktike (Wavelets. From the theory – to the practice). Solon-R. Moskva. (Rus). (2004)
33. Stockwell, R.G., Mansinha, L., Lowe, R.P.: Localization of the complex spectrum: the S transform. IEEE Trans. Signal Process. **44**(4), 998–1001 (1996). https://doi.org/10.1109/78.492555
34. Assous, S., Boashash, B.: Evaluation of the modified S-transform for time-frequency synchrony analysis and source localization. EURASIP J. Adv. Signal Proc. **49**(1). (2012). doi: https://doi.org/10.1186/1687-6180-2012-49
35. Rilling, G., Flandrin, P., Gonçalves, P.: On empirical mode decomposition and it's algorithms. In Proceedings of the 6th IEEE/EURASIP Workshop on Nonlinear Signal and Image Processing (NSIP '03). Grado. Italy. 8–11 July 2003. (2003)
36. Battista, B.M., Knapp, C., McGee, T., et al.: Application of the empirical mode decomposition and Hilbert-Huang transform to seismic reflection data. Geophysics **72**(2), H29–H37 (2007). https://doi.org/10.1190/1.2437700
37. Ding, Q., Kay, S.: Inconsistency of the MDL: on the performance of model order selection criteria with increasing signal-to-noise ratio. IEEE Trans. Signal Process. **59**(5), 1959–1969 (2011). https://doi.org/10.1109/TSP.2011.2108293
38. Kitamura, M., Takada, J., Araki, K.: A model order estimation in the matrix pencil method for the transient response of a microwave circuit discontinuity. IEICE Trans. Electr. **E82-C**(11), 2081–2085. (1999). doi: 10.1.1.29.7869

39. Butkevych, O.F.: Problemno-orientovanyi monitoryng rezhymiv OES Ukrainy (Problem-oriented monitoring of Ukrainian IPS's operational conditions). Tekhnichna elektrodynamika **5**, 39–52. (Ukr) (2007)
40. IEEE Recommended Practice for Excitation System Models for Power System Stability Studies (IEEE Std 421.5–2016)
41. Fault recorder FR947-M PowerProbe:LogicLab S. R. L. (2009)
42. Liu, Y., Zhan, L., Zhang, Y., et al.: Wide-area measurement system development at the distribution level: an FNET/GridEye example. IEEE Trans. Power Delivery **31**(2), 721–731 (2016). https://doi.org/10.1109/TPWRD.2015.2478380
43. Thambirajah, J., Thornhill, N.F., Pal, C.B.: A multivariate approach towards inter-area oscillation damping estimation under ambient conditions via independent component analysis and random decrement. IEEE Trans. Power Syst. **26**(1), 315–322 (2011). https://doi.org/10.1109/TPWRS.2010.2050607

Hybrid Diagnostics Systems for Power Generators Faults: Systems Design Principle and Shaft Run-Out Sensors

Ievgen Zaitsev, Anatolii Levytskyi, and Victoriia Bereznychenko

Abstract One of the ensuring stable and reliable electricity production problems is determine the technical condition of the means of generating electricity. This is necessary since more than 80% of the electricity in the Ukraine energy system is generate by powerful generators of nuclear power plants (NPP), thermal power plants(TPP), hydroelectric power plants (HPP) and pumped storage power plants (PSPP) with wear from 70 to 90%. One of the ways out of the situation it is the replacement of equipment on the new. This approach requires the attraction of significant monetary investments, which in the context of the global economic crisis is a rather difficult task. Another way is to use systems for diagnosing the actual technical state of powerful generators. The use of such systems will improve operational efficiency equipment to reduce the time and cost of maintenance and repairs, reduce the risk of accidents and failures by timely detection of defects in the machine during its operation, as well as make the right decisions to eliminate them and move from scheduled repairs to repairs on the actual condition of powerful generators.To assess the condition of generators as mechanical systems, diagnostic systems in addition to vibration sensors are use meters of mechanical parameters—the air gap between the stator and the rotor, the radial and axial beating of the shaft, mechanical forces in the tensioning prisms and others special sensors. Improving the metrological and technical characteristics of such meters will make better the control and diagnostic systems, and as a result—increase the reliability and durability of machines. So, this chapter presents:

– Ukraine power generators current state;
– design principle for developing hybrid fault control and diagnosis system for diagnostics mechanical faults in power generators;
– capacitive shaft run-out sensors structures;
– influence work magnetic field and temperature on capacitive shaft run-out sensor characteristics;
– influence technological factors on capacitive shaft run-out sensor characteristics.

I. Zaitsev (✉) · A. Levytskyi · V. Bereznychenko
Institute of Electrodynamics of NAS of Ukraine, Kyiv, Ukraine
e-mail: zaitsev@i.ua

O. Kyrylenko et al. (eds.), *Power Systems Research and Operation*, Studies in Systems, Decision and Control 388, https://doi.org/10.1007/978-3-030-82926-1_4

Keywords Generator · Measurement · Experimental research · Capacitive sensor · Distance · Grounded surface · Run-out

1 Introduction

Energy—a complex set of processes for obtaining natural energy resources, conversion to working types of energy and their transmission [1]. Under the terms of the Association Agreement with the EU and the Energy Community Treaty, it is envisaged that Ukraine must change the model of the electricity market, as required by the Third Energy Package, and move towards a modern, open and competitive pan-European electricity market. energy from renewable sources.

In June 2017, Ukraine signed an agreement with the Association of Network Operators ENTSO-E on the terms of the future integration of Ukraine's energy systems with the energy system of continental Europe [2]. From that moment on, the processes taking place in a particular country directly affect the development of energy in other countries. In this regard, the issues of the technical condition of the electrical equipment of the UPS of Ukraine, constant control over them and their safe operation in general is one of the priority tasks of the energy industry.

2 Current State of Power Generators in Ukraine

Integrated power system of Ukraine consists of 49 power plants with 16 heat, 8–hydro, 6–wind, 6–sleepers, 6–heat and power plants, 4–atomic and 3–hydroaccumulating power plants [3]. According to the Ministry of Energy of Ukraine, in January-August 2020, the volume of electricity production by power generating enterprises that are part of the IES of Ukraine reached 96,337,500,000 kWh. At the same time, TPPs and CHPPs generated 31,212,400,000 kWh of electricity (32.4%), nuclear power plants 51,135,600,000 kWh (53.1%) were produced, electricity generation by HPPs and PSPs was 5,016,900,000 kWh (5.2%), For 8 months of 2020 RES (WPP, SPP, biomass) electricity production amounted to 7657.0 million kW·h (7.9%) [4].

As shown on Fig. 1, the largest share of electricity production falls on the NPP, however, it should be remembered that over the past 7 years, the NPP faced the maximum tasks for the production of electricity due to the disconnection of the stations located in the Autonomous Republic of Crimea from the UPS of Ukraine and in the eastern part of Ukraine. The need to cover the shortage of electricity has led to the postponement of scheduled and anticipatory repairs of some power units in which turbine generators are the most unreliable components [5] and in most cases do not have standard systems for online monitoring of their actual technical condition. All this can lead to the exit of the equipment from working condition in the nearest future.

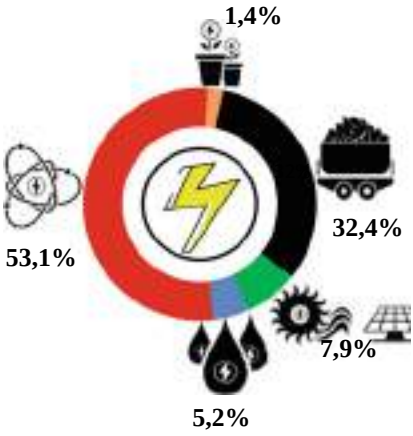

Fig. 1 The structure of electrical energy production in Ukraine

Thermal power plants are next in terms of productivity. Unfortunately, today TPPs operate at an extremely low utilization factor of the installed capacity. The technical condition of the majority of TPP generators is characterized by the fact that the service life of the majority of machines, according to regulatory documents, is already running at the end or will end in the coming years, and therefore it is necessary to carry out urgent work to update and modernize machines [6–11], not always are appropriate given the Paris Climate Agreement. In accordance with which the transition to the reduction of greenhouse gas emissions and the complete decarbonization of the energy system are expected. In the next 10–15 years Ukraine has undertaken to bring the levels of emissions of toxic substances into the atmosphere from coal-fired TPPs in line with European standards, or to close TPPs that violate the maximum permissible levels of emissions [2].

The third main supplier of electricity is generation from renewable energy sources, which include sleepy, wind and hydropower. Today, hydropower is the only "green" energy sector that can collect surplus energy and save it until there is a shortage in the network. In addition, hydropower, unlike solar and wind, are almost independent of weather conditions and can cover electricity generation deficits at any time. HPPs can adapt very quickly and at any time to the changing needs of the energy market, increasing or decreasing production. For example, in large power systems, most of the generation may be the capacity of thermal and nuclear power plants, which are not able to quickly reduce electricity output during the night reduction of energy consumption or do so with significant losses. This leads to a significant increase in the commercial cost of peak electricity compared to that generated at night. In such conditions, the use of PSP is economically feasible and increases both the efficiency of other capacities (including transport) and the reliability of the system as a whole. Reservoirs can protect against floods by retaining excess water. In addition, reservoirs perform an important social function: as reservoirs of drinking water, as a place of summer recreation, as a plane for various water sports, as water supplies for irrigation,

etc. The main advantages of HPPs and PSPs are the lack of costs for “fuel” and long-term “use” (up to 100 years.) As a result, the final cost of electricity is much lower than in other types of power plants [12].

However, during operation under the influence of different conditions and modes of operation the initial state of the equipment is constantly worse, reduced operational reliability, which leads to an increased risk of failure. In addition, the situation significantly complicated by the peculiarities of operation of generating equipment in recent years, which are characterized by a large number of starts and stops, “extreme” maneuverability of active-reactive load and other things that inevitably accelerate the operation of units and increase their damage.

The complete replacement of the generators connected to the Ukraine integrated power system with the new ones in the short term is too problematic. Therefore, ensuring reliable and trouble-free operation of generating equipment necessitates the use of monitoring and diagnostic systems together with full or partial modernization of generators and other power grid equipment of the Ukraine integrated power system [13–26], to enable power plants to provide ancillary services [27–32], and ensuring reliable operation of transmission lines [28, 33]. Usually, after modernization, the nominal capacity of the generating equipment increased by 8 - 15% and stable operation of additional equipment ensured.

Before integrating any system, it is necessary determine the list of requirements that it must meet. In this case, the system must be able to detect dangerous situations for the generator and provide information about the defects of individual components.

Shaft beam and vibration control is widely used to obtain information on the condition of the hydrogenerator, as the increase in shaft beating and vibration of the supporting structures of the hydraulic unit clearly indicate the deterioration of the technical condition and its performance, especially during operation under load or in transient modes [34].

Measurement of vibration and additional parameters of shaft beating allows to estimate the level of vibration and to establish which perturbing forces—mechanical, hydraulic or electric—cause increased vibration, but does not allow determining the causes of these perturbing forces. To determine the causes, it is necessary to use additional sensors that directly measure the parameters of the main components of the generator through the control of their thermo mechanical condition [35]. In addition, in order to be highly informative about the results of the study, it is necessary to correctly select sensors of the study to monitor objects, taking into account the complex relationships of defects in the generator nodes with the diagnostic parameters of the shaft [36–47].

3 Design Principle of Hybrid Faults Diagnosis System in Power Generators

3.1 Hybrid Faults Diagnosis System Architecture

The architecture of electric machines faults diagnostic system incorporates a wide range of the mechanical sensors for control many technological parameters. However, in practice, during operation of the machine, external influences (electromagnetic fields, temperature, etc.) act on the measuring equipment. For avoiding external influence on the sensor and control systems operation unit are used fiber optic and other electro-optical components. The benefits of the optics components make possible to use HFOS in applications for measurement parameters of mechanical faults in working environment of large generator with high-EMI field, temperature, pressure, explosive, and noisy, etc. [26, 32, 45, 48, 49].

Figure 2 shows simplified structure of control system processing tools with a complete mapping of microelectronic and optoelectronic components in functional groups structure with sensors. Figure 2 used next notation: PSCS—primary special capacitive sensor of the mechanical parameters with capacitance-to-digital converter on board; SW—switch; SigPr—microcontroller unit or signal processing

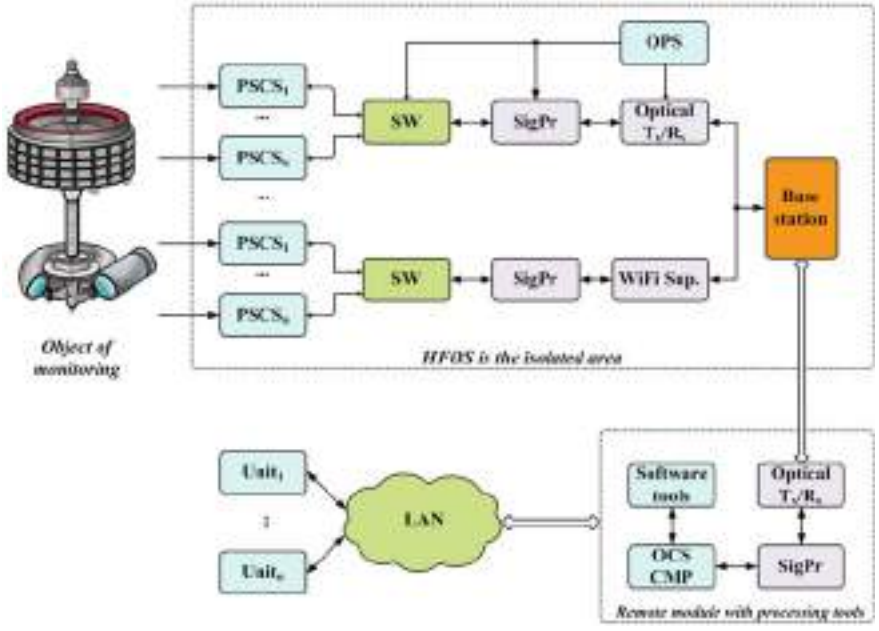

Fig. 2 Structure of the monitoring system

unit; OPS—converter optical energy to power supply of sensor unit; Optical Tx/Rx—in direct way it's converter optical digital code to electrical digital code with digital controller and reversed way it's electrical to optical digital code; OCS CMP—control systems operation unit for large generator fault diagnostic system.

The system consists from two parts: sensors in isolated area and monitoring system processing tools. The monitoring system processing tools located at isolated area on safe distance which provides a low level of external influences (electromagnetic fields, temperature, etc.) [45, 50].

Group of unit of HFOS in isolated area integrates a capacitance-to-digital converter (CDC) AD7745/AD7746 from Analog Devices, Inc. (Norwood, MA, USA) [51] on primary capacitive sensor circuit board material made from FR4 copper clad laminate printed circuit board (PCB) [46], Optical Tx/Rx implementations by analogy described in [44] with low power microcontroller and vertical cavity surface emitting semiconductor laser with very low threshold current, semiconductor photovoltaic energy converter (labeled as the "OPS").

In the system described in the work [45], a pair of optical fibers connects the OPS and vertical cavity surface emitting semiconductor laser to the external system to receive power energy by optical cable and measurements data by fiber optic. Moreover, one optical fiber to receive control data to microcontroller from main system used.

The group of blocks in safe area integrates "optical Tx/Rx", SigPr system and digital part with special software solution for detection and monitoring mechanical faults of the electric machines. In the remote zone there is a user interface through which the operator controls the operation of the system and receives information about the state of the object. Providing user "Unit" access to the data received from the sensors, which are contained in the system "Remote module" can be done in two ways through direct access and connection via LAN.

The proposed hierarchical structure of the monitoring system allows implementing the concepts of Smart Grid. Application of Smart Grid in monitoring system allows to carry out: initial selection and preparation of diagnostic signals; primary mathematical processing, making primary diagnostic decisions, signaling of possible defects; accumulation, full-fledged processing and in-depth analysis of data, rapid response to alarms from the lower level, making diagnostic decisions about the object as a whole, archiving statistics. The main advantages of the proposed structure: multilevel, implemented principles of Smart Grid, implementation in the form of a distributed modular complex, the ability to use both wired and wireless technologies.

3.2 Microelectronic Components Work Principle

The base of the principle of operation the system shows on Fig. 2 is described in [45] and is as follows: the primary measuring transducer (sensing element PSCS) converts the value of a controlled parameter of a mechanical defect into a digital code like NRZ. Then the SigPr communication subsystem collects measurement information

from the PSCS and converts the information data into a modulated optical signal [45]. The signal is transmitted by optic fiber-cable (OF) to optical Tx/Rx module where optical signal converted into an electrical signal. The electrical signal as digital code like NRZ send to processing tools as data information processing system OCS CMP and use for analysis with special software tools. In the case of the transmission of digital control data signals for PSCS transducers, the OCS CMP system works in the similarly [45]. Architecture of sensor and network with sensor was detail analysis in work [45, 50, 52].

For converter capacitance value of primary sensor to digital code chosen capacitance-to-digital converter (CDC) AD7745/AD7746 (Analog Devices, Inc., Norwood, MA, USA) with temperature sensor. The use of a 24-bit sigma-delta converter allows the resolution of the measurement range of an informative capacity of 4fF [51].

3.3 Power Optoelectronics Components Work Principle

The benefits of fiber optics make it possible to use capacitive censor in applications for measurement mechanical parameters of power generator in their working environment with high-EMI and magnetic field, temperature, pressure, hazardous, explosive, noisy and etc. Data sent by data optic fiber. Power supply for primary measuring converters HFOS in an isolated area can transmit by the following ways [53–64]:

- using battery power wherein energy from sources located directly beside of sensor be used;
- using energy single fiber-optical channel, wherein energy transmission from optically powering system optical energy into single optical fiber be used;
- using energy multiple fiber-optical channels, wherein energy transmission from optically powering system optical energy into multiple optical fiber be used;
- using data-energy fiber-optical channel, wherein used multiplexing energy and data for transmission into single core fiber-optical channel by “Wavelength-Division Multiplexing".

Using appropriate WDM multiplexing and demultiplexing technology to accommodate also the power delivery system to one OF with control and measuring signals transmission systems we obtain more compact solution. And this is solution can be used for power of HFOS. For more optical power for HFOS we use more than one fiber optic power channels.

In the system that we are reporting, the second option was used when light connected to one optical fiber with a unique photovoltaic converter on the one hand, and a powerful laser that was located in SigPr on the other, was used to power it. For photovoltaic energy converter it proposed to use semiconductor photovoltaic cells based on crystalline GaAs.

3.4 Software Solution Work Principle

Remove module of the monitoring system consist optical converters with microcontroller for communication and a personal computer, which functions under the control of specialized software. Its functions designed for [65]:

- the definition of the class of possible defects (the most important or most frequently encountered) that must be identified;
- selection of diagnostic signals available for measurement, and control points on the object under study;
- development of a mathematical model of the diagnostic object, the analysis of which allows to substantiate possible diagnostic parameters;
- development of algorithms for obtaining numerical values of selected diagnostic parameters;
- construction of decisive rules for identifying and classifying defects; creation of means implementing certain steps of the diagnostic process from the selected measurement and diagnostic signals before making diagnostic solutions.

The system software (primary data acquisition and processing module) consists of the following parts: a data processing software module from CDC and CDC control, a microcontroller configuration module, a primary data processing module. The special designed software is used for the control system for data collection, processing and analysis. This software is used for the operation control CDC AD7745/AD7746, to organize other hardware and software modules, for the primary process implementation [66], data collection and data transmission from the transducers to designed devices for the secondary processing, for the statistical data analysis, storage and control data display in a simple form for the operator.

The CDC control module algorithm for converter capacitive value to code and receive the digital data to the monitoring system use algorithm from [51] for "AD7746", The data exchange for designed to provide the organization of data exchange between hardware and software monitoring system and CDC.

Operations of calculating the value of the mechanical parameters special software solution is used. Processing of the received data in the control module of mechanical parameters state of the control is use for the value of the mechanical parameter and analyzed its status and changes. In turn, obtained at the work of the module of mathematical processing and module of automatic control of the state of the electrical equipment node is transferred to the data storage organization module for database management based on the history of measurements. In this case, it is possible to create knowledge bases with diagnostic features, which depend on the value of the physical parameter that is control of the certain state of the power equipment.

The connection of the monitoring system and HFOS module in the isolated area is transfer with developed communication protocol for the fiber-optic line communication. In addition, the module for input and output information SigPr is designed for organize the exchange data between the modules of the system.

4 Capacitive Shaft Run-Out Sensors for Diagnostics Shaft Faults in Power Generators: Work Principle and Characteristics

Improving the accuracy of determining a significant number of defects of rotating machines, in which the main unit is plain bearings can be done by measuring the relative and absolute parameters of the beating of the shafts [44, 45, 67]. To measure the beating parameters of the shafts, it is advisable to use capacitive contactless sensors [68–71].

When designing and manufacturing sensors, it is necessary to take into account operational factors—parameters and type of environment in which the sensor is operated, technological capabilities of sensor placement to control changes in object parameters, etc., which affects its metrological characteristics and manufacturing technology. So, this section is devoted to the study of the limits of application of the sensor and presents the research result as follows:

- design shaft run-out sensor for generator fault control system is developed;
- it's sensor conversion function is calculated depending on the change of the air gap between the active plane of the sensor and the shaft surface;
- the influence of temperature change in the range –30 to + 80 °C and electromagnetic field on the operating characteristics of the sensor was studied;
- the influence of technological factors on the transformation function is investigated.

4.1 Sensors Located and Construction

Capacitive sensors can be applied for measuring different kind of non-electrical quantities [52, 54, 72], such as mechanical parameters of electric machines equipment: geometrical dimensions change, displacement and vibration of grounded surfaces, air gap and position of the object, core compression ratio and others. Capacitive mechanical sensors are the most widely used non-optical sensors in short-range positioning applications owing to their excellent resolution [52].

The principle of measurement of a capacitive sensor is based on the change in the capacitance with the distance of capacitor with parallel electrodes. Figure 3 has shown the typical design of coplanar sensor. Electrodes 1 and 2 separated from each other by thin dielectric spaces in width h, which depends on the technology of manufacturing [52].

Electrical capacity C of coplanar sensor between electrodes 1 and 2 will change when moving a grounded surface as imitation changes of the air gap between sensor and shaft plane [50].

Existing capacitive *C* sensors made in the shape of flat capacitor geometry do have high values of sensitivity. In this case, the electrical *C* capacitance sensor depends on the size of the air gap d and can be written as [47, 71]:

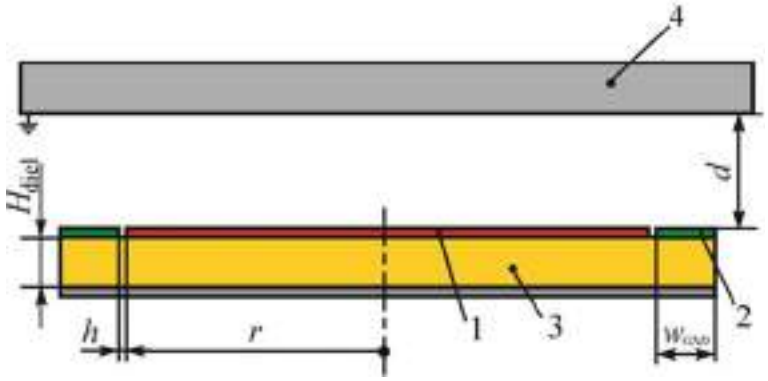

Fig. 3 Capacity sensor with electrodes

$$C = \varepsilon_0 \varepsilon_r \pi r^2 / d. \tag{1}$$

Based on this principle by Eq. (1) was implemented mechanical sensor for measuring value of shaft run-out and other mechanical parameters in the generator.

4.2 Determination Sensor Response Characteristic

Figure 4. shows scheme of the placement run-out sensor and control system for measure the run-out of a shaft. Sensors are located according to [73]. In this case, the shaft beating meters installed at several levels near the shaft of the hydrogenerator, which allows you to control the beating of the shaft in several sections [47, 71, 74–76]. The control carried out near the guide bearings of the generator and turbine. 4–6 sensors installed on the unit, 2 sensors with an angle of 90º on each of the bearings of the hydraulic unit, because in addition to the generator and turbine bearing, with a significant length of the shaft, can be installed an intermediate bearing.

Figure 4 has following notation: 1—fault diagnostic system with special processing tools, 2—data acquisition, 3— rotor shaft, 4—sensors, 5—housing, 6—bearing.

When using the scheme of the placement run-out sensor shown in Fig. 4, information signals received from sensors 4 are processed in electronic units 2 of preprocessing. Information from the electronic preprocessing units 2 is transmitted to the technical diagnostics tools 1 of powerful generators. The two sensors 4 are located at an angle of 90° to each other in the same plane in pairs at least three points (in the area of the lid, above the thrust bearing and below it). The orthogonal placement of sensors 4 along the axes on the stationary parts of the bearing 4 directly above the surface of the shaft 3 improves the diagnostic capabilities, since with the appropriate software and mathematical monitoring tools for example: they can visually observe

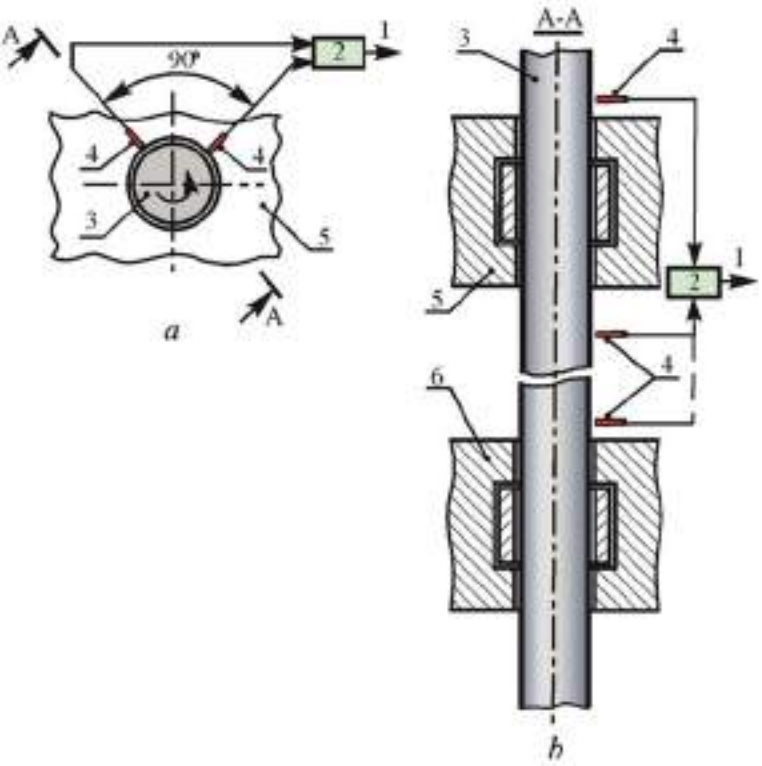

Fig. 4 Position of shaft run-out sensors on large vertical hydro generator for measurements run-out on rotating shafts: **a** horizontal view; **b** vertical view

the orbit of the shaft in the radial plane, rotor imbalance or angular eccentricity. Also, the received signals can be used in the diagnosis of some mechanical defects of high-power generators [66].

Figure 5 showed constructive scheme of the capacitive measuring transudes with the shaft run-out sensor. Scheme has following notation: h—gap between the electrode; b—width guarding ring "Kelvin"; r— the radius of the working area of the sensor electrode; w_{GND}—grounded ring width; d—controlled distance, which varies depending on the beating parameters of the shaft.

The scheme of the capacitive sensor with a concentric plane-parallel system of electrodes is shown in Fig. 6.

The sensor, which measures the distance d to the ground plane 4, consists of an active electrode 1 with radius r, a protective electrode 2 with a width b and a grounded electrode 3, the size of which is determined for design reasons. The guard electrode width b depends on the ratio d/r. Electrodes 1 and 2 separated by a dielectric gap h, which for greater uniformity of the field must have a minimum width. The working capacity of the sensor calculated by formula.

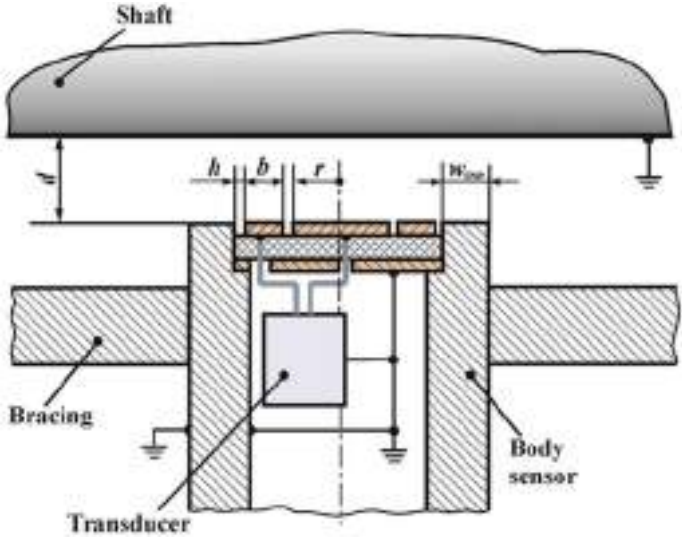

Fig. 5 Capacitive measuring transudes constructive scheme

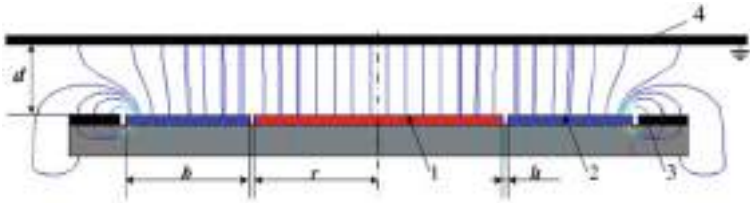

Fig. 6 Scheme for measuring the distance to the grounded surface with capacitive sensor with concentric plane-parallel electrode system

$$C = \varepsilon_0 \varepsilon_r \pi r^2 / d \tag{2}$$

where $\varepsilon_0 = 8.8542 \cdot 10^{-12}$ Ф/м—vacuum dielectric constant; $\varepsilon_r = 1.00056$ —ir relative dielectric constant; r—active electrode 1 radius.

Figure 7 shows capacitive coplanar run-out sensor response characteristic by air gap distance d depending.

4.3 Sensor Temperature Stability

Generally the coplanar air-gap sensor is developed and designed for work in temperature range from −30 to + 80 °C. The low-limit of temperature can be during in

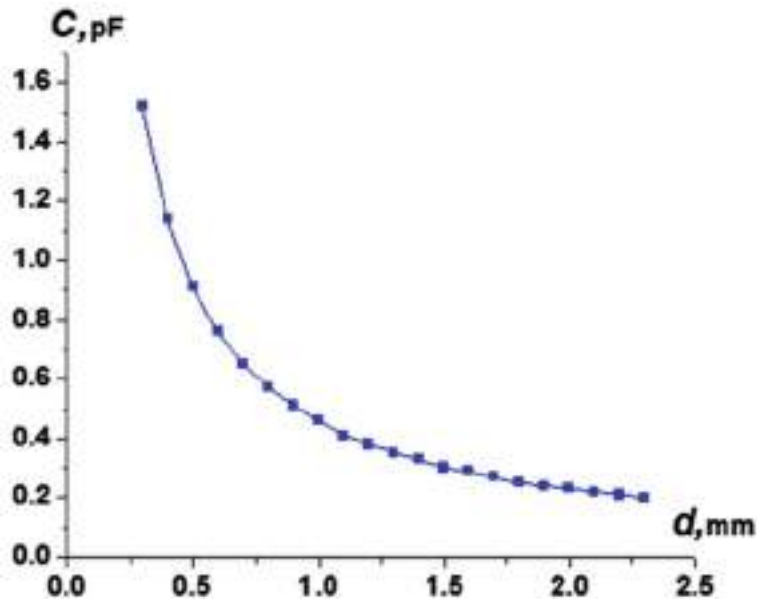

Fig. 7 Depending response characteristic of capacitive run-out sensor by air gap distance d

initial setup or during a planned inspection of the hydrogenerators. In the operator, the hydrogenerators have temperature nearly 70–80 °C.

For the influence calculation of temperature variations on the measuring accuracy of coplanar air-gap sensor capacitance "TABAI Hot and Cold Chamber MC-71, #865,267" is used. The test of censor by measuring electrical capacitance between the sensor electrodes 1 and 2 in the temperature change with inside the chamber. The hot chamber temperature was set to 80 °C while the cold chamber was set to − 40 °C. The parts were held at each temperature for a minimum of 10 min for each exposure. Figure 8 shows the dependence of measurement capacitance C_{12P} for the direct change of temperature in the chamber calculated by the next equations:

$$\Delta C_{12P} = C_{12P} - C_H, \tag{3}$$

where $C_H = 805.010^{-15}$ F—capacitance sensor value at room temperature 20 °C, before start the test.

And for measurement capacitance C_{12Z} for the reverse change of temperature by the next equation:

$$\Delta C_{12Z} = C_{12Z} - C_H. \tag{4}$$

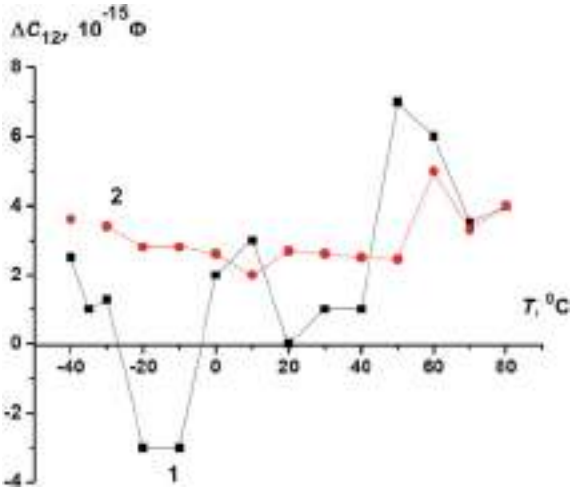

Fig. 8 Plots of the capacitance values in temperature range from −30 to + 80 °C: 1—plot of capacitance C_{12P} for the direct change; 2—plot of capacitance C_{12Z} for the reverse change

4.4 Sensor Electromagnetic Stability

In experiments values of electromagnetic field varied in range between 0.1 T and 0.68 T. For experiments was designed special stand. Stand is works as follows: variable voltage from the source is creating magnetic field in the air gap of coil. This magnetic field is modeling of electromagnetic field industrial frequency in turbo generator [44, 77, 78].

The results of natural experimental study of electromagnetic field influence on the measurement accuracy error of the run-out sensor shown in Fig. 9.

Study industrial frequency magnetic field influence on microcontroller functioning stability is described detail in work [43, 45, 79].

4.5 Technological Factors Influence on Capacitive Shaft Run-Out Sensor Characteristics

The most common method of manufacturing cheap capacitive sensors in the form of printed circuit boards is the method of photolithography. The application of the method leads to technological defects that affect the design parameters of capacitive sensors, which leads to an error in the conversion function of the sensors. The main technological defects that occur during manufacture and are shown in Fig. 10.

Conducted review of the literature [80–84] showed that research capacitive sensors technical characteristics in powerful hydrogenerators is practically absent.

The metrological characteristics of capacitive sensors significantly depend on the materials and technology used in their manufacture in accordance with international

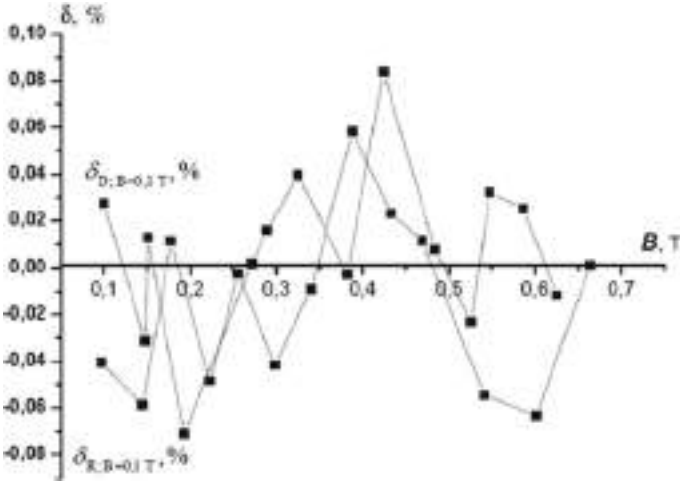

Fig. 9 Dependence of capacitive measurement error by electromagnetic field:$\delta_{D;B=0,1,T}$, %—for the direct change induction of electromagnetic field;$\delta_{R;B=0,1,T}$, %—for the reverse change induction of electromagnetic field

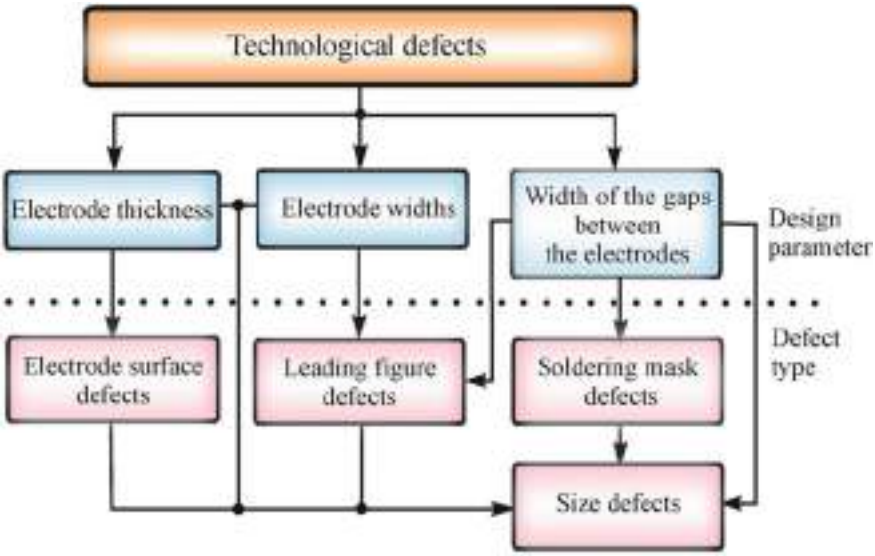

Fig. 10 Scheme of technological factors and their influence on capacitive shaft run-out sensor characteristics

Table 1 Technical characteristics of materials

Name	Characteristic
Standard thickness of the base material of the board, mm	0.5, 0.71, 1.0, 1.5, 2.0 all with tolerance ± 10%
Minimum inter-electrode gap, μm	100 170 200 250 300
Foil thickness (coating), μm	18 μm, tolerance ± 30 μm 35 μm, tolerance ± 50 μm 50 μm, tolerance ± 70 μm 70 μm, tolerance ± 100 μm 105 μm, tolerance ± 120 μm

standards IPC-2221B [85] and ANSI/IPC A-600H [86]. Such sensors are essentially printed circuit boards made from FR4, and therefore may have the following limitations and disadvantages:

1. The width of the gaps between the electrodes cannot be chosen less than (40–50) μm to avoid the possibility of complete or partial shorting of the electrodes by dust particles, as well as due to the complexity of the process of cleaning the gaps.
2. t is difficult to achieve uniformity of gaps in length due to inaccuracy in the manufacture of individual electrodes and inaccuracy in the installation of their mutual position.
3. An error may occur due to non-coplanarity of the electrodes.

Parameters such as dielectric substrate thickness, electrode thickness and inter-electrode gap can be selected from the technical characteristics of the materials listed in Table 1, which are selected in accordance with the standards [85, 86].

4.5.1 Inter-Electrode Gap

Figure 11 shows scheme of capacitive sensor idealized software model. This model retaliated in a software solution to determine the influence of the size of the inter-electrode gap on the response function of the sensor.

The idealized model of the sensor consists of a high-potential electrode, security and grounded electrodes, which were taken as lines with zero thickness $H_{foil} = 0$ mm. Voltage is applied to the high-potential and guard electrodes $U = 1$ V, grounded electrode and shaft grounded.

In this model, only the inter-electrode gap was changed h in the range 0.1, 0.17, 0.2, 0.25, 0.3 mm (see Table 2.1) in accordance to ANSI/IPC A-600H [86].

The results of the study presented in Table 2 and in Fig. 12.

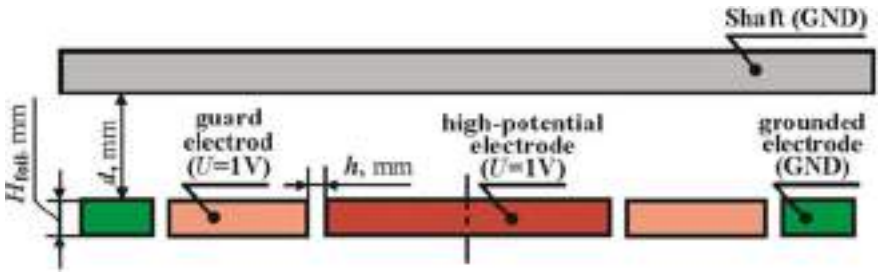

Fig. 11 The capacitive sensor scheme for modeling influence considering inter-electrode gap h to response characteristic of capacitive run-out sensor

Table 2 Results of studies on the influence of the size of the inter-electrode gap on the response function of the sensor

d, mm	$h = 0.1$ mm	$h = 0.17$ mm	$h = 0.2$ mm	$h = 0.25$ mm	$h = 0.30$ mm
	C_M, pF				
0.3	1.57	1.60	1.60	1.62	1.63
0.4	1.19	1.21	1.22	1.23	1.24
0.5	0.97	0.98	0.99	0.99	1.00
0.6	0.81	0.83	0.83	0.84	0.85
0.7	0.71	0.72	0.72	0.73	0.73
0.8	0.62	0.63	0.64	0.64	0.65
0.9	0.56	0.57	0.57	0.58	0.58
1	0.51	0.52	0.52	0.53	0.53
1.1	0.47	0.48	0.48	0.48	0.49
1.2	0.43	0.44	0.44	0.45	0.45
1.3	0.41	0.41	0.41	0.42	0.42
1.4	0.38	0.39	0.39	0.39	0.39
1.5	0.36	0.36	0.37	0.37	0.37
1.6	0.34	0.34	0.35	0.35	0.35
1.7	0.32	0.33	0.33	0.33	0.33
1.8	0.31	0.31	0.31	0.32	0.32
1.9	0.29	0.30	0.30	0.30	0.31
2	0.28	0.29	0.29	0.29	0.29
2.1	0.27	0.28	0.28	0.28	0.28
2.2	0.26	0.27	0.27	0.27	0.27
2.3	0.25	0.26	0.26	0.26	0.26

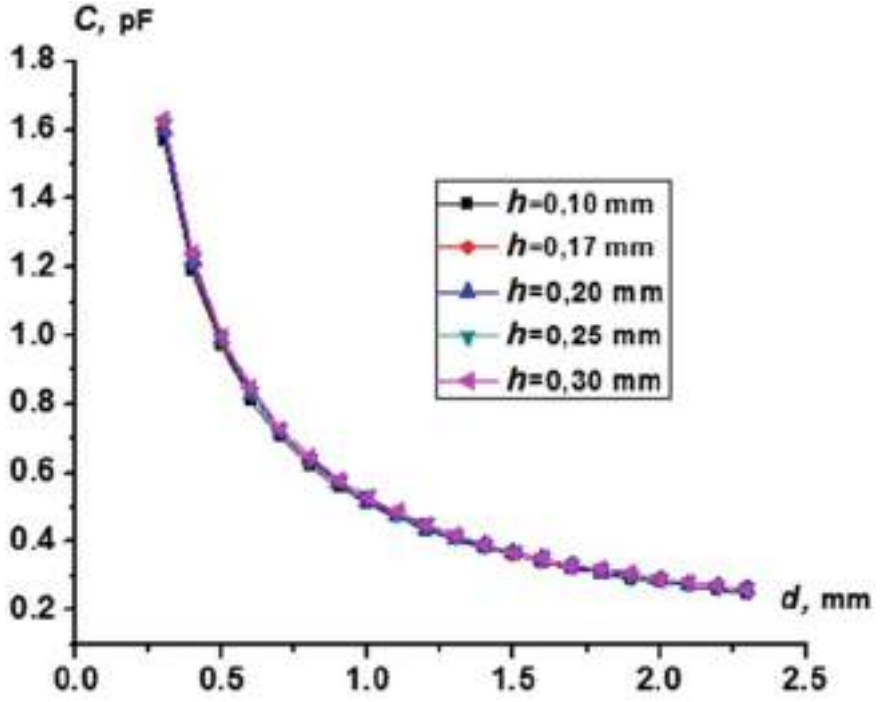

Fig. 12 Dependence of capacitive measurement error by interelectrode gap

The results of the studies presented in Fig. 12 and Table 2. So, result show that the inter-electrode gap has a direct effect on the conversion function and with increasing inter-electrode gap increase the value of the capacitance.

Based on the obtained results and analyzing the market for the production of printed circuit boards [87–89], we can conclude that the optimal size of the inter-electrode gap for the capacitive sensor is 0.1 mm.

4.5.2 Electrode Thickness

To determine the optimal thickness of the electrodes for constructed capacitive run-out sensor was retaliated model by scheme that presented in Fig. 13.

electrodes thickness H_{foil} to response characteristic of capacitive run-out sensor.

The difference from the previous case is that the thickness of the electrodes (foil) is taken as a variable value H_{foil} which is changed in the range 0.018, 0.035, 0.05, 0.07, 0.105 mm (see Table 2.1), and the determination of the distance between the electrode gap is taken to be infinitesimal $h \rightarrow 0$. The results of the study are presented in Table 3 and in Fig. 14.

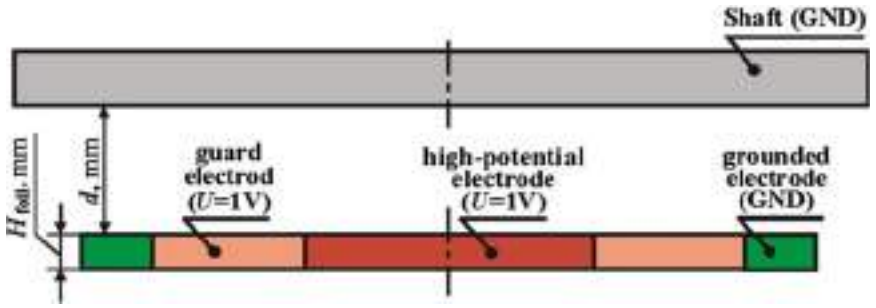

Fig. 13 The capacitive sensor scheme for modeling influence electrode thickness

Table 3 Results of studies on the influence of the electrodes thickness size of the inter-electrode gap on the response function of the sensor

d, mm	H_{foil} = 0.018 mm	H_{foil} = 0.035 mm	H_{foil} = 0.05 mm	H_{foil} = 0.07 mm	H_{foil} = 0.105 mm
	C_m, pF				
0.3	1.57	1.57	1.57	1.57	1.57
0.4	1.19	1.19	1.19	1.19	1.19
0.5	0.97	0.97	0.97	0.97	0.97
0.6	0.81	0.81	0.81	0.81	0.81
0.7	0.71	0.71	0.71	0.71	0.71
0.8	0.62	0.62	0.62	0.62	0.62
0.9	0.56	0.56	0.56	0.56	0.56
1	0.51	0.51	0.51	0.51	0.51
1.1	0.47	0.47	0.47	0.47	0.47
1.2	0.43	0.43	0.43	0.43	0.43
1.3	0.41	0.41	0.41	0.41	0.41
1.4	0.38	0.38	0.38	0.38	0.38
1.5	0.36	0.36	0.36	0.36	0.36
1.6	0.34	0.34	0.34	0.34	0.34
1.7	0.32	0.32	0.32	0.32	0.32
1.8	0.31	0.31	0.31	0.31	0.31
1.9	0.29	0.29	0.29	0.29	0.29
2	0.28	0.28	0.28	0.28	0.28
2.1	0.27	0.27	0.27	0.27	0.27
2.2	0.26	0.26	0.26	0.26	0.26
2.3	0.25	0.25	0.25	0.25	0.25

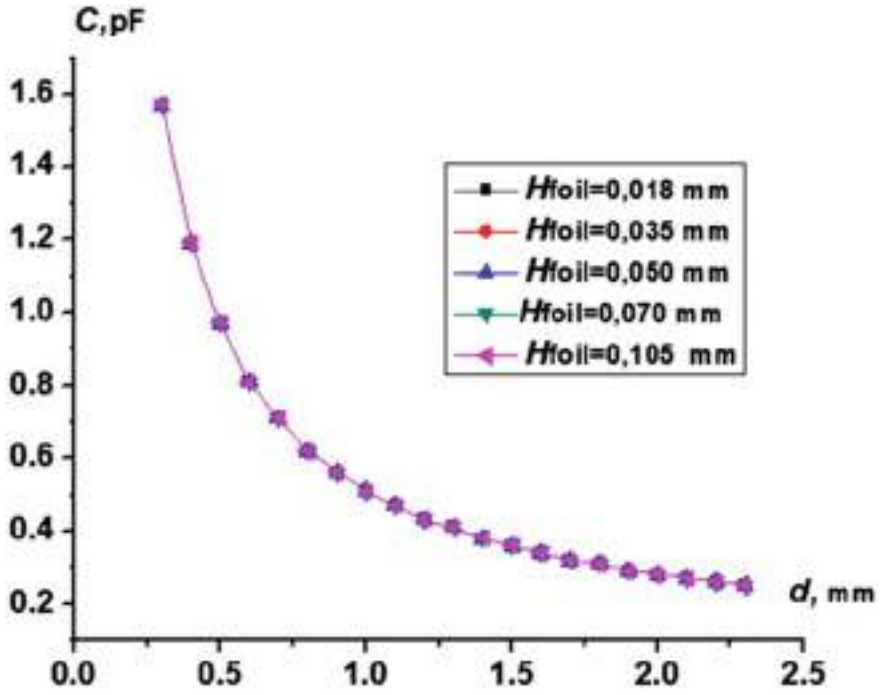

Fig. 14 Dependence of capacitive measurement error by electrode thickness

Figure 14 shown graphs of dependence capacity on the distance when changing the thickness of the electrodes almost curve into one line. This behavior of the function indicates that the thickness of the electrodes has almost no effect on the conversion function. So, choice of the optimal thickness of the electrodes is based on the total thickness of the sensor and the thickness of the dielectric substrate.

4.5.3 Dielectric Substrate Thickness

The international standard for printed circuit boards ANSI / IPC A-600H [86] states that the standard thicknesses of printed circuit boards, taking into account the thickness of the dielectric substrate (FR4) and the thickness of the foil (electrodes), are 0.5, 0.71, 1.0, 1.5, 2.0 mm.

At the same time, in [71, 86] it is noted that the optimal total thickness of the sensor is approximately 1.5 mm, as at a smaller thickness is likely to have a significant error from the curvature of the stator bore [45], and at a larger—decreases the informative measurement range. Given the above, the standard range of thicknesses of the foil (electrodes) and the design of the sensor, you can calculate the range of possible thicknesses of the dielectric substrate by the formula:

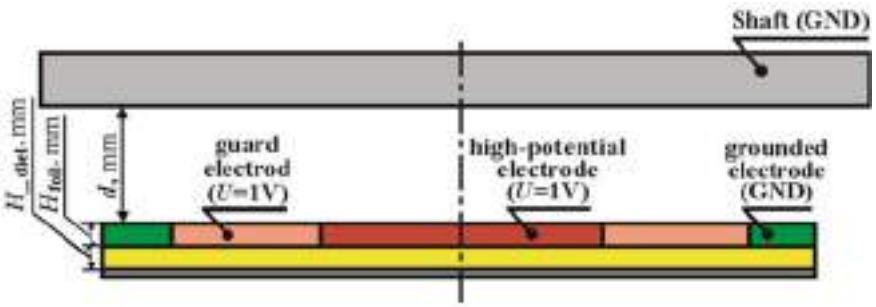

Fig. 15 The capacitive sensor scheme for modeling influence thickness of the dielectric substrate H_{diel} and its dielectric constant to to response characteristic of capacitive run-out sensor

$$H_{diel} = H_{sens} - \left(H_{foil} + H_{foil2}\right), \tag{5}$$

where $H_{sens} = 1.5$ mm—the total thickness of the sensor; H_{foil}—electrode thickness; H_{foil}—the thickness of the metal substrate of the sensor.

Thus, the range of possible thicknesses of the dielectric substrate H_{diel} is 1.29, 1.36, 1.4, 1.43, 1.46 mm.

Similar to the previous ones, a relatively idealized model of the capacitive sensor was created according to the scheme presented in Fig. 15.

During the simulation, the thickness of the dielectric substrate H_{diel} changes within the range calculated by formula (2.8), and the thicknesses of the electrodes and the metal substrate are taken as lines of zero thickness. The selected thickness of the dielectric substrate (FR4) is 1.43 mm, and the thickness of the foil (electrodes) – 0.035 mm according to the standard IPC-4101C [90] for thicknesses from 1.0 mm to 3.0 mm. The results are presented in Table 4 and Fig. 16.

The results of the research showed that with increasing the thickness of the dielectric substrate, the capacitance of the sensor increases. The dependence of the increase in the value of the capacitance on the thickness of the dielectric substrate is additive.

5 Conclusions

This chapter provides an overview integration of Ukraine's energy systems powerful generators condition. In order to be able to diagnose generators, a structure of hardware and software was proposed and developed, which combines the advantages of capacitive, optoelectronic and microelectronic technologies, which allowed to improve the theoretical foundations of systems for diagnosing mechanical parameters of generators, which include computerized information and measurement channels. The proposed hierarchical structure of the monitoring system allows implementing the concepts of SMART Grid.

Table 4 Results of studies on the influence thickness of the dielectric substrate H_{diel} and it's dielectric constant to response characteristic of capacitive run-out sensor

d, mm	$H_{diel} = 1.29$ mm	$H_{diel} = 1.36$ mm	$H_{diel} = 1.4$ mm	$H_{diel} = 1.43$ mm	$H_{diel} = 1.46$ mm
	C_m, pF				
0.3	1.87	1.85	1.84	1.84	1.83
0.4	1.49	1.47	1.46	1.46	1.45
0.5	1.26	1.25	1.24	1.23	1.22
0.6	1.11	1.09	1.09	1.08	1.07
0.7	1.00	0.99	0.98	0.97	0.96
0.8	0.92	0.91	0.90	0.89	0.88
0.9	0.86	0.84	0.83	0.83	0.82
1	0.81	0.79	0.78	0.77	0.77
1.1	0.77	0.75	0.74	0.73	0.73
1.2	0.73	0.72	0.71	0.70	0.69
1.3	0.70	0.69	0.68	0.67	0.66
1.4	0.68	0.66	0.65	0.64	0.64
1.5	0.66	0.64	0.63	0.62	0.62
1.6	0.64	0.62	0.61	0.60	0.60
1.7	0.62	0.60	0.59	0.59	0.58
1.8	0.61	0.59	0.58	0.57	0.56
1.9	0.59	0.58	0.57	0.56	0.55
2	0.58	0.56	0.55	0.55	0.54
2.1	0.57	0.55	0.54	0.54	0.53
2.2	0.56	0.54	0.53	0.53	0.52
2.3	0.55	0.53	0.52	0.52	0.51

The elements of information-measuring channels are small, are noise-resistant to the influence of powerful magnetic fields of diagnostic objects, and provide their use on generators of different types due to the variation of primary measuring transducers (sensors). All this makes it possible to increase the reliability of the assessment of the technical condition of generators.

The design of a capacitive radial beating sensor with a concentric plane-parallel electrode system considered and its transformation function was determined.

The main advantages of using computer simulation tools to study the metrological characteristics of capacitive sensors in comparison with analytical methods identified:

– reduction of time spent on research of influence of constructive parameters of the sensor on function of transformation of the capacitive sensor;
– simplified calculations due to the implementation of automatic calculations;
– visual reflection of research results.

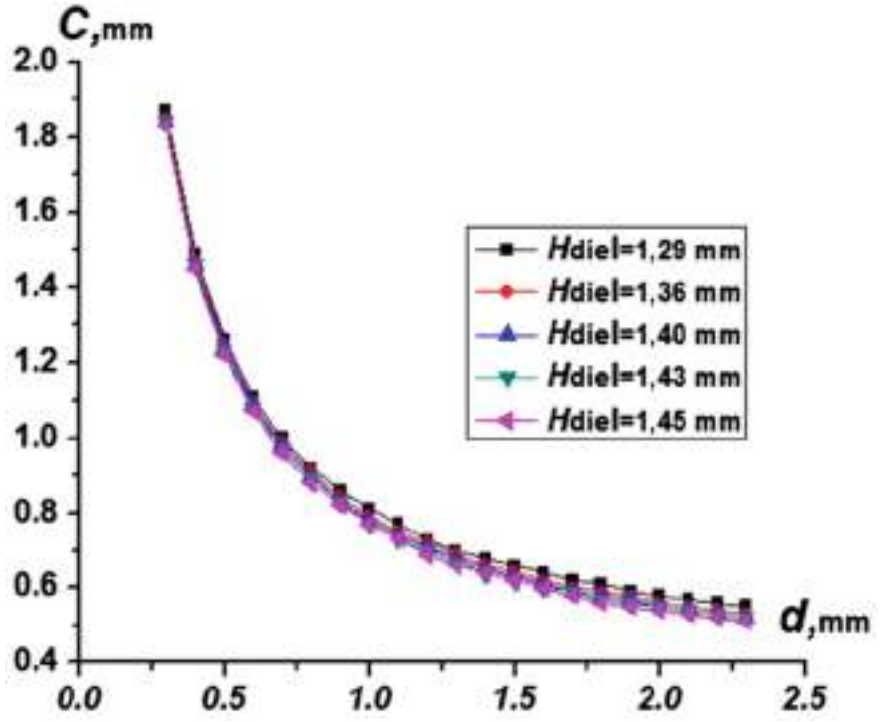

Fig. 16 Dependence of capacitive measurement error by dielectric substrate thickness

When studying the influence of structural characteristics (geometric parameters) of materials (textolite FR4) from which sensors made and technological errors that occur in the manufacture of the sensor on its conversion function. It was determined that:

- Inter-electrode gap has a direct effect on the conversion function, ie with increasing inter-electrode gap increases the value of the capacitance.
- Change in the thickness of the electrodes has almost no effect on the conversion function.
- Increasing the thickness of the dielectric substrate increases the capacity of the sensor.

The conducted researches allowed receiving a family of functions of transformation of the sensor for implementation of a choice of its optimum design and manufacturing technology depending on design features of the generator and an admissible error of definition of size of parameters of beating of a shaft.

The conducted theoretical researches allowed developing the concept of construction of the system of diagnosing mechanical defects of generators and components of its information-measuring channels.

References

1. Shevchenko, V.V.: A systematic approach to the assessment of the technical condition of electrical equipment of power systems of Ukraine. Electric. **1**, 6–11 (2013) (Rus)
2. CAN Climate Action Network: https://infoclimate.org/budushhee-ukrainskoy-elektroenergetiki. Accessed 21 Mart 2021
3. Energy of Ukraine (oil and gas sector/electricity): https://energybase.ru/country/ukraine#power-plant-tabs-widget-tab2(Rus). Accessed 21 Mar 2021
4. Generation and consumption by energy of Ukraine (oil and gas sector/electricity): https://kosatka.media/category/elektroenergiya/analytics/generaciya-i-potreblenie-elektroenergii-v-yanvare-avguste-2020-goda. Accessed 21 Mar 2021
5. Kensitsky, O.G., Klyuchnikov, A.A., Fedorenko, G.M.: Safety, reliability and efficiency of operation of electrical and electric power equipment of NPP units. Chernobil 240 (2009) (Rus)
6. Zozulin, Yu.V., Antonov, O.Y., Bichik, V.M., Borichevskiy, A.M., Kobzar, K.O., Livshits, O.L., Rakogon, V.G., Rogoviy, I.H., Khaimovich, L.L., Cherednik, V.I.: Development of new types and modernization of electric turbine generators for thermal power plants. Kharkiv 228 (2011) (Ukr)
7. Gruboi, O.P., Kobzar, K.O., Cheremisov, I.Ya., Khaimovich, L.L., Bogdanov, O.A., Gladkiy, V.V.: Creation of new types and ways of modernization of operating turbogenerators for thermal power plants, in Thermal Energy-New Challenges of Time, pp. 209–225. Lviv (2009) (Ukr)
8. Matsevity, Yu.M., Shulzhenko, N.G., Goloshchapov, V.V. et al.: Improving the energy efficiency of turbine plants at TPPs and CHPs through modernization, reconstruction and improvement of their operation modes, Matsevity, Yu. M. (ed.), p. 366. Kiev (2008) (Rus)
9. Subotin, V.G., Shevchenko, E.V., Shvetsov, V.L., et al.: Creation of new generation steam turbines with a capacity of 325 MW. Kharkiv 256 (2009) (Ukr)
10. Gruboy, O.P., Kuzmin, V.V., Cheremisov, I.Ya., Kobzar, K.O., Bogdanov, O.A.: Problems and prospects of development of turbogenerator construction in Ukraine. Hydropower Ukraine **2**, 27–35 (2006) (Ukr)
11. Cherednik, V.I., Kobzar, K.A., Zozulin, Yu. V., Livshits, A.L., Rakogon, V.G., Rogovoy, I.H., Bychik, V.N., Borichevsky, A.M.: Modernization of the TGV turbogenerator -200M, in Proceedings of the Institute of Electrodynamics of the National Academy of Sciences of Ukraine, Vol. 24, pp. 43–49. Kiev (2009) (Ukr)
12. Ukrgidroenergo: https://uhe.gov.ua/media_tsentr/novyny/chomu-ges-i-gaes-neobkhidni-energetichniy-sistemi-kraini (Ukr). Accessed 21 Mar 2021
13. Blinov, I., Zaitsev, Ie.O., Kuchanskyy, V.V.: Problems, methods and means of monitoring power losses in overhead transmission lines. In: Babak, V., Isaienko, V., Zaporozhets, A.(eds.) Systems, Decision and Control in Energy I, pp. 123–136. Springer (2020) https://doi.org/10.l007/978-3-030-48583-2_8
14. Zaitsev, I.O., Kuchanskyy, V.V.: Corona discharge problem in extra high voltage transmission line. In: Zaporozhets, A., Artemchuk, V. (eds.) Systems, Decision and Control in Energy II, pp. 3–30. Springer (2021). https://doi.org/10.1007/978-3-030-69189-9_1
15. Kuchanskyim, V., Zaitsev, I.: Corona discharge power losses measurement systems in extra high voltage transmissions lines, In: Proceedings of 2020 IEEE 7th International Conference on Energy Smart Systems (ESS), pp. 48–53. Kyiv, Ukraine (2020). https://doi.org/10.1109/ESS50319.2020.9160088.
16. Levytskyi, A.S., Zaitsev, I.O., Kobzar, K.O.: Measuring the stroke of cone disk springs in power accumulators of the turbogenerator stator core using a capacitive sensor. Devices Methods Meas. **9**(2), 121–129 (2018). https://doi.org/10.21122/2220-9506-2018-9-2-121-129 (Index in Web Of Science)
17. Zaitsev, I., Shpylka, A., Shpylka, N.: Output signal processing method for fiber bragg grating sensing system. In: Proceedings of the 15th International Conference on Advanced Trends in Radioelectronics, Telecommunications and Computer Engineering (TCSET-2020), pp. 152–155. Lviv-Slavske(Ukraine) (2020) https://doi.org/ https://doi.org/10.1109/TCSET49122.2020.235412

18. Zaitsev, I.O., Levytskyi, A.S., Sydorchuk, V.E..: Air gap control system for hydrogenerators **8**(2), 122–130 (2017). https://doi.org/10.21122/2220-9506-2017-8-2-122-130
19. Braginets, I.A., Zaitsev, I.O.: Noise immunity of phase laser vibration sensors. Tekhnichna Elektrodynamika **3**, 67-73 (2010)
20. Braginets, I.A., Zaitsev, I.O.: Dynamic characteristics of the phase laser vibration sensor. Tekhnichna Elektrodynamika **5**, 75-79 (2010)
21. Braginets, I.A. and other: Laser vibration sensor based on the phase-frequency method for measuring distances. Tekhnichna Elektrodynamika **1**, 66–70 (2011)
22. Braginets, I.A. and other: Phase-frequency laser displacement and vibration meters with optical calibration. Tekhnichna Elektrodynamika **6**, 71–77 (2011)
23. Levitskyi, A.S., Zaitsev, L.O, Panchik, M. V.: Method for monitoring the stator core of a powerful turbo generator. ENERGETIKA. Proc. CIS High. Educ. Inst. Power Eng. Assoc. **64**(4), 303–313 (2021). https://doi.org/10.21122/1029-7448-2021-64-4-303-313
24. Levytskyi, A.S., Zaitsev, L.O., Panchyk, M.V.: Assembly defects detection in the stator core of a powerful turbine generator. Visnyk Vinnytsia Politechnical Inst. **156**(3), 47–53 (2021). https://doi.org/10.31649/1997-9266-2021-156-3-47-53
25. Braginets, I.A., et al.: Increasing the noise immunity of the phase laser ranging systems. Tekhnichna elektrodynamika. **3**, 91–96 (2014) (Rus)
26. Zaitsev, E.O.: A study of synthesizers for multi frequency phase range finder system with using LABVIEV. Tekhnichna elektrodynamika. **2**, 84–88 (2014) (Rus)
27. Blinov, I., Parus, E.: Approach of reactive power pricing for ancillary service of voltage control in Ukraine. In: Proceedings of the 2014 IEEE International Conference Intelligent Energy and Power Systems (IEPS), 145 – 148 (2014)
28. Kyrylenko, O.V., Blinov, I., Parus, E.: Operation evaluation of power plants in the provision of ancillary services of primary and secondary frequency control in the Ukrainian power system. Techn. Electrodyn. **5**, 55–60 (2013)
29. Latenko, V.I. and other: Digital converters metrological specification for resistant thermal thermosensors compare. Tekhnichna Elektrodynamika **1**, 84–89 (2021) (Ukr). https://doi.org/10.15407/techned2021.01.084.
30. Blinov, I.V., Parus, Y.V.: Approach of reactive power pricing for ancillary service of voltage control in Ukraine. In: Proceedings of IEEE International Conference on Intelligent Energy and Power Systems (IEPS-2014). https://doi.org/10.1109/IEPS.2014.6874167
31. Braginets, I.A., Masyurenko, Y.A., et al.: Appling of compensatory measuring method of phase shift for laser range finder. Tekhnichna elektrodynamika. **3**, 75–80 (2015) (Rus)
32. Bereznychenko V.O.: Definition of the shafts radial beating capacitive sensor response function by computer modeling. Praci Institutu elektrodinamiki Nacionalanoi akademii nauk Ukraini **2021**(58), 107–112 (2021). https://doi.org/10.15407/publishing2021.58.107
33. Senderovich, G.A., Zaporozhets, A.O., Gryb, O.G., Karpaliuk, I.T., Shvets, S.V., Samoilenko, I.A.: Experimental studies of the method for determining location of damage of overhead power lines in the operation mode. In: Sokol, Y.I., Zaporozhets, A.O. (eds.) Control of Overhead Power Lines With Unmanned Aerial Vehicles (UAVs), pp. 55–77. Springer (2021). https://doi.org/10.1007/978-3-030-69752-5_4
34. STO 70238424.27.140.001–2011: Hydroelectric power plants methods for assessing the technical condition of the main equipment. Moscow (2011) (Rus)
35. Komshin, A.S.: Development of Scientific Foundations of Measuring and Computational Phase-Chronometric Technologies for Supporting the Life Cycle of Mechanical Engineering Objects. Moscow (2017) (Rus)
36. Dyakov, A.Y.: Control systems and automatic diagnostics of a hydraulic unit. Sayanogorsk, 83 (2017) (Rus)
37. Ivanchenko, I.P., Prokopenko, A.N.: Analysis of monitoring systems and diagnostics of the technical condition of hydraulic turbines **2**(23), 24–30 (2011) (Rus)
38. Levytskyi, A.S., Zaitsev, I.O., Bereznychenko, V.O.: Features of measurement of radial beating of cylindrical surfaces of a shaft of the hydraulic unit. Hydropower Ukraine **1–2**, 39 –44 (2019) (Ukr)

39. Levytskyi, A.S., Zaitsev, I.O., Bereznychenko, V.O.: Relative and absolute radial vibration of the shaft of the vertical unit. Hydropower Ukraine **3–4**, 36–39 (2019) (Ukr)
40. Zaitsev, Ie.O., Levytskyi, A.S., Novik, A.I., Bereznychenko, V.O., Smyrnova, A.M.: Research of a capacitive distance sensor to grounded surface. Telecommun. Radio Eng. **78**(2), 173–180 (2019). https://doi.org/10.1615/TelecomRadEng.v78.i2.80.
41. Levytskyi, A.S., Zaitsev, I.O., Bereznychenko, V.O., Sukhorukova, O.E.: Measuring transducer for air gap capacitive sensor in hydrogenerator. Devices and methods of measurements. **11**(1), 33–41 (2020) (Rus). https://doi.org/10.21122/2220-9506-2020-11-1-33-41
42. Zaitsev, I., Panchyk, M.V.: Physical processes and their influence on the development of defects in the stator core of powerful generators. Sci. Educ. New Dimension Nat. Techn. Sci. (224), 81–84 (2020). https://doi.org/10.31174/SEND-NT2020-224VIII27-20.
43. Zaitsev, I., Levytskyi, A., Kromplyas, B., Panchyk, M., Bereznychenko, V.: Study influence industrial frequency magnetic field on capacitive pressing sensor for large turbogenerator core clamping system. In: Proceedings of the 2019 IEEE Ukraine International Conference on Electrical and Computer Engineering (UKRCON-2019), , pp. 566–569, Lviv(Ukraine) 2–6 Jule 2019. https://doi.org/10.1109/UKRCON.2019.8879949
44. Zaitsev, I.O., Levytskyi, A.S., Kromplyas, B.A.: Capacitive distance sensor with coplanar electrodes for large turbogenerator core clamping system. In: Proceedings of the 2019 IEEE 39th International Conference on Electronics and Nanotechnology (ELNANO), pp. 644–647. Kiev(Ukraine) 16–18 Apr 2019. https://doi.org/10.1109/ELNANO.2019.8783916
45. Zaitsev, I.O., Levytskyi, A.S., Kromplyas, B.A.: Hybrid capacitive sensor for hydro- and turbo generator monitoring system. In: Proceedings of the International conference on modern electrical and energy system (MEES-17) 15-17 Nov 2017, pp. 288–291. Kremenchuk(Ukraine) (2017). https://doi.org/10.1109/MEES.2017.8248913
46. Zaitsev, I.O., Levytskyi, A.S.: Determination of response characteristic of capacitive coplanar air gap sensor. In: Proceedings of the 2017 IEEE Microwaves, Radar and Remote Sensing Symposium (MRRS-2017), Aug 29–June 30 2017, pp. 85–88. Kyiv(Ukraine) (2017). https://doi.org/10.1109/MRRS.2017.8075034
47. Shkolnik, V.E.: Measurement of the radial run-out of the cylindrical surfaces of the rotor shaft of electrical machines. Sci. Pap. "Electrosila". **40**, 60–66 (2001) (Rus)
48. Zaitsev, L.O.: Analysis of sampling error on the accuracy of laser range finders based on the discrete hilbert transform. Tekhnichna elektrodynamika. **4**, 89–94 (2015) (Rus)
49. Braginets, I.A., Sydorchuk, V.E., et al.: Analysis of phase system of automatic frequency correction in laser rangefinder. Tekhnichna elektrodynamika. **1**, 91–94 (2015) (Rus)
50. Zaitsev, I.O.: Electric machines faults monitoring system with hybrid electro-optic capacitive mechanical sensors. In: Abstracts of the 2017 IEEE International Young Scientists Forum on Applied Physics and Engineering (YSF-2017), 17–20 Oct 2017, pp. 15–18. Ukraine, Lviv (2017)
51. AD7745/46 24-Bit: Capacitance-to-Digital Converter with Temperature Sensor. https://www.analog.com/media/en/technical-documentation/data-sheets/AD7745_7746.pdf Accessed 21 Mar 2021
52. Zaitsev, I.O., Levytskyi, A.S.: Hybrid electro-optic capacitive sensors for the fault diagnostic system of power hydrogenerator. In: Ebrahimi, A. (ed.) Clean Generators-Advances in Modeling of Hydro and Wind Generators, pp. 25–42. Intechopen (2020) https://doi.org/10.5772/intechopen.77988.
53. Turan, J., Ovsenik, L., Turan, J.: Optically powered fiber optic sensors. Acta Electrotechnica et Informatica, 5–7 (2005)
54. Levytskyi A., Zaitsev I.: Hybrid fiber-optic measuring tools for control and diagnostic parameters of hydrogenerators. Hydropower Ukraine **3–4**, 32–33 (2016) (Ukr)
55. Zadvornov, S.A.: Issledovaniye metodov postroyeniya gibridnykh volo-konno-optikoskikh izmeritel'nykh sistem. MPEI 119 (2009) (Rus)
56. Rosolem, J.B., Floridia, C., Sanz, J.: Optical system for hydrogenerator monitoring. In: Proceedings of the International Council for Power Electroenergetical Systems CIGRE 2010, pp. 1–8. France (Paris) (2010)

57. Riesen, S., Schubert, U., Bett, A.W.: GaAs photovoltaic cells for laser power beaming at high power densities. In: Proceedings of the 17th European Photovoltaic Solar Energy Conference, pp. 182–185. Germany (2001)
58. Pena, R., Algora, C., Anton, I.: GaAs Multiple Photovoltaic Converters with an Efficiency of 45% for Monochromatic Illumination. In: Proceedings of the 3rd World Conference on Photovoltaic Energy Conversion, pp. 228–231. Osaka (Japan) (2003)
59. Dakin, J., Brown, R.: Handbook of optoelectronics. Boca Raton, p 1563 (2006)
60. PV-Cells for Optical Power Transmission: https://www.ise.fraunhofer.de/content/dam/ise/de/documents/infomaterial/brochures/photovoltaik/14e_ISE_Flyer_III-V_OpticalPowerTransmission.pdf Accessed 21 June 2019
61. Herb, J.: Commercialization of new lattice-matched multi-junction solar cells based on dilute nitrides. Subcontract Report NREL/SR-5200–54721, p 28. San Jose(California) (2012)
62. Wang, M.R., Chen, R.T., Sone,k G.J., Jannson T.: Wavelength-division multiplexing and demultiplexing on locally sensitized single-mode polymer microstructure waveguides. Opt. Lett. **15**(7), 363–365 (1990)
63. Haid, M., Armbruster, C., Derix, D., Schöner, C., Helmers, H.: 5 W Optical power link with generic voltage output and modulated data signal. In: Proceedings of the 1st Optical Wireless and Fiber Power Transmission Conference (OWPT2019), Yokohama (Japan) (2019)
64. Sunmee, P., Borton, D., Kang, M., Nurmikko, A., Song, Y.: An implantable neural sensing microsystem with fiber-optic data transmission and power delivery. Sensors **13**, 6014–6031 (2013)
65. Babak, S.V., Myslovich, M.V., Sysak, R.M.: Statistical diagnostics of electrical equipment, p 456. IED NANU, Kiev (2015) (Rus)
66. Zaitsev, I.O., Levytskyi, A.S., Sydorchuk, V.E.: Air gap control system for hydrogenerators. Devices Methods Meas. **8**(2), 122–130 (2017) (Rus)
67. Bereznychenko, V.O., Zaitsev, I.O.: Contactless capacitive sensor of the system for monitoring the parameters of the beating of the powerful electrical machines shafts Works of the Institute of Electrodynamics of the National Academy of Sciences of Ukraine **57**, 81–88 (2021) (Ukr). https://doi.org/10.15407/publishing2020.57.081
68. Knapp, B.R., Arneson, D.A., Martin, D.L.: Electrical runout using an eddy-current sensor for roundness measurements. In: Proceedings of the 28th ASPE (2013)
69. Smirnov, V.I.: Methods and means of functional diagnostics and control of technological processes based on electromagnetic sensors. Ulyanovsk State Technical University, p 190 (2001) (Rus)
70. Zaitsev, I., Levytskyi, A., Bereznychenko, V.: Development shaft run-out measurement transducers for powerful generators fault control system with capacitive coplanar concentric sensor. In: Proceedings of the 1st International Scientific and Practical Conference Theory and Practice of Science: Key Aspects, pp. 1014–2021. Rome (Italy) (2021). https://doi.org/10.51582/interconf.19-20.02.2021.103
71. Levytskyi, A.S, Fedorenko, G.M., Gruboj, O.P.: Monitoring of the status of powerful hydro and turbo generators using capacitive meter for the parameters of mechanical defects. Kyiv, 242 (2011) (Ukr)
72. International Measurement Confederation (IMEKO) 209: www.imeko.org Accessed 21 Mar 2019
73. Gorbova, G., Gorbov, M., Meyer, M.: Precise capacitance calculation of sensing elements capacitive sensors by method of direct field strength determination. In: Proceedings of the lEfct Sensor 2002, pp. 1239–1243. Orlando (2002)
74. Beloglazov, A.V. Glazyrin, G.V.: Development of monitoring tools for hydraulic unit shaft beats. Collect. Sci. Pap. NSTU. **3**(53), 79–84 (2008) (Rus)
75. XY Measurements for Radial Position and Dynamic Motion in Hydro Turbine Generators. Orbit **30**(1), 32–39 (2010)
76. Ungureanu, G., Covaciu, F., Balaj, A., Ciulbea, C.: Vibration monitoring system of hydroelectric turbine-generator sets. In: Proceedings 2002 IEEE-TTTC International Conference on Automation, Quality and Testing, Robotics, Vol. 11, pp. 382–385. Clui-Napoca (Romania) (2002)

77. Milykh, V.I., Vysochin,A.I.: Principles of calculation of the magnetic field in the end of the turbo generator in various regimes of its work. Electrical engineering, Electrical engineering, Vol.3, pp.19–24 (Rus) (2010)
78. Milykh, V.I., Dubinina, O.N.: Numerical calculation of the magnetic field in the end zone of the turbogenerator under load conditions. Electr. Eng. Electr. Mech. **1**, 64–69 (2003) (Rus)
79. Zaitsev, I., Levytskyi, A.S., Kromplyas, B.A., Panchyk, M.V., Bereznychenko V.O.: Study industrial frequency magnetic field influence on STM32F051K8T6 microcontroller functioning stability. In: Works of the Institute of Electrodynamics of the National Academy of Sciences of Ukraine, Vol. 52, pp. 80–86 (2019) (Ukr). https://doi.org/10.15407/publishing2019.52.080
80. Levytskyi, A.S., Zaitsev, I.O., Kromplyas, B.A.: Determination of the response characteristic of the capacitive sensor of the air gap in the hydrogenerator СГК538/160–70М. In: Works of the Institute of Electrodynamics of the National Academy of Sciences of Ukraine, Vol. 43, pp. 134–136 (2016) (Ukr)
81. Levytskyi, A.S., Zaitsev, I.O., Kromplyas, B.A.: The errors of the capacitive measurer gap in the hydrogenator. In: Works of the Institute of Electrodynamics of the National Academy of Sciences of Ukraine. Vol. 44, pp. 50–55 (2016) (Ukr)
82. Bao, M.H.: Electrostatic driving and capacitive sensing. In: Handbook of Sensors and Actuators, vol. 8, pp. 139–198 (2000)
83. Dzhezhora, A.A.: Electric capacitive converters and methods of their calculation. Belarusian Sci. 305 (2008) (Rus)
84. Evstigneev, V.V., Khomutov, O.I., Gorbova, G.M.: Prospective directions of design and principles of calculation of non-contact capacitive microdisplacement meters. Polzunovsky Almanac. **2**, 45–58 (1999) (Rus)
85. IPC-2221B: Generic Standard on Printed Board Design, p. 207 (2012)
86. ANSI/IPC A-600H: Acceptability of Printed Boards, p.168 (2010)
87. Company SEA: https://www.sea.com.ua (Rus). Accessed 21 Mar 2021
88. Company “PCB ETAL": https://pcbetal.com/ (Rus). Accessed 21 Mar 2021
89. Company “SK-Techno": http://spcb.com.ua/ (Rus). Accessed 21 Mar 2021
90. IPC-4101C: Specification for Base Materials for Rigid and Multilayer Printed Boards, p. 127 (2009)

Operating Modes Optimization of Bulk Electrical Power Networks: Structural and Parametrical Methods

Vladislav Kuchanskyy, Denys Malakhatka, and Artur Zaporozhets

Abstract One of the main elements of the power system is the extra high voltage transmission lines, which are system-forming for the bulk electric networks. The normal operation of the integrated power system depends on the reliability and efficiency of operation transmission line. To ensure efficient operation of the extra high voltage transmission line, it is necessary to optimize the voltage mode and reactive power. Optimization of the transmission line mode operation by minimizing the losses of active power in it, should be based on solving problems of optimization of voltage and reactive power. The control of the operating mode of the transmission line is the correct choice of the composition of the charging power compensation devices in order to regulate the voltage levels and power factors on the bus terminals. Optimization of the transmission line modes operation in this problem statement is performed, focusing on some of the most significant mode parameters. It should also be noted that previous studies have not addressed issues related to the corona discharge of wires and its impact on voltage distribution and the feasibility of depth regulation in lines of this voltage class. One of the measures to reduce electricity losses is to optimize the operating modes of transmission lines in terms of voltage and reactive power. In this formulation of the problem of transmission lines is considered in isolation for the three most common modes: minimum, maximum and operational operating mode of power transmission. The optimal voltage value at the beginning or end of the transmission line, as a rule, usually cannot be achieved due to the inability to increase the operating voltage to the maximum allowable value under the condition of equipment insulation and insufficient power and regulation of the installed compensating devices. By using modern devices for controlled charging compensation of the power line, you can achieve deeper regulation of reactive power and voltage, and, accordingly, minimize the loss of active power. A complex of interrelated mathematical models has been created to determine the economic effect of optimizing the mode of an electric network with extra high voltage transmission

V. Kuchanskyy (✉) · D. Malakhatka
Institute of Electrodynamics of NAS of Ukraine, Kyiv, Ukraine

A. Zaporozhets
Institute of Engineering Thermophysics of NAS of Ukraine, Kyiv, Ukraine
e-mail: a.o.zaporozhets@nas.gov.ua

O. Kyrylenko et al. (eds.), *Power Systems Research and Operation*, Studies in Systems, Decision and Control 388, https://doi.org/10.1007/978-3-030-82926-1_5

lines in terms of voltage and reactive power, taking into account the probabilistic nature of corona losses. Techniques, algorithms and methods have been developed for the operational optimization of the modes of individual power transmission lines, taking into account corona losses. Expressions for the optimal voltage of power lines and voltage control laws are obtained. A methodology and an algorithm for operational optimization of the mode of an electrical network with power lines in terms of voltage and reactive power have been developed. The verification of the adequacy and effectiveness of the proposed methods and algorithms was carried out by means of comparative calculations for real extra high voltage overhead lines and circuits of electrical systems with operating extra high voltage overhead lines.

Keywords Corona discharge power losses · Deep voltage regulation · Controlled reactive power compensation · Minimizing criterion · Parametrical and structural optimization methods

1 Introduction

The formation of modern electric power systems, covering large areas, is based on the use of over and extra high voltage power lines. The current stage of energy development is characterized by the use of more advanced mathematical models of individual elements, as well as the entire system as a whole, that is why it largely depends on the rate of implementation of scientific and technical achievements. The development of energy in the context of rising fuel prices, increasing requirements for improving the technical and economic indicators of the energy system, requires improving the methods of managing the processes of transmission and distribution of electrical energy. At the same time, a special role is assigned to automated dispatch control systems, the development of which makes it possible to gain the greatest effect [1–10].

The load of the bulk network of 330 kV and above began to increase, the flows between energy systems increased. The share of losses in 330–750 kV lines reached 20% of the total losses. The total length of the networks tends to grow. In this regard, additional consideration is required of a number of fundamental questions of the methodology for studying normal processes in overhead power lines and in complex electrical power systems with overhead power lines, in particular, issues of modeling taking into account the phenomenon of corona wire.

Important aspects of the operational analysis and control of the extra high voltage overhead lines are the measurement and isolation of the components of power losses and the operational correction of its parameters. One of the main reasons for non-optimal modes of electric power systems and, accordingly, additional losses of electricity during its transport and distribution is the obstacle of the normal exploitation of electrical systems. Obstacle is a design parameter of the extra high voltage line, therefore, it negatively effects on its modes throughout the entire operation time of the

system. This chapter considers a comprehensive solution to the problem of compensating for the negative impact of electrical power systems (EPS) heterogeneity on the optimality of the processes of transmission and distribution of electricity in it on the basis of structural and parametric optimization methods. A decrease in the measure of inhomogeneity of the EPS is achieved by installing in it installations of controlled transverse compensation of reactive power [11–14].

The formation of modern electric power systems, covering large territories, is based on the use of over and extra high voltage power lines. The current stage of development of energetics is characterized by the use of more advanced mathematical models of individual elements, as well as the entire system as a whole, and largely depends on the rate of implementation of scientific and technical achievements.

2 Development Technical and Economic Analysis Methods for Comparison Measures and Technical Means of the Bulk Electrical Networks

Controlled compensation devices are the most promising as means of transverse compensation in extra high voltage lines. Their main purpose is to smoothly change the consumption of excess reactive power of power lines in order to normalize voltage levels. Using the example of a 750 kV power transmission line, the chapter shows a method for evaluating the additional effect of using a controlled compensation device to reduce active power losses in lines.

As is known, shunt reactors (SR) are used as a means of compensating for the overage reactive power of overhead transmission lines (OTR) of higher voltage classes. In addition, these devices limit internal overvoltages when overhead lines are switched on and off, and help cutting off the recharge arc in the single-phase automatic re-closing cycle (SPAR). They are characterized by relatively small losses of active power (0.3%) and the lowest specific design cost among reactive power compensation devices [1–3]. At the same time, it is known that in many cases the installation of SR has a negative impact on the transmission capacity of power lines, and also leads to increased losses of active power in power lines in modes of significant overhead line loads [14–18].

This is appear due to the impossibility of their frequent switching due to the low operational reliability of reactor switches and their insufficient switching life, as well as due to unacceptable voltage fluctuations with a cutting change in the significant reactive capacities of these reactors. Thus, in the 750 kV overhead line scheme, the capacity of which was only about 40% of its natural capacity due to the use of unregulated shunt reactors as reactive power compensation devices. The presence of permanently connected reactors to the overhead line, regardless of its load, leads not only to a decrease in the transmission capacity of the power line, but also to increased losses of active power. The latter circumstance was well known earlier, but the method of quantifying active power losses was not previously carried out [4–6].

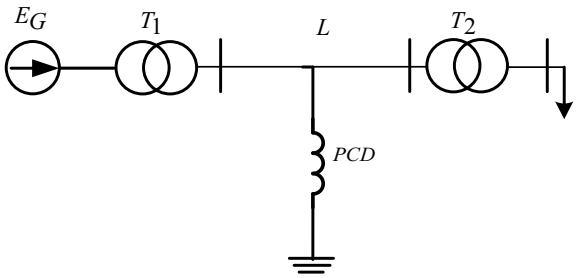

Fig. 1 Extra high voltage power line

The real effect of reducing active power losses caused by the replacement of controlled shunt reactors with (CSR) or static synchronous compensators (STATCOM) is so significant that only this circumstance allows a very short payback period for additional costs for installing controlled reactive power compensation devices (PCD). Technique on the example of 750 kV class power transmissions line for two cases—when the CSR or STATCOM is installed at an intermediate substation shown on Fig. 1.

To obtain equivalent transmission parameters, taking into account the SR, we present the circuit in the form of three four-poles connected in series.

In this case, the parameters of an equivalent four-pole are defined as:

$$\begin{bmatrix} A_{eq} & B_{eq} \\ C_{eq} & D_{eq} \end{bmatrix} = \begin{bmatrix} \cos\lambda & jz_W \sin\lambda \\ j\frac{\sin\lambda}{z_W} & \cos\lambda \end{bmatrix} \times \begin{bmatrix} 1 & 0 \\ -jb_p & 1 \end{bmatrix} \times \begin{bmatrix} \cos\lambda & jz_W \sin\lambda \\ j\frac{\sin\lambda}{z_W} & \cos\lambda \end{bmatrix}. \quad (1)$$

After the transformations, we get the longitudinal lines of parameters (including PCD parameters):

$$\dot{B}_{eq} = jz_W \sin 2\lambda + jb_p \sin^2\lambda. \quad (2)$$

In relative units:

$$B_{eq} = \sin 2\lambda + b_P^* \sin^2\lambda, \quad (3)$$

where $b^*{}_{\mathrm{P}}$ is the PCD conductivity in relative units:

$$b_P^* = 2tg\frac{\lambda}{2}. \quad (4)$$

Expression for determining the angle δ on a plot:

$$\delta = \frac{\pi B_P}{4}. \quad (5)$$

Expression for determining the voltage at the reactor installation site—U_P^*

$$U_P^* = \frac{\sin(\lambda)}{\sin(\delta)}. \tag{6}$$

Expression for determining the reactive power of the PCD (in terms of angular power characteristics):

$$Q_P^* = 2\frac{U_P^*}{\sin\lambda}(\cos\delta - U_P^*\cos\lambda). \tag{7}$$

Active power losses in section λ when the SR is installed:

$$\Delta P_{SR}^* = \frac{P^{*2} + (Q_P^*/2)^2}{U_P^{*2}} r_l^*, \tag{8}$$

where $r_l^* = \frac{r_0}{n} l \frac{1}{z_w}$—radius of the split phase wire.

In the case of establishing a CSR or STATCOM $U_P^* = 1$, $Q_P^* = 0$, due to the fact that natural power is transmitted over the line without loss of power in the reactive elements:

$$\Delta P_{PCD}^* = \frac{P^{*2}}{U_P^{*2}} r_l^*. \tag{9}$$

Difference in losses in named units (per length 2λ):

$$\Delta P^* = \Delta P_{SR}^* - \Delta P_{PCD}^*. \tag{10}$$

We will take into account the active power losses in the SR at the rate of 0.5 MW for 3 phases; we will ignore the losses in the PCD in the natural power transmission mode.

$$\Delta W = \Delta P \tau. \tag{11}$$

The cost of these losses at a unit cost of 50 USD per MWh is:

$$C = W \cdot 50. \tag{12}$$

The unit cost of SR is assumed to be 10 USD for 1 kVar, CSR—20 USD for 1 kVar, the STATCOM is 50 USD for 1 for 1 kVar.

Cost of SR:

$$C_{SR} = C^{SR} \cdot Q_P^* \cdot 10^3. \tag{13}$$

Cost of CSR:

$$C_{CSR} = C^{CSR} \cdot Q_P^* \cdot 10^3. \tag{14}$$

Cost of STATCOM:

$$C_{STATCOM} = C^{STATCOM} \cdot Q_P^* \cdot 10^3. \tag{15}$$

The cost of installing CSR or STATCOM instead of SR is recouped only by reducing losses in overhead lines and SR over the period:

$$\Delta C = \frac{C_{PCD} - C_{SR}}{C}. \tag{16}$$

In Table 1 the results of calculating the cost and payback period when setting the CSR or STATCOM are presented.

As can be seen from (Table 1) when installing CSR of the same capacity in comparison with the STATCOM, a shorter payback period is achieved. A part of the 750 kV transmission line with substations where CSR groups are installed in Fig. 2 is shown.

In the literature sources [3, 4], optimization of actual modes is performed, without analyzing the use of specific devices. Recently developed, a new generation of CSR and STATCOM significantly expands the possibilities of their application for the implementation of coordinated voltage and reactive power regulation in ultra-high voltage transmission lines [7–11]. Charging power compensation and power

Table 1 The results of calculating the cost and payback period

PCD characteristics	Reactive power compensation device		
	SR	CSR	STATCOM
Power, MWAr	330		± 330
Cost mil. USD	3.3	6.6	16.5
Payback period	1.1	–	4.5

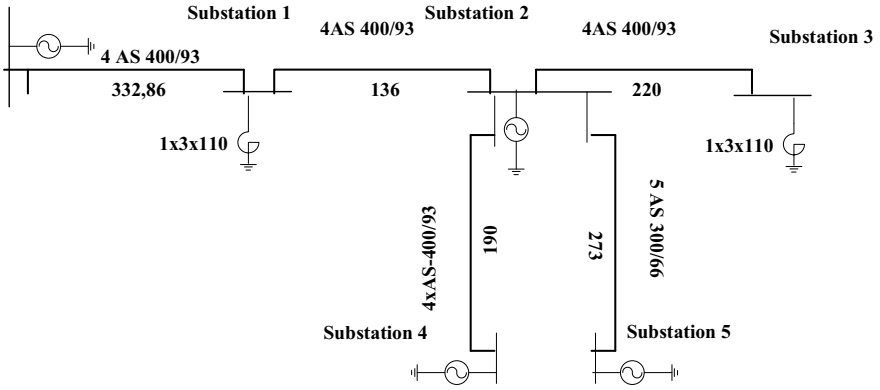

Fig. 2 The part of the 750 kV bulk electrical power system

flow control are performed to analyze the operating modes of extra high voltage transmission lines with controlled shunt reactors.

It can be seen that in the case of the use of CSR, an additional reduction in technological losses occurs due to more accurate transverse compensation. But, of course, crucial from the point of view of saving electricity is a possibility of using CSR to control flow distribution in heterogeneous networks of the system in order to obtain an economical normal regime.

3 Assessment of the Efficiency Reducing the Active Power Losses in Electric Power Transmission Lines by Structural Means

Optimization of the mode of operation of the transmission line, which is considered as a local object, by minimizing the loss of active power in it, should be based on solving problems of optimizing the voltage mode and reactive power. The control of the operating mode of the EHV transmission line is the correct choice of the composition of the charging power compensation devices in order to regulate the voltage levels and power coefficients on the busbars of the terminal substations. It should be noted that the optimization of the modes of operation of the transmission line EHV in this problem statement is performed, focusing on some of the most significant mode parameters. It should also be noted that previous studies have not addressed issues related to the consideration of wire corona and its impact on voltage distribution and the feasibility of deep voltage regulation in lines of this voltage class.

One of the measures to reduce electricity losses is to optimize the operating modes of EHV transmission lines in terms of voltage and reactive power. In this statement, the problem of transmission lines EHV is considered in isolation for the three most common modes: minimum, maximum and operational operating mode of power transmission. Expressions for determining the loss of active power in the transmission line contain components of idling and short circuit losses.

The latter, respectively, are directly and inversely proportional to the square of the voltage on the bus terminals, which determines the possibility of choosing the optimal voltage level that provides a minimum amount of these components. The optimal voltage value at the beginning or end of the transmission line, as a rule, cannot be achieved due to the inability to increase the operating voltage to the maximum allowable value under the condition of equipment insulation and insufficient power and regulation of the installed compensation devices.

By using modern devices of controlled compensation of charging power of the transmission line, it is possible to achieve deeper regulation of reactive power and voltage, and, accordingly, minimization of active power losses: Power loss ΔP_{loss} without charging compensation devices is determined by the following expression:

$$\Delta P_{loss} = G \cdot (B^2 \cdot A1 - 6 \cdot (A2 + A3) + G^2 \cdot (R^2 + X) + 8) \cdot U^2 + (\frac{G \cdot A1}{2} + R) \cdot \frac{P^2 + Q^2}{U^2} + ((A3 \cdot (3 \cdot A2 - 4(A3 - 4)) - \frac{A4^2 + G^2 \cdot X^2}{2}) \cdot P + (\frac{A4 \cdot A2 - A4 \cdot A3 - 7 \cdot G \cdot A2}{2} - A4 + 15 \cdot G \cdot X) \cdot Q, \quad (17)$$

where R—active resistance Ohm; X—inductive resistance Ohm; G—active conductivity, Sm; B—reactive conductivity, cm; U—rated voltage, kV; P—MWatt active power, Q—reactive power, MWAr. For the sake of convenience, additional coefficients have been introduced. $A = R^2 + X^2; A2 = BX; A3 = GR\ A4 = BR$.

In the literature [15–20] the optimization of the actual modes is performed, without analysis of the use of specific devices. The recently developed new generation of controlled shunt reactors and STATCOM significantly expands the possibilities of their application for the implementation of coordinated regulation of voltage and reactive power in ultra-high voltage power transmission lines. For the analysis of operating modes of NVN transmission lines with control shunt reactors, charging power compensation and power flow regulation are performed. In this case, the loss of active power will be recorded:

$$\Delta P_{loss} = (\frac{A \cdot G \cdot (B^2 + A7) + 2 \cdot \left[B^2 \cdot R - B \cdot n \cdot B_{\text{Reac}} \cdot G \cdot A5 - 3 \cdot R \cdot A7\right] - 3 \cdot R \cdot A7}{8} + \frac{B^2 \cdot R - B \cdot n \cdot B_{\text{Reac}} \cdot G \cdot A5 - 3 \cdot R \cdot A7}{4} + \frac{B \cdot (n \cdot B_{\text{Reac}} \cdot R - G \cdot X) + 3 \cdot n \cdot B_{\text{Reac}} \cdot G \cdot X}{2} + G)U^2 + (\frac{G \cdot A}{2} + R) \cdot \frac{P^2 + Q^2}{U^2} + (\frac{B^2 \cdot A5}{2} - B_{\text{Reac}} \cdot n \cdot A + 2 \cdot G \cdot R \cdot X(B - B_{\text{Reac}} \cdot n) + 2 \cdot B \cdot X + \frac{B_{\text{Reac}}^2 \cdot n^2 \cdot A5}{2}) - \frac{G \cdot (G \cdot A + 4 \cdot R)}{2} \cdot P + (G \cdot X - B \cdot R - \frac{B_{\text{Reac}} \cdot n \cdot G \cdot A - B \cdot G \cdot A5}{2} + B_{\text{Reac}} \cdot n \cdot R) \cdot Q, \quad (18)$$

where n—the number of installed groups of controlled shunt reactors; $B_{\text{Reac}} \in [0; 6 \cdot 10^{-4}]$ See the range of conductivity changes of the installed KSR, in case of installation of uncontrolled shunt reactors $B_{\text{Reac}} = 5.328 \cdot 10^{-4}$Sm. For the sake of convenience, additional coefficients have been introduced.$A5 = R^2 - X^2$, $A6 = X^2 - R^2$, $A7 = n^2 \cdot B_{\text{Reac}}^2 + G^2$.

Table 2 The minimum mode of operation of transmission lines EHV $P = 350$ mW and $Q = 100$ MWAr, $U = 780$ kV

	Charging power compensation device		
	Controlled SR	Shunt reactor	Without compensation
ΔP, mW	7.459	7.715	9.267
η,%	97.86	97.8	97.35

Table 3 Operational mode of transmission lines EHV $P = 1800$ mW and $Q = -500$ MWAr,$U = 750$

	Charging power compensation device		
	Controlled SR	Shunt reactor	Without compensation
ΔP, mW	50.368	56.879	66.095
η,%	97.2	96.84	96.3

Table 4 The maximum mode of operation of the transmission line EHV $P = 2500$ mW and $Q = -500$ MWAr,$U = 750$kV

	Charging power compensation device		
	Shunt reactor	Without compensation	Shunt reactor
ΔP, mW	96.359	99.681	108.897
η,%	96.145	96.01	95.64

Tables 2, 3 and 4 show the results of calculations of active power losses.

The efficiency of the controlled shunt reactor is shown in Fig. 3. As can be seen from Fig. 3, the values of active power losses vary widely depending on the inductance of the controlled shunt reactors. It should be noted that in (17, 18) the total losses consist of technological and losses on corona wires. In the case of controlled shunt reactors, there is a reduction of technological losses and, consequently, total losses, thereby increasing the efficiency of the transmission line NVN. In operational mode, the task is to control groups of controlled shunt reactors in which the value of active power losses will be minimal.

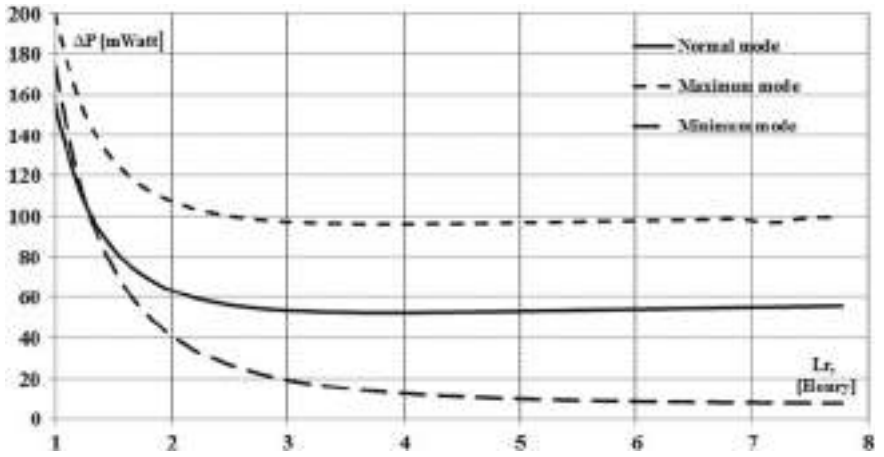

Fig. 3 Reduction of total losses of active power at application of CSR

4 Optimization of Bulk Electrical Networks Operating Modes by Controlled Lateral Compensation Using

Schemes of electrical networks contain many closed circuits, which in general increases the reliability of electricity supply to consumers and helps to increase the capacity of the electrical network. The circuits are formed by lines of one voltage step and several stages of rated voltages. If the circuit consists only of transmission lines made of wires of the same brand, the X/R ratio for all branches of the substitution circuit in such a circuit is the same and the network is homogeneous. At different cross-sections of the transmission line wires included in the circuit or for a network with transformers, the X/R ratio is different for different branches and the network is inhomogeneous. We show that in an inhomogeneous closed network, power flows are distributed suboptimal over the branches and that for such a network it is possible to reduce losses by forcibly changing the flow distribution in the circuit.

The total loss of active power in the main electrical network is described by the expression:

$$\Delta P_{\Sigma} = \sum_{i \in 1}^{n} \sum_{i \in 1 j \neq 1}^{n} \Delta P_{ij}, \tag{19}$$

where ΔP_{ij}—losses of active power of the transmission line, determined by the formula (18); $_{ij}$—substation numbers.

To increase the efficiency of electrical networks, various measures are taken to reduce electricity losses both at the stage of operation and at the design stage. At the stage of operation, the optimization of operating modes is performed using various methods, among which the optimization of steady-state modes of voltage and redistribution of power flows in heterogeneity closed networks is often used.

At a given transmitted active power, the amount of load power losses in the lines and windings of transformers can be reduced by increasing the mains voltage and reducing the amount of transmitted reactive power. The latter can be provided through the rational use of installed compensating devices. In extra high voltage power lines, in bad weather, the losses on the corona can in some cases exceed the load losses. In these cases, it may be appropriate to reduce the voltage level slightly, which will reduce the total line loss. Thus, the change in voltage level in the network affects the amount of losses in them.

In existing electrical systems, there are often closed electrical networks of different voltages (for example, 750 kV), connected by transformers and autotransformers. In these heterogeneous closed networks, in some cases it is possible to reduce power and energy losses by applying special measures.

High and extra high voltage electrical networks are made in such a way that the intersection of the wires of the transmission line with increasing nominal voltage increases in proportion to the voltage. This achieves such parameters of overhead lines, at which their natural capacities correspond to the allowable thermal load

current. As a result, the networks are heterogeneous, and with increasing range of nominal voltages of the networks of the integrated power system, the degree of heterogeneity increases. Therefore, the advantages of closed networks, which are greater reliability of power supply, better quality of transmission and greater efficiency are realized due to the presence of heterogeneity is not always. The impact of heterogeneity can be so significant that special measures have to be taken to improve the operating conditions of such networks.

The sharpest heterogeneity is manifested in cases of transmission of large transit power through a network consisting of parallel connected (through transformers) sections of different rated voltages. The mismatch of the inductive resistances of the branches to their active resistances leads to a decrease in network capacity. The distribution of loads in the network is unfavorable: while one of the branches (lower rated voltage) is fully loaded, the other (higher rated voltage) is not loaded.

The currents are distributed along the lines according to the total resistance of the longitudinal branches of the substitution circuits, as well as transformers. This is a natural flow distribution. The minimum of losses of active power in a network can be reached if to provide flow distribution according to active support of longitudinal branches. This flow distribution is optimal, economical. Studies have shown that the natural flow distribution is significantly—1.5 times less economical in terms of losses, creates an overload of lower voltage networks with transit power flows, reduces the capacity of "multilayer" sections of the entire network. To eliminate this phenomenon, it is recommended to use various controls and measures.

In its own turn, the reactive urge to lie down in the pool of compensatory attachments of the charging strain line. When the robotics mode of the EHV transmission line is regulated, it is necessary to determine the minimization of the function of the consumption (17–18) according to the independent operating parameters.

$$\frac{\partial \Delta P}{\partial U} = 0, \quad \frac{\partial \Delta P}{\partial B_{reac}} = 0. \tag{20}$$

The Eq. (19) allows obtaining the conditions of optimal regulation of the flows of the reactive power of the transmission line, the power of the CSR and the voltage at the connection point.

Due to the active and reactive power flow of power system can be approximate decoupled, the impact of reactive power compensation for power flow is negligible, so that the primarily impact of reactive power compensation for active loss of the branch is ΔP. According to the "proportional sharing" principle, ΔP could decomposed to each load node, the factor of load node i for active power loss could be defined as power loss distribution coefficient.

If there are more reactive source nodes serve reactive power for load node i, and the reactive power transmissions through branch is larger than others, thereby j would be larger than others. So, the active power loss of the system would be reduced effectively, if load node i was compensated properly. Assume the number of node allowed compensating, then i of all load nodes were sorted descending, the largest load node would be former elected optimal reactive compensation points.

Compensation of reactive power in networks is one of the possible and effective measures to reduce losses in electrical networks; however, the effectiveness of this measure largely depends on how well the locations of installation of additional compensating devices in the electrical network are selected. At the same time, the algorithms for finding the most effective places for installing additional compensating devices still require development and improvement, since with the wrong choice of installation sites, their efficiency decreases, which leads to an increase in costs without obtaining a noticeable positive effect.

5 Analysis and Optimization of Power Systems Operating Modes According to the Minimizing Criterion of Active Power Losses

Currently, in the power industry of the country, great importance is attached to the creation of managed or flexible power lines, which are part of the "smart" networks with smart devices FACTS (Flexible Alternative Current Transmission Systems). Highly efficient means of regulating the flows of both active and reactive power are necessary for the optimal management of such power systems.

To control the modes of voltage and reactive power, along with the traditional use of generators, synchronous and static compensators, switched reactors and capacitor banks in the last decade, more and more widely used new devices—controlled shunt reactors. The combination of CSR with a parallel battery of static capacitors (BSC) allows not only providing smoothly adjustable compensation (consumption) of reactive power, but also its issuance in accordance with the power of BSC when unloading CSR to idle mode.

An important task of modeling a power system is to determine the optimal modes. The goal of optimization is to find acceptable economical modes that are, satisfying the conditions of reliability of power supply and proper quality of energy. This allows for virtually no additional cost savings through reduction of losses in electrical networks, measured on the scale of the energy sector. The task of calculating the optimal mode is to find the optimal values of all parameters characterizing its admissibility and efficiency, in particular active and reactive powers and voltages. The main indicator, by which the efficiency of work is assessed energy system, is the amount of electricity losses in the electrical network.

This indicator largely depends on the distribution of the load between the supply substations and the cost of electricity. For example, loading substations with less the cost of electricity, but removed from consumers, you can reduce the cost of electricity, but increase electricity losses in the network [20–40]. Having two separate, indicators that depend on each other makes it difficult to assess the efficiency of modes energy system and measures to improve it, especially in cases where in one of the compared modes, the cost of electricity per supplied 1 kWh is higher, and the losses in the network is smaller than in the other.

If the electrical network is represented by nodal equations in the form of a power balance:

$$\begin{aligned} P_i &= g_{ii}U_i^2 - \sum_{j=1}^{N_i} U_i U_j (b_{ij}\sin\delta_{ij} - g_{ij}\cos\delta_{ij}) = P_i(\delta_i, \delta_j, U_i, U_j); \\ Q_i &= g_{ii}U_i^2 - \sum_{j=1}^{N_i} U_i U_j (b_{ij}\sin\delta_{ij} - g_{ij}\cos\delta_{ij}) = Q_i(\delta_i, \delta_j, U_i, U_j), \end{aligned} \tag{21}$$

where P, Q, U, δ—powers (active and reactive) and voltages (modules and angles), then the active power losses ΔP_Σ during the transmission of electrical energy through the network can be defined as the algebraic sum of active powers generated and consumed in all N nodes:

$$\Delta P_\Sigma = \sum_{j=1}^{N_i} P_i(\delta_i, \delta_j, U_i, U_j). \tag{22}$$

The power losses of the ΔP_{ij} in each branch ij and in the network as a whole (22) are explicit functions of the nodal voltages U_i, U_j and, at the same time, implicit functions of the powers S_i at the nodes of the network, since the latter, through the power balance Eq. (21), determine U_i, U_j.

Changes in reactive powers at Q_i nodes lead to changes in network nodal voltages in accordance with (21). The consequence of this, in turn, is a change in power losses in the network, as can be seen from (22). At the same time, changes in reactive powers should correspond to the available range of sources regulation and not cause unacceptable voltage deviations in the network nodes:

$$Q_{\min} \le Q_i \le Q_{\max}; U_{\min} \le U_i \le U_{\max}. \tag{23}$$

Expressions (21)–(23) constitute a mathematical formulation of the optimization problem, which consists in determining the installation locations and power of additional, at which the minimum of the objective function (22) is ensured and the constraints in the form of equalities (21) and inequalities (23). In solving this general problem, it is advisable to single out two narrower ones: (1) the choice of the place for installing additional KU in the network; (2) determination of the optimal capacities of the CSR in the modes. This article deals with the solution of the first of these two tasks.

Objective function (22) and Eq. (21) are expressed by continuous differentiable functions; therefore, the solution of the problem is possible based on the use of gradient methods. Derivatives of power losses ΔP_Σ by the parameters of the mode U_i, δ_i can be obtained by differentiating function (22):

$$\frac{\partial P_\Sigma}{\partial U_i} = \frac{\partial P_i}{\partial U_i} + \sum_{j=1}^{N} \frac{\partial P_j}{\partial U_i}, \tag{24}$$

$$\frac{\partial P_\Sigma}{\partial \delta_i} = \frac{\partial P_i}{\partial \delta_i} + \sum_{j=1}^{N} \frac{\partial P_j}{\partial \delta_i}. \tag{25}$$

Objective $\frac{\partial P_i}{\partial U_i}, \frac{\partial P_j}{\partial U_i}, \frac{\partial P_i}{\partial \delta_i}, \frac{\partial P_j}{\partial \delta_i}$ function (24–25) are elements of matrix Jacobi, which are used for analyses normal mode of networks. Derivatives of power losses ΔP_i, ΔQ_i by the parameters ΔU_i, $\Delta \delta_j$ are related by the ratios:

$$\begin{aligned} &\sum_{j=1}^{N} \frac{\partial \Delta P_i}{\partial \delta_j} \Delta \delta_j + \sum_{j=1}^{N} \frac{\partial \Delta P_i}{\partial U_j} \Delta U_j = \Delta P_i; \\ &\sum_{j=1}^{N} \frac{\partial \Delta Q_i}{\partial \delta_j} \Delta \delta_j + \sum_{j=1}^{N} \frac{\partial \Delta Q_i}{\partial U_j} \Delta U_j = \Delta Q_i; \end{aligned} \tag{26}$$

obtained from (21). That is why increment ΔU_i, $\Delta \delta_j$ vectors of nodal voltages caused by the inclusion of additional reactive power in one of the network nodes can be determined by solving the linearized system of Eq. (26), in which the column vector of given values on the right side contains only one nonzero element—the increment of reactive power ΔQ_i in the node i.

Knowing the derivatives (24–25) and calculating the increment of the modules and angles of the nodal voltages when the additional power ΔQ_j is switched on, in the node i, in accordance with the theory of implicit functions [30–40], it is possible to determine the increment of the losses ΔP caused by the inclusion of ΔQ_j:

$$\Delta P = \sum_{j=1}^{N} \frac{\partial \Delta P}{\partial U_j} \Delta U_j + \sum_{j=1}^{N} \frac{\partial \Delta P}{\partial \delta_j} \Delta \delta_j. \tag{27}$$

Then the ratio of the increment in the losses of the ΔP to the increment in the reactive power ΔQ_j in the node i at small ΔQ_j, can be taken equal to the corresponding derivative of the can be obtained by differentiating function:

$$\frac{\partial P_\Sigma}{\partial Q_i} \approxeq \frac{\Delta P_\Sigma}{\Delta Q_i}. \tag{28}$$

To determine the derivatives of losses when changing reactive power in each of the N nodes of the network, you need to obtain the Jacobi matrix once, perform its inversion and, setting the increment on the right side of Eq. (26) in turn in each of the N nodes, calculate the corresponding increment vectors $\Delta \delta_i$, ΔU_i and then—the increment of losses by expression (27).

Table 5 Influence of additional CSR on power losses

Compensation node number	Active power loss, ΔP_Σ, mWatt	Reduction of losses $\frac{\Delta P_\Sigma}{\Delta Q_i}$, mW/MVAr	Node numbers in order of priority
1	85.5924	0.094	4
2	73.5931	0.087	3
3	63.5928	0.090	2
4	53.5919	0.099	1
5	79.5923	0.095	5

Calculations of the derivatives of losses ΔP_Σ by reactive power, carried out for real electrical networks 330–750 kV, show that the numerical values of these derivatives vary over a very wide range - from 1 10^{-5} to 1 10^{-1}. For illustration in Table 5 is shown the results of such calculations for a fragment of the 750 kV electrical network.

Losses of active power in the initial normal mode are 63.6018 mW. Table 5 shows losses after installing additional compensating devices for a number of network nodes, specific (per 1 MVAr) loss reduction, node numbers in priority order (first 10 nodes).

The value of the derivative $\frac{\partial P_\Sigma}{\partial Q_i}$ can be considered as the indicator for the efficiency of installing additional compensating device in node i, since it characterizes a decrease in power losses in the corresponding node by 1 MVAr of installed additional reactive power. Consequently, when choosing a place for installing additional CSR in order to reduce power losses in the electric network, preference is needed to give to the nodes with the highest value $\frac{\partial P_\Sigma}{\partial Q_i}$ and as exhaustion per the possibilities of regulation in such nodes to go over (if it is economically justified) to nodes with smaller ones $\frac{\partial P_\Sigma}{\partial Q_i}$.

Calculations for compensation from reactive power in electrical networks also show that, judging only by $\frac{\partial P_\Sigma}{\partial Q_i}$ partial derivatives, then among the nodes that followed per If you would like to choose additional CSR as installation sites, there may be nodes located both in a heavily and in a weakly loaded part of the network. An indicator characterizing the degree of line congestion can be considered the ratio of the power P_{ij} transmitted through the overhead line to its natural power P_{nat} (load factor of the overhead line):

$$k_l = \frac{P_{ij}}{P_{nat}} \tag{29}$$

on the grounds that when transmitting power through overhead lines, more natural. ($k_l > 1$) consumption of reactive power exceeds its generation by the line, which leads to an increase in active power losses. Therefore, when choosing a place for installing additional CSR, it is also necessary to take into account the network load from nodes with the same or $\frac{\partial P_\Sigma}{\partial Q_i}$ close ones give preference to the nodes to which they adjoin per lines with a load factor $k_l > 1$.

(1) In accordance with the above, to select the optimal places for installing additional CSR when solving the optimization problem (20–23), it seems appropriate to use the following algorithm:
(2) Calculate the initial mode and select the loaded part of the network;
(3) Form the Jacobi matrix corresponding to the linearized nodal power balance equations by the voltage of the initial steady state, and learn the inverse Jacobi matrix;
(4) Calculate partial derivatives of power losses in the electrical network by modules and angles of nodal voltages according to formulas (24);
(5) Calculate the increments of modules and angles, nodal voltages corresponding to additional reactive power $\Delta\delta_i$, ΔU_i in each of the network nodes according to Eq. (5);
(6) Calculate the gains of ΔP_i losses in the loaded part of the network caused by additional CSR and derivatives of power losses of additional CSR;
(7) Choose the place of installation of additional compensating device, taking into account private $\frac{\partial P_\Sigma}{\partial Q_i}$ derivatives and network loading.

The main purpose of controlled shunt reactors is to regulate voltage and reactive power. In CSR with magnetization for smooth regulation of the consumed reactive power, and hence voltage in a connection point, saturation of steel with a constant stream created by the rectified current in a special control winding is used. In fact, for a powerful high voltage transformer device uses the principle of a magnetic amplifier, when as the saturation of the rods of the theater decreases the inductance of the network winding located on them, and also proportionally reduces its inductive resistance.

As the inductive resistance of the reactor winding decreases or increases, its current increases proportionally or decreases, which means that the power consumption of the reactor in the range from idling (about 1%) to rated power or allowable overload (100–120%). Thus, the use of sections of steel of the core in modes from unsaturated state to deep saturation, close to the limit, when the magnetic permeability approaches the magnetic permeability of air, allows obtaining a range of smooth regulation of reactive power with a multiplicity of more than 100%.

The approach proposed in the dissertation allows modeling corona losses for different meteorological conditions, taking into account the intensity of precipitation, the effect of heating by the load current on losses for overhead lines with wires and lightning protection cables arbitrarily located in space. For a specific design of overhead lines and weather conditions, it is convenient to represent corona losses as a function of voltage. For this purpose, an algorithm and program for obtaining specific corona losses from voltage have been developed in the form of a power function and polynomials up to the fourth degree for the main four and additional weather groups.

In the problems of calculating the normal modes of electrical networks, it is convenient to represent the corona of overhead lines in the form of: constant selection; the conductivity of the shunt to ground [40–46].

In turn, formulas for determining technological power losses were derived:

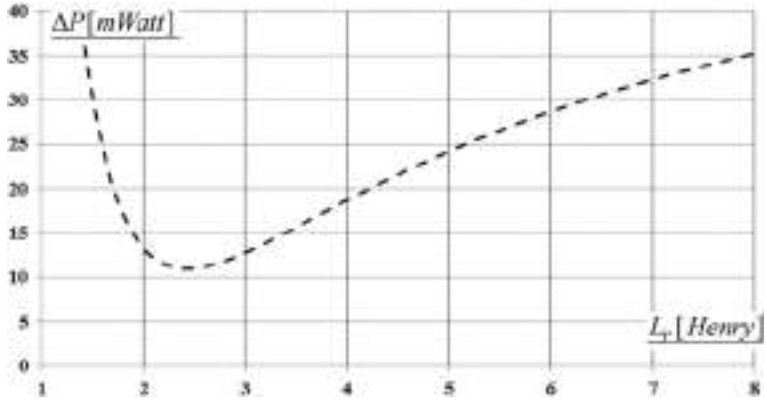

Fig. 4 Reduction of total losses of active power at application of CSR

$$\Delta P^{Tech} = \frac{R \cdot (X \cdot B^2 \cdot Q^2 \cdot U^2 - R \cdot B^2 \cdot P \cdot U^2 - 2 \cdot B \cdot Q \cdot U^2 + 2 \cdot P^2 + 2 \cdot Q^2)}{2U^2}. \quad (30)$$

Expression of determination of corona power losses:

$$\begin{aligned} \Delta P^{Corona} = & \frac{G \cdot (2 \cdot B^2 \cdot U^4 \cdot X^2 - 7 \cdot B \cdot Q \cdot U^2 \cdot X^2}{2U^2} \\ & + \frac{G \cdot (2 \cdot G^2 \cdot U^4 \cdot X - 12 \cdot B \cdot U^4 \cdot X)}{2U^2} \\ & + \frac{G \cdot (2 \cdot G^2 \cdot U^4 \cdot X^2 - G \cdot P \cdot U^2 \cdot X^2 + P^2 \cdot X^2 + Q^2 \cdot X^2)}{2U^2} \\ & + \frac{G \cdot (30 \cdot Q \cdot U^2 \cdot X^2 - 16 \cdot U^4)}{2U^2}. \end{aligned} \quad (31)$$

Depending on the degree of compensation, the values of active power losses vary widely (Fig. 4) taking into account the losses on the crown.

6 Conclusions

The most time-consuming computational operations (items 1–3), necessary for the implementation of the algorithm are an integral part of the calculations of the normal modes of the electrical network, and to solve the problem it is only necessary to supplement them with the calculation of the derivatives of the power losses of additional compensating controlled device. The proposed algorithm for selecting the installation sites for additional compensating controlled device is effective in combination with the program for calculating the steady-state regime by Newton's method, when solving linearized equations on the calculation step by the block method of

double factorization, which is confirmed by calculations on the choice of means of compensation for reactive power in electrical networks.

The lack of a controlled balance of capacities in the power system can lead to negative consequences, the prevention of which should be carried out at the pace of the processes, occurring in the power system. FACTS combination with modern information and computer technologies allow solving these problems and contribute to creation of intelligent power supply systems. To ensure consistent voltage regulation, the voltage regulation range of transformers must be economically justified according to specific conditions. The presence of intermediate systems on long-distance power transmissions favors practical implementation modes of coordinated voltage regulation.

Within the framework of this chapter which is considered far from all possible control actions: in addition to changing the resistance (conductivity) of the network element, it can also be turning on or off the network element, changing the EMF of the generator. It can be shown that for such control actions the dependences of the operating parameters will have a fractional-polynomial character. For further significant interest represents the optimization of power systems of various configurations according to the criterion of increasing the limit of static stability, as well as optimization according to complex (vector) criteria that include simultaneously several criteria of reliability and quality the work of the power system.

In this work, on the example of modeling the power network, the optimization problem is investigated and the method of its solution. Parameters defined mathematical model of the investigated electrical network. Results are given modeling the parameters of the operating mode of the electrical network of the power system, established the amount of loss reduction depending on the degree of reactive power compensation load.

Functional dependencies have been obtained for assessing the degree of reduction of active power losses in power transmission lines when compensating for the reactive power of the consumer, depending on the voltage level supplied to the capacitor units, taking into account the dielectric losses in the capacitors. A mathematical analysis of the obtained functional dependencies, which can be used when making decisions on the compensation of reactive power in the power supply systems of industrial facilities, has been carried out.

References

1. Kundul, S., Ghosh, T., Maitra, K., Acharjee, P., Thakur, S.S.: Optimal location of SVC considering techno-economic and environmental aspect. 2018 ICEPE 2nd International Conference on Power, Energy and Environment: Towards Smart Technology, Shillong, India, India pp. 15–19. (1–2 June 2018). DOI: https://doi.org/10.1109/EPETSG.2018.8658729
2. Gu, S., Dang, J., Tian, M., Zhang, B.: Compensation degree of controllable shunt reactor in EHV/UHV transmission line with series capacitor compensation considered. Proceedings of International Conference on Mechatronics, Control and Electronic Engineering (MCE 2014), Shenyang, China, pp. 65–68. (August 29–31, 2014). https://doi.org/10.2991/mce-14.2014.14

3. Chandrasekhar, R., Chatterjee, D., Bhattarcharya, T.: A hybrid FACTS topology for reactive power support in high voltage transmission systems IECON 2018—44th Annual Conference of the IEEE Industrial Electronics Society October 21–23, 2018 at the historic Omni Shoreham Hotel, Washington DC, USA, pp. 65–70. (2018). DOI: https://doi.org/10.1109/IECON.2018.8591988
4. Bryantsev, A.M., Bryantsev, M.A., Bazylev, B.I., Dyagileva, S.V., Negryshev, A.A., Karymov, R.R., Makletsova, E.E., Serguei Smolovik.: Power compensators based on magnetically controlled shunt reactors in electric networks with a voltage between 110 kV and 500 kV. 2010 IEEE/PES Transmission and Distribution Conference and Exposition: Latin America (T&D-LA), pp. 239–244. (2010)
5. Kuchanskyy, V.V.: The prevention measure of resonance overvoltges in extra high voltage transmission lines. 2017 IEEE First Ukraine Conference on Electrical and Computer Engineering (UKRCON), pp. 436–441. DOI: https://doi.org/10.1109/UKRCON.2017.8100529
6. Kuchanskyy, V.V.: Application of controlled shunt reactors for suppression abnormal resonance overvoltages in Assymetric modes. 2019 IEEE 6th International Conference on Energy Smart Systems (ESS), pp.122–125. DOI: https://doi.org/10.1109/ESS.2019.8764196
7. Kuchanskyy, V., Zaitsev, I.O.: Corona discharge power losses measurement systems in extra high voltage transmissions lines. 2020 IEEE 7th International Conference on Energy Smart Systems (ESS), Kyiv, Ukraine, pp. 48–53. (2020). doi: https://doi.org/10.1109/ESS50319.2020.9160088
8. Kuchanskyy, V., Malakhatka, D., Ihor, B.: Application of reactive power compensation devices for increasing efficiency of bulk electrical power systems. 2020 IEEE 7th International Conference on Energy Smart Systems (ESS), Kyiv, Ukraine, pp. 83–86. 2020. doi: https://doi.org/10.1109/ESS50319.2020.9160072
9. Kuchanskyy, V.: Application of controlled shunt reactors for suppression abnormal resonance overvoltages in assymetric modes. 2019 IEEE 6th International Conference on Energy Smart Systems (ESS), Kyiv, Ukraine, pp. 122–125. (2019) doi: https://doi.org/10.1109/ESS.2019.8764196
10. Yu. I., Tuhay, V.V., Kuchansky, I.Yu.: Tuhay The using of controlled devices for the compensation of charging power on ehv power lines in electric networks. Technical Electrodynamics, (1), 53–56. (2021)
11. Kuznetsov, V., Tugay, Y., Kuchanskyy, V.: Overvoltages in open-phase mode. Tekhnichna Elektrodynamika, No. 2, pp. 40–41. (Ukr). (2012)
12. Kuznetsov, V., Tugay, Y., Kuchanskyy, V.: Influence of corona discharge on the internal ovevoltages in highway electrical networks. Tekhnichna Elektrodynamika, No. 6, pp. 55–60. (Ukr). (2017)
13. Kuchanskyy, V.: Criteria of resonance overvoltages occurrence in abnormal conditions of extra high voltage transmission lines. Visnyk naukovykh prats Vinnytskoho Nastionalnoho Tekhnichnoho Universytetu, no. 4, pp. 51–54. (2016)
14. Blinov, I.V., Zaitsev, I.O., Kuchanskyy, V.V.: Problems, methods and means of monitoring power losses in overhead transmission lines. In V.P. Babak, V. Isaienko, A.O. Zaporozhets (ред.). Systems, Decision and Control in Energy I (p. 123–136). Springer. (2020)
15. Kuznetsov, V.G., Tugay, Y.I., Kuchansky, V.V., Likhovid, Y.G., Melnichuk, V.A.: Resonant overvoltages in non-sinusoidal mode of the main electric network. Elektrotehnika ta Elektromehanika. **2**, 69–73. (Ukr). (2018)
16. Hunko, I., Kuchanskyi, V., Nesterko, A., Rubanenko, O.: Modes of electrical systems and grids with renewable energy sources—LAMBERT Academic Publishing, p. 184. (2019). ISBN 978–613–9–88956–3
17. Kuchanskyy, V.: Olena Rubanenko Influence assesment of autotransformer remanent flux on resonance overvoltage UPB Scientific Bulletin. Series C: Elect. Eng. **82**(3), 233–250 (2020)
18. Vladislav Kuchanskyy, Paul Satyam, Olena Rubanenko, Iryna Hunko Measures and technical means for increasing efficiency and reliability of extra high voltage transmission lines PRZEGLĄD ELEKTROTECHNICZNY **2020**(11), 135–141. (2020). doi:https://doi.org/10.15199/48.2020.03.27

19. Martinich, T., Nagpal, M., Manuel, S.: Damaging open-phase overvoltage disturbance on a shunt-compensated 500-kV line. IEEE Trans. Power Deliv. **30**(1), 412–419. (Feb. 2015)
20. Bollen, M.H.J.: What is power quality? Review. Elect. Power Syst. Res. **66**(1), 5–14 (July 2003)
21. Wenjuan, Z., Tolbert, L.M.: Survey of reactive power planning methods. in Proc. 2005 PES General Meeting, pp. 1430–1440. (2005)
22. Liu Chengxi, Qin Nan, Bak, C.L., Xu Yini.: A hybrid optimization method for reactive power and voltage control considering power loss minimization. in Proc. IEEE Eindhoven PowerTech, pp. 1–6. (2015)
23. Herman, L., Papič, I.: Optimal control of reactive power compensators in industrial networks. in Proc. 14th Int. Conf. On Harmonics and Quality of Power (ICHQP), Bergamo, Italy, pp. 1–6. (26–29 Sept. 2010)
24. Eajal, A.A., El-Hawary, M.E.: Optimal capacitor placement and sizing in distorted radial distribution systems. Part II: Problem formulation and solution method. in Proc. 14th Int. Conf. on Harmonics and Quality of Power (ICHQP), Bergamo, Italy, pp. 1–6. (26–29 Sept. 2010)
25. Lukomski, R., Wilkosz, K.: Optimization of reactive power flow in a power system for different criteria: stability problems. in Proc. The 8th Int. Symp. on Advanced Topics In Electrical Engineering, Bucharest, Romania, s. 1–6. (May 23–24, 2013)
26. Ionescu, C.F., Bulac, C., Capitanescu, F., Wehenkel, L.: Multi-period power loss optimization with limited number of switching actions for enhanced continuous power supply. in Proc. 16th Int. Conf. on Harmonics and Quality of Power (ICHQP), Bucharest, Romania, pp. 34–38. (25–28 May 2014)
27. Pham, V.-H., Erlich, I.: Online optimal control of reactive power sources using measurement-based approach. in Proc. 2014 IEEE PES Innovative Smart Grid Technologies Conference Europe, Istanbul, Turkey, pp. 1–5. (12–15, Oct. 2014)
28. Mori, H., Hayashi, T.: New parallel tabu search for voltage and reactive power control in power systems. in Proc. IEEE Int. Symp. on Circuits and Systems, Monterey, CA, pp. 431–434. (May–Jun. 1998)
29. Khiat, M., Rehiel, D., Chaker, A., Frioui, Z.: Optimal reactive power dispatch and voltage control using interior point method. Acta Electrotehnica **52**(2), 81–85 (2011)
30. Trochim, W.: The research methods knowledge base, 2nd edn. OH, Atomic Dog Publishing, Cincinnati (2000)
31. van Cutsem, T.: Voltage instability: phenomena, countermeasures, and analysis methods. Proc. of the IEEE **88**(2), 208–227 (2000)
32. Kessel, P., Glavitsch, M.: Estimating the voltage stability of the power system. IEEE Trans. on Power Delivery **1**(3), 346–354 (1986)
33. Moghavvemi, M., Omar, F.M.: Technique for contingency monitoring and voltage collapse prediction. IEE Proce. Generat. Trans. Dist. **145**(6), 34–640. (November 1998)
34. Moghavvemi, M., Faruque, O.: Real-time contingency evaluation and ranking technique. IEE Proce. Generat. Trans. Distrib. **145**(5), 517–524. (1998)
35. Moghavvemi, M., Omar, F.M.: A line outage study for prediction of static voltage collapse. IEEE Power Engineering Review. (1998)
36. Reis, C., Maciel Barbosa, F.P.: A comparison of voltage stability indices. Proc. of IEEE MELECON, Málaga, Spain, pp.1007–1010. (2006)
37. Reis, C., Maciel Barbosa, F.P.: Line indices for voltage stability assessment. Proc. of IEEE Bucharest PowerTech Conference, Bucharest, Romania, pp. 1–6. (2009)
38. Karbalaei, F., Soleymani, H., Afsharnia, S.: A comparison of voltage collapse proximity indicators. Proc. of IPEC Conference, pp. 429–432. (2010)
39. Deb, K.: Multi-objective optimization using evolutionary algorithms", Wiley Press, pp. 113–125. (2002)
40. Liping, L., Jian, Z., Qi, W., Zhao, Y., Yizhe, W., Ying, L.: Theoretical calculation and evaluation of the line losses on UHV AC demonstration project. 2015 IEEE International Conference on Cyber Technology in Automation, Control, and Intelligent Systems (CYBER), Shenyang, pp. 1299–1303. (2015)

41. So, E., Arseneau, R.: Traceability of no-load loss measurements of high voltage transmission lines. 2016 Conference on Precision Electromagnetic Measurements (CPEM 2016), Ottawa, ON, pp. 1–2. (2016)
42. Netake, A, Katti, P.K.: Design aspect of 765kV transmission system for capacity enhancement. 2015 International Conference on Circuits, Power and Computing Technologies [ICCPCT-2015], Nagercoil, pp. 1–9. (2015)
43. Liping, L., Jian, Z., Qi, W., Zhao, Y., Yizhe, W, Ying, L.: Theoretical calculation and evaluation of the line losses on UHV AC demonstration project. 2015 IEEE International Conference on Cyber Technology in Automation, Control, and Intelligent Systems (CYBER), Shenyang, pp. 1299–1303. (2015)
44. Meah, K., Ula, S.: Comparative evaluation of HVDC and HVAC transmission systems. 2007 IEEE Power Engineering Society General Meeting, Tampa, FL, pp. 1–5. (2007)
45. Hanqing, L.: Operation losses and economic evaluation of UHVAC and HVDC transmission systems. Power Syst. Technol. **36**(2), 1–6 (2012)
46. Rickard, D.A., Waters, R.T., Dupuy, J.: Frequency effects in alternating current Corona. Sixth International Symposium on Gaseous Dielectrics, pp. 413–419. (1991)
47. Shu, Y.-B., Hu, Y.:Research and application of the key technologies of UHV AC transmission line. Proc. CSEE, vol. 36, pp. 2. (Dec. 2017)

Short Term Renewable Energy Forecasting with Deep Learning Neural Networks

Volodymyr Miroshnyk, Pavlo Shymaniuk, and Viktoriia Sychova

Abstract Renewable energy sources (RES) are sources of electricity production with a sharply uneven load coverage schedule. Unsatisfactory accuracy of RES forecasts leads to additional production/consumption imbalances and additional costs for settling these imbalances. The need to unload or load flexible electricity producers to compensate for the potential imbalance created by electricity producers at the feed-in tariff will lead to a significant increase in the cost of electricity in such organized market segments as Balancing Market and Ancillary services market. Created imbalances of RES will lead to an even greater increase in electricity prices in terms of the transmission tariff of the Transmission System Operator due to both the payment of electricity produced for feed-in and the increase of imbalances created by them. In such conditions, you can improve the quality of decision-making when planning regimes using accurate forecasts for day-ahead and intraday markets. Statistical methods for forecasting time series have become widespread in the problem of forecasting the RES energy generation. The essence of the methods of this class is to select the parameters of statistical models by minimizing the error of the forecast on historical data. The simplest are one-factor models that take into account only the previous values of generated energy volume. In this class, the most common models are ARIMA (Box-Jenkins in various modifications), exponential smoothing (Holt-Winters in various modifications), and models based on the Kalman filter. The development of machine learning theory and artificial intelligence has led to effective mathematical tools for constructing complex hierarchical models such as support vector machines (SVMs) and artificial neural networks (ANNs) including deep learning methods. The advantages of models of this class are their flexibility, high generalization ability (the ability to make accurate predictions on data that are not in the learning process), and the ability to work with data without prior selection of significant features by an expert. Usually for a neural network of deep learning requires much more data than for classical models. Their disadvantages include the complexity of developing a network architecture and calibration of the learning process. By choosing successful architecture and learning procedure parameters, it is possible to fully automate the neural network learning process for new objects and

V. Miroshnyk (✉) · P. Shymaniuk · V. Sychova
Institute of Electrodynamics of NAS of Ukraine, Kyiv, Ukraine

O. Kyrylenko et al. (eds.), *Power Systems Research and Operation*, Studies in Systems, Decision and Control 388, https://doi.org/10.1007/978-3-030-82926-1_6

adapt to changes in existing data. In this chapter, we propose a novel architecture for short-term energy forecasting of aggregated RES generation.

Keywords Short term generation forecast · Renewable energy sources · Neural network · Deep learning

1 Introduction

There is a trend in the world to reduce capital costs for the construction of renewable energy sources (RES) power plants. The greatest reduction is observed for solar power plants, due to cheaper and more efficient panels and scaling of their production processes. To estimate the price of electricity at which the profitability of the power plant will be equal to the value set in the project, the indicator of levelized cost of energy (LCOE) is used. According to consulting company Lazard [1], the average LCOE for industrial solar photovoltaic plants fell from $ 359 in 2009 up to $ 37 in 2020 per MWh, for wind power plants LCOE decreased from 135 to 40 $ per MWh.

According to the annual report "Renewable power generation costs" published by the International Renewable Energy Agency (IRENA) [2] in 2019, the trend of decreasing LCOE worldwide continues. Since 2010, the average LCOE for solar power plants decreased from 371 to 68 $ per MWh in 2019.

Data from both organizations indicate that the cost of RES power plants in recent years has been lower than the cost of stations with traditional energy sources.

According to the NGO "Laboratory of Clean Energy" [3], LCOE for RES power plants built in Ukraine also decreased significantly between 2012 and 2018. For solar power plants LCOE decreased by an average of 71% from 403 EUR / MWh to 116 EUR/MWh for wind power of 28% from 107 EUR/MWh to 77 EUR/MWh for hydropower plants from 271 EUR / MWh to 177 EUR/MWh (35%), for biomass from 168 EUR/MWh to 104 EUR/MWh.

The average "green" tariff for stations commissioned in 2018 and LCOE data are shown in Table 1. Exchange rate 28.2 UAH / USD and 1.18 USD/EUR. Hydropower plants of any capacity were taken into account in the calculation of IRENA.

Table 1 Comparison of feed-in tariff in Ukraine with LCOE

Energy source type	Feed-in tariff, USD/MWh	LCOE, USD/ MWh		
		CEL	Lazard	IRENA
PV	178	137	43	85
Wind	120	91	42	56
Hydro	138	209		47
Biogas	146	123		62
Biomass	146	123		62

Table 2 Coefficients of ideality of the diode

Technology of production of photocells	Coefficient of ideality
Si-mono	1.2
Si-poly	1.3
a-Si–H	1.8
Tandem a-Si:H	3.3
Triple a-Si:H	5
CdTe	1.5
CIS	1.5
AsGa	1.3

According to the OECD in 2017 [4] feed-in-tariff for solar power plants is higher than in Ukraine (178 USD/MWh) was only in Australia, Japan, Italy, and Portugal.

Support for RES producers is undoubtedly necessary to achieve the goals of sustainable development and fulfillment of Ukraine's international obligations, but incentives without the unconditional issuance of a "green" tariff can lead to financial crises and affect the reliability of Ukraine's energy system. A similar situation led to the termination of the subsidy program for RES producers in Spain in 2010.

The peculiarity of electricity production from RES is the low accuracy of generation forecasting, which is due to the stochastic nature of meteorological conditions. The inability to determine in advance the schedule of electricity supply from RES and responsibilities for the purchase of all electricity produced in combination with the peculiarities of the power system leads to the so-called "coal-green" paradox, which is a forced increase in production at TPP/CHP (most of which are worn out with an efficiency of 30%) to balance possible imbalances caused by RES [5]. In some power systems, due to limited line capacity, this replaces the base capacity of nuclear power plants with shunting units of coal-fired power plants, which further increases the price for the final consumer, atmospheric emissions, and reduced reliability of the power system. For further development of RES production in Ukraine, it is necessary to develop fast maneuvering capacities, battery energy storage systems, network capacity and improve the quality of forecasting the generation of electricity by RES stations [6].

Improving the accuracy of forecasting total generation of RES producers will reduce the size of imbalances in the power system and thus reduce the price of electricity for end-users, as the difference between the market price of electricity and the "green" tariff is partially offset by the transmission system operator [7].

Approaches to forecasting the supply of electricity by power plants with RES are divided into three groups [8]:

– forecast with the help of physical models of stations and meteorological forecasts [9];
– forecast using methods of time series analysis, including artificial neural networks [10];
– combining two approaches [11].

In the first approach, the projected value of meteorological parameters fed into a mathematical model, based on known physical dependence and geometric parameters of platform and station. More complex models take into account the features of the terrain around the site, the effect of wind shadow from adjacent installations, and others. Complex global numerical weather forecasts (NWP) are most often used for day-ahead forecasting. Given the significant amount of computing resources and the significant spatial distribution of measurement points, the construction of such forecasts is quite expensive and is usually developed by large collaborations of government and research institutions.

The best known are NWP National Oceanic and Atmospheric Administration (NOAA, USA), National Weather Service (USA), AROME, European Center for Medium-Range Weather Forecasts (ECMWF), North American Mesoscale (NAM), Global Forecast System (GFS), Rapid Update Cycle (RUC), Mesoscale Model Version 5 (MM5), Navy Operational Global Atmospheric Prediction System (NOGAPS), Coupled Ocean/Atmosphere Mesoscale Prediction System (COAMPS). The combination of several NWPs increases the accuracy and reliability of forecasts.

At intervals of less than a day, forecasts of meteorological factors are usually obtained based on measurements at remote sites. Solar power plants use cloud video monitoring systems for operational forecasts.

To predict the total output using the first approach, a physical model is required for each station. This requires high-quality meteorological forecasts for each location. Also, for an accurate forecast, the model must take into account local terrain and atmospheric parameters. At present, Ukrainian manufacturers do not have significant economic incentives that can offset the costs associated with the acquisition of weather forecasts and the construction of physical models. Therefore, the vast majority of producers are limited to naive forecasts, which significantly affects the imbalances in the IPS of Ukraine.

On the other hand, the geographical dispersion of locations and the presence of different types of RES do not create significant obstacles to statistical methods of forecasting total generation, which allow solving the problem centrally with minimal investment.

Statistical methods for forecasting time series have become widespread in the field of forecasting RES plants generation. The essence of the methods of this class is to select the parameters of statistical models by minimizing the error of the forecast on historical data. The simplest is one-factor models that take into account only the previous values of leave. In this class, the most common models are ARIMA (Box-Jenkins in various versions), exponential smoothing (Holt-Winters in various modifications), and models based on the Kalman filter.

2 Mathematical Models of Wind and Solar Plants for Generation Forecasting

The development of mathematical models for predicting wind or solar energy is due to nonlinear dependences of their parameters. Articles [12–16] describe the development and comparison of models for forecasting wind and solar energy production.

For wind farms, the forecast of wind energy depends on the relationship between wind speed and wind energy. The dependence of wind speed and wind power is nonlinear, so the forecast of wind energy in some cases can be asymmetric or multimodal. Based on the relationship between wind speed and wind power is determined forecast error distribution of the energy of the wind. The error of the wind speed forecast for the day before is determined using the technology of numerical weather forecasting. The accuracy of wind speed forecasts is influenced by the location, altitude, geographical environment of the wind power plants, as well as the forecast period. The distribution of wind energy can be obtained in accordance with the energy conversion ratio of the wind turbine. The energy of the wind is also affected by the density of the air, and this value changes rather slowly over a short period of time in the same zone. Therefore, the normal distribution of wind energy can be considered as the relationship between wind speed and power, which can be described as a formula:

$$f(v) = \frac{1}{\sqrt{2\pi}\sigma_v} e^{\frac{(v-\mu_v)^2}{2\sigma_v^2}},$$

where v—wind speed; μ_v—expected wind speed;σ_v—standard deviation of wind speed.

The Weibull distribution is used to analyze wind speed information. Weibull's distribution contains two main parameters: shape and scale. The distribution itself can be predicted using the wind speed distribution, the distribution function is given below:

$$f(v) = \frac{k}{c}\left(\frac{v}{c}\right)^{k-1} \cdot e^{-\left(\frac{v}{c}\right)^k},$$

where $c > 0$—scale parameter; $k > 0$—shape parameter. If the wind speed is less than the speed of the turbine, the wind generator is not able to output power, and if the wind speed is within the specified (starting) and nominal speed, the output increases with increasing wind speed. When wind speed exceeds cut-out value, the energy of the wind is equal to 0. To display the connection between energy and wind speeds are presented equation of "wind speed–wind power" [12]:

$$P(v) = \begin{cases} 0 & 0 < v < V_{in}; \\ a_0 + a_1 v + a_2 v^2 + a_3 v^3 & V_{in} \le v < V_r; \\ P_r & V_r \le v < V_{out}; \\ 0 & v \ge V_{out}, \end{cases}$$

where V_{in}—cut-in wind speed; V_{out}—cut-out wind speed; V_r—rated wind speed; P_r—power rating.

If the wind speed is in near or exceeds the cut-out speed, the wind power value is 0. Thus, the probability that the wind energy will be equal to 0 corresponds to the cumulative probability of wind speed $v \in (-\infty, V_{in}) \cup (V_{out}, +\infty)$. Also, when the wind speed is equal $v \in (V_{in}, V_r)$, the probability of wind energy is derived from the direct ratio of wind energy to wind speed. If the wind speed is between the rated wind speed and the cut-off speed $v \in (V_r, V_{out})$, the wind energy will be kept within the maximum value.

Main features for developing physical model for photovoltaic generation are [15]: the photoelectric current, current reverse saturation resistance of serial connection, the resistance of the parallel connection (or shunt resistance) and coefficient of ideal diode.

$$I_{ph} = (I_{sc} + K_i(T - 298)) \cdot \frac{I_r}{1000},$$

where I_{ph}—photoelectric current; I_{sc}—short circuit current (A); K_i—short-circuit current at a temperature of 25 °C and 1000 W/m^2; T—operating temperature (K); I_r—solar irradiation (W/m^2).

In addition to the photo of the electric current for forecasting it is necessary to obtain the reverse saturation current I_{rs}, it is determined by the formula:

$$I_{rs} = \frac{I_{sc}}{\exp\left(\frac{q V_{oc}}{N_s k n T}\right) - 1},$$

where q—electron charge, $= 1.6 \cdot 10^{-19}$ C; V_{oc}—open circuit voltage; N_s—number of cells connected in series; k—Boltzmann's constant $= 1.3805 \cdot 10^{-23}$ J / K; n—the ideality factor of the diode.

The coefficient of ideality of the diode is a parameter that depends on the technology of manufacturing photocells. In [16] describes the features of modeling solar modules and the choice of the coefficient of ideality. The table with the coefficients of ideality is given below:

Also, to determine the photovoltaic current of the module, it is necessary to determine the saturation current I_0, this parameter depends on the cell temperature and is determined by the formula below:

$$I_0 = I_{rs}(\frac{T}{T_r})^3 \exp\left(\frac{qE_{go}}{nk}\left(\frac{1}{T} - \frac{1}{T_r}\right)\right),$$

where T_r—nominal temperature, = 298.15 K; E_{go}—band gap energy of the semiconductor, 1.1 eV.

The output current of the photovoltaic module is defined as:

$$I = N_p I_{ph} - N_p I_0(\exp\left(\frac{\frac{V}{N_s} + \frac{IR_s}{N_p}}{nV_t}\right) - 1) - I_{sh};$$

$$V_t = \frac{kT}{q};$$

$$I_{sh} = \frac{\frac{VN_p}{N_s} + IR_s}{R_{sh}},$$

where N_p—the number of photovoltaic modules connected in parallel; R_s—resistance of series connection; R_{sh}—shunt resistance; V_t—thermal voltage of the diode; I_{sh}—shunt current.

The use of advanced forecasting models can provide better wind speed, solar irradiance and power forecasting results than reference models. However, quite important specify which model is best, reason is their location. Although the forecasting model works well it does not guarantee that it will work well elsewhere. In this case, the change in the overall accuracy of the forecast is described by the following statements [16]:

The accuracy of the forecast decreases with increasing duration of the forecast. The average absolute error of short-term forecasts of the mean average error (MAE) is usually in the range of 5–15%, but with increasing forecasting horizon, it grows rapidly. Thus, for the forecast period of 1–2 days, the MAE is in the range of 13–21%, and when forecasting for three days, the error increases to 20–25%.

The average value of normal MAE for the 12-h forecasting horizon can be compared with different sweets of the terrain where the wind farm is located. Much less IEA is observed in low-lying wind farms than in difficult areas. A significant increase A significant increase in the values of MAE occurs with increasing complexity of the terrain. In addition, offshore wind farms have slightly higher MAE values compared to lowland wind farms.

The effectiveness of prediction models and surf ‘ related to seasonal variability (change, change of seasons). Smaller forecasting errors are observed in winter, and then in summer, this is due to higher wind speeds on greater uncertainty in summer storm situations, with a separate low-pressure system with fast front areas containing complex wind structures.

The forecast error is compared as a function of the meteorological risk index (MRI), which assesses weather stability. The prediction error increases linearly with

increasing MRI (increasing MRI means instability of the weather regime). In addition, the prediction error does not depend on wind speed, but on pressure. The prediction error in the case of low pressure is greater than in the case of high pressure.

3 Forecasting Using Deep Neural Networks

All forecasting methods could be divided into physical and statistical methods. Physical methods include methods that are based on data on weather forecast, temperature, pressure, solar radiation and other physical parameters.

Statistical methods use historical data to model and analyze the input–output relationship to predict future results. These methods can directly predict wind speed based on historical wind speed data. Statistical methods can also be divided into time series methods, artificial intelligence methods and reference vector methods. Each of these statistical methods has its positive and negative aspects: time series methods can affect the local trend but are not able to correspond to nonlinear relationships between variables, and the effectiveness of the method depends on the forecast period. Artificial intelligence methods do not require previous model parameters but require a large amount of data for training, and also have time for training. In most cases, combined methods using deep learning are used for RES forecasting tasks. As a basis using recurrent neural networks, convolution neural networks and multilayer Perceptron [17–22] and neural and networks and radial basis function. Also for the problems of forecasting wind speed used wavelet transformations or decomposition of the data to study characteristics of signals.

In [17], studies of wind speed prediction using various algorithms based on artificial neural networks, namely multilayer perceptrons, convolutional neural network of a recurrent neural network and the method of k-nearest neighbors are described. The study was conducted with mountains and an umbrella ahead of 12 h. In [18] LSTM model was used for multivariate wind speed forecasting and called it optimally and density peaks weighting coefficients long short-term memory (OWDPC-LSTM). In the article [19], the analysis of variance and the grouping function of the auto- encoder for noise reduction were used to obtain accurate results of wind speed forecasting. And as the basis for the combined architecture for forecasting for various time intervals was LSTM. The average absolute error and the root mean square error are used as estimation model accuracy. In [20] to test the effectiveness of machine learning tools compared three methods: classical ARIMA, support vector machine and deep neural networks with adaptive distributed learning (ATL-DNN). Several data sets from wind farms located in Europe were used. In [21, 22] present hybrid networks and how their data is first fed to the autoencoder to reduce noise and data dimension, and then the encoded data fed to the deep learning network LSTM. To predict wind energy in general use such basic parameters as: wind speed, wind direction, zonal component of wind, meridional component of surface wind, relative humidity, temperature also use atmospheric pressure and the number of generators under repair.

Photovoltaic technologies, along with wind energy, are also evolving rapidly to meet electricity needs, and photovoltaic panels convert solar radiation into electricity through semiconductor materials. As well as wind energy forecasting, photoelectric energy forecasting strongly depends on meteorological conditions that can change over time. The use of photovoltaic panels is highly dependent on solar irradiation, ambient temperature, and geographical location. In [23] a hybrid model was proposed which included a machine learning model and a statistical model. LSTM, GRU and Auto-LSTM were compared as machine learning models.

The LSTM module has the ability to start on long-term dependencies, the architecture of this module is given below:

$$f_t = \sigma\left(W_f \cdot \left[h_{t-1}, x_t\right] + b_f\right);$$

$$i_t = \sigma\left(W_i \cdot \left[h_{t-1}, x_t\right] + b_i\right);$$

$$\tilde{C}_t = \tanh\left(W_c \cdot \left[h_{t-1}, x_t\right] + b_c\right);$$

$$C_t = f_t \cdot C_{t-1} + i_t \cdot \tilde{C}_t;$$

$$o_t = \sigma\left(W_o \cdot \left[h_{t-1}, x_t\right] + b_o\right);$$

$$h_t = o_t \cdot \tanh(C_t),$$

where σ—activation function; W_f, W_i, W_c, W_o—weights; b_f, b_i, b_c, b_o—bias coefficients; x_t—input vector; h_{t-1},h_t—output vector; $\tilde{C}_t$—memory cell correction vector; C_t, C_{t-1}—memory cell state.

GRU-controlled recurrent unit is a special LSTM architecture allows you to reduce the learning time of LSTM, this module has fewer inputs, and thus is simpler, the architecture of this module is as follows:

$$r_t = \sigma\left(W_r \cdot \left[h_{t-1}, x_t\right] + b_r\right);$$

$$z_t = \sigma\left(W_z \cdot \left[h_{t-1}, x_t\right] + b_z\right);$$

$$\hat{h}_t = \sigma(W_h \cdot x_t + U_h(r_t \cdot h_{t-1}) + b_h);$$

$$h_t = (1 - z_t) \cdot h_{t-1} + z_t \cdot \hat{h}_t,$$

where r_t—input; z_t—update vector; W_r, W_z, W_h, U_h, U—weights; b_r, b_z, b_h—biases; $h_t, \widehat{h}_t$—output and correction.

In [23] proposed hybrid architect which called MLSHM. In [24] presented a comparison of several variants of architectures and neural networks of deep learning which were compared with the model of physical photoelectric forecasting. For comparison, were used a multilayer perceptron, an LSTM model, an in-depth belief network, and an Auto-LSTM and a physical photoelectric P-PVFM forecasting model. At the same time, deep learning methods showed better results in comparison with the physical model of photoelectric generation forecasting. In [25] compared deep learning network with a simple neural network and method of predicting based on a sequence of samples. Several data sets were used to test the effectiveness: data from the photovoltaic system only, PV data with the addition of weather data, and data with the addition of weather forecast data. The following were used as weather data: daily maximum and minimum temperatures, precipitation per day, daily solar activity in hours, maximum daily wind speed, relative humidity, cloudiness and wind speed at 9 and 15 h, as well as daily solar radiation. The following were used as weather forecast data: forecast daily maximum and minimum temperatures, forecast daily precipitation and forecast daily radiation. Also, to check the effectiveness of the deep learning network, the optimal number of hidden layers and neurons in them was checked.

Estimation of solar irradiance is an important step to determine the effective photovoltaic power station to determine its use multiple options for land or satellite measurements using photos and analysis of air masses in the atmosphere. The disadvantage of satellite analysis is the inaccuracy in determining the magnitude of solar radiation through images in clear and cloudy weather. Also, methods that use satellite observation data do not take into account the attenuation of solar radiation through the atmosphere, so such studies require additional ground-based observation data. Thus, in [26], based on the method of satellite analysis, a method of numerical weather forecasting of NWP using recurrent artificial neural networks was proposed to predict real-time solar irradiation. To check the used network type LSTM and forecast carried out for a period of 1–4 h in advance. Preliminary data preparation is a rather important step for photoelectric energy forecasting. Since the forecast requires data on solar radiation and at night the solar radiation is 0 so the data is cleared of this type of data. In the article [27] for the prediction of solar radiation, preparations were made with the data from which only data during the period of solar radiation were selected. As a model for prediction, a recurrent neural network of deep learning type LSTM was used, which was compared with the usual single-layer perceptron and the method of reference vectors, respectively, deep learning methods showed better forecasting accuracy.

Based on the studies in [26], historical weather data do not improve forecasting results. A possible reason for this may be that the weather data can already be taken into account in the photovoltaic system data, as the PV data are highly volatile in side one hour, so the addition of weather data does not provide any important information for forecasting.

Adding data forecast to forecast a day in advance to data FS improves network performance deep compared to the forecast data only on PV. Also, the noise of the weather forecast data does not affect the forecasting results. Adding weather forecast data to PV data with weather data also does not improve MAE forecasting results, but when checking RMSE the error does not improve due to the large difference between actual and forecast values as well as the square. Therefore, adding weather forecast data improves the MAE error but does not improve the RMSE.

The use of PV data and weather forecast does not change the errors of MAE and RMSE. When you add to them data about the current weather and an increase in noise from 10 to 20%, the errors are uniform but increase with a noise level of 30%. So the more noise the less accurate at forecasting PV data current weather data and weather, while for yes or no current forecast accuracy does not change.

For deep networks, the best data sources that can be used are PV data and weather forecast data. Although if you estimate the error through the RMSE, it is more appropriate to use only the PV data.

When forecasting on the PV data with weather forecast data, the best results are demonstrated by the network of deep learning, even with increasing noise in the data. When forecasting PV data with weather forecast data and actual weather data, the usual neural network shows the best result. Therefore, it can be argued that in-depth learning networks are best for forecasting on PV data and when adding weather forecast data.

In general, a large number of tasks related to the management of a power system with RES [28–31] rely on an accurate forecast of generation volumes.

The model presented in [10] was adapt for RES generation forecasting in this chapter. The architecture of the neural network is shown in Fig. 1. This neural network consists of 3 blocks of autoencoding type (AE) with shortcut-connections.

A feature of this type of architecture is the same number of input (d_x) and output (d_y) neurons and fewer hidden (d_h) neurons $d_x = d_y > d_h$. It is known that the use of shortcut connections can significantly increase the number of layers of the neural network, which increases the accuracy and stability of the prediction results. This architecture is equivalent to an ensemble of simple neural networks. Due to the presence of shortcut connections, information is transmitted from input to output in several ways with different number of layers, which significantly reduces the effect of the gradient instability during training (decrease or increase the gradient rate when passing through neural network layers).

The output of the last block of the AE is fed into the usual fully connected layer to reduce the dimensionality of the data. The output of the fully connected layer is fed in parallel to the final fully connected layers. A separate source layer is used for each forecast value, this is a necessary condition for correct training.

The output of the AE unit is given by the formula:

$$x_{AE} = selu(selu(x \cdot W_1 + b_1) \cdot W_2 + b_2) + x,$$

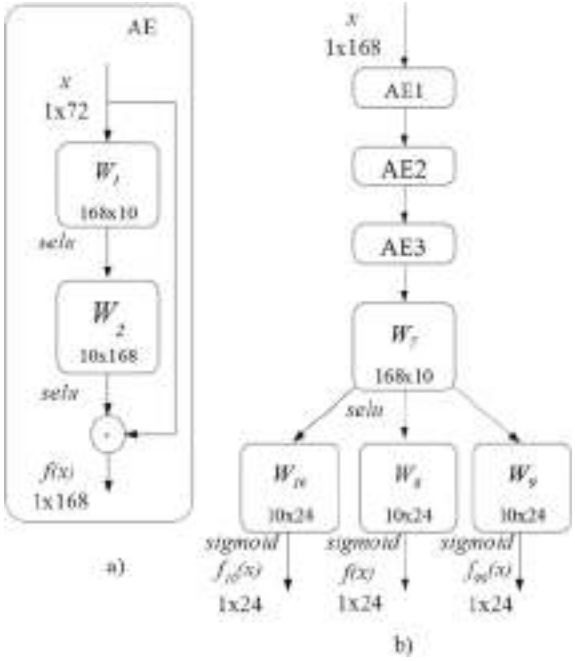

Fig. 1 Components of the neural network: **a** AutoEncoding unit; **b** eResNet network architecture

where x_{AE}—AE output; x—the input of the AE unit, for the first is equal to the input value of the neural network; W_1, W_2—weights; b_1, b_2—bias.

Function *selu* (scaled exponential linear unit):

$$selu(z) = \lambda \begin{cases} z & z > 0; \\ ae^z - a & z \leq 0, \end{cases}$$

where z—is the scalar product of the output of the previous layer and the matrix of weights:

$$z = Wx,$$

$a = 1.6733$, $\lambda = 1.0507$.

The output of the entire network is given by the formulas:

$$\begin{cases} \hat{y}_{90} = sigmoid\,(selu(x_{AK3} \cdot W_7 + b_7) \cdot W_9 + b_9); \\ \hat{y} = sigmoid\,(selu(x_{AK3} \cdot W_7 + b_7) \cdot W_8 + b_8); \\ \hat{y}_{10} = sigmoid\,(selu(x_{AK3} \cdot W_7 + b_7) \cdot W_{10} + b_{10}), \end{cases}$$

where, $\hat{y}$, $\hat{y}_{10}$, $\hat{y}_{90}$—respectively, the forecasts of the most probable value, 10 and 90 percentiles of the distribution.

The number of hidden neurons of each AE unit $d_h = 10$, the dimension of the input vector $d_x = 168$, the dimension of the output for each predictive value $d_y = 24$.

The input of the neural network is fed a vector of previous values from the predicted time series with a lag of 1 to 168 h relative to the first hour of the forecast day. Previously, all input (x) and target (y) values are scaled in the range from 0 to 1 relative to the set power. Thus, the output of the neural network is the power utilization factor. When forecasting the aggregate time series of the entire balancing group of the guaranteed buyer, the total installed capacity of PDE stations is used for rationing.

To limit the output of the neural network in the range from 0 to 1, the sigmoid function is used:

$$sigmoid(z) = \frac{1}{1 + e^{-z}}.$$

To estimate the forecast error of the most probable value, the root mean square error is used:

$$MSE = \frac{1}{n} \sum_{i=1}^{n} \left(y_i - \hat{y}_i\right)^2,$$

where y_i—the actual value of the training sample; $\hat{y}_i$—the most probable forecast value; n—the number of hours in the sample.

In the general case, the loss function for quantile regression is as follows:

$$QE_q = \frac{1}{n} \sum_{i=1}^{n} \begin{cases} k\left(y_i - \hat{y}_{qi}\right), \left(y - \hat{y}_{qi}\right) \geq 0; \\ (1-k)\left(y_i - \hat{y}_{qi}\right), \left(y - \hat{y}_{qi}\right) < 0, \end{cases}$$

where q—the required distribution percentile, in this case 10 or 90; k—coefficient in the range from 0 to 1 which corresponds to the required percentile of distribution (0.1 or 0.9); $\hat{y}_{qi}$—the predicted value of the q-th percentile of the distribution.

To simplify the calculations in the program used the equivalent formula:

$$QE_q = \frac{1}{n} \sum_{i=1}^{n} \max\left(k\left(y - \hat{y}_q\right), (1-k)\left(y - \hat{y}_q\right)\right).$$

General loss function:

$$\mathcal{L} = MSE + QE_{10} + QE_{90}.$$

The training was conducted in a mini-package mode using the ADAM optimization algorithm. This algorithm uses the gradient of the error function to refine the

weights and the square of the gradient to estimate its curvature. The weights are updated according to the following procedure:

$$w_t = w_{t-1} - \alpha \frac{\widehat{m}_t}{\sqrt{\widehat{v}_t} + \epsilon},$$

where *t*—*t* is the iteration number of the training procedure; w_t, w_{t-1}—vectors of weights on iterations *t* and *t-1*; α—learning step, recommended value 0.001; ϵ—constant that prevents calculation errors when dividing by 0, usually $\epsilon = 10^{-8}$; $\widehat{m}_t$—vector of adjusted exponentially smoothed values of the gradient, which is calculated by the procedure; $\widehat{v}_t$—vector of adjusted exponentially smoothed values of the gradient square:

$$\begin{cases} \widehat{m}_t = \frac{m_t}{1-\beta_1^t}; \\ m_t = \beta_1 m_{t-1} + (1-\beta_1) g_{t;} \\ \widehat{v}_t = \frac{v_t}{1-\beta_2^t}; \\ v_t = \beta_2 v_{t-1} + (1-\beta_2) g_t^2, \end{cases}$$

where m_t—exponentially smoothed gradient vector; v_t—exponentially smoothed vector of the gradient square; g_t—gradient of the error function; β_1, β_2—smoothing coefficients, values of which are equal to 0.9 and 0.999, respectively.

The square of the gradient is calculated element by element. Vectors m_0 and v_0 initialized by zero.

This learning procedure adaptively adjusts the value of the learning step for each individual parameter and reduces it with each iteration. This algorithm has shown high efficiency in optimization problems with a large number of parameters which include neural networks of deep learning.

The number of examples in the package varied cyclically depending on the learning epoch. The examples themselves are selected from a training sample at random according to a uniform distribution law. From the rest of the data, a training sample was formed, in which 15% of randomly selected examples were used for cross-checking in the selection of hyperparameters of the training procedure.

The size of the mini-package of the educational sample for each epoch is calculated by the formula:

$$m_e = m_{init} \cdot k \cdot (1 + floor(mod(e, r)),$$

where m_e—mini-batch size at epoch *e;* m_{init}—initial mini-batch size $m_{init} = 100$; *k*—increment step, an integer, in these example k = 1, the packet size is increased by 100 examples at each iteration before restarting the cycle; *r*—the number of epochs before restarting the size of the mini-batch, in these calculations r = 6.

With these parameters, the packet size increases from 100 to 600 for 6 epochs with a step of 100, for 7 epochs the number of examples becomes equal to 100 and the cycle is restarted.

These schedule allows resizing mini-batch out of the local minimum loss function and reduce the error of generalization of artificial neural network, as increasing mini-batch is equivalent to learning rate reduction.

The total number of epochs was determined by the method of cross-validation and was $e_{max} = 28$.

4 Model Evaluation

To assess the effectiveness of the proposed architecture of the artificial neural network of deep learning, calculations were made on hourly data on the total electricity supply of producers from RES for the period from 01.07.2015 to 06.06.2019, which were published by SE "Energorynok".

Monthly data on the installed capacity of renewable energy generation facilities published by the National Energy and Utilities Regulatory Commission (NERC) were used for rationing. For the period from 01.07.2015 to 31.12.2016 there is no data on the installed capacity, so to normalize the values of actual leave for the specified period, the value for January 2017 was used. during the specified period.

Data for the period from 06.05.2019 to 06.06.2019, only 744 values were not used in the training of models. At the first stage of the study, software tools for automatic collection of data on the supply of electricity from renewable energy sources from the site of the branch "Guaranteed Buyer" SE "Energorynok" and their statistical analysis were developed.

To compare the efficiency of the proposed deep learning neural network, an experimental program was developed to predict hourly values of electricity produced from alternative energy sources using basic models including linear regression (LinReg), ε-SVR, SARIMA and multilayer perceptron with one hidden layer of neurons.

For LinReg, ε -SVR and MLP, the input vector included 168 previous values. The output is 24 predicted values for the next day. In the case of linear regression, a separate model is built for each hour. The Python programming language scikit-learn was used to build these models. The output of the SARIMA model is one forecast value for the next hour and to obtain a forecast for 24 h, the previous forecast values were submitted to the model input. A software implementation from the statsmodels package was used to build SARIMA.

The hyperparameters of the models were selected on the basis of a search of combinations of parameters with quality criterion control. For LinReg, E-SVR and MLP, the values of the loss function were compared in the test samples, which were selected sequentially from the initial sample (K-fold cross validation).

The Akaike information criterion (AIC) was used to select the parameters of the SARIMA model:

$$\mathrm{AIC} = 2k - 2\ln(L),$$

where k—number of model parameters; L—value of the likelihood function after training with the selected hyperparameters.

Among the set of candidate models, the model with lower AIC values is selected.

Evaluation parameters SARIMA conducted at camping using BFGS optimization algorithm, which belongs to a class of quasi-Newton methods.

For LinReg, the form of the regularization function (L_2 or L_1 norm) and the value of the regularization parameter λ were selected. The ε -SVR model determined the form of the kernel function, the regularization coefficient C, and the value of the parameter that means the share of reference vectors in the training sample. Activation function, number of hidden neurons (h) and regularization parameter (λ) were selected for MLP. For SARIMA, the orders of autoregression, integration and moving average for seasonal (P, D, Q) and non-seasonal (p, d, q) components were determined for a period of 24 h. The defined values of the parameters are given in Table 3.

Using the forecast interval eResNet, you can get another version of the forecast of the most probable value in the form of averaging the values of the 10th and 90th percentiles:

$$eResNet_q = \frac{\widehat{y}_{90} + \widehat{y}_{10}}{2}.$$

The calculation of forecast quality indicators for different models was performed using statistical data for the period from 05/06/2019 to 06/06/2019. Table 4 summarizes the evaluation results for these models.

Among the considered classical models, the average and maximum error is the smallest when predicting using linear regression. This result can be explained by the fact that LinReg builds a separate model for each hour of the day, while in the case of MLP and ε - SVR the output of the model is 24 values of the daily vacation schedule. The worst predictions, in terms of average accuracy, show SARIMA, which can be explained by the effect of the accumulation of error in a multi-step forecast.

Table 3 Hyperparameters

Model	Parameters
LinReg	$\lambda = 0$
ε - SVR	linear core, $C = 1$,
MLP	logistic function, $h = 100$, $\lambda = 0$
SARIMA	$p = 1, d = 1, q = 1, P = 1, D = 0, Q = 1$

Table 4 Results of evaluation models forecast

Model	RMSE		MAX	
	% of P_{ins}	MWh	% of P_{ins}	MWh
LinReg	4.56	158	15.22	527
ε - SVR	4.58	159	15.51	536
MLP	4.59	160	15.35	539
SARIMA	4.87	169	16.2	559
GEN	4.78	166	21.18	732
eResNet	4.46	155	12.81	466
eResNet_q	4.74	165	12.78	465

All the presented models show a significant increase in the stability of forecasts compared to the forecast of power plant owners (GEN).

Model of artificial neural network depth study shows the best results in terms of average error, and maximum. The fact of a significant reduction in the maximum error is extremely important, as this indicator has the greatest impact on the need for reserves to balance consumption and generation and thus on the price in the balancing market.

In Fig. 2 actual and forecast graphs (GEN and eResNet) for 06.05.2019 are given. Maximum observed prediction error GEN at this day at 14:00, which is 732 MWh, with an average level of accuracy of 342 MWh. For eResNet this day maximum error of 409 MWh 13 h, the average error of 200 MWh.

Figure 3 shows the deviation of the GEN and eResNet forecasts from the actual values. The forecast interval is presented in the form of deviations of percentiles from the eResNet forecast.

The graphs show the dynamics of the forecast interval, which increases in the hours with the greatest uncertainty of the forecast. For three days the average

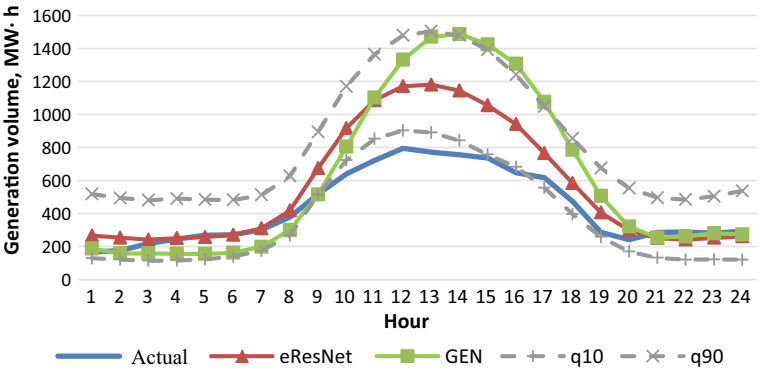

Fig. 2 Actual and forecast graphs (GEN and eResNet)

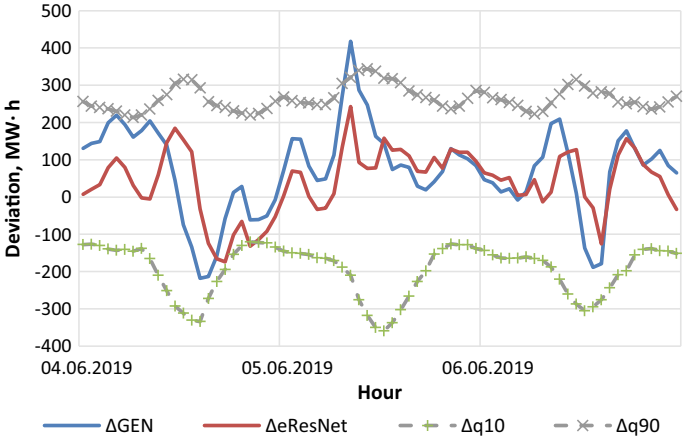

Fig. 3 Deviation of GEN and eResNet forecasts from the actual value

errors $RMSE_{GEN} = 140$ MWh $RMSE_{eResNet} = 90$ MWh, and maximum $MAX_{GEN} = 418$ MWh $MAX_{eResNet} = 243$ MWh.

The value of the PICP indicator for the entire test period from 05/06/2019 to is 0.82, which is close to the target 0.8.

Based on the calculations, we can conclude that the use of an artificial neural network of deep learning can reduce the average error of predictions and significantly increase the stability of the results.

A common technique for improving the quality of forecasts is to build "ensembles" of models. When constructing different models, different assumptions are made about the statistical nature of the forecast value, which can be complementary, which leads to a synergistic effect in which the accuracy of the forecast "ensemble" is higher than the accuracy of each model. The simplest method of constructing "ensembles" is to average the forecasts of different models.

The study conducted a complete search of possible combinations of "ensembles" from the available 7 models. A total of 120 variants of combining models were tested. The mean and maximum error values for all combinations are given in Appendix 2. The rows are sorted in ascending order of RMSE. The model with the minimum maximum error is marked in bold. Table 5 shows the value of errors for the first 5 models and models with minimum MAX errors.

All models listed in Table 1.3 include eResNet forecasts. The above data show that the combination of forecasts significantly reduces the average forecasting error from (4.46 to 3.84%). However, the maximum error of model 1 is much higher than the maximum error of eResNet, which of course is an undesirable effect and indicates an increase in forecast instability. But if the primary criterion for selecting combinations is the smallest maximum error, then in this case we can also expect a decrease in the average error. The use of model 6 in this case reduces the average error from 4.46 to

Table 5 Errors of combinations of models

	Combinations of models	RMSE		MAX	
		% of P_{ins}	MWh	% of P_{ins}	MWh
1	GEN + SARIMA + eResNet	3.84	133	15.42	533
2	GEN + SARIMA + $eResNet_q$	3.85	134	15.58	538
3	GEN + SARIMA + eResNet + $eResNet_q$	3.88	135	14.64	506
4	GEN + LinReg + SARIMA + eResNet	3.90	136	14.52	502
5	GEN + ε-SVR + SARIMA + eResNet	3.90	136	14.39	497
6	**ε-SVR + SARIMA + eResNet + $eResNet_q$**	**4.10**	**142**	**12.41**	**429**

4.10%, while the maximum error remains at the level of eResNet, 12.41% of model 6 against 12.81% of eResNet.

The inclusion of SARIMA in all combinations with the lowest error values is due to the low correlation of forecasts of this model with others. The Pearson correlation for SARIMA compared to other models does not exceed 0.94.

Figure 4 shows basic parameters of the laws of distribution of forecast errors, and make more accurate conclusions about the relative stability of the forecasts of different models.

This graph explains the effectiveness of combining SARIMA and eResNet. The SARIMA model on average underestimates the actual values ($\hat{y} < y$) while eResNet on the contrary overestimates ($\hat{y} > y$) and when averaging the deviations are mutually compensated.

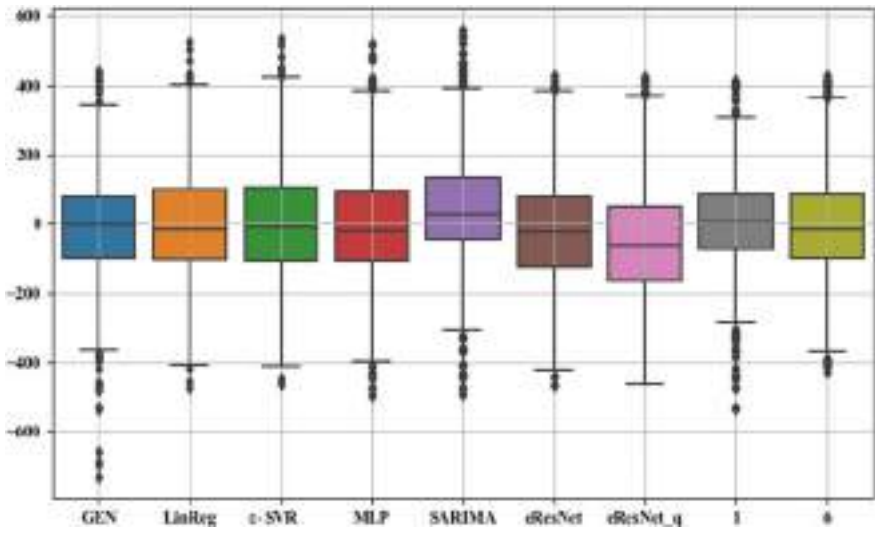

Fig. 4 Comparison of the quality of forecasts obtained by different models

Thus, the proposed architecture of the artificial neural network provides more accurate forecasts of the total supply of electricity by producers from renewable energy sources. In particular, its standard error is lower by 8.5% than the forecast error of the respective manufacturers, while the maximum error decreased by 43%, which indicates a much higher stability of the neural network forecasts.

Combining several models into an "ensemble" showed an additional improvement in the quality of forecasts. The eResNet model is used in all 5 best combinations. On the other hand, the forecast of the most expected value through the calculation of the 50th percentile, assuming the symmetric distribution of the error, was less effective than the forecast of the artificial neural network. However, in some cases, its use in the "ensemble" can reduce the error of the forecast.

In general, the proposed approach allows you to build predictive intervals with the probability of actual values within the range close to the target values. while ensuring the efficiency of the forecast interval at the level of 0.82 at the expected values of 0.8. For further research and reduction of forecasting error, it is necessary to expand the input information and explicitly use the signs of annual and daily periodicity, as well as meteorological factors.

5 Conclusions

The architecture of an artificial neural network of deep learning is proposed for simultaneous forecasting of the most probable value of the total volume of electricity supply by producers with RES and the upper and lower limits of the forecast interval. A feature of this architecture is the use of autoencoding units with shortcut connections. The training procedure of this neural network has been improved due to the cyclic change of the number of samples on which the gradient of the loss function is calculated, which allows to significantly increase the speed and efficiency of training. The use of the proposed neural network reduces the average forecast error for the day ahead to 4.46 from 4.78% and the maximum error from 21.18 to 12.81% compared to the forecast of manufacturers. Under the conditions of averaging neural network forecasts, SARIMA model and manufacturers forecast, the average error is reduced to 3.84 from 4.78%. The developed mathematical methods and models are implemented in the form of a computer program.

References

1. Lazard. Levelized Cost of Energy and Levelized Cost of Storage—2020. https://www.lazard.com/perspective/levelized-cost-of-energy-and-levelized-cost-of-storage-2020/
2. IRENA. Renewable Power Generation Costs in 2019. https://www.irena.org/publications/2020/Jun/Renewable-Power-Costs-in-2019
3. CEL. LCOE of renewable energy sources in Ukraine. https://cel.com.ua/reports/lcoe-ukraine-2019/

4. OECD. The Organisation for Economic Co-operation and Development. https://stats.oecd.org/Index.aspx?DataSetCode=RE_FIT
5. Kyrylenko, O.V., Basok, B.I., Baseyev, Y., Blinov, I.V.: Power industry of Ukraine and realities of the global warming. Technical Electrodynamics **3**—C, 52–61 (2020). DOI: https://doi.org/10.15407/techned2020.03.052
6. Kulyk, M., Zgurovets, O.: Modeling of power systems with wind, solar power plants and energy storage. Part of the Book Studies in Systems, Decision and Control book series (SSDC, volume 298), pp. 231–245. Springer. (2020). DOI:https://doi.org/10.1007/978-3-030-48583-2_15
7. Ivanov, H., Blinov, I., Parus, Y.: Simulation model of new electricity market in Ukraine. IEEE 6th International Conference on Energy Smart Systems. (2019). DOI:https://doi.org/10.1109/ESS.2019.8764184
8. Liu, H., Chen, C., Lv, X., Wu, X., Liu, M.: Deterministic wind energy forecasting: a review of intelligent predictors and auxiliary methods. Energy Convers. Manage. **195**, 328–345 (2019)
9. Dybowski, R., Roberts, S.: Confidence intervals and prediction intervals for feed-forward neural networks. Clinical Applications of Artificial Neural Networks, pp 298–326. U.K. Cambridge University Press (2000)
10. Chernenko, P., Miroshnyk, V.: Short-term electrical load forecasting for the electrical supply company with deep neural network. The proceedings of the Institute of Electrodynamics of the National Academy of Sciences of Ukraine, **50**, 5–11. (2018). DOI**:** https://doi.org/10.15407/publishing2018.50.005
11. Lezhniuk, P., Kravchuk, S., Netrebskiy, V., Komar, V., Lesko, V.: Forecasting hourly photovoltaic generation on day ahead. 2019 IEEE 6th International Conference on Energy Smart Systems (ESS). DOI:https://doi.org/10.1109/ESS.2019.8764245
12. Yuan, K., Zhang, K., Zheng, Y., Li, D., Wang, Y., Yang, Z.: Irregular distribution of wind power prediction. J. Modern Power Syst. Clean Energy **6**, 1172–1180 (2018). https://doi.org/10.1007/s40565-018-0446-9
13. Nazir, M.S., Alturise, F., Alshmrany, S., Nazir, H.M.J, Bilal, M., Abdalla, A.N., Sanjeevikumar, P., Ali, Z.M.: Wind generation forecasting methods and proliferation of artificial neural network: a review of five years research trend. Sustainability **12** (2020). DOI:https://doi.org/10.3390/su12093778
14. Chen, Q., Folly, K.A.: Wind power forecasting. IFAC-Papers On Line **51**(28), 414–441. (2018). DOI: https://doi.org/10.1016/j.ifacol.2018.11.738
15. Nguyen, X.H., Nguyen, M.P.: Mathematical modeling of photovoltaic cell/module/arrays with tags in Matlab/Simulink. Environ. Syst. Res. **4**(24). (2015). DOI https://doi.org/10.1186/s40068-015-0047-9
16. Tsai, H.-L., Tu, C.-S., Su, Y.-J.: Development of generalized photovoltaic model using MATLAB/Simulink. Proceedings of the World Congress on Engineering and Computer Science, San Francisco, USA (2008).
17. Manero, J., B´ejar, J., Cort´es, U.: Deep learning is blowing in the wind. Deep models applied to wind prediction at turbine level. Journal of Physics: Conference Series, vol.1222, IOP Publishing, Spain (2019). DOI:https://doi.org/10.1088/1742-6596/1222/1/012037
18. Huang, Y., Li, J., Hou, W., Zhang, B., Zhang, Y., Li, Y., Sun, L.: Improved clustering and deep learning based short-term wind energy forecasting in large-scale wind farms. J. Renew. Sustain. Energy **12**(6). (2020). DOI: https://doi.org/10.1063/5.0016226
19. Chen, L., Li, Z., Zhang, Y.: Multiperiod-ahead wind speed forecasting using deep neural architecture and ensemble learning. Hindawi Mathem. Probl. Eng. (2019). https://doi.org/10.1155/2019/9240317
20. Qureshi, A.S., Khan, A.: Adaptive transfer learning in deep neural networks: wind power prediction using knowledge transfer from region to region and between different task domains. Comput. Intell. **35**(4), 1088–1112 (2019). https://doi.org/10.1111/coin.12236
21. Qureshi, A.S., Khan, A., Zameer, A., Usman, A.: Wind power prediction using deep neural network based meta regression and transfer learning. Appl. Soft Comput. **58**, 742–755 (2017). https://doi.org/10.1016/j.asoc.2017.05.031

22. Torres, J., Aguilar, R.M., Zúñiga, K.V.: Deep learning to predict the generation of a wind farm. J. Renew. Sustain. Energy **10**(1). (2018). DOI: https://doi.org/10.1063/1.4995334
23. AlKandari, M., Ahmad, I.: Solar power generation forecasting using ensemble approach based on deep learning and statistical methods. Appl. Comput. Infor. (2020). https://doi.org/10.1016/j.aci.2019.11.002
24. Assimakopoulos, V., Nikolopoulos, K.: The theta model: a decomposition approach to forecasting. Int. J. Forecasting **16**(4), 521–530 (2000)
25. Gensler, A., Henze, J., Sick, B., Raabe, N.: Deep learning for solar power forecasting—an approach using AutoEncoder and LSTM Neural Networks. IEEE International Conference on Systems, Man, and Cybernetics 2016, Budapest, Hungary. (2016). DOI: https://doi.org/10.1109/SMC.2016.7844673
26. Torres, J.F., Troncoso, A., Koprinska, I., Wang, Z., Martínez-Álvarez, F.: Big data solar power forecasting based on deep learning and multiple data sources. Exp. Syst. **36**(4). (2019). DOI: https://doi.org/10.1111/exsy.12394
27. Mishra, S., Palanisamy, P.: Multi-time-horizon solar forecasting using recurrent neural network. 2018 IEEE Energy Conversion Congress and Exposition, Portland, USA. (2018). DOI: https://doi.org/10.1109/ECCE.2018.8558187
28. Ivanov, H.A., Blinov, I.V., Parus, E.V., Miroshnyk, V.O.: Components of model for analysis of influence of renewables on the electricity market price in Ukraine. Tekhnichna Elektrodynamika **4**, 72–75. (2020). DOI: https://doi.org/10.15407/techned2020.04.072
29. Karp, I.M., Nikitin, Y.Y., Pyanykh, K.Y.: Renewable sources in the energy supply systems of Ukrainian cities. Tekhnichna Elektrodynamika **1**, 40–49. (2021). DOI: https://doi.org/10.15407/techned2021.01.040
30. Agamalov, O.: Grid-forming/following control for converters of renewable energy sources. Tekhnichna Elektrodynamika **1**, 50–52. (2021). DOI: https://doi.org/10.15407/techned2021.01.050
31. Shavelkin, A., Shvedchykova, I.: Management of generation and redistribution electric power in grid-tied photovoltaic system of local object. Tekhnichna Elektrodynamika **4**, 55–59 (2020). DOI: https://doi.org/10.15407/techned2020.04.055

Grids Transfer Capacity: Calculation Methodology and Features

Vsevolod Pavlovsky, Lukian Lukianenko, Andrii Zakharov, and Anna Prykhodko

Abstract Nowadays, secure and reliable operation and control of large interconnected power systems is mainly focused on the use of information on Total Transfer Capacity (TTC). TTC is important indicator of any system interfaces used to preserve system stability in market environment. Under the current conditions, it is necessary to recalculate TTC every day or even every hour to estimate reliability margins for all power transfers through each grid's interfaces. Therefore, a big advantage for TSO to bring into system planning and control the advanced tool of TTC calculations, which is based on a high-level automation of several repetitive load flow calculations. Under proposed approach, users will spend their time on tuning and preparing big data for calculations. While variable calculations should be performed fully automatically. Such an approach significantly reduces the time required to TTC calculation and reduces the number of errors of operational personnel in performing calculations.

Keywords Total Transfer capacity · Power system · Voltage stability · Inter-area interface

1 Introduction to the Grid Transfer Capacity Problem

Today, an operation and control in power systems (PS) are mainly focused on the use of different software tools and hardware systems. Analysis of a large-scale accidents that have occurred over the past 10 years has shown that one of the main reasons for their occurrence is an incomplete and inadequate representation of real situations by data gathering systems, analysis, and data visualizations [1]. Therefore, one of the actual task of PS operation and control is to improve and to develop new information systems to support operational and dispatching staff in decisions making process. Among such information systems is the system of definition of boundary regimes and estimation of margins by static stability are allocated in separate group [2, 3]. Considering the features of the European and CIS countries power systems, it can be

V. Pavlovsky · L. Lukianenko · A. Zakharov · A. Prykhodko (✉)
Institute of Electrodynamics of NAS of Ukraine, Kyiv, Ukraine
e-mail: anna.prykhodko@dmcc.com.ua

O. Kyrylenko et al. (eds.), *Power Systems Research and Operation*, Studies in Systems, Decision and Control 388, https://doi.org/10.1007/978-3-030-82926-1_7

argued that the most common problem of static stability analysis has become in the CIS countries. It is an aperiodic static stability analysis of power system. European power systems are characterized by a high level of connectivity of the power grid (330…400 kV). In such power grids, the problems of calculation of total transfer capacity (TTC) of interfaces by the criteria of aperiodic static stability most often do not occur at all. In most cases, it is enough to analyze the reliability criteria «N − 1». On the other hand, in the CIS countries and the IPS of Ukraine as a rule, the transfer capacity through the networks is usually limited by static or transient stability criteria. It helped to development of methods and tools for power system stability analysis. The point at issue is tasks of determining the boundary regimes of the power system and their solution at operational management of the PS.

Today, operational personnel for ensure aperiodic static stability uses instructions, which regulate the allowable transfer capacity through controlled interfaces in different system conditionals. For each of the controlled interfaces numerous calculations of the allowable grid transfer capacity in the most difficult system conditionals are performed in advance. The main disadvantage of this approach is that it is almost impossible to consider and calculate all situations, especially their combinations that may occur during the power systems operation. Thus, the value of the allowable grid transfer capacity determined in the instruction materials may not fully correspond to the real situation in the power system.

Also, the promising development of electrical grids leads to the need for updating and clarification of existing operational and dispatching instructions. Therefore, operational personnel are forced to focus on approximate situations, which can lead to suboptimal or erroneous decisions.

In addition, the definition of boundary regimes by static stability is associated with the use of several methods and approaches, which are created with the introduction of several simplifications and assumptions and make some inaccuracies in determining the boundary of stability. Without claiming the completeness of the stability theory, the following are the basic simplifications and assumptions that are traditionally used in the calculation of boundary modes by static stability.

In general, a model described by a system of nonlinear differential equations are used to analyze the stability of the PS:

$$x = f(x, u, t), \tag{1}$$

where x—state vector, u—vector of inputs to the system, t—time.

If the derivatives of the state vector are implicit functions of time, then such a system is considered autonomous and can be written as:

$$x = f(x, u). \tag{2}$$

Such an autonomous system allows modeling of stationary processes and processes which are not exposed to external influences. All these processes are

completely determined by the initial values of the state variables and do not depend on the choice of the initial value of the argument t.

The stability of a nonlinear system is determined at small or large disturbances and, accordingly, there are traditionally two aspects of stability—"stability in the small" and "stability in the large". In terms of the PS, "stability in the small" is the stability of constant (stationary) motion, which is constantly exposed to small disturbances. In the following, the processes in the PS at small disturbances are considered, assuming that before the disturbances the system was in a steady state operation. In this case, the equations system can be linearized around the equilibrium point, based on the assumption that the system parameters changes (angle, voltage, electrical power) are quite small. Then the equations system decomposes into a power series (usually a Taylor series) around some point x_0 and its members above the first order are rejected.

Linearized model of equations of the power system for small disturbances:

$$\Delta = f[(x_0 + \Delta x), (u_0 + \Delta u)]; \tag{3}$$

$$\overline{\Delta} = A\Delta x + B\Delta u, \tag{4}$$

where Δx—state vector of dimension n; Δu—input vector of dimension r; A—state or plan matrix of size $n \cdot m$; B—control or input matrix of size $n \cdot r$.

In the study of power system stability, as a rule, for convenience, it is assumed that the disturbances that occurred in the PS later disappear. That is, the free movement of the power system is analyzed. The power system is stable if it returns to its previous state after the disturbances.

To simplify the analysis of the static stability of the PS, the transition from differential equations to their images (using the Laplace transform) is performed and the characteristic equations (equations) are determined:

$$det(A - \lambda I) = 0. \tag{5}$$

Expansion of the determinant gives the characteristic equation. The n solution of $\lambda = \lambda_1, \lambda_2, \ldots, \lambda_n$ are eigenvalues of A.

According to the method of the first Lyapunov approximation, the system is stable "in the small" if all the equation's roots have a negative real part. But in practice, the calculation of all equation's roots for specific PSs, the processes of which are described by thousands of differential equations, is a rather nontrivial computational problem even with the current computational capabilities of computers. Therefore, even more simplified methods of analysis of static stability of the PS are often used, estimating only the signs of the equation's coefficients. In this case, the system is considered stable if all the signs of the equation's coefficients the same.

As a rule, on the way to simplification go even further and analyze not all the equation's coefficients, but only some of their ratios (for example, a_n/a_0—the ratio of the higher equation's coefficient to the free member or a_{n-1}/a_0). Changing the sign

of such an expression allows us to conclude that the loss of aperiodic static stability. In practice, to determine the aperiodic static stability further simplify the analysis procedure, focusing only on the sign of the coefficient of the equation's free member a_n. While not even defining it, but using the criterion of degeneracy of the Jacobi matrix in the iterative method of Newton–Raphson calculation, which under several conditions [4] coincides with a_n. Several other simplified methods using frequency and algebraic stability criteria are also known.

As we can see, for determining the aperiodic static stability boundary regime of the PS provides the introduction of several simplifications and assumptions. Therefore, the introduction of additional assumptions about grid in complex system conditions is impractical and can significantly distort the representation of the real situation. In addition, no less significant disadvantage of the use of reference instructions by operational personnel is the imperfection of the procedure for analyzing the current regime in complex contingencies cases. All this leads to underutilization of the amount of transfer capacity in controlled interfaces.

Therefore, new methods of determining the boundary regimes and estimation of margins by aperiodic static stability are considered. They are aimed at automation and acceleration of all processes and allow to solve these problems in the operational management of the PS considering current system conditions.

Today, among the known approaches to the automated assessment of aperiodic static stability of the PS can be divided into several groups of methods [2, 3, 5]. The first group of methods—provides off-line basic calculations related to the assessment of the admissibility of PS regimes for aperiodic static stability.

The second group of methods for determining the boundary regimes by aperiodic static stability are based on the performance of all necessary calculations in the operational management of the PS or close enough to it. It consists that all calculations on interfaces weighting and definition available transfer capacity on them doing in an operational regime in process of receipt of new data concerning regime's parameters. The main problem that arises with this approach is the complexity of all calculations in the operational regime. This imposes certain restrictions on the number of calculations. It should be noted that the second approach is implemented in some European software [1–3]. The Quick Stab system is part of the SCADA/EMS system.

2 Voltage Stability and Features of Calculation of Total Transfer Capacity of Interfaces

2.1 Methodology for Determining the Limits for Aperiodic Static Stability of Power System Regimes in the Time Frame of Power System Operational Control

Determination of regimes that are limited by the static stability usually is performing by the method of electrical regime "weighting". The weighting can be done in

different ways. These ways may differ in the composition and type of weighting trajectories, methods of determining the weighting step, criteria for achieving the margin regime, etc. There is no approach that allows you to choose the optimal weighting trajectories. Traditionally, the trajectory is determined by a certain algorithm that implements the procedure of the power consumption/generation changing and aims to increase the active power flow through the interface (or through the separate line). The change of power flows between the systems can be done in different ways. The possibility of their implementation in practice is the single requirement only. After calculations by several trajectories, the minimum value of transfer capacity is chosen.

In the process of the margin regimes determining, for every step of the weighting, the assessment of the five main criteria is carried out:

1. The value of the reciprocal angle δ between two voltages on different sides of the interfaces and reaching the margin value. In this case, usually, the limit is set at the level $\delta < 90°$.
2. Determination of the PV curve inflection point. An illustration of the PV curves used for the voltage levels analysis on certain system buses in relation to the increasing of active power flow through the interface [6] is shown in Fig. 1. The use of PV curves makes it possible to identify situations where the change in the sign of the Jacobi matrix determinant used in the Newton–Raphson method (the traditional approach to determining the margin regimes) does not match with the state where the system loses the stability.
3. Voltage limits control (control of critical voltage values);

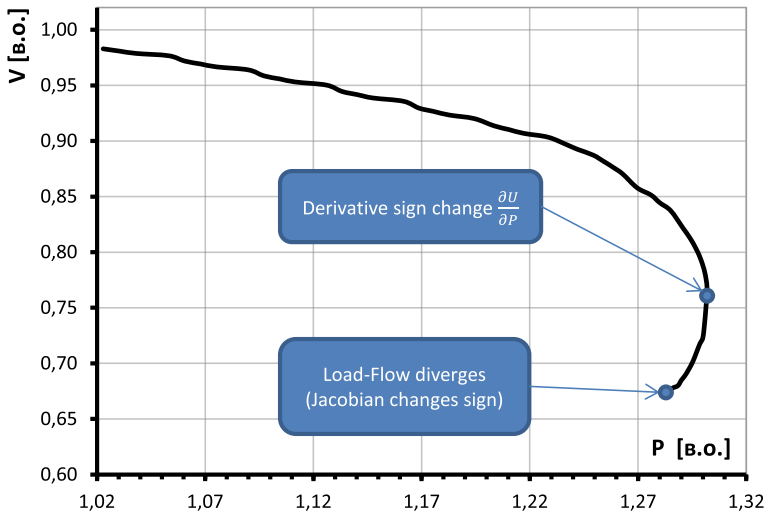

Fig. 1 An example of the PV curves using for the analysis of voltage levels in the process of regime weighting

4. PS elements (lines, transformers, etc.) loading control. These elements may be included in the interface or not;
5. Convergence of the iteration process by the Newton–Raphson method.

The first two criteria for achieving the margin regime (1 and 2) are related to the detection of regime static stability loss in terms of angle and voltage. The next criterion 3 is aimed to control the voltage stability of consumers [6, 7]. It is similar to the second criterion but can be decisive in the grids with a significant level of equivalence. The fourth criterion is not related to the assessment of stability directly but is used to assess the regime in terms of preventing damage of electrical equipment.

The fifth criterion can be considered indirect. Moreover, in the case of reaching the margin values according to one of the criteria 1–4, it is possible to clearly determine the reason for reaching the margin regime. For the fifth criterion, a clear answer about the cause of the limit regime and loss of stability is almost impossible. In addition, special attention needs the assumption analysis of the equivalence of the criterion of existence of the regime by static aperiodic stability and the convergence of the iterative process of solving nonlinear algebraic equations describing the steady-state.

In the general case it is necessary to allocate three basic grid restrictions on the value of power flow under conditions of static stability:

Aperiodic loss of angle stability. The study of the conditions for ensuring angle stability has traditionally been carried out at the stage of development of power systems, including considering the peculiarities of the long power lines operation. Indeed, in the transmission of electricity over long distances, we can take as an example the high-voltage overhead line (OHL) “Kuibyshev-Moscow”, the angles between the endpoints of such OHL in some steady-state regime can reach the critical values, which may cause loss of static stability of PS parallel operation. Although as shown in the results of numerical calculation experiments, aperiodic loss of angle stability in the IPS of Ukraine is almost impossible due to the lack of long lines.

Loss of voltage stability. The study of the conditions of loss of voltage stability is the most urgent task for the PS of many countries and IPS of Ukraine also. A characteristic feature of this phenomenon is the power lines/interfaces transfer capacity limitation due to the inability to provide sufficient voltage levels and reserves of reactive power. For the IPS of Ukraine, the loss of voltage stability is the main limitation that must be considered during the transfer capacity calculations.

The thermal resistance of wires and PS equipment. In this case, if the power system is stable according to the above mention criteria, the transfer capacity of lines/interfaces will be limited by the thermal stability of the line wires only. This situation is typical for most energy systems in the European Union. This determines the features of the application of different methods of analysis of the transfer capacity of interfaces. In ENTSO-E the transfer capacity is limited by N-1 criterion mainly. The level of construction of new power lines and the volume of compensating equipment installation in the IPS of Ukraine has not yet reached the level when the capacity of the interfaces will be limited only by the thermal stability of wires and PS equipment.

In general, it should be noted that the choice of the type of restrictions on the amount of transfer capacity is determined by the structure and characteristics of the power system. IPS of Ukraine in this case respect to the European energy systems. All this allows us to conclude that today the main factor in limiting the transfer capacity of IPS of Ukraine interfaces, in terms of ensuring static stability, is the voltage stability [6]. At the same time, as mentioned above, the issues of determining the parameters of the margin regimes should be addressed at the time frames of operational management of the PS.

2.2 Introduction to Voltage Stability

Due to the complexity of the phenomena and processes that take place in power systems, the "physical" concept of stability for the convenience of modeling is traditionally decomposed into components. In the countries of the former USSR, the mathematical decomposition of stability into the concepts of "stability of parallel operation of power systems" and "load stability" was quite common [8]. At the same time, the countries of the European Energy Union use a slightly different classification of this phenomenon: «angle stability», «voltage stability» and «frequency stability» [9–11]. These different mathematical idealizations do not contradict each other, but only differently consider the single physical essence of the power systems' stability. At the same time, the use of the latter approach makes it possible to divide the general concept more clearly into separate mathematical components. In addition, considering the prospects of Ukraine for membership in the European Energy Community, it is advisable to determine in some way and use modern global approaches to the analysis of the sustainability of energy systems.

Voltage stability is the ability of the power system to maintain stable and acceptable voltage levels on all bus systems in both normal and postemergency and repair regimes. The main reason for the uncontrolled voltage reduction and loss of stability is the inability of the power system to maintain at any time the balance of reactive power. The criterion for the power system voltage stability is increasing voltage with the increasing of reactive power at the same busbar. Therefore, the system is stable with $\delta Q/\delta V > 0$. The magnitude of the voltage that corresponds to the transition from steady state to unstable (at $\delta Q/\delta V = 0$), is called the "critical voltage", and the corresponding level of reactive power - "margin on reactive power". For further analysis, we use the following classification of voltage stability.

Transient voltage stability associated with the assessment and maintenance of voltage for 1–2 s immediately after the "large" disturbance. It is about the response of the automatic voltage regulator (AVR) of generators in the case of a short circuit (SC). The problem of transient voltage stability becomes especially acute together with the growth of the share of renewable energy in the generation structure. Unconventional generators (at wind farms) have insufficient capacity to maintain voltage during a short circuit or other accidents in the power system. When the voltage decreases, generators at wind farms can be switched off, which leads to a deterioration in

the level of transient voltage stability in such power systems. Therefore, system operators in many European countries [12] have established requirements for the parallel operation of "nontraditional" generators. We are talking about LVRT (Low Voltage Ride Through) or the ability of generators to pass short-term "voltage dips" without disconnection from the power system.

Static voltage stability belongs to the form of stability, which is determined mainly by static load characteristics and network parameters, which are known to be independent of time and current regime, which can be considered as stable for 2–10 s. Loss of the power system element or increase of load is considered as a disturbance.

Long-term voltage stability takes into account the impact on the voltage level of the response of control systems on generators, as well as processes associated with the expiration of reactive power reserves over time, operation of on-load tap changing (control under voltage) auto- (AT) and transformers (T), static capacitors batteries switching, shunt reactors and the operation of regime automation.

Even though the phenomenon of voltage instability is usually local in nature, its occurrence can lead to global consequences. Violation of stability is associated with the occurrence of a voltage collapse, which can cover large power regions or even the entire power system. Therefore, the analysis of the margin regimes in which the voltage violation is observed is important. For large modern power systems, such analysis is quite complex since from a physical point of view, the violation of stability is influenced by many factors. These are the characteristics of consumer loads, the structure and parameters of the grid, the regime parameters (power flows on power lines and AT, the composition of generating equipment), power characteristics and current settings of control systems on generators and other compensation devices (SVC—static var compensators, capacitor batteries) and redistribution (on-load tap changing of AT and transformers) of reactive power.

Given the above, it should also be noted that the violation of voltage stability, as a rule, occurs in the system sporadically, more often the operational and dispatching staff is faced with the phenomenon of voltage instability at certain busbar. The concept of voltage stability determines the degree of oscillation of the voltage level at the busbar in the oscillations of reactive power at the same busbar or in the system in general. This situation is characterized by the fact that the voltage resistance requirements are generally met (criterion $\delta Q/\delta V > 0$), but the voltage is unstable, that is even small fluctuations in reactive power lead to significant voltage fluctuations.

2.3 Voltage Stability Indicators for TTC Calculation

Ensuring the conditions of reliable operation of power systems is associated with compliance with the criteria of regime safety defined at the planning stage. Among others, the next criteria's are observed:

- limitations on the thermal stability of transmission lines and AT;

- required levels of reactive power reserves on generators and SVC (or capacitor batteries);
- permissible voltage levels;
- the value of reserves by voltage stability.

The differences between restrictions on voltage levels and voltage stability reserves should be noted. For normal and repair (emergency) schemes the permissible limits of voltage deviation from the nominal are set. Most of the ENTSO-E Grid Codes set a deviation of ±10% [12]. Reserves of voltage stability can be determined by each system operator separately. For example, in Ukraine, such reserves according to are 10 and 15% and are determined from voltage levels as 0.7 (0.75) p.u. from the nominal (normal) for busbars 110 kV. It is obvious that critical voltage points where the voltage deviates by more than 10%, are potentially dangerous in terms of the possibility of further voltage reduction and conversion of these busbars in points of the power system, where voltage stability reserves do not meet the allowable values.

However, voltage stability can be violated in situations where the voltage at all busbars 110 kV exceeds the standard value of 0.7 (0.75) p.u. from the nominal (normal), and the critical voltage may be higher than that set in [10].

This phenomenon is possible in the grids with powerful reactive power compensators (SVC) or with the implementation of a secondary voltage regulation system on generators. In such cases, a busbar with a critical voltage of more than 0.9 p.u. can be a critical point by the criterion of insufficient margin by voltage stability. As shown in [13], in the analysis of voltage stability in margin regimes with high critical voltage, the best indicator of the stability losses point are the reserves of reactive power than the voltage level.

During voltage stability analysis, it is important not only to determine the margin regime and the corresponding critical voltage level, but also to investigate how exactly the parameters of the electrical grid and its operating regimes affect the value of the critical voltage. This analysis is the basis for the development of effective measures to prevent voltage stability loss.

To assess the degree of “severity” of the voltage stability, various indicators are used that evaluate the degree of approximation of the current regime to the voltage limit, in which an avalanche of voltage can be observed. They are based on different definitions and ideas about the physical nature of resilience and complement each other. Here are the following most common indicators [9, 10, 13]:

- reactive power reserve at power plants and means of compensation, which determines the magnitude of the approach in Mvar to the margin by voltage stability.
- deviation of voltage from nominal (or normal) values that allows estimating degree of regime “severity".
- loss of reactive power in the transmission line. In particular, the rapid increase in the ratio of losses (Mvar) in the transmission line to the transfer capacity of interfaces (MW) determines the degree of approximation of the regime to the occurrence of a voltage collapse [13].

- voltage sensitivity to the magnitude of oscillations of reactive power at the busbar used to identify voltage-critical areas of the grid or individual busbar. Such "weak" busbar can be considered as the most dangerous places from the point of view of the loss of stability during the regime weighting.
- the value of the Jacobian determinant in the equations of the load flow (LF). Under certain assumptions (for example, regarding the simulation of generators), the transition of the determinant through "0" occurs in the vicinity of the zone of static stability. The margin regime can be identified with a certain probability by the convergence of the iterative process of calculating the LF.
- results of the modal analysis of inverse abbreviated Jacobian.

3 Methodology of Calculation of Grid Transfer Capacity

In the world, there are various techniques of calculation of Grid Transfer Capacity. In this chapter, the approach based on consideration of power system margins is presented. In the frame of this approach, all specific stability parameters should be determined and provided for dispatching staff with consideration of different power system margins. In particular, the following margins should be applied to Grid Transfer Capacity:

- active power margin (20% for normal condition and 8% for contingencies condition);
- voltage margin (15% for normal condition and 10% for contingencies condition);
- current margin (100% equipment loading for normal condition and 120% loading of lines and 140% loading of transformers for contingencies condition).

The process of implementation of power system margins during the calculation of Grid Transfer Capacity are shown in Fig. 2. To determine abovementioned specific system margins, which are very importance for dispatching engineers the next approach is used. Process of calculation all above mentioned margins for normal system conditionals and contingencies cases are shown in Figs. 2 and 3.

So, there are different rules and margins for uninterrupted operations and for contingencies cases. The resulting allowable grids transfer capacity for one selected case (it can be normal system condition, or any maintenance system conditions) can be determined as the minimum of margin transfer capacity for normal system condition and for contingencies cases. It can be illustrated as following:

$$TTC_i = MIN\left\{\begin{array}{c} margins for normal condition \\ margins for Contingency case 1. \\ \cdots \\ margins for Contingency case n. \end{array}\right\}, \tag{6}$$

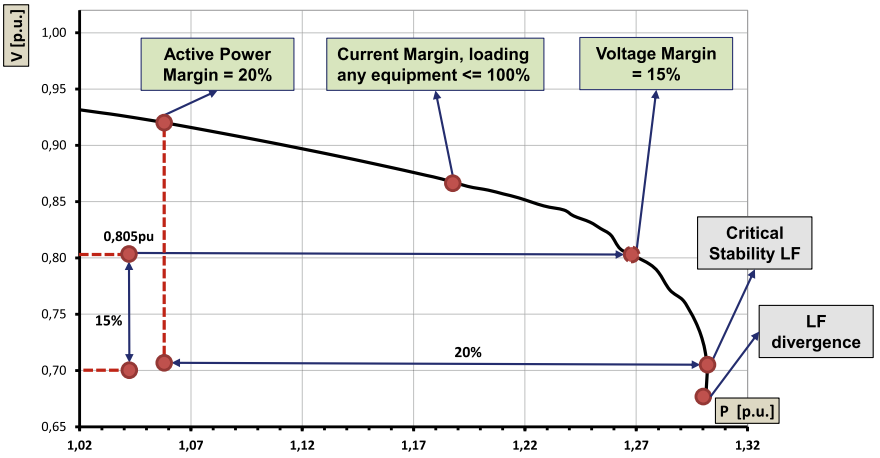

Fig. 2 Implementation of power system margins to TTC for normal system conditions

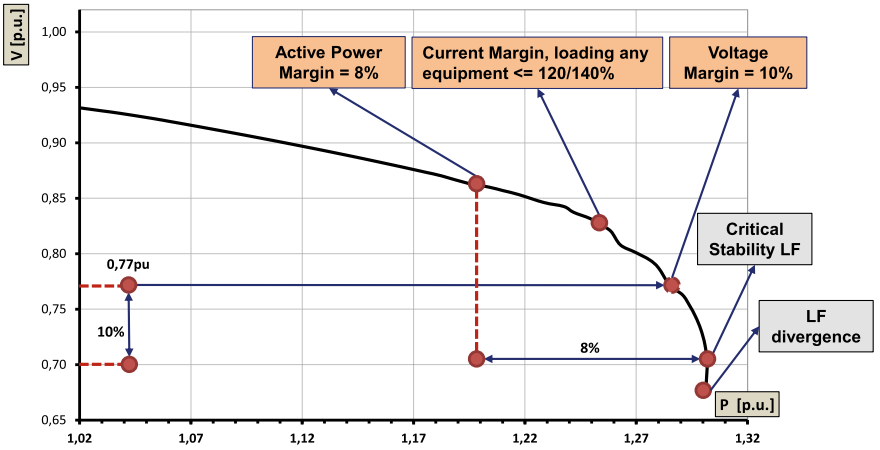

Fig. 3 Implementation of power system margins to TTC for normal system conditions

where TTC_i—grids transfer capacity for one selected system condition considering the margins and contingencies cases.

4 The Sensitivity of Grid Transfer Capacity to Various System Parameters

4.1 The Sensitivity of TTC to Consideration of PQ-Characteristics of Generators

Quite often, with a shortage of network compensating devices, the main reactive power compensation reserve is concentrated in generators of working power plants (for example, this is typical situation for the IPS of Ukraine [14]). In this situation, the accurate simulation of the working modes of synchronous generators is a necessary condition for adequate determination of the allowable transfer capacity. In particular, the main issue is to adequate simulation of ranges of reactive power operation limits for generation. Therefore, considering their dependences of the operation reactive power range from the current active power and voltage on the generator busbars. All this makes it possible to determine not theoretically possible values of Grid transfer limits, but to calculate more realistic values considering the limitations of the condition of existing equipment and its modes of operation.

In general, there are several ways to consider the limitations of the reactive power of SG in the simulation. One of the most simplify, but common use in practice is the approach associated with using minimum, maximum reactive power and voltage setting at control busbar (Q_{min}, Q_{max}, U_{set}) as are shown in Fig. 4.

The main disadvantage of this method is the assumption that Q_{min}, Q_{max} do not depend on the active power of the generator and on voltage on the generator busbars. However, this is far from real situation, and their consideration can significantly

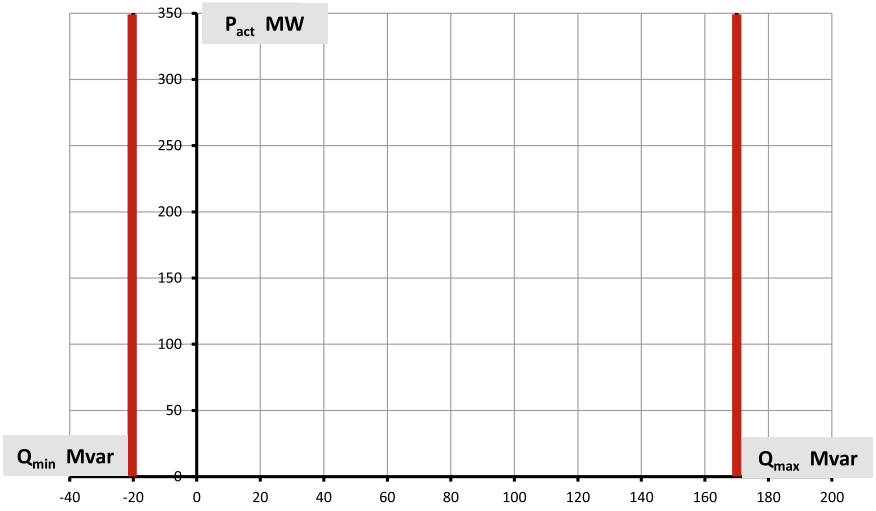

Fig. 4 Representation of generator reactive control range by constant values

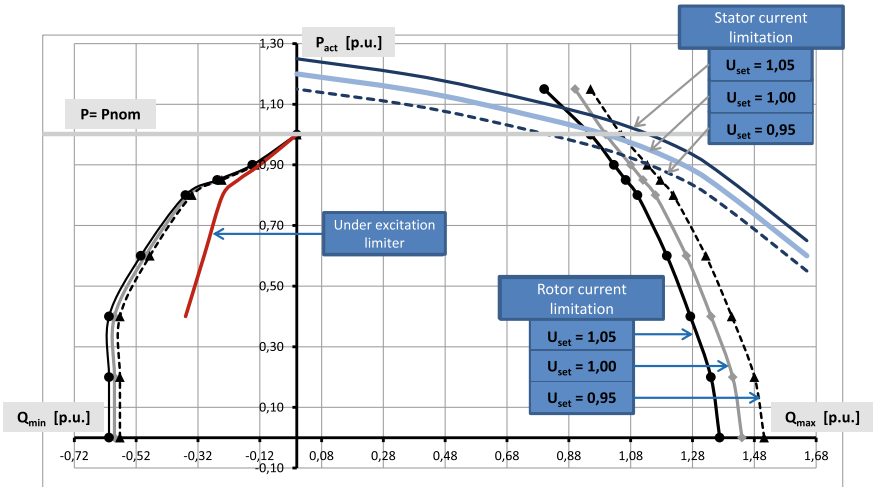

Fig. 5 Typical PQ-characteristics of a synchronous generator with specific limitation of the value of reactive power

affect the results of the calculation. In Fig. 5 a typical PQ-characteristic of generator with specific limitation for reactive power compensation is presented.

The analysis of the dependences presented in the Fig. 5 allows us to draw a conclusion, that Q_{max} quite significantly depends on the loading of SG at active power and the voltage on the generator busbars. The dependence of Q_{min} on the voltage is rather weak, so ignoring this dependence when solving the current problem does not significantly reduce the accuracy of the calculation.

Another important aspect of the correct modeling of the SG is to consider the action generator protection devices. As can be seen from Fig. 5, under excitation limiter imposes stricter restrictions on the consumption of reactive power SG than other factors. Thus, the available reactive power control reserve on the SG and its accurate consideration are of exceptional importance for the calculation of TTC.

4.2 Different Approaches to Build of Weighing Trajectory for TTC Calculation

Also, there are technological limitations of SG on the minimum and maximum allowable active power. In other words, in practice, it is not possible to operate with a sufficient level of reliability and long-term of TPPs and NPPs with maximum loads, for example, with 40 or 110% of rated capacity. The allowable active power capacity of the SG can vary only in a certain range, which is approximately is 0.60…1.05 of the rated capacity. Ignoring these real limitations will leads to the fact that the calculated

TTC values will characterize only the capacity of the lines, without considering the practical operating conditions of a particular power system.

Thus, to more accurately consider the limitations of synchronous generators on the minimum/maximum allowable active power, it is necessary to change the weighting algorithm.

In common practice, most existing programs use an approach that assumes a constant weighting step for each generator or load. But such a simplified approach incorrect working in the case of considering the PQ-characteristics and the active power limitations of the SG. The main issue is that set of the generators for "loading" and "unloading" will be constantly changing in the process of weighting if active power limitations of SG are used. To solve this, it is proposed to use a constant weighting step, not for each generator/load, but for the selected interface. So, the "permanent" weighting step can be selected for the interface, and then the "personal" weighting step will be recalculated at each iteration for each SG, considering the allowable active power.

The calculation of the "personal" weighting step for each SG can be performed according to various criteria proportionally:

- the rated power of each SG;
- operational limit for loading/unloading of SG at active power;
- available reserve for loading/unloading of SG at active capacity.

After reaching the maximum or minimum active power limit for all SGs used in weighting trajectory, further increase of transfer power flow through the interface can be performed by a corresponding change in the active power of loads.

Also, in the case of using this type of weighting trajectory with consideration of active power limits, a new situation in the power system can be defined. When the maximum load flow will be reached without violating any of the network constraints (stability criteria) and will be determined only by the physically possible operation of power systems.

4.3 Example of Grid Transfer Capacity Calculation

Considering the abovementioned approach, the calculated studies for the selected real inter-area interface were carried out (considering the confidential agreement the specific information was anonymized). The results of the TTC calculations are given in Table 1. In particular, the following combinations of different configurations were considered:

- The basic case, which corresponds to the current practice of calculating the transfer capacity of interface (#1 in Table 1); This is base for comparison.
- Cases with enable the simple PQ-characteristics—without voltage dependence (#3 and #4 in Table 1).

Table 1 Grid transfer capacity calculation for selected testing interface

##	Study cases	Normal system condition		Maintenance condition (one OHL 330 kV)	
		Critical transfer capacity, MW	Difference from basic	Critical transfer capacity, MW	difference from basic
1	Basic case	4669	–	3688	–
2	PQ-characteristics = disable Active Power limit = enable (P ≥ 0,70*Pnom)	4489	−180	3688	0
3	Simple PQ-characteristics = enable. Active Power limit = disable	4620	−49	3465	−223
4	Simple PQ-characteristics = enable. Active Power limit = enable (P ≥ 0,70*Pnom)	4436	−233	3465	−223
5	Full PQ-characterist. = enable. Active Power limit = disable	4619	−50	3497	−191
6	Full PQ-characterist. = enable. Active Power limit = enable (P ≥ 0,70*Pnom)	4423	−246	3497	−191

- Cases with enable the full PQ-characteristics—with considering the voltage dependence (#5 and #6 in Table 1).
- Cases with enable of active power limitations for SG (#2, #4 and #6 in Table 1).

Thus, based on the analysis of the TTC of the selected interface (Table 1) for the normal system condition, we can conclude that the PQ characteristics (with/without voltage dependences) have less impact on the TTC value than the active power limits SG. The cumulative impact of both factors is enhanced.

In the maintenance system conditionals, voltage stability issues are sharped. The influence of PQ-characteristics, in this case, has crucial value.

Ignore the influence of PQ-characteristics and values of the minimal and maximum active power limitation of SG can lead to obtaining a non-real value of grid transfer

capacity. In this situation, dispatching personnel will work with distorted TTC value, which may be a risk of loss of stability of the power system.

5 Automated Procedure of Identification of Allowable Transfer Capacity and Other Control Data for TSO

Secure and reliable operation and planning of large interconnected power systems nowadays is mainly focused on the use of information on TTC. Integration of many local power systems into a few large power systems has become the TTC calculation much more complicated and strongly requires the full automation of this process. During last decades, information about TTC values was quite stable and it was recalculated very rarely, usually once every one or two years. It was enough for yesterday's power systems all over the world. However, under the current conditions, it is necessary to recalculate the TTC every day to estimate all power transfers through each grid's interfaces.

Therefore, a big advantage for TSO will bring the specific tools of TTC calculations, which is based on a high level of automation of calculations. Under this approach, users will spend their time tuning and prepare big data for calculations. While variable calculations should be performed fully automatically with the automated determination of all control data for TSO. Such an approach significantly reduces the time required to TTC calculation and reduces the cost of error of operational personnel in performing calculations.

It is intended to determine the allowable power flow through selected interface considering various stability criteria. The Script automatically considers the various trajectories of load/generation increase, contingency, and maintenance schemes. The function features automatic assessment of interface stability parameters (with the report output in MS Excel format). The last version features automatic definition of load increase trajectories, step size, etc. This Script is an engineering tool for.

DigSilent PowerFactory software package. This module is allowed to calculate the weighted load-flow of power systems, taking into account the following items:

- Automatic building the specific weighting trajectory for each interarea interface.
- Automatic identification of the specific weighting step for each interface.
- Taking into account the combination of contingencies and maintenance situations and other system conditions during the calculation.
- Automatic determination of specific system parameters for dispatching engineers (as shown in Figs. 2 and 3).

The use of the developed software allows to fully automate the calculation of the transfer capacity of interfaces, considering the various maintenance and contingencies system condition in power systems. This approach significantly reduces the calculation time of one interface and allows you to approach the calculations in the pace of decision-making.

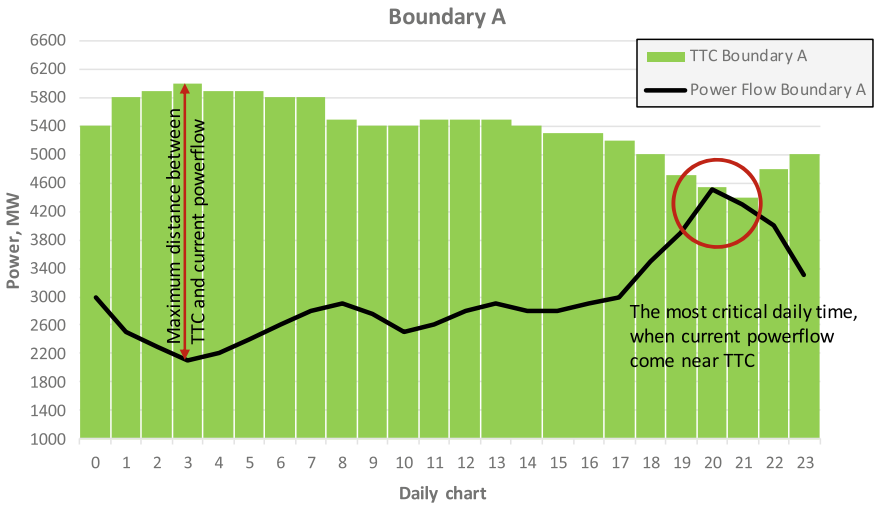

Fig. 6 TTC evaluation for "Boundary A" for the day ahead with 1-h resolution in comparison with forecasted power flow through selected interface

Additionally, this approach (and tools) can be used to calculate the Day Ahead Transfer Capacity Forecast (Estimation). This approach allows to estimate the value of TTC for different interfaces for 24 h ahead. Simple example of such calculation can be illustrated in the Fig. 6.

This new approach provides the intelligent tool for the evaluation of values of Total Transfer Capacity for selected system interfaces for the day ahead and intraday markets in fully automatic mode. All calculations of TTC are automated, such as:

- auto-selection one by one interface from the specific list;
- auto-define the uploading trajectory, weighting factors on each step and other specific parameters for the selected interface;
- auto-define the rated contingency cases for the selected interface;
- auto storing of detailed calculation results with consideration of the stability, voltage, and current power system margins;
- auto calculation for 24 h ahead.

References

1. Final Report on the August 14, 2003 Blackout in the United States and Canada: Causes and Recommendations (2003)
2. Gao, B., Morison, G.K., Kundur, P.: Towards the development of a systematic approach for voltage stability assessment of large-scale power systems. IEEE Trans. Power Syst. **11**(3), 1314–1324 (1996)

3. Savu, C.: Savulescu: Real-time Stability Assessment in Modern Power System Control Centers, 425 p. John Wiley & Sons (2009)
4. Gurevich, Y.E., Libova, L.E., Okin, A.A.: Calculation of stability and emergency automation in power systems. M. Energoatomizdat, 390 (1990)
5. Butkevich, O.F.: Problem-oriented monitoring regimes of IPS Ukraine. Tekhnichna Elektrodynamika (5), 39–52 (2007)
6. Kyrylenko, O.V., Pavlovsky, V.V., Lukyanenko, L.M., Zorin, E.V.: Analysis of the stability of energy systems by voltage. Tekhnichna Elektrodynamika (3), 59–66 (2010)
7. Kyrylenko, O.V., Pavlovsky, V.V., Lukianenko, L.M.: Features of application of the modal analysis for research of resistance on pressure. Tekhnichna elektrodynamika. Thematic issue Power Electron. Energy Efficiency (Part 2), 241–242 (2010)
8. Venikov, V.A.: Electromechanical transients in electrical systems. M. Vysshaya shkola, 536 (1985)
9. Kundur, P.: Power System Stability and Control, 1176 p. McGraw-Hill (1994)
10. Cutsem, V., Vournas, T., Kluwer, C.: Voltage Stability of Electric Power Systems, 379 p. Kluwer Academic Publishers Group, Boston (1998)
11. Kundur, P., Paserba, J., Ajjarapu, V., other: Definition and classification of power system stability IEEE/CIGRE joint task force on stability terms and definitions. IEEE Trans. Power Syst. **19**(2), 1387–1401 (2004)
12. Transmission Code 2007: Network and System Rules of the German Transmission System Operators. BDEW (2007)
13. Stogniy, B.S., Kyrylenko, O.V., Pavlovsky, V.V., Levkonyuk, A.V.: Increasing the capacity of "weak" interfaces of power systems using technology FACTS. Tekhnichna Elektrodynamika (2), 63–68 (2009)
14. Kyrylenko, O.V., Pavlovsky, V.V., Lukianenko, L.M.: Estimation of reactive power reserves in the IPS of Ukraine taking into account the problem of ensuring voltage stability. Tekhnichna Elektrodynamika. (Thematic issue Probl. Mod. Electri. Eng.) (Part 3), 53–56 (2010)

Frequency Stability of the Bulk Isolated Power System with a High Share of Renewables and Nuclear Generation

Vsevolod Pavlovskyi, Anton Steliuk, Oleg Lenga, and Viacheslav Hrechko

Abstract Frequency stability is one of the principal tasks of providing the security and reliability of power system operation. This chapter covers the various aspects of frequency stability study in power systems. The chapter consists of three parts. In the first part, the identification methodology of the frequency characteristics of the power system is presented. The second part covers the questions of the local frequency control to mitigate the impact of the renewable generation on highly loaded tie-line flows. The third part of the frequency stability study considers the frequency emergency systems and AGC simulation.

Keywords Frequency stability · Power flow · Special protection automatics · Primary and secondary frequency control · Automatic generation control · Power system

1 Introduction

Frequency stability is one of the paramount tasks of the security and reliability of power systems operation. The importance of this task is confirmed by many cases of blackouts and system faults that occurred during past decades, including the last system emergency that happened in the ENTSO-e grid on January 8, 2021. Due to the outages of the transmission network elements, the ENTSO-e grid has been split into two parts (the active power imbalance was 6300 MW). As a result, the North-West part of the ENTSO-e grid was operated with a decreased frequency, while a significant frequency increasing has been observed in the South-East part.

Another factor, which increases the importance of frequency stability is the penetration of renewables. Nowadays, renewables, primarily windfarms and PV solar power plants, are widely used all over the world. One of the features of such a plant is a variable and stochastic generation that influences frequency stability and complicates frequency control in power systems.

V. Pavlovskyi · A. Steliuk (✉) · O. Lenga · V. Hrechko
Institute of Electrodynamics of NAS of Ukraine, Kyiv, Ukraine

O. Kyrylenko et al. (eds.), *Power Systems Research and Operation*, Studies in Systems, Decision and Control 388, https://doi.org/10.1007/978-3-030-82926-1_8

In power systems with nuclear power plants (NPPs), the frequency deviation is strictly limited. It is due to the special protection automatics (SPA) used at NPPs to disconnect generating units from the grid in case of the significant frequency decreasing. In its turn, a usage of under-frequency load-shedding (UFLS) relays allows preventing the SPA operation in case of the significant frequency decreasing. Considering mentioned above, the study of frequency stability is an important and actual task. This study is based on the development of the appropriate dynamic models, such as SPA models of NPPs, under-frequency load shedding (UFLS) relays.

2 Frequency Characteristics Identification of the Power System

To study the frequency stability, it is necessary to identify the frequency characteristics of the power system. The important parameters are stiffness coefficients of the interconnected power systems, which define the active power change in MW in case of the frequency change by 1 Hz. Below, the identification methodology of these coefficients is presented on the example of 1000 MW generating unit disconnection at NPP [1, 2]. For this purpose, the frequency and net interchange power recorded data of SCADA-EMS have been used. Let us consider the synchronous operation of two power systems PS1 and PS2. The installed capacity of the power system PS1 is much greater than one of PS2. According to these data, the initial total generating capacity of the power system is $P_g{}^0 = 22{,}455$ MW, frequency —$f^0 = 49.994$ Hz, and net interchange power —$P_{net}{}^0 = -696.75$ MW. The disconnection of the NPP generating unit with the loading 882 MW leads to a new active power balance at a deviated frequency. When the primary control ends up the generating capacity decreases to $P_g{}^1 = 21{,}633$ MW, the frequency—$f_1 = 49.962$ Hz, and net interchange power changes to $P_{net}{}^1 = 12.184$ MW. During the primary control, the decreasing of the total generating capacity is

$$\Delta P_g = P_g^0 - P_g^1. \tag{1}$$

The change of the net interchange power can be defined as

$$\Delta P_{net} = P_{net}^0 - P_{net}^1. \tag{2}$$

Respectively, the frequency change is

$$\Delta f = f^0 - f^1. \tag{3}$$

Based on known ΔP_g and Δf the total stiffness coefficient of interconnected power systems *PS1−PS2* can be defined

$$K_f^{PS1-PS2} = \Delta P_g / \Delta f. \tag{4}$$

During the primary control, the change of the net interchange power defines the reaction of the first power system PS1 on a disturbance in the second power system PS2. Thus, the stiffness coefficient of the first power system PS1 is

$$K_f^{PS1} = \Delta P_{net} / \Delta f. \tag{5}$$

Considering that the total stiffness coefficient of *PS1–PS2* is equal

$$K_f^{PS1-PS2} = K_f^{PS1} + K_f^{PS2}, \tag{6}$$

the stiffness coefficient of the second power system PS2 can be defined as

$$K_f^{PS2} = K_f^{PS1-PS2} - K_f^{PS1}. \tag{7}$$

Using the foregoing formulas, the stiffness coefficients can be defined $K_f{}^{PS1}$ = 22,154.18 MW/Hz (absolute value), $K_f{}^{PS2}$ = 3533.32 MW/Hz and $K_f{}^{PS1-PS2}$ = 25,687.5 MW/Hz. The calculation results are consistent with experimentally obtained ones.

Additionally, on basis of the recorded data, the frequency characteristics of the total generation (see Fig. 1) and net interchange power (see Fig. 2) of PS2 can be defined. These characteristics depict the dependency of the total generation and net interchange power on the frequency in the second power system PS2 in the initial steady-state and during the primary and secondary frequency control. On

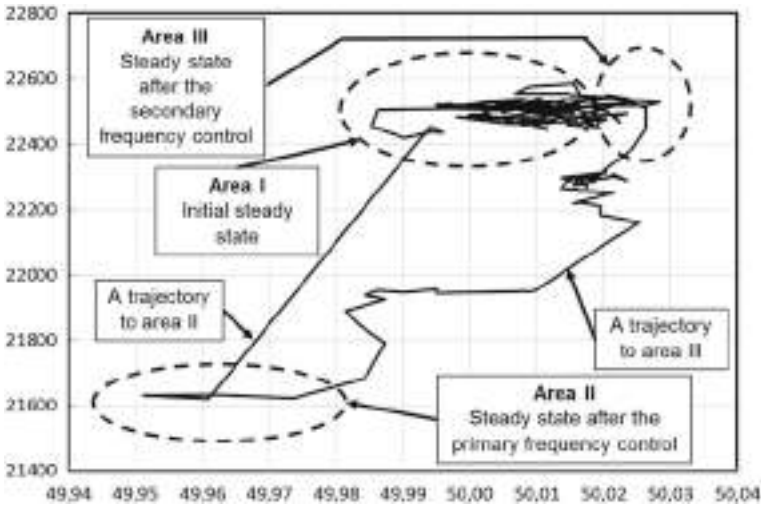

Fig. 1 The trajectory of the total generation depending on the frequency

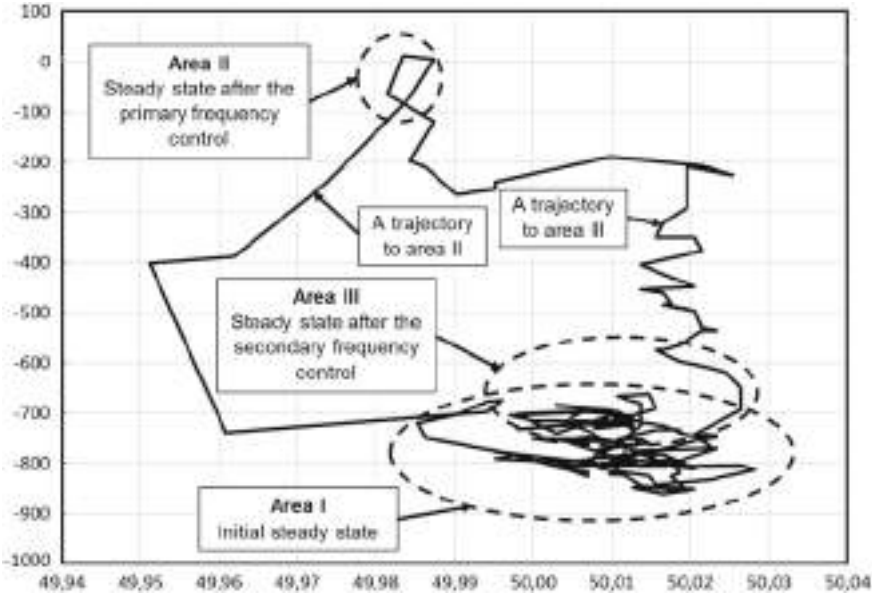

Fig. 2 The trajectory of the net power flow depending on the frequency

both characteristics, the following areas and trajectories can be shown. The area I defines the initial steady-state before the disconnection of the NPP generating unit (see Fig. 1). In this area, the frequency fluctuates around its nominal value while the net interchange power changes considerably (see Fig. 2).

In the case of disturbance, the frequency has been decreased and net interchange power has also been changed. As shown in Fig. 1 the slope of the trajectory from the area I to area II depends on the total stiffness coefficient $K_f^{PS1-PS2}$ [1, 2].

Area II defines the steady-state after the primary frequency control. During the secondary frequency control, the generating power change of the regulating power plants in PS2 allows recovering the set values of the frequency and net power flow. Thus, area III defines the steady-state after the secondary frequency control.

3 Development of the Local Load–frequency Controller Considering the Impact of the Renewables

In recent years, the installed capacity of wind and solar power plants is increasing in the world. One of the features of these renewables is a variable generation that influences the power system operation. Since renewables are used mainly in the distribution networks, they have a great influence on power system operation in the regional networks. The elimination of this impact requires improvements in supervisory control as well as in voltage and reactive power control, power quality,

etc. In the chapter, the influence of the solar power plants (SPP) on load–frequency control is considered. To eliminate the influence of SPP generation on power flows change, the local active power controller (LAPC) is proposed. The schematic diagram of the frequency control organization in the power system considering the generation of the renewable and LAPC is presented in Fig. 3.

Let us consider the LAPC operation in detail. The structure diagram of LAPC is depicted in Fig. 4.

The input signals of the LAPC are tie-line power flows P_{flowj}^{loc}, current frequency f, and a reference signal ΔP_{ref}^{LAPC} from the system level AGC. Based on power flow signals, the net interchange power P_{net}, which is a sum of power flows P_{flowj}^{loc}, and control error (CE) signals are calculated

$$CE = \left(P_{net} - P_{net.ref}\right) + K_f\left(f - f_{ref}\right) + \Delta P_{ref}^{LAPC}, \tag{8}$$

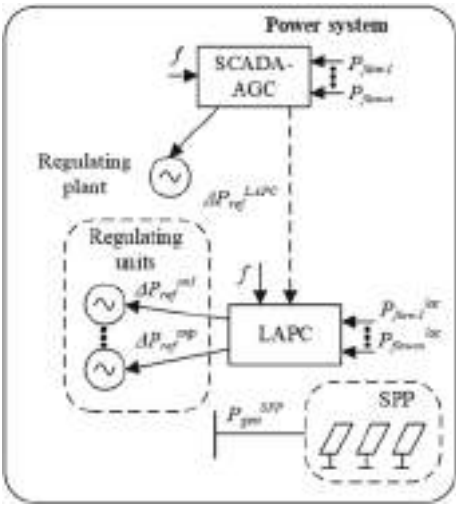

Fig. 3 Organization of the frequency control in the power system including LAPC

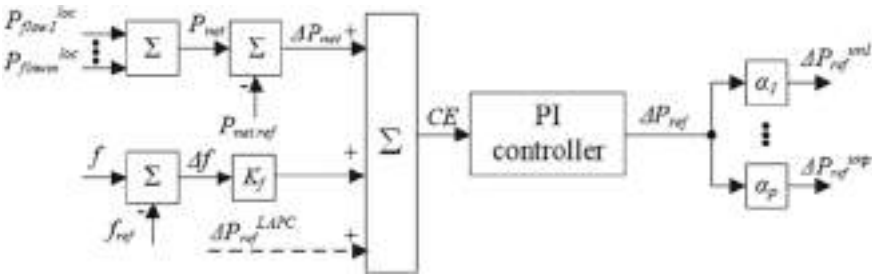

Fig. 4 The structure diagram of LAPC

where $P_{net.ref}$—reference net interchange power; K_f—frequency coefficient; f_{ref}—reference frequency.

Considering the frequency Δf and net interchange power ΔP_{net} deviations, the *CE* signal can be defined as follows

$$CE = \Delta P_{net} + K_f \Delta f + \Delta P_{ref}^{LAPC}. \tag{9}$$

Considering (9), the control signal ΔP_{ref} calculated by the proportional and integral (PI) local controller is

$$\Delta P_{ref} = K_P^{LC} CE + K_I^{LC} CE/p, \tag{10}$$

where ${K_P}^{LC}, {K_I}^{LC}$—proportional and integral gains of the local controller; p—differential operator.

The control signals ${\Delta P_{ref}}^{unk}$ transmitted from LAPC to the k-th unit of the regulating power plant are calculated as follows

$$\Delta P_{ref}^{unk} = \alpha_k \Delta P_{ref}, \tag{11}$$

where α_k—participation factor of the k-th generating unit in the frequency control.

Thus, the generation power of the regulating units changes in such a way, to compensate for the SPP generation changes.

As a disturbance, the SPP generation power has been considered. The synthesized plot of SPP generation is depicted in Fig. 5. It should be noted that this characteristic corresponds to the actual measured generation power of the solar power plants.

As seen in Fig. 5, in the morning and evening hours the generation of the solar power plants is insignificant due to the decreasing of the solar irradiation. At the

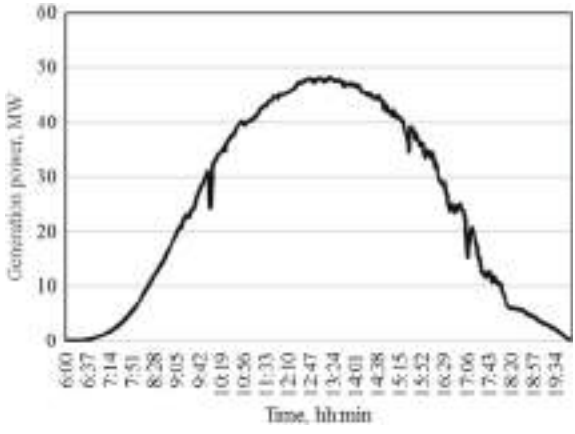

Fig. 5 The generation of solar power plants

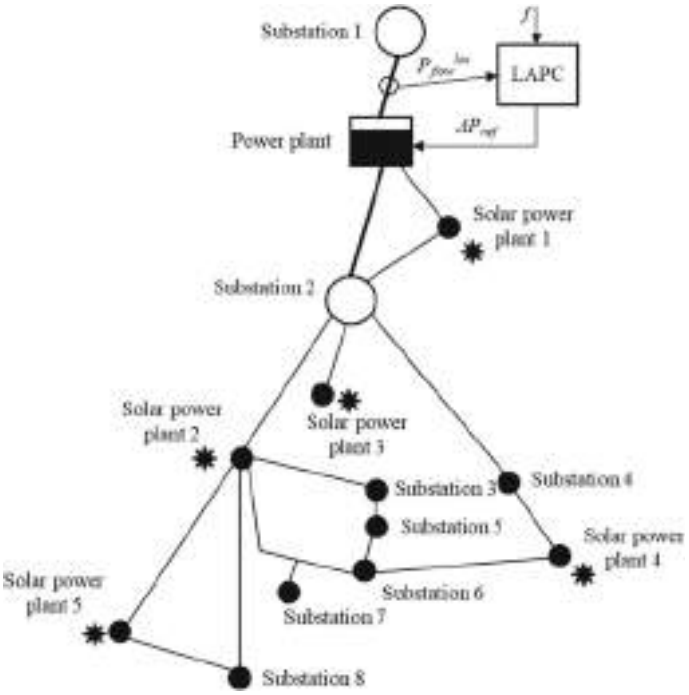

Fig. 6 A test model of the power system

same time, the maximum value of the generation power is observed in the afternoon that corresponds to the maximum solar irradiance.

The simulation of the LAPC operation has been performed using the test model of the power system which is depicted in Fig. 6.

As seen in Fig. 6, the local controller regulates the power flow on the overhead line between Substation 1 and the thermal power plant. Five solar power plants are in the distribution network. Respectively, the generation of the solar power plants impacts on power flow of the active power from Substation 1.

The obtained simulation results: generation power of the regulating power plant controlled by LAPC as well as power flow of the overhead line are presented in Figs. 7 and 8. As seen in Fig. 8, a SPP generation leads to the power flow change on the overhead line. As a result, LAPC generates a control signal to the regulating power plant (see Fig. 7) to maintain a scheduled net interchange power (see Fig. 8).

As seen, the participation of LAPC in the load–frequency control allows mitigating active power fluctuations on power flows due to the stochastic generation of the renewables. It should be noted that the connection of the additional regulating power plants to LAPC will improve load–frequency control at the local levels of power systems. The proposed computer model allows studying frequency control at the local levels of the power systems with high renewables penetration.

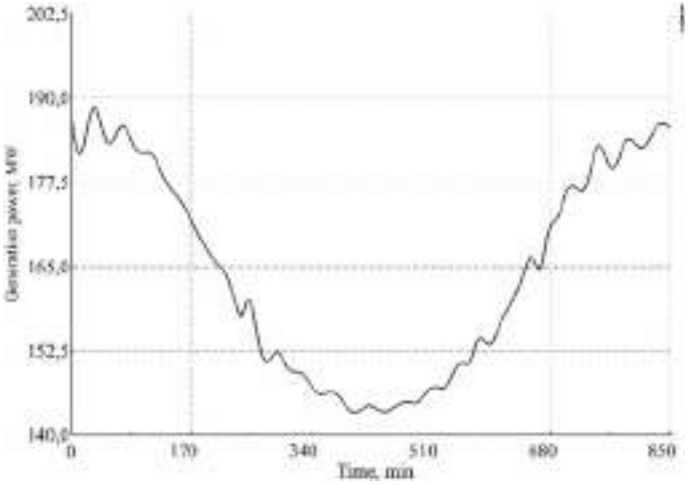

Fig. 7 The generation power of the regulating power plant

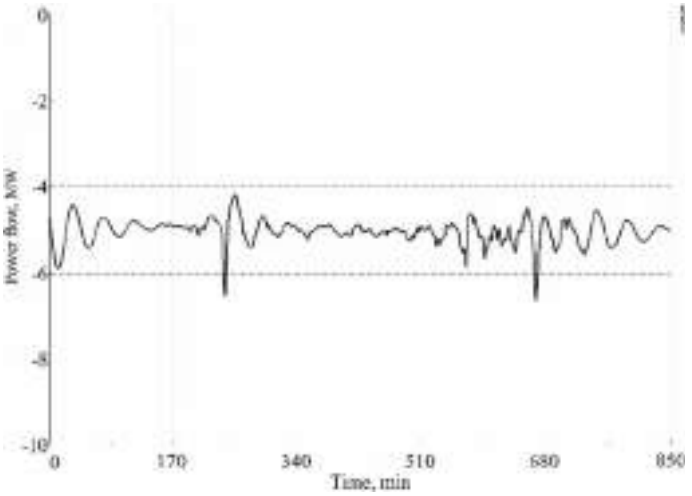

Fig. 8 Power flow change on the interface controlled by LAPC

4 Frequency Stability Simulation Considering the Operation of the Under-Frequency Load Shedding Relays and Special Protection Automatics of the Nuclear Power Plants

To preserve the frequency stability of the power system in case of more severe disturbances, which lead to large frequency deviations, UFLS relays are used in the

power system [3, 4]. Depending on the settings for frequency values and operation times, there are five categories of UFLS used in IPS/UPS [5, 6]:

1. Special UFLS is used to prevent a frequency decreasing to operation settings of UFLS-2. The frequency pick-up setting is 49.2 Hz, pick-up time is 0.3–0.5 s.
2. Protective UFLS is used to prevent an operation of SPA, which decreases the generation of the nuclear power plants in case of a dangerous frequency drop (less than 49 Hz) in the system. The frequency pick up of this UFLS is 49.1 Hz, pick up time is 0.3–0.5 s.
3. UFLS-1 (the first category) is used to prevent a deep frequency decreasing. This category of high-speed devices UFLS has different frequency settings to adapt to various disturbances in the power system (or its isolated parts) and to eliminate a frequency decreasing. Frequency pick-up settings are in the range 48.8–47.2 Hz; pick-up time 0.3–0.5 s.
4. UFLS-2n—not combined UFLS-2 (the second category). This is a slow category that is not combined with UFLS-1 and used to increase the frequency after UFLS-1 operation when frequency decreases at an unacceptably low level. The frequency pick-up setting is 49.1 Hz and time pick-up settings are in the range from 5 to 20 s with intervals of 3 s.
5. UFLS-2c—combined UFLS-2 (the second category), used to eliminate frequency decrease with relatively slow power deficit increase (frequency drift) and to increase the frequency in case of UFLS-2n inefficient operation. Frequency pick-up settings are in the range from 48.7 to 49 Hz; time pick-up settings are in the range from 21 to 60 s.

The diagram, illustrating consumption, disconnected by UFLS relays, is shown in Fig. 9.

Besides, to ensure the safe operation of NPPs, SPA relays are also used. The SPA has several settings groups: if frequency lower than 47 Hz then operation time is less than 10 s (<47 Hz, < 10 s.); lower than 48 Hz—not exceeding 1 min (<48 Hz, <60 s) and lower than 49 Hz—less than 5 min (<49 Hz, < 300 s.). If the frequency is

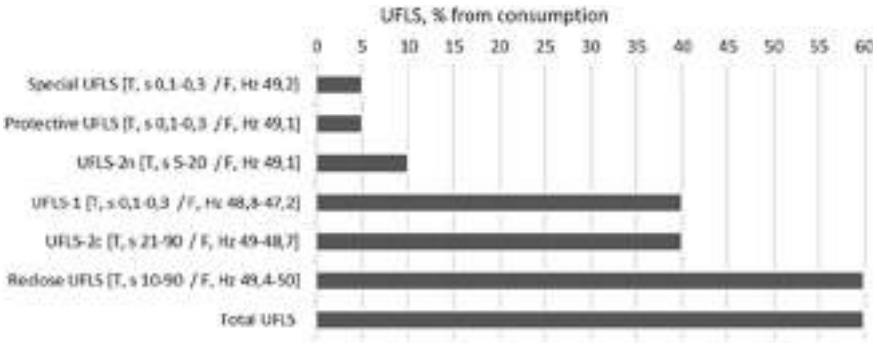

Fig. 9 The consumption disconnected by UFLS relays

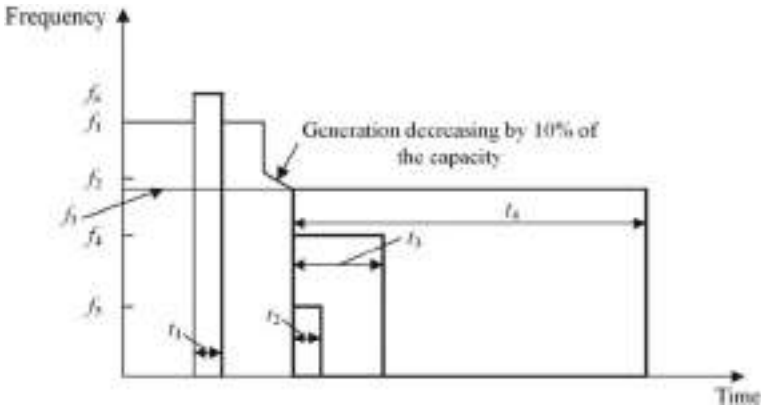

Fig. 10 The diagram of SPA operation

increased by more than 50.5 Hz, the operation time is 10 s. The diagram of the SPA operation used at the nuclear power plants is depicted in Fig. 10.

The normal operation of the power system is defined by the frequency f_1. In case of the frequency decreasing below f_2, the output power of nuclear units is being decreased by 10% by SPA operation. In the event of the further frequency decreasing below f_3 (but above f_4) and if the frequency restoration is not achieved during time setting t_4, the generating unit is disconnected by SPA operation. If the frequency is decreased below f_4 and f_5, the corresponding time settings are t_3 and t_2 respectively. The frequency increasing above f_6 with a time greater than t_1 also leads to the generator disconnection from the network. Thus, as seen above, the duration of the frequency decreasing (or increasing) should not exceed the corresponding SPA time setting. Otherwise, it will lead to the generator disconnection followed by a great frequency drop and possible blackout.

Some simulation results for UFLS relay operation in the case of two 1000 MW generating unit's disconnection (2000 MW imbalance) are presented in Figs. 11 and 12.

As seen in Fig. 12, up to 20 s. after disturbance, consumption power is decreasing due to the frequency drop (self-regulation effect) [3]. In case of the frequency decreasing to the UFLS relay setting, the load is reduced by UFLS operation [7]. The total load reduction is equal to 190 MW.

The simulation results of the SPA operation of the nuclear power plants in case of the significant frequency decreasing are presented in Figs. 13 and 14. As seen in Fig. 14, the initial generation power of the unit is 1023 MW. When the frequency decreases below 49 Hz (see Fig. 13) SPA begins to operate. As the frequency is below 48 Hz during 60 s the generating unit is disconnected from the grid by SPA operation. It should be noted that the loss of such a significant generation power is worsening the system emergency and can lead to a blackout.

To estimate the quality of the frequency control, the model of the automatic generation control (AGC) has been developed as well [8]. Simulation results of AGC

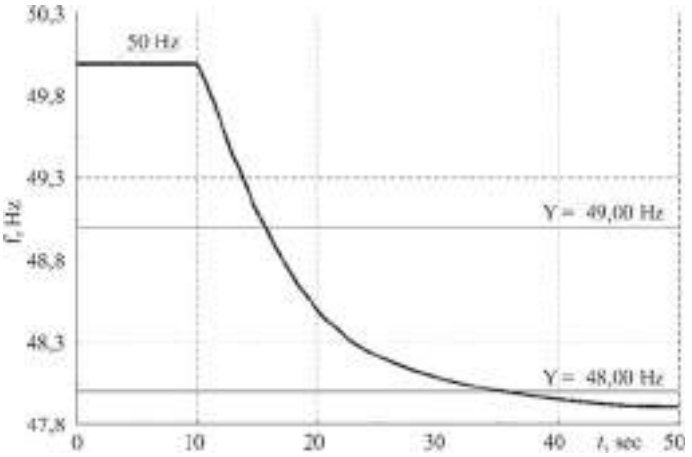

Fig. 11 Frequency change in the power system

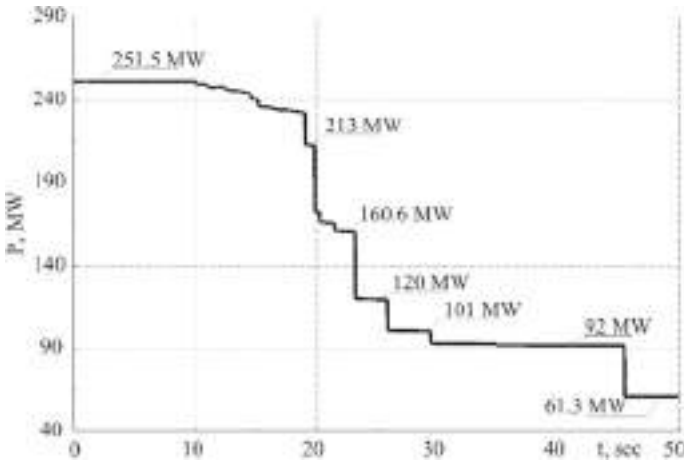

Fig. 12 Load change as a result of UFLS operation

operation in case of generating unit disconnection are presented in Figs. 15 and 16. The participation factors of the regulating power plant in the secondary frequency control are equal to 0.2; 0.14; 0.2; 0.16; 0.18 and 0.12 pu. As seen in Fig. 15, the generator loss is fully compensated by the power change of the regulating power plant according to their participation factors in the secondary frequency control. After secondary frequency control, the net interchange power at the interface between power systems PS1 and PS2 is also restored at its scheduled value as well (see Fig. 16).

It should be noted, that in this work the simulation of the load frequency control has been performed considering the normal operation of the interconnected power

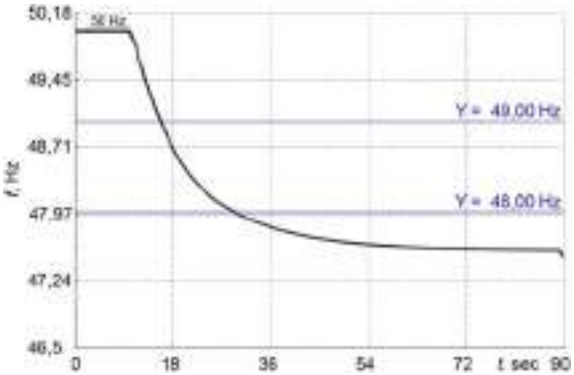

Fig. 13 Frequency change in the power system to simulate SPA operation

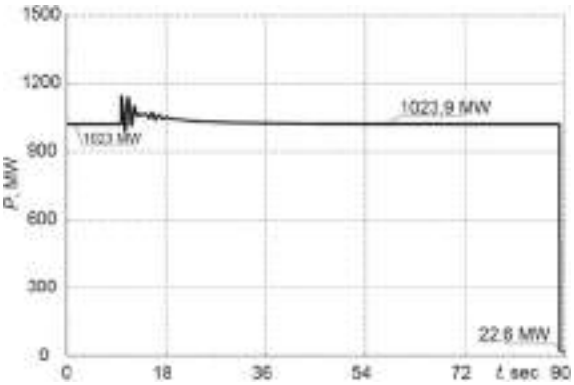

Fig. 14 Unit generation at the nuclear power plant

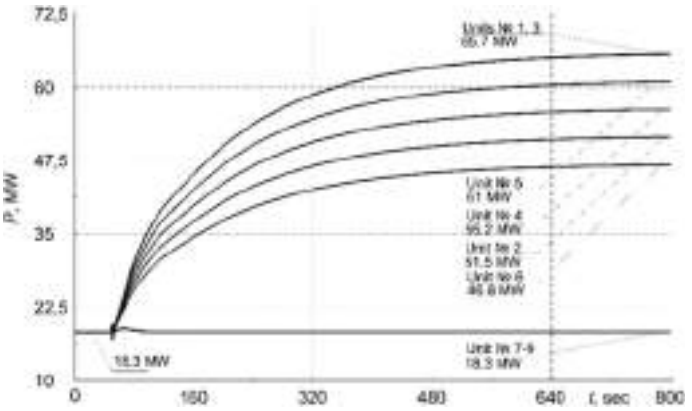

Fig. 15 Generation of the regulating power plant under AGC control

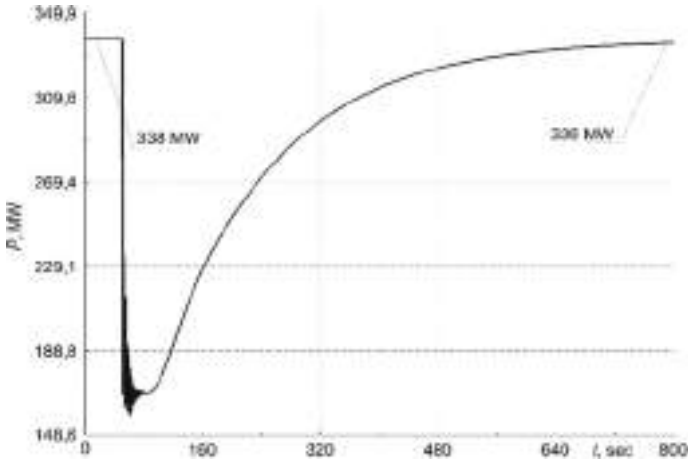

Fig. 16 Net power flow during the secondary frequency control

system. At the same time, identifying the critical loading of overhead lines in emergency operation conditions will allow defining these overloadings to prevent their possible disconnection.

The presented results of the time-domain simulation demonstrate an accurate operation of the proposed dynamic user-defined specific models of UFLS, SPA, and AGC during electromechanical transients after applying different disturbances. The developed advanced software model is realized in DIgSILENT PowerFactory software [3, 6, 9].

The developed models can be used to study all aspects of frequency stability (inertial system response, primary active power control, UFLS, and SPA operation, secondary control) for various scenarios of power imbalances in power systems. The mentioned study also including a market study [10, 11] is actual in the case of the power systems interconnection.

References

1. Kundur, P.: Power System Stability and Control. McGraw-Hill (1994)
2. Machowski, J., Bialek, J., Bumby J.: Power system dynamics. In: Stability and Control, 2nd edn. John Wiley & Sons (2008). https://www.wiley.com/en-us/Power+System+Dynamics%3A+Stability+and+Control%2C+2nd+Edition-p-9781119965053. Accessed 25 Mar 2021
3. Ramavathu, S.N., Datla, V.T., Pasagadi, H.: Islanding scheme and auto load shedding to protect power system. Int. J. Comput. Electr. Eng. **1**(4), 508–512 (2013)
4. Shahgholian, G., Salary, M.E.: Effect of load shedding strategy on interconnected power systems stability when a blackout occurs. Int. J. Comput. Electr. Eng. **4**(2), 212–217 (2012)
5. Pavlovsky, V., Steliuk, A., Lenga, O., Zaychenko, V., Vyshnevskyi, M.: Frequency stability simulation considering under-frequency load shedding relays, special protection automatics and

AGC software models. In: Proceedings of IEEE PowerTech Conference, pp. 1–5. Manchester (2017). https://doi.org/10.1109/PTC.2017.7981043
6. Pavlovsky, V., Steliuk, A., Lenga, O., Zaychenko, V., Vyshnevskyi, M.: Determination of the optimal UFLS settings of the IPS of Ukraine taking into account the experience of ENTSO-e. In: Second Southeast European Regional CIGRE Conference. Kyiv (2018)
7. Pavlovsky, V., Steliuk, A., Lenga, O., Zaychenko, V., Vyshnevskyi, M., Antoniuk, Y.: Influence of the frequency and voltage change on load power considering automatic frequency load shedding. Energ. Electrif. **4**, 7–12 (2016). http://electromagazine.com.ua/uploads/files/mag1/energetika_4_2016.pdf. Accessed 25 Mar 2021
8. Gonzalez-Longatt, F., Steliuk, A., Hinojosa V.H.: Flexible automatic generation control system for embedded HVDC links. In: Proceedings of IEEE PowerTech Conference, pp. 1–6. Eindhoven (2015). https://doi.org/10.1109/PTC.2015.7232555
9. Gonzalez-Longatt, F., Luis Rueda, J. (eds.): PowerFactory applications for power system analysis. Springer (2015). https://doi.org/10.1007/978-3-319-12958-7
10. Blinov, I., Parus, E.: Congestion management and minimization of a price difference between coupled electricity markets. Tekhnichna Elektrodynamika **5**, 81–88 (2015). http://dspace.nbuv.gov.ua/handle/123456789/134106. Accessed 25 Mar 2021
11. Kyrylenko, O., Blinov, I., Parus, E., Ivanov, G.: Simulation model of the day-ahead electricity market with implicit consideration of power systems network constraints. Tekhnichna Elektrodynamika **5**, 60–67 (2019). https://doi.org/10.15407/techned2019.05.060